Integrating geochemical and microbiological information for better modeling of the N-cycle – past and present

by

Céline Chantal Michiels

MSc, Université Libre de Bruxelles, 2012
BSc, Université Libre de Bruxelles, 2010

A DISSERTATION SUBMITTED IN PARTIAL FULFILLMENT OF
THE REQUIREMENTS FOR THE DEGREE OF

DOCTOR OF PHILOSOPHY

in

The Faculty of Graduate and Postdoctoral Studies

(Microbiology and Immunology)

THE UNIVERSITY OF BRITISH COLUMBIA

(Vancouver)

April 2019

The following individuals certify that they have read, and recommend to the Faculty of Graduate and Postdoctoral Studies for acceptance, the dissertation entitled:
Integrating geochemical and microbiological information for better modeling of the N-cycle – past and present
Submitted by Céline C. Michiels in partial fulfillment of the requirements for the degree of Doctor of Philosophy in Microbiology and Immunology

Examining Committee:

Prof. Sean A. Crowe, Microbiology and Immunology & Earth, Ocean and Atmospheric Sciences

Supervisor

Prof. Steven J. Hallam, Microbiology and Immunology

Supervisory Committee Member

Prof. Mary O'Connor, Zoology

University Examiner

Prof. Susan Baldwin, Chemical and Biological Engineering

University Examiner

Prof. Gregory Dake, Chemistry

Chair

Additional Supervisory Committee Members:

Prof. Philippe Tortell, Earth, Ocean and Atmospheric Sciences

Supervisory Committee Member

Prof. Roger François, Earth, Ocean and Atmospheric Sciences

Supervisory Committee Member

Abstract

Cycling of N occurs through a multitude of microbial reactions used by microorganisms to harness energy and generate growth. These microbial reactions are the main controls on the availability of fixed-N and can often limit primary production in marine ecosystems. The microorganisms involved in the N-cycle are diverse and the metabolic pathways are further distributed across many taxa, rendering the modeling of the N-cycle complex. Indeed, models of N-cycling fall short of making robust and explicit predictions, in part due to a lack of ecophysiological information describing the relevant processes at a molecular scale. Direct ecophysiological information is obtained from process rate measurements, yet these generally lack coupled information on microbial community composition limiting their extensibility across multiple environments. This dissertation creates a new framework for the modeling of the N-cycle by measuring the rates and pathways of N-cycling in anoxic pelagic environments. This new and quantitative knowledge is incorporated into models of N-cycling to improve reconstructions of past and future N-cycle. I describe the rates and pathways of Fe-dependent NO_3^- reduction in a ferruginous pelagic environment, analogous to the Proterozoic oceans. I then describe the nutrients status and the implications of NO_3^- reduction through DNRA and denitrification for biological production through a flux-balance model for ancient oceans. I also study the environmental factors that influence the partitioning of N-loss between anammox and denitrification in an anoxic fjord (Saanich Inlet). A flux-balance model was built to describe the competition between anammox and denitrification based on the rates of N_2 production as well as changes in microbial community composition and ecophysiological parameters. We show that recycling of N through DNRA, rather than N-loss, dominates annual NO_3^- reduction in Saanich Inlet, challenging current assumptions that DNRA does not need to be considered as an important pathway of N-cycling in the ocean. Overall, the work presented here offers a new and integrated approach that combines geochemical information such as nutrient profiles and process rate measurements, microbiological information such as microbial community composition, structure and functions analysis, and applies it to quantitative models that can be used to further test hypotheses about the N-cycle.

Lay Summary

Availability of oxygen is an organizing principle for life in marine ecosystems. As oxygen declines, microbial metabolisms prevail over higher trophic activities. Low oxygen conditions are found in large zones of the modern oceans where anaerobic microbial activities play an important role in biogeochemical cycling of essential elements like nitrogen, which affects nutrient availability, primary production, and CO_2 sequestration. These low oxygen conditions also existed on the Early Earth, and microbial activities would have been primordial regulators of biogeochemical cycling of essential nutrients, which likely impacted biological productivity and climate. My thesis creates new knowledge on how nitrogen is used under low-oxygen conditions by specific groups of microorganisms, for past and present marine systems. I then apply this new information to modeling approaches that inform on biogeochemical cycles in the Earth system, for the ancient and modern moceans, which can lead to better predictions for future climate.

Preface

This work was made possible through the contributions and dedication of many collaborators. Dr. Sean Crowe, as the research advisor was involved in all aspects of this work including experimental design, data analysis and interpretation and writing. Sections of this work are partly or wholly published, in press, or in review. Copyright licenses were obtained and are listed below.

- Chapter 1: Céline C. Michiels wrote the main text with editorial support from Sean A. Crowe.

- Chapter 2: Céline C. Michiels wrote the main text with Sean A. Crowe. Sean A. Crowe and Franois Darchambeau designed the research. Sean A. Crowe and Franois Darchambeau collected samples. Sean A. Crowe, Franois Darchambeau and Fleur Roland performed laboratory work, Céline C. Michiels and Sean A. Crowe analyzed and interpreted the data, as well as developped the model found in the published paper. Editorial support was received from the entire list of authors. The reference for the published paper can be found as follows:

  C. C. Michiels, F. Darchambeau, F. A. E. Roland, et al. Iron-dependent nitrogen cycling in a ferruginous lake and the nutrient status of proterozoic oceans. Nature Geoscience, 10(3):217U176, Mar 2017.

- Chapter 3: Céline C. Michiels wrote the main text with help from Sean A. Crowe. K.E. Giesbrecht and D. E. Varela supplied the Chlorophyll *a* data. J. A. Huggins, R. L. Simister and J. S. Spence helped in the analysis of the isotope pairing technique and taxonomic data. S. J. Hallam and D. E. Varela reviewed the mauscript and provided editorial support.

  This chapter was submitted to the journal Frontiers in a special edition titled "Facing Marine deoxygenation". The manuscript was accepted in January 2019.

  The citation can be found as: C. C. Michiels, J. A. Huggins, K. E. Giesbrecht et al. Rates and pathways of N_2 production in a persistently anoxic fjord: Saanich Inlet, British Columbia. *Frontiers in Marine Science*, 6:27, 2019.

- Chapter 4: Céline C. Michiels wrote the main text with editorial support from Sean A. Crowe. Céline C. Michiels and Sean A. Crowe interpreted the data. J. A. Huggins helped in the analysis of the isotope pairing data. C. Morgan-Lang and R. L. Simister helped in

the processing of the metagenomic data. S. J. Hallam provided help in the analysis of the metagenomic data and editorial support.

- Chapter 5: Céline C. Michiels wrote the main text.

Throughout this dissertation the word 'we' refers to Céline C. Michiels unless otherwise stated.

None of the work encompassing this dissertation required consultation with the UBC Research Ethics Board.

Table of Contents

Appendices

List of Tables

List of Figures

Acknowledgements

This thesis has profoundly changed my life by uprooting me from my birth country. Although I have missed my Belgian family and friends dearly, I can with certainty say that I now have a Canadian family and have gathered around me some dear friends in Vancouver. This thesis also allowed me to visit some amazing places in BC, the middle of the Pacific Ocean and Indonesia. I have met some incredible people along this journey and would like to thank them all for their kindness. However, the list is long, and I will try to keep it more concise in a few dedicated thank yous. First and foremost, I would like to thank Sean A. Crowe for welcoming me in his brand-new lab in 2013 and expanding my vision on how to "do science". Your incredibly vast knowledge has been a never-ending source of new ideas and I am very grateful to have been able to thrive under your supervision. Thank you to my committee, Steven J. Hallam, Philippe Tortell and Roger François for your support during our meetings. Thank you to my External Examiner, Prof. Gregory Dick from U. Michigan, who reviewed my thesis carefully and thoughtfully. Thank you to my lab mates in the Crowe lab, past and current members – Kate Thompson, Ashley Davidson, Julia Huggins, Jenifer Spence, Rachel Simister, Niko Finke, Arne Sturm, Kohen Bauer, Andrew Hefford – for your help and guidance in the lab, your knowledge, the discussion at bread and beer meeting (!!), and numerous coffee dates! A special thank you to Annie Cheng and Belle Cheng who have helped me measure my million samples without ever complaining. To all the "Saanichers" – Jade Shiller, Monica Torres-Beltran, Melanie Sorensen, Andreas Muller, Chris Payne and Lora Pakhomova, and the crew from the Strickland, thank you! And finally, a special "thank you" to a few Hallam lab members – CarriAyne Jones, Aria Hahn, Connor Morgan-Lee, Colleen Kellogg, Alyse Hawley. When I sought out your expertise, you were always there and willing to share it with me and more

Dedication

À mes parents et Camille, pour leur soutien inconditionnel malgré les 7825km de distance qui nous séparent.

To Kev for being there no matter what.

Chapter 1

Introduction

Nitrogen (N) is required as an elemental constituent for all life on Earth, as it is one of the most abundant elements in nucleic acids and proteins. For every 100 atoms of carbon, cells typically require between 2 to 20 atoms of nitrogen depending on the specific organism [6]. The majority of Earth's accessible nitrogen resides in the atmosphere, with nitrogen comprising 78% by mass in its inert form N_2 gas. This N_2 gas is primarily made available to life through the bioenergetically expensive microbial reaction of N-fixation, which requires an enormous activation energy (16 ATPs or $\sim$544 kJ mol^{-1} [7]) to break the triple bound found in the N_2 molecule. Rates of N-fixation can limit primary production both in terrestrial and marine ecosystems, and this limitation of productivity is a first-order control on biological CO_2 sequestration globally [8, 9]. Bioavailable N is thus fundamental to sustaining life on Earth, and has the potential to further influence the global carbon pump and climate.

The modern biogeochemical cycling of N, its biological availability, and operation under different redox states depends almost entirely on a suite of oxidoreductive metabolic reactions conducted by a complex network of microorganisms (Fig. 1.1). N_2 is incorporated from the atmosphere into the biosphere through the fixation of gaseous N_2 into organic amines (R-NH_3), which upon biomass degradation are liberated to the surrounding environment as NH_4^+ via ammonification (Fig. 1.1). NH_4^+ is then sequentially oxidized to NO_2^- and NO_3^- through the process of nitrification, requiring molecular oxygen to operate (Fig. 1.1). These oxidized N-species are important to eukaryotic primary producers and are usually assimilated as a source of fixed-N (Fig. 1.1). NO_3^- is alternatively either reduced back to the atmosphere as N_2 through the chemotrophic reactions of denitrification and anaerobic ammonium oxidation (anammox) or reduced back to NH_4^+ through the chemotrophic reaction of dissimilatory nitrate reduction to ammonium (DNRA) (Fig. 1.1). When assimilated into biomass, N can be released through organic

matter remineralization and ammonification. However, a small portion of this organic matter escapes the remineralization process and ends up buried in sediments [10]. During subduction, some of the buried N (bound to the organic matter) returns to the atmosphere but a significant part leaves the biosphere for the geosphere and is sequestered in the solid Earth [11].

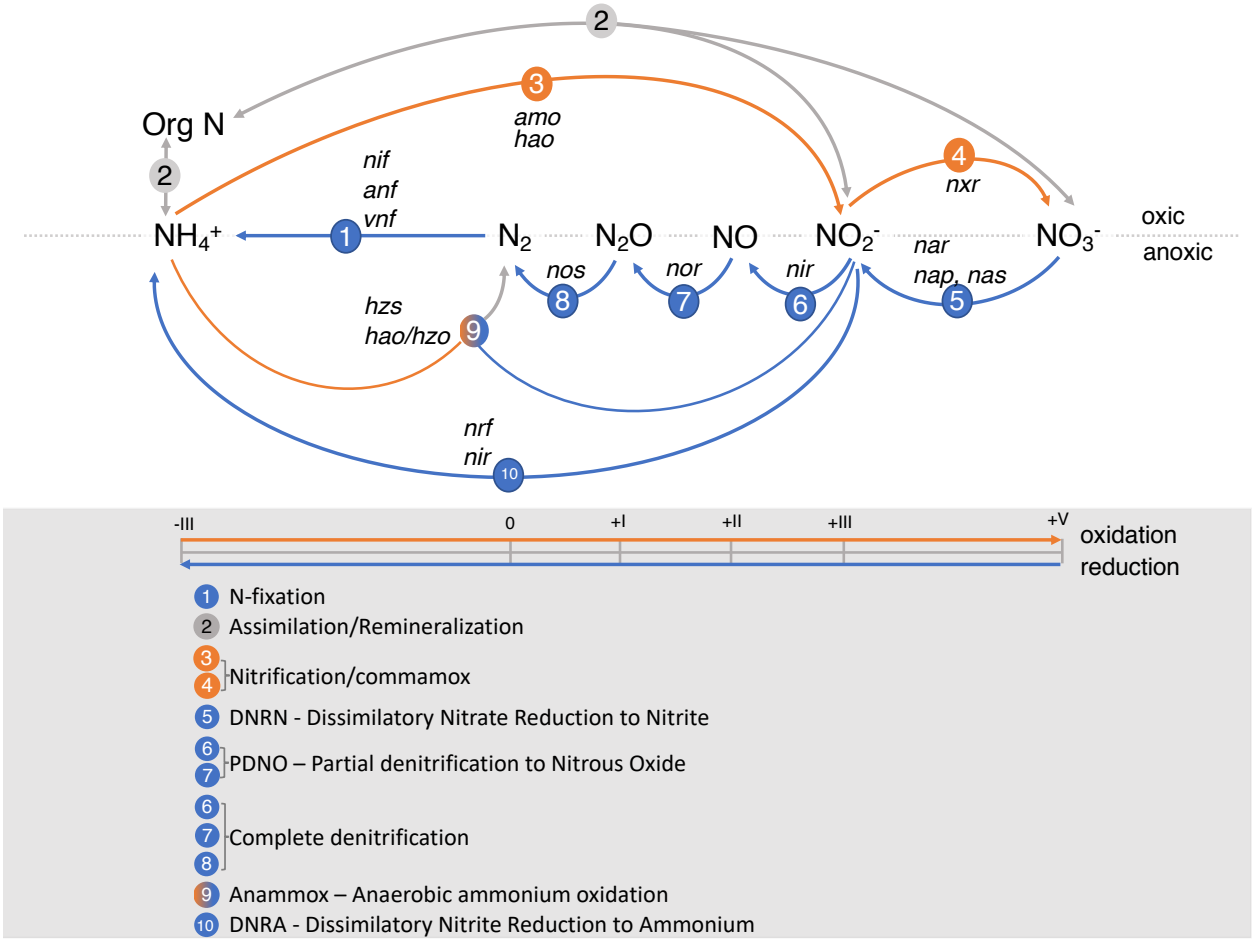

Figure 1.1: *Overview of the microbial reactions constituting the N-cycle.* Reactions are defined in the grey box. Orange arrows correspond to an oxidation reaction of the N-species whereas blue arrows show a reduction of the N-species. The grey arrows encompass assimilation of the N-species by an organism and remineralization of organic N-species. Reactions with arrows above the dotted line are generally considered to be done under oxic conditions whereas arrows drawn below the dotted line are usually considered done under anoxic conditions. Chemical N-species follow the redox state highlighted in the grey box. In italic are the main genes found to execute the corresponding enzymatic reaction. This figure was made with the help of Julia Huggins and is inspired from Kuypers et al. (2018) [3].

The main pools of N in the Earth system are distributed between the atmosphere and the solid Earth: the crust and the mantle [12]. Recycling of N between these different pools occurs both

rapidly through biological processes (Fig. 1.1 and description above) with a turnover time for atmospheric N_2 of $\sim$1000 years [2], and slowly through tectonics of the crust and mantle over timescales of 1 Ga [13]. Biological reactions govern the processes of N fixation and remineralization, which, in combination, determine the overall rate at which biomass is buried in marine sediments and subducted into the mantle. Thus, the rapid turnover of N through biological activity could have caused long-term changes in atmospheric N abundance. Such dynamics in atmospheric N abundance through time can further influence climate and impose a negative feedback on biological productivity. For example, lower rates of N-fixation result in higher N_2 pressure in the Earth's atmosphere, which increases the greenhouse effect of existing gases by broadening their absorption lines [14]. A lowering of N_2 pressure through high rates of N-fixation and burial of organic matter will in turn induce a negative feedback on N-fixation, which would become limited by lower N_2 partial pressure [15]. Despite best efforts to date, however, likely changes in atmospheric N_2 over Earth's history, and in the future, remained unconstrained due to high uncertainties in the sizes and exchange rates between the different reservoirs and their corresponding mechanisms of regulation [16, 17].

Cycling of N through biological activity is mainly conducted by microorganisms through the many metabolic reactions transforming N, between its oxidized and reduced states under oxic and anoxic conditions (Fig. 1.1). The metabolic potential for these reactions are widely distributed across the 3 domains and across mutliple phyla within these domains [3] (see example in Fig. 1.2c). Furthermore, microorganisms have established specific niches and have developed complex interactions between functional metabolic groups in order to carry out these transformations [18]. The complexity of the microbial metabolic network responsible for N-cycling has, as a consequence, rendered biogeochemical modeling of this element challenging. Biogeochemical modeling approaches often use thermodynamic calculations in combination with susbtrate availability, as well as ecophysiological parameters for the relevant microorganisms. Ecophysiological parameters remain elusive, however, due to the fact that the majority of relevant microorganisms remain uncultivated and that there is a lack of mechanistic links between process rate measurements and the underlying microbial community in environmental systems (see section 1.4). Modeling efforts of N-cycling, to date, are, therefore, hampered by the lack of information needed to constrain

these models.

The emergence of humans as geobiological agents is causing changes to the Earth system at unprecedented rates, and specifically to the N-cycle [2, 19]. An acute example is the doubling of global rates of N-fixation through the use of the Haber-Bosch process to produce fertilizers since the early 20th century [2]. Such rapid perturbations to fluxes of matter and energy strongly deviate from the pre-industrial dynamics in biogeochemical cycles that were established over billions of years; this will almost certainly alter rates of pathways in the N-cycle and have unconstrained feedbacks on climate. Such changes in rates and pathways will be largely determined by changes in the fluxes of N through the different metabolic pathways. It is currently difficult, however, to predict these responses and feedbacks either qualitatively or quantitatively, since we lack sufficient information on these metabolic pathways to construct meaningful models that will ultimately allow robust forecasts. In particular, we need new ecophysiological information on the relevant microorganisms involved in key metabolic pathways in the N-cycle. The extent of current knowledge and gaps will be discussed in the following sections.

This chapter introduces the evolution of the N-cycle over time, the details of different metabolic pathways comprising the modern N-cycle, the distribution of these pathways amongst a broad diversity of microorganisms, and the controls that constrain the rates of these processes. It also aims to highlight the existing gaps in current knowledge of the N-cycle and the uncertainties associated with global budgets and N-cycling modeling. The following chapters of the thesis are then outlined in the last section. Overall, my thesis creates new knowledge on the N-cycle through direct measurements of rates and pathways of N-cycling in anoxic pelagic environments. This new and quantitative knowledge can be incorporated into models of N-cycling to improve reconstructions of the past and make predictions about the future.

1.1 The emergence of the N-cycle

The distribution of N-species in modern pools of N is the product of billions of years of feedback between biological N-cycling and geophysical processes (tectonics). Dynamics in the N-cycle and the distribution of N between Earth's major N inventories is archived in the rock record,

which reveals exchange between atmospheric N and the solid Earth mediated through biological N-fixation, transfer of fixed-N into marine sediments, and subduction of these sediments into the mantle [17]. Life emerged on Earth approximately 4.2 Ga ago [20] and N-fixation likely emerged as a key metabolic pathway as early as 3.8 Ga [21], in a plausible response to scarcity of bioavailable N in the early biosphere. It was not until the advent of oxygenic photosynthesis, however, and the introduction of molecular oxygen (O_2) into Earth's surface environments, that the full-suite of oxidative and reductive pathways in the biological N-cycle likely emerged (Figs. 1.1 and 1.2) [16, 22].

Before biological N-fixation evolved ∼3.8Ga ago, bioavailable N came only from extraterrestrial input and slow photochemical and hydrothermal activities [23–25]. It is assumed that bioavailable N was extremely limited, which likely restricted life on the early Earth [2]. Initial input of N on Earth occurred through the bombardment of the proto-Earth with solid ammonia that then outgassed to the atmosphere under extreme heat conditions [2]. Heat shock in the atmosphere, associated with lightning activity and meteorite impacts, turned N_2 into NO, which, through photochemical and aqueous reactions, could have been oxidized to NO_2^- and NO_3^- [23, 25, 26]. These processes were extremely slow and yielded up to $2 \cdot 10^8$ mol N yr^{-1} [27], producing only a fraction of todays marine biological fixation ($10 \cdot 10^{12}$ mol N yr^{-1} or 10 Tmol N yr^{-1} [1]). In addition to atmospheric reactions, hydrothermal activity could have theoretically transformed $N_2/NO_3^-/NO_2^-$ into NH_4^+. However, there is no evidence for such reactions today and their operation in the past thus seems unlikely [28, 29]. A need for alternative pathways to fix N would have emerged when biological activity exhausted geological sources.

In the absence of atmospheric oxygen, the early biological N-cycle was only composed of biological N-fixation, NH_4^+ assimilation and release of the NH_4^+ through biomass degradation, also called ammonification (Fig. 1.2a), followed by transfer of this fixed-N to the sediments. With the advent of biological N-fixation during the PaleoArchean (4.0 – 3.2Ga), NH_4^+ would likely have emerged as the principal N-species, accumulating in the oceans under anoxic and ferruginous (Fe^{2+}–rich) marine conditions. N-fixation is known to have a relatively small fractionation effect, leaving the N-pool fixed in the biomass with a small negative fractionation relative to the source N_2 [30], thus agreeing with the N isotopic fractionation observed in the geological record, which shows

a small excursion of $\delta^{15}N$ between 0 and -4‰. In addition to the rock record, the phylogenetic diversity of well-conserved nitrogenase, the enzyme necessary for N-fixation, shows that the metabolic potential for N-fixation is widespread across two domains of life, implying a strong need for this reaction to occur [31] and suggesting that it evolved early in the evolution of life and was subsequently spread through vertical inheritance and horizontal gene transfer [32]. Altogether, the evidence suggests that biological N-fixation evolved early in Earth's history, not long after the capacity to assimilate NH_4^+ into biomass.

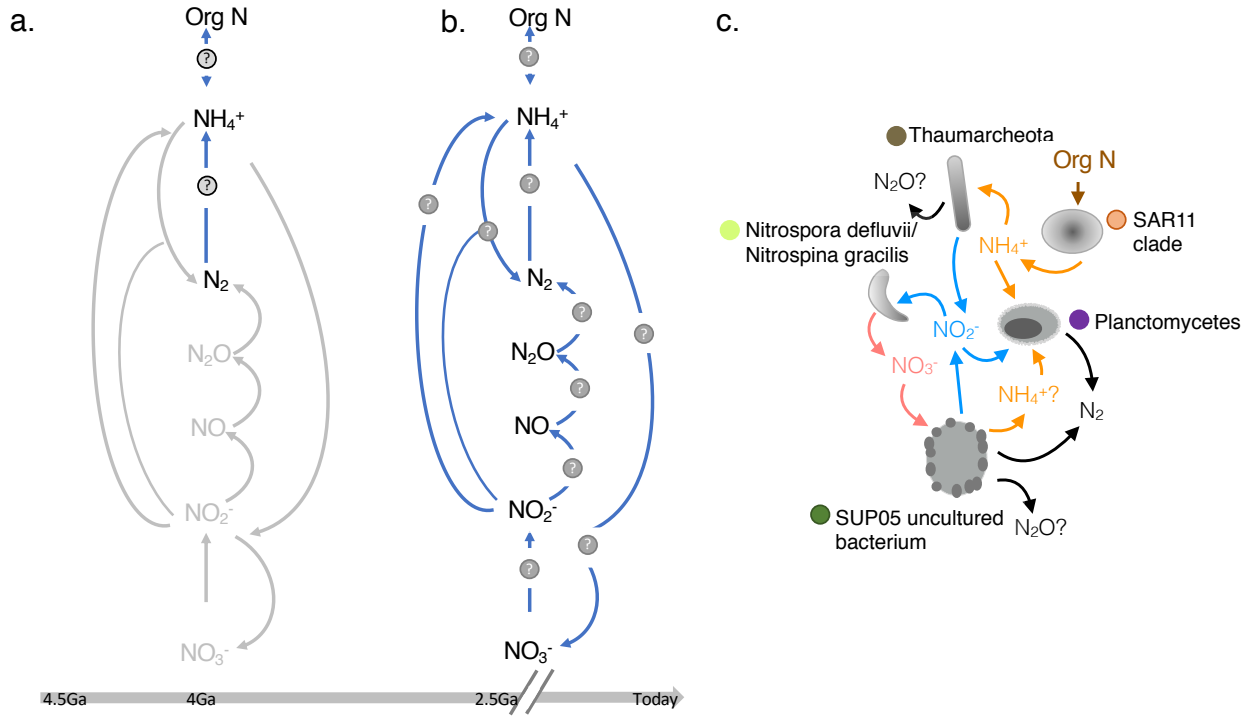

Figure 1.2: *Schematics of distributed metabolisms within the N-cycle over time.* Colored circles represent microbial species, when known, performing a reaction (function) shown by the arrows. Several species can perform the same reaction, and the same species can perform multiple reactions depending on the metabolic potential contained in their genomes and their expressed metabolism. For the ancient N-cycle, however (a and b), it is, to date, impossible to associate species with pathways (a) represents the early biosphere with constrained chemical N-species present. (b) highlights the changes to a modern N-cycle due to the oxygenation of the atmosphere and thus the presence of oxidized N-species such as NO_3^- and NO_2^- 2.5 Ga ago (c) is a specific example of the modern N-cycle with the distribution of the N-cycle reactions through the microbial communities in Saanich Inlet (BC, Canada). (c) was adapted from Hawley et al. (2014) [33].

Oxygenic photosynthesis likely evolved around 3.0 Ga, during the Meso-Neo Archean (3.2 – 2.5Ga) [34–37], and the local accumulation of O_2 in regions known as "O_2 oases" [38] triggered the

onset of the oxidative part of the biological N-cycle (Fig. 1.2b). This allowed for the development of nitrification and, for the first time, the accumulation of oxidized N-species (NO_3^-/NO_2^-) in the oceans (Figs. 1.1 and 1.2b). Denitrification and/or anammox likely evolved shortly thereafter as NO_3^- became increasingly available. The advent of biological N_2 production has been implicated in a bottleneck for biological productivity, because the NO_3^- produced through nitrification would have been effectively returned to the atmosphere through denitrification/anammox, with the corresponding re-imposition of N-limitation on biological productivity [39–41]. It was only when atmospheric O_2 increased appreciably, likely in the late Proterozoic (1.6 – 0.6 Ga), that the marine NO_3^- pool started to stabilize and become more widely available and similar to modern concentrations [41]. The rock record supports the evolution to a modern N-cycle, showing positive excursions of δ^{15}N throughout the late Archean and Proterozoic, indicating an early onset of nitrification and denitrification processes associated with a small pool of NO_3^- in the oceans [22, 40–43]. Indeed, denitrification is associated with isotopic fractionation that leads to a heavier NO_3^- pool, which is subsequently recorded in sediment biomass containing assimilated NO_3^-. This signal can be amplified if the pool of NO_3^- is small in the water column, leading to increased positive δ^{15}N signal. However, the δ^{15}N of the Meso- and Neoproterozoic (1.6 – 0.6 Ga) is close to that of modern marine sediments (+5‰) implying a stabilization of the NO_3^- pool in the ocean, which indicates the widespread establishment of the modern N-cycle due to the stabilization of O_2 in the atmosphere and the ocean [41, 43].

Most information about the ancient N-cycle comes from the rock record [21, 22, 40–43] and from associated modeling using information from the rock record [39, 42, 44, 45]. Few models integrate microbial and molecular information in their design in part due to a lack of essential quantitative ecophysiological information on the relevant microbial processes. One way to infer what the microbial activities would have looked like during the Archean and the Proterozoic is to study modern environments that harbor geochemical conditions analogous to the ancient oceans (e.g. ferruginous conditions), and host microbial communities that manifest metabolic potential relevant to the past. The oceans in the Archean and Proterozoic eons were mainly ferruginous [46] with transient occurrences of euxinic (sulphide-rich) conditions in coastal and closed basin areas in the late Archean and through the Proterozoic [47–49]. Finding ferruginous conditions

under the modern oxidized atmosphere has proven challenging, however, because ferrous iron (Fe^{2+}) oxidizes to ferric iron (Fe^{3+}) when oxygen is present, thus restricting the occurrence of such conditions on today's Earth. Nevertheless, a few modern analogues to the ferruginous Archean and Proterozoic oceans exist on Earth today and information from these analogues can be used to inform our view of the past [Kabuno Bay in Lake Kivu (RDC) [50], Lake La Cruz (Spain) [51], Lake Pavin (France) [52], Lake Lugano (Switzerland) [53] and Lake Matano (Indonesia) [54]]. For example, studies in these environments reveal the ecological role of photoferrotrophy (anoxygenic photosynthesis with Fe^{2+}) in illuminated Fe-rich environments. By extension, studies in these same environments may inform qualitative and quantitative models of N-cycling under these conditions.

The Neo-Archean and the Proterozoic oceans transitioned periodically from ferruginous to euxinic conditions in coastal areas and closed basins, as a result of increases in organic carbon availability in the water column and/or with increased seawater sulphate concentrations [41, 49]. These euxinic conditions appear to have been transient and mainly restricted to coastal shelves where biological activity would have been high [47–49, 55]. This could have influenced rates of N-recycling through denitrification and anammox as it has been shown that microorganisms performing denitrification can use sulphide as an electron donor and the presence of sulphide might be an inhibitor of anammox [56]. However, we are lacking quantifiable microbial information to assess how the transition from ferruginous to euxinic conditions would have affected the N-cycle.

1.2 The modern N-cycle

The modern N-cycle is comprised of multiple biological and geochemical processes and the transmission of N between the different pools at the Earth's surface depends almost entirely on the activity of microorganisms. Throughout the oceans and in soils, microorganisms called diazotrophs fix N_2 from the atmosphere and incorporate it into their biomass [57]. When these microorganisms die and decompose, fixed-N contained in their biomass is released into the surrounding environment as NH_4^+ through the process of ammonification (Fig. 1.1). Under oxic

conditions, this NH_4^+ can be oxidized sequentially to NO_2^- and then NO_3^-, through the microbial reactions of nitrification. Under the low oxygen conditions that can develop when respiration rates exceed oxygen supply from photosynthetic production and/or advective and diffusive transport from the atmosphere, specific microorganisms use NO_3^- as a terminal electron acceptor in respiration instead of oxygen, through canonical denitrification, leading to the production of N_2 and closing the N-cycle by returning N to the atmosphere (Fig. 1.1).

In addition to complete denitrification, several other microbial reactions also utilize NO_3^- or NO_2^- as an electron acceptor (Fig. 1.1): dissimilatory NO_3^- reduction to NO_2^- (DNRN), partial denitrification to nitrous oxide (PDNO), and anaerobic ammonium oxidation (anammox) [3]. These processes, like complete denitrification, usually operate under low oxygen or anoxic conditions. Microorganisms that carry out partial denitrification (DNRN and PDNO) are often grouped with complete denitrifies and collectively are often referred to simply as 'denitrifiers'. Thus, many 'denitrifiers' lack the metabolic potential to perform all the steps of complete denitrification, and even when they do, environmental conditions may favour incomplete denitrification. Denitrifiers oxidize inorganic (HS^- [2], Fe(II) [58, 59]) and/or organic electron donors (e.g. formate, lactate, and other C-containing compounds [60]) depending on their metabolic potential and the substrates available. Anammox bacteria, on the other hand, reduce NO_2^- while oxidizing NH_4^+ autotrophically [61]. This metabolism is confined to the bacterial phylum Planctomycetes and is phylogenetically restricted in comparison to the very broad diversity of the denitrifiers which spans bacterial and archaeal phyla [3, 62]. Together, complete denitrification and anammox contribute to the loss of bioavailable nitrogen back to the atmosphere, often referred to as N-loss [63].

The microbial reaction of DNRA provides a shunt in the N-cycle (Fig. 1.1) and precludes N recycling back to the atmosphere. Indeed, as it reduces NO_3^- and NO_2^- to NH_4^+, DNRA retains fixed-N, possibly enhancing the transfer of N_2 from the atmosphere to marine sediments. As DNRA consumes NO_2^-, it also competes with PDNO, complete denitrification, and anammox for the same substrates in the environment. This process has, however, rarely been measured, and it could be cryptically active where/when anammox is also present, as anammox consumes the NH_4^+ produced rather than allowing its accumulation [64]. This renders DNRA invisible to many techniques used to determine rates and pathways of microbial N transformations [64]. Therefore,

the extent to which DNRA contributes to global N-cycling is poorly defined, so far [3].

Overall, the relative fluxes of N between anammox, DNRN, PDNO, complete denitrification and DNRA likely influence global climate and biogeochemical processes. These processes affect the rates of N transfer between different reservoirs, the availability of N to primary producers, and the interactions of N with other biogeochemical cycles in soils, sediments, and pelagic environments. The differential movement of N through this metabolic network has the potential to tip the balance between export of fixed-N to marine sediments versus N recycling back to the atmosphere through N_2 production. Naturally, this balance plays an important role in global biological productivity and climate over multiple time-scales. Moreover, leakage of intermediates such as greenhouse active N_2O gas can have feedbacks on climate. The complex metabolic pathways that underpin the N-cycle have thus influenced Earth's climate over geological time-scales by regulating fluxes of N from the atmosphere, to the crust, and the mantle. Today, climate change is mainly driven by human activity and this will have specific feedbacks on primary production and microbial activities. However, the extent to which primary production and microbial activities will respond to these changes is poorly constrained.

Current anthropogenic activities have lead to the increased loading of agricultural soils with N through the industrial Haber-Bosch process, at a current rate of 9.7 Tmoles yr^{-1} [2], the equivalent of current estimates for marine N-fixation. The increase in soil NO_3^-, in turn, leaches N to coastal waters and causes eutrophication by increasing biological productivity in coastal areas. Indeed, an increase in organic matter promotes aerobic respiration that consumes oxygen, and, without sufficient ventilation, can lead to the development of anoxia. Oxygen minimum zones (OMZs) form under similar conditions, with upwelling of nutrient-rich deep waters promoting primary production in surface water and aerobic respiration in underlying waters. Anoxia in coastal areas and OMZs supports heavy N-loss [60, 65–69] in its anoxic cores [0.1% of the oceanic volume, [63]], and to the development of transient plumes of HS^- [70, 71]. As coastal anoxia and marine OMZs are currently expanding, due to global warming leading to poor ventilation of these zones and increased nutrient loading with increased primary production [72], it is likely that N-loss will be enhanced in the oceans. Thus, a shift in the balance between N-fixation and N-loss could occur, but our current knowledge of the N-cycle is insufficient to enable consistent and robust

predictions of future N-cycling. It is therefore important to improve quantitative models that will enable us to make predictions for the future biogeochemical cycling of essential elements for life on Earth.This will be discussed in the next three sections of this introduction.

1.3 Environmental distribution of anammox, denitrification and DNRA

It is currently unknown whether the global N-cycle is balanced, and this is due to uncertainties in the estimates of N-budgets and rates of N-species transformations. The abundance of fixed-N in the environment is controlled by the balance between sources and sinks, which are primarily biological N-fixation and N-loss through N_2 production and NH_4^+ burial. Some analyses suggest global N-budgets (Table 1.1), are currently balanced ([1] and references therein) while others imply that anthropogenic activities have increased atmospheric N-fixation to such a degree that it outpaces N-loss back to the atmosphere ([2] and references therein). Analyses that indicate balance, however, are based primarily on estimates that carry large uncertainties of up to 20 to 50%, or more [1]. Global input and output fluxes for the N-cycle are mostly based on extrapolation from budgets built at smaller scales based on process rate measurements that are limited both spatially and temporally. Refinements and expansions of these measurements would likely lead to more robust scaling and could promote consensus on global N-budgets; such concensus is essential to the predictions of future N-cycling and climate models.

Robust measurements of N transformation rates can be measured by amending soils, sediments, and waters with ^{15}N labeled N-species and tracking their movement through different N-pools [73, 74]. ^{15}N is not naturally abundant [0.4% [75]] and thus mass spectrometry provides a sensitive way to detect the accumulation of small amounts of excess ^{15}N in natural N pools that results from amendments of ^{15}N labeled reactants or substrates. For example, it is possible to measure N_2-fixation by exposing environmental microbial communities to $^{15}N_2$ and following the incorporation of labeled ^{15}N into biomass (Fig. 1.3a). In the same way, it is also possible to discriminate N_2 production between anammox and denitrification by separately providing microbial communities with $^{15}NO_3^-$ / $^{15}NO_2^-$ or $^{15}NH_4^+$ and following the production of $^{15}N_2$ (Fig.

Table 1.1: N-budgets for the Earth system (marine and terrestrial) based on 1) Gruber and Galloway (2008) [1] and 2) Canfield et al. (2010) [2] and references therein. Inputs are characterized by positive numbers whereas outputs from the systems are negative. * indicates that this flux was not mentioned but could have been merged with another flux without mention

System	Input/Output	Flux (Tg yr^{-1}) Gruber and Galloway (2008)	Flux (Tg yr^{-1}) Canfield et al. (2010)
Terrestrial	N-fixation	145	110.6
	Atmospheric deposition	40	25.2
	Anthropogenic activity	205	182
	N-loss	-317	-99.4
	Riverine export to ocean	-80	-68.6
		Δ= -7	Δ=149.8
Marine	N-fixation	140	140
	Atmospheric deposition	50	?*
	Riverine export to ocean	80	68.6
	N-loss	-244	-238
	N-burial	-25	?*
		Δ= 1	Δ= -29.4
		ΔΔ = -6	ΔΔ = 120.4

1.3a). Nitrification and DNRA can be quantified in these same experiments by tracking the accumulation of $^{15}NO_3^-$ / $^{15}NO_2^-$ or $^{15}NH_4^+$, respectively (Fig. 1.3a). The $^{15}N/^{14}N$ composition of the tracked products (usually $^{15}N_2$) can be measured by using gas source isotope ratio mass spectrometry (IRMS). If the resulting products are dissolved species ($^{15}NH_4^+$ or $^{15}NO_3^-$ / $^{15}NO_2^-$ through DNRA or nitrification, respectively), these products are first chemically reduced or oxidized to $^{15}N_2$ before being measured by Istotope Ratio Mass Spectrometry (IRMS [76]). ^{15}N labeling incubations and the subsequent measurement of ^{15}N excess by IRMS has proven to be sensitive [74], with detection limits depending on the variation in sensitivity between instruments. Measurements based on this ^{15}N-labeling technique form the backbone of my thesis and a schematic figure detailing the handling of the samples can be found in Fig. 1.3b. A fully detailed protocol can be found in Appendix A.

Other approaches to measuring rates of N-cycling include analyses of N_2:Ar ratios to determine production/consumption of N_2 relative to atmospheric levels [77], measuring variability in the natural abundance of N isotopes [78], and application of inhibitors such as acetylene which blocks

the final step in denitrification [79]. These methods are less widely used today as they are usually less sensitive and allow for a less detailed insight into processes and are generally blind to specific metabolic pathways. In addition to these methods, another way to look at N-cycling is to compare concentrations of NO_3^- and PO_4^{2-}, i.e. N*. Concentrations of NO_3^- and PO_4^{2-} in the ocean follow a trend directed by the Redfield ratio (16N:1P, [80]), corresponding to the average composition of marine photosynthetic community and its following remineralization. Thus, concentrations of NO_3^- and PO_4^{2-} are commonly compared by calculating N* according to Eq. 1.1.

$$N^* = [NO_3^-] - 16 * [PO_4^{2-}] + 2.9\mu M \tag{1.1}$$

The inference of N-loss based on N* relationship between the two nutrients is constant for the entire ocean, and a negative deviation from it indicates a NO_3^- deficit due to more N-loss than N-fixation, signifying active denitrification or anammox. The advantage of N* is that it allows investigation of the effect of N-fixation and N-loss on nutrient levels in the ocean without having to use direct rate measurements, which can be costly and time-consuming [81]. However, similar to the other methods mentioned in this paragraph, N* calculations cannot discriminate specific processes and are semi-quantitative estimates of N-loss. Overall, application of these tools and techniques over the last century has yielded remarkable insights into how N-cycling operates in a diverse suite of environments. For example, the anammox process was discovered in a wastewater reactor in the early 1990's [82] and, shortly after, found to operate all over the world in sediments [83] and pelagic environments [84, 85]. Rates and pathways of N-loss and N-processes operating under low oxygen conditions, namely anammox, denitrification and DNRA, were compiled in Fig. 1.4, and Tables A.1, A.2 and A.3 to provide a summary of available information (spatial distribution and magnitude of rates) on rates and pathways of microbial N transformations. We specifically inventoried benthic and pelagic rates found for both lacustrine and marine systems. Anammox, denitrification, and DNRA do, however, operate in terrestrial soils as well, and more information about this can be found in the following references and references therein [86–89].

N-cycling is intense in most marine and lake sediments, contributing to more than 50% of global marine N-loss [9]. N-cycling processes in sediments are vertically distributed, with

nitrification occurring in the oxic sediments, often causing a subsurface accumulation of NO_3^- and NO_2^-. Denitrification, anammox and DNRA occur below this where O_2 is depleted and NO_3^- accumulates. This vertical distribution of N metabolism is intrinsically linked to other biogeochemical cycles such as oxygen, carbon, sulfur, and iron-cycles. Indeed, respiration in sediments generally proceeds using a suite of terminal electron acceptors, in order of progressively decreasing free energy yields ($O_2 > NO_3^- > Fe^{3+} > SO_4^{2-}$). This respiration is fueled by organic matter deposited from the overlying water column, acting as an electron donor for respiration. The progressive depletion of electron acceptors and donors below the sediment-water interface leads to a vertical cascade in redox couples, which leads to stratified microbial communities. When O_2 is exhausted, NO_3^- is generally used as the next most favourable electron acceptor for anaerobic microbial respiration. This is where heterotrophic denitrification and DNRA usually occur, as well as anammox supplied with NH_4^+ from the remineralization of organic matter and NO_2^- from NO_3^- reduction. Rates of denitrification, anammox and DNRA have been reported mostly on coastal shelves, in riverine estuaries, in lakes, and, on a few accounts, on the continental slope (Tables A.1 and A.2). Rates vary over several orders of magnitude, with rates of DNRA varying between 0.024 [90] to $24 \cdot 10^7$ μmoles m^{-2} d^{-1} [91], rates of anammox between 1.2 [92] and $5 \cdot 10^3$ μmoles m^{-2} d^{-1} [93], and rates of denitrification between 10 [94] and $2.4 \cdot 10^7$ μmoles m^{-2} d^{-1} [91](Tables A.1 and A.2). The magnitude of the rates generally appears to increase with decreasing latitude, with the highest rates of DNRA and denitrification reported in tropical estuaries and marine sediments [91, 93, 95–97]. However, an overwhelming majority of the measurements have taken place in northern latitude temperate regions and more measurements in tropical sediments are needed to accurately assess the contribution of these systems to global N-loss.

Pelagic environments support 30 to 50% of the global marine N-loss [9]. In these environments, anammox and denitrification have been reported in coastal and open ocean OMZs, in closed basins (e.g. fjords), and in inland waters such as stratified lakes (Fig. 1.4ab and Table A.3). Usually, denitrification and anammox operate near oxic-anoxic boundary layers, where O_2 is low and NO_3^- is available. When detected, volumetric rates of denitrification vary between 0.05 nM d^{-1} in the ETSP [98] and 1700 nM d^{-1} in Wintergreen Lake (USA) [99]. Rates of anammox vary between 0.12 nM d^{-1} in the Arabian Sea [69] to 480 nM d^{-1} in the Golfo Dulce (Costa Rica) [100]. Out

of 27 studies (Table A.3), only 11 studies have attempted to measure DNRA. Rates of DNRA range between 0.48 nM d^{-1} in the Eastern Tropical South Pacific (ETSP) [60] and 151 nM d^{-1} in a sulphidic hydrothermal vent [101] . Most of these studies represent single measurements at single stations or along transects, likely missing spatial and temporal variability that can be found in such environments. A specific example would be a drastic change in nutrients with the occurrence of a transient plume of HS^- [102], or increased N_2-production through meso-scale eddy events in the Peruvian upwelling system [103]. These events are extremely transient and could therefore elude sampling. Thus, without sampling coverage of such events, we might be overlooking the true variations in rates and pathways of N-cycling in marine anoxic waters, preventing accurate descriptions of marine N-budgets, and overlook important controls on these pathways, such as nutrient availability.

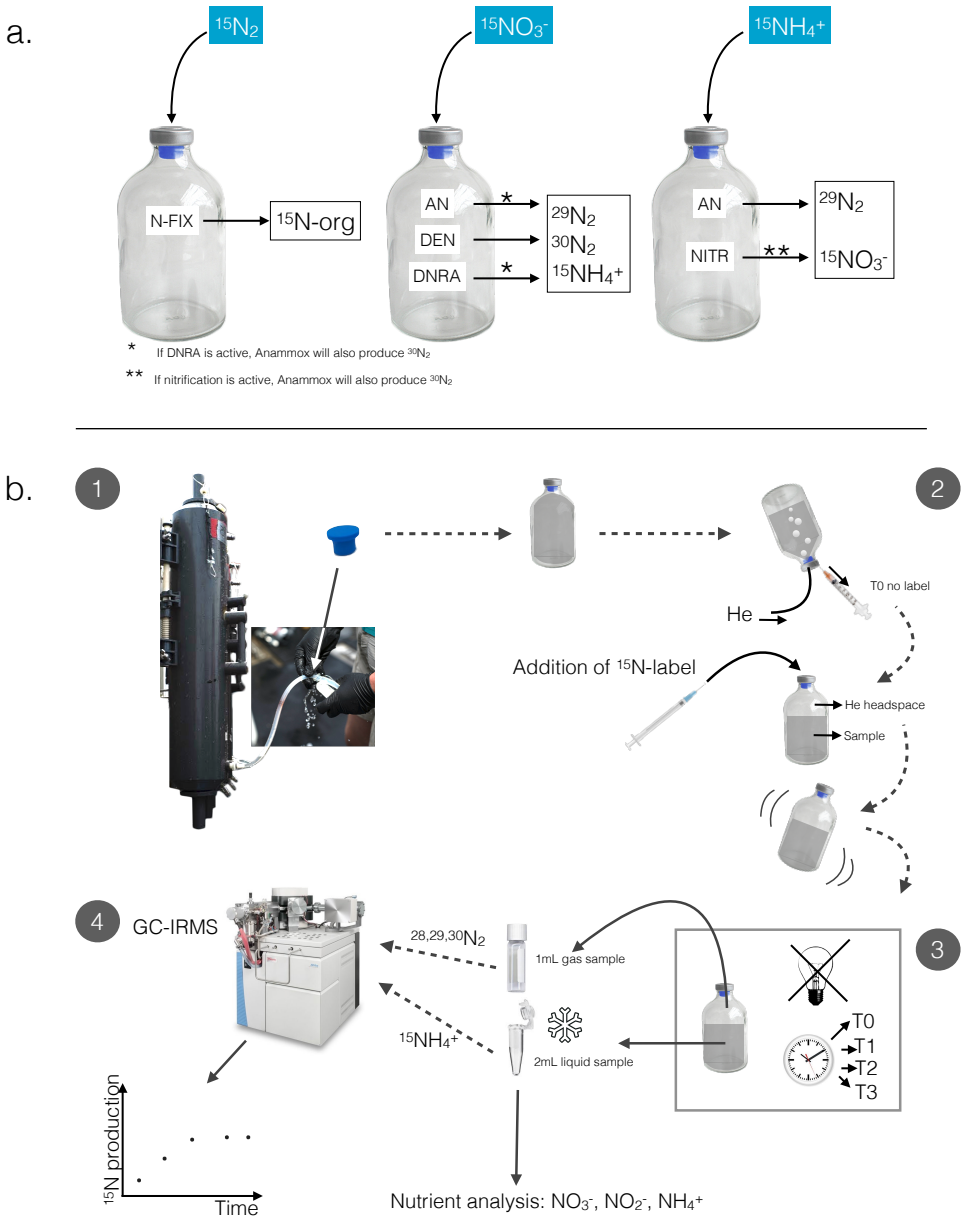

Figure 1.3: *^{15}N-labeling incubations workflow.* (a) shows which active processes of the N-cycle can be measured based on specific addition of ^{15}N-labels. In blue shows the addition of the label. In the serum bottles, the reactions (N-FIX=N-fixation, AN=anammox, DEN=Denitrification, NITR=nitrification) that can be detected by adding the specified labels and in the white outlined box, the products coming from the transformation of the labeled N-species with the processes that will be measured. (b) is a workflow diagram of the incubation experiment. (1) The serum bottle is filled with anoxic water, overflowed 3x and then closed with blue butyl stoppers to limit O_2 contamination. (2) A headspace is added to the serum bottle to further limit O_2 contamination, the 15N-label is added to the sample and the bottle is then shaken for gas species to equilibrate. (3) The samples are incubated in the dark and several time points are taken to follow the course of $15N^2$ production. (4) The production of labeled N-species can be measured by GC-IRMS and the concentration of nutrients can be measured by spectrophotometry.

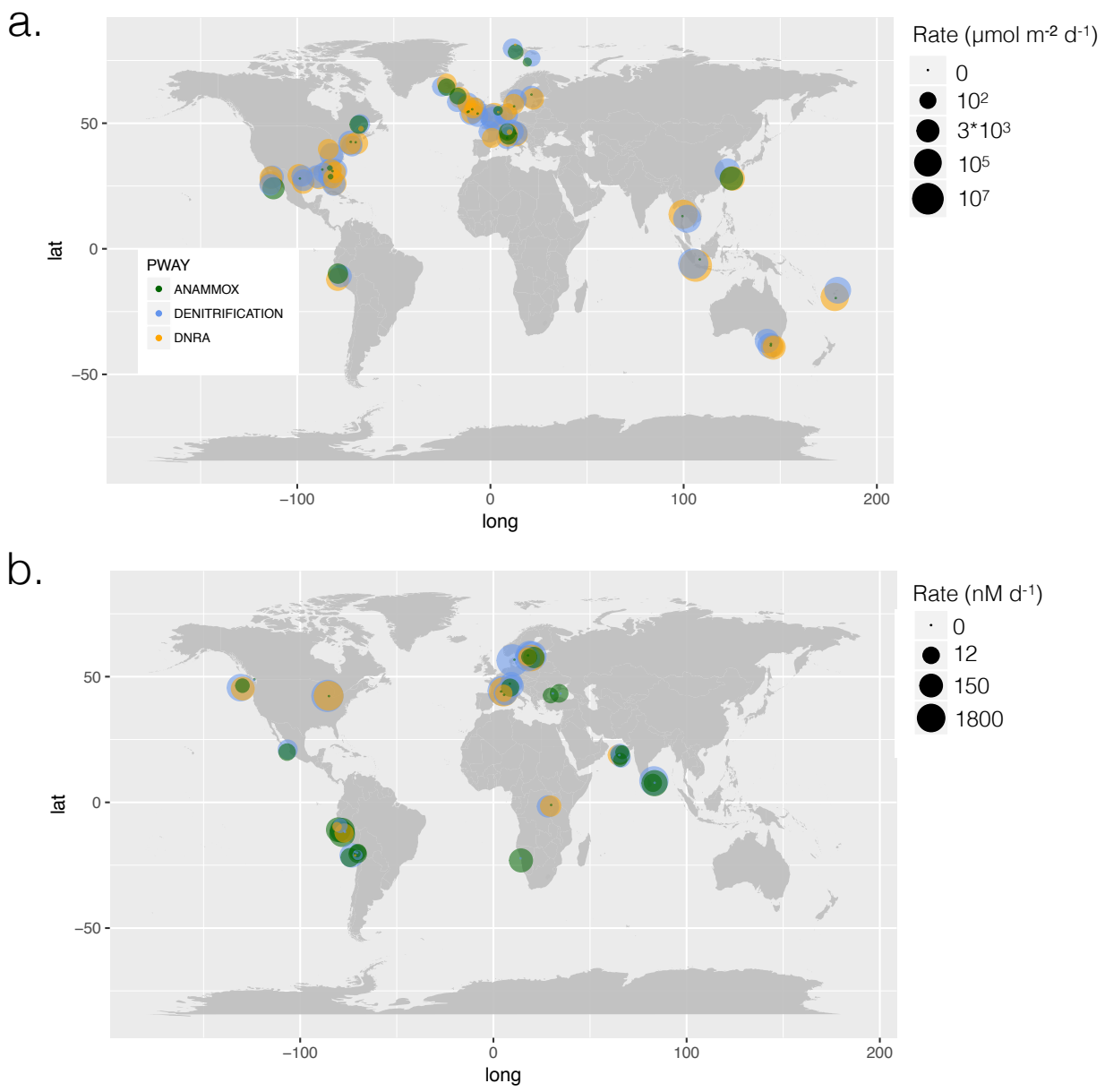

Figure 1.4: *Environmental distribution of anammox, denitrification and DNRA.* (a) Rates of anammox, denitrification and DNRA found in marine and freshwater sediments (in μmol m^{-2} d^{-1}). (b) Pelagic lacustrine and marine rates of DNRA, denitrification, and anammox (in nM d^{-1}). Rate magnitude is described by the black circle on the right of the figure. Anammox is in green, denitrification in blue and DNRA in orange. A dot in the circle indicates that the process was looked for but not detected. No dot or no circle indicates that there was no experiment done to measure this process.

1.4 Controls on anammox, denitrification and DNRA

Most biogeochemical models, when attempting to reproduce the specific rates and pathways of N-cycling, will need constraints on the controls for the different processes described in these models. Metabolic processes are usually controlled primarily by whether or not a reaction is thermodynamically favourable, and can lead to the harnessing of energy and growth for the microorganisms conducting the reaction. For example, it is usually considered that microorganisms will consume first the available electron acceptors that are the most energetic, then consume the next most energetic available acceptors, if their metabolic potential allows it, when the first one is drawn down to inaccessible concentrations [68, 104]. Thus free energy yield calculations for the metabolic reactions will be a first-order determinant on which pathways can occur under specific conditions of the system in a model. Secondly, the metabolic pathways conducted by specific enzymes are limited by how fast these enzymes can process the substrates, depending on the concentrations of these substrates. This is defined by the kinetic features of the enzymes, which can limit the rates of reactions. These parameters can be measured either for lab cultured organisms or for environmental microbial communities, which is non-taxon specific. However, because the kinetic parameters usually vary between the type of enzyme and are also taxon-specific, environmental kinetic parameters are not extensible to other environments, without previous knowledge of the microorganisms involved in the pathways and their individual kinetic traits (or ecophysiological parameter). Beyond thermodynamic and kinetic information, other factors can also control the rates and pathways of N-cycling, such as inhibitors and physical factors (e.g. temperature). These factors further confound attempts at modeling the dynamics in rates and pathways under changing system conditions. Below is summarized the state of the knowledge for the controls on anammox, denitrification and DNRA, and how they are currently used in modeling approaches.

Organisms catalyze redox reactions to harness energy from electron transport that allows them to perform anabolic metabolism for growth and reproduction. The yield obtained from these biochemical reactions is constrained by thermodynamic properties, which dictate how much energy a given reaction yields under specific conditions. This energy can be quantified as the

Gibbs free energy or ΔG° of a reaction and is calculated based on the free energy of formation for the reactants and products involved in the reaction (Eq. 1.2). These are based on standard-state reference conditions, which are rarely found in natural environments. These standard state Gibbs free energies of reaction can be translated from the standard-state reference to any set of environmental conditions by correcting for the activities of the individual products and reactants in the reaction (Q=quotient of products and reagents activities), as well as temperature and pressure (Eq. 1.3).

$$\Delta G^\circ = \Delta G^\circ_{\text{fprod}} - \Delta G^\circ_{\text{freac}} \tag{1.2}$$

$$\Delta G = \Delta G^\circ + RT * ln(\frac{Q_{\text{prod}}}{Q_{\text{reac}}}) \tag{1.3}$$

Using Gibbs free energies it is possible to assess whether a particular biochemical reaction is favorable under a given set of environmental conditions. Negative Gibbs free energies signify exergonic reaction yields, which release energy and can power microbial metabolism. Reactions with positive Gibbs free energies require energy input to occur, whereas Gibbs free energies of 0 signify equilibrium. Because changes in product and reactant concentrations affect the value of the Gibbs free energy of reaction, it follows then that specific metabolisms yield different quantities of energy based on the concentrations of the substrates present. Reaction free energy yield is thus a first order determinant on microbial niche partitioning. This is a particularly relevant consideration for the N-cycle where multiple pathways competing for the same substrates have very different geochemical outcomes. Denitrification, for example, produces N_2 and leads to a return of N to the atmosphere. Whereas DNRA generates NH_4^+ that remains bioavailable or can be sequestered in sediments and ultimately subducted to the mantle. In this case, concentrations of electron donors and acceptors influence which reaction, DNRA or denitrification, is the most energetically favorable. We calculated the free energy yield of the reactions with different organic and inorganic electron donors (ED), as both DNRA and denitrification can be chemolithotrophic or heterotrophic [56, 65, 105–107]. We estimated the free energy yield of the half-reaction for

natural organic compounds as follows:

$$\Delta G_{oxidation} = 60.3 - 28.5 * NOSC \text{ [108]} \tag{1.4}$$

Where NOSC is the nominal oxidation state of carbon, calculated as:

$$NOSC = -(\frac{e^-}{a}) + 4 \text{ [108]} \tag{1.5}$$

for the generic half reaction:

$$C_aH_bN_cO_dP_e + (3a + 4e - d)H_2O$$
$$\Rightarrow aHCO_3^- + cNH_4^+ + ePO_4^{2-} + (5a + b - 4c - 2d + 7e)H^+ + (4a + b - 3c - 2d + 5e)e^- \text{ [108]} \tag{1.6}$$

The results show that DNRA is more competitive with an organic ED than denitrification per mole of NO_3^- reduced, no matter the C/N ratio content of the organic ED studied (Table 1.2 and Fig. 1.5a). Denitrification, however, was more competitive with HS^- as an inorganic ED than DNRA (Fig. 1.5b). In comparison, H_2 as an inorganic ED was more favorable for DNRA when the ratio between H_2 and NO_3^- is high. Fe(II) was favorable for denitrification only at very high ratios as well, and was endergonic for DNRA. Thus, thermodynamics are an effective way to determine whether a reaction will occur or not based on the conditions present in the ecosystem and provide a first-order approach to predicting the outcomes of potential competition between reactions using the same substrate. However, other factors, such as enzyme kinetics and inhibition, growth yield, and viral infection are also important considerations.

Although thermodynamics are useful in determining whether a reaction will occur and how much energy can be harvested out of it, reaction rates also play a role in predicting the outcome of competition. The kinetics of enzymatic reactions can often be described using a Michaelis-Menten model which describes rates as a function of a limiting-substrate concentrations, a half-saturation constant (K_m), which is the concentration of a substrate at half of the maximum rates, and the

Table 1.2: Thermodynamic calculations for denitrification and DNRA with different organic and inorganic ED. We varied the N-content of the organic molecules. The ΔG° for each reaction was calculated based on the second law of thermodynamics.

	Reactions	ΔG° (kJ moles N^{-1})
DNRA/Redfield	$C_{106}H_{263}N_{16}O_{110}P + 53\ NO_3^- + 53\ H_2O + 14\ H^+ \Rightarrow 106\ HCO_3^- + 69\ NH_4^+ + HPO_4^{2-}$	-559.01
DNRA/Redfield -50% N	$C_{106}H_{239}N_8O_{110}P + 53\ NO_3^- + 53\ H_2O + 6\ H^+ \Rightarrow 106\ HCO_3^- + 61\ NH_4^+ + HPO_4^{2-}$	
DNRA/Redfield -75% N	$C_{106}H_{227}N_4O_{110}P + 53\ NO_3^- + 53\ H_2O + 14\ H^+ \Rightarrow 106\ HCO_3^- + 57\ NH_4^+ + HPO_4^{2-} + 2\ H^+$	
DNRA/Redfield +50% N	$C_{106}H_{287}N_{24}O_{110}P + 53\ NO_3^- + 53\ H_2O + 22\ H^+ \Rightarrow 106\ HCO_3^- + 77\ NH_4^+ + HPO_4^{2-}$	
Denitr/Redfield	$C_{106}H_{263}N_{16}O_{110}P + 84.8\ NO_3^- \Rightarrow 106\ HCO_3^- + 16\ NH_4^+ + 42.4\ N_{2(g)} + HPO_4^{2-} + 42.4\ H_2O + 7.2\ H^+$	-524.87
Denitr/Redfield -50% N	$C_{106}H_{239}N_8O_{110}P + 84.8\ NO_3^- \Rightarrow 106\ HCO_3^- + 8\ NH_4^+ + 42.4\ N_{2(g)} + HPO_4^{2-} + 42.4\ H_2O + 15.2\ H^+$	
Denitr/Redfield -75% N	$C_{106}H_{227}N_4O_{110}P + 84.8\ NO_3^- \Rightarrow 106\ HCO_3^- + 4\ NH_4^+ + 42.4\ N_{2(g)} + HPO_4^{2-} + 42.4\ H_2O + 19.2\ H^+$	
Denitr/Redfield +50% N	$C_{106}H_{287}N_{24}O_{110}P + 84.8\ NO_3^- + 0.8\ H^+ \Rightarrow 106\ HCO_3^- + 24\ NH_4^+ + 42.4\ N_{2(g)} + HPO_4^{2-} + 42.4\ H_2O$	
DNRA/ HS^-	$NO_3^- + HS^- + H_2O + H^+ \Rightarrow SO_4^{2-} + NH_4^+$	-487.54
Denitr/ HS^-	$8\ NO_3^- + 5\ HS^- + 3\ H^+ \Rightarrow 5\ SO_4^{2-} + 4\ N_{2\,(g)} + 4\ H_2O$	-480.20
DNRA/ H_2	$NO_3^- + 4\ H_2 + 2\ H^+ \Rightarrow NH_4^+ + 3\ H_2O$	-679.61
Denitr/ H_2	$2\ NO_3^- + 5\ H_2 + 2\ H^+ \Rightarrow N_{2\,(g)} + 6\ H_2O$	-600.24
DNRA/ Fe^{2+}	$NO_3^- + 8\ Fe^{2+} + 21\ H_2O \Rightarrow NH_4^+ + 8\ Fe(OH)_3 + 14\ H^+$	401.99
Denitr/ Fe^{2+}	$NO_3^- + 5\ Fe^{2+} + 12\ H_2O \Rightarrow \frac{1}{2}\ N_{2\,(g)} + 5\ Fe(OH)_3 + 9\ H^+$	75.76

maximum rate of reaction (V_{max}) when the enzyme is substrate-saturated (Eq. 1.7).

$$R_{reaction} = \frac{V_{max} * [S]}{[S] + K_m} \tag{1.7}$$

These kinetic parameters can either be measured in pure culture or in the environment. The latter involves an added layer of complexity, as interactions with the environment and other members of *in situ* microbial communities are likely to influence the rates measured. However, as most microorganisms have not been cultured to date, environmental kinetics are likely to give us the most environmentally relevant information. Unfortunately, only a handful of studies, summarized here for marine settings, have measured these parameters. Half-saturation constants (K_m) are usually reported as apparent substrate dependency constants for environmental studies.

Denitrification, anammox and DNRA compete for NO_3^- and NO_2^- as substrates. Denitrification was shown to have an apparent NO_3^- dependency (or k_m) of 2.9 μM in an anoxic fjord of the Baltic Sea [56]. Contrary to this, another study in the Baltic Sea reported no effect of NO_3^- addition between 1 to 10μM, suggesting high NO_3^- affinity and enzymatic saturation above 1μM [106]. NO_2^- dependency (or k_m) for anammox was reported to be below 3μM [109], and as low as 0.1μM in marine sediments [110]. This finding was supported by a comparison to rates of anammox and

the corresponding ambient NO_2^- concentrations from OMZs, showing no correlation between the two [68]. Thus, it appears that anammox bacteria are likely not limited by NO_2^- concentrations in the environment and may have a higher affinity for NO_2^- than denitrifiers. It is, however, harder to conclude something about NO_3^- and NO_2^- dependency for denitrification, as it has not been tested extensively. Moreover, only one study has tested the NO_3^- dependency of DNRA and this study found no effect of NO_3^- concentration on rates of DNRA [106].

Electron donor (ED) availability appears important in regulating rates of denitrification and DNRA as well, with increasing electron donor concentrations often correlating to high rates [105, 106, 111]. Both denitrification and DNRA have been reported to be either organotrophic (organic ED) or lithotrophic (inorganic ED) processes [56, 65, 105–107]. Addition of different ED can thus help to determine how the N-cycle is coupled with other cycles such as the C-, S- and Fe-cycles. Only denitrification has been shown to depend on organic matter in marine waters [105, 106] and marine sediments [90, 112]. The reactive DOC dependency constant reported for denitrification in marine waters was 0.08 μM [106], and rates of denitrification increased in marine sediments with shallowing depth as well as with increased organic matter loading [90, 112]. Additionally, denitrification has been shown to depend on sulphide in sulphidic environments such as the Mariager fjord in the Baltic sea [56], and other stations in the Baltic Sea chemocline [106], with k_m for HS^- varying between 1.7 and 3.5 μM in the Baltic Sea [106]. A linear dependency was, however, observed in Mariager fjord, suggesting that enzyme saturation was not reached under the concentrations studied (0-50μM HS^- - [56]). DNRA also responded to HS^- amendments in the Baltic Sea and sulphidic sediments [106, 113], with a k_m between 6.8 and 8.6 μM [106]. Finally, DNRA appears to be coupled with Fe(II) oxidation in estuarine sediments with a k_m of 33.8μM [111]. Denitrification, although it was simultaneously detected with DNRA, did not respond to increased Fe(II) concentrations.

NH_4^+ is the ED used in the anammox process, and can also be a limiting substrate for anammox in marine pelagic environments, as NH_4^+ concentrations are very low ($<5\mu$M - [68]). A single measurement of enrichment cultures of *Ca.* Scalindua sp. suggests a k_m for NH_4^+ of 3μM for anammox bacteria [109]. A collection of rates of anammox compared to ambient NH_4^+ concentrations in OMZs reveals a positive correlation between the two, implying that the supply

rate or concentration of NH_4^+ in seawater can regulate rates of anammox in OMZs [68]. A positive correlation can also be found between rates of anammox and organic matter concentrations [105]. Indeed, when organic matter is remineralized through heterotrophic processes, such as denitrification under low oxygen conditions, NH_4^+ is released and available to be used by anammox. Hence, it has been argued that organic matter stoichiometry controls N-loss in open ocean OMZs, constraining the amount of NH_4^+ released during respiration and its supply rate to anammox [105]. In addition to the stoichiometry of organic matter, it has been argued that organic matter concentrations could regulate the partitioning of N-loss between anammox and denitrification in marine sediments [83, 90]. However, organic matter quality and quantity cannot always explain the partitioning between denitrification and anammox as other processes can also be active, such as sulphate reduction, organotrophic or sulphide-dependent DNRA, and sulphide-dependent denitrification making the deciphering of the different interactions complex. Therefore, other factors, such as inhibitors, could be at play in regulating rates of anammox, denitrification and DNRA, in addition to substrate availability.

Oxygen also regulates and sometimes inhibits the occurrence of anammox, denitrification, and DNRA at different levels. It has been shown that anammox proceeds at O_2 concentrations up to 13.5μM [114], whereas denitrification proceeds at concentrations up to 20μM [115]. It has also been reported that rates of DNRA in sediments increased with increasing concentrations of O_2 in overlying estuarine waters [96]. Similarly, nitrification was shown to have a very high affinity for oxygen, rendering the operation of nitrification possible under very low oxygen concentrations (k_m = 0.3 to 0.8 μM) [116]. This is generally unexpected and could indicate that many canonically anaerobic metabolisms operate under mildly oxygenated conditions, whereas some canonically aerobic metabolisms proceed at vanishingly low oxygen blurring the lines between geochemical conditions and the corresponding energy driven metabolic cascade.

Other factors also likely contributed to the regulation of anammox, denitrification and DNRA and their absolute and relative rates. For example, HS^- appears to inhibit anammox with thresholds as low as 1.5μM HS^- [114]. Temperature was tested as another factor influencing rates of anammox and denitrification with the highest rates between 15 and 35°C for both processes [110]. Salinity was also shown to influence certain processes such as DNRA and denitrification in

a oligohaline estuary, with higher salinity corresponding to high rates of DNRA and low rates of denitrification [117] Both temperature and salinity are likely to influence the physiology of the microorganisms responsible and thus should also be considered as important regulating factors of N-cycling.

Overall, we need to expand the current knowledge about how substrate availability and the presence of potential inhibitors control DNRA, anammox and denitrification across environments. Only a few studies, described above, have explored the kinetics of anammox, DNRA and denitrification, and a consensus has not always been found for these processes (i.e. HS^- for denitrification or NO_3^- for DNRA), leaving kinetics for these processes poorly constrained. Further, it is essential to link the environmental kinetic information with the individual microbial taxa associated with N-cycling in order to construct ecophysiologically-constrained biogeochemical models associated with specific community compositions, such as gene-centric modeling approaches [118, 119]. Indeed, if these microbial taxa are found more broadly, this ecophysiological information can be extensible to other environments and used to constrain modeling efforts globally.

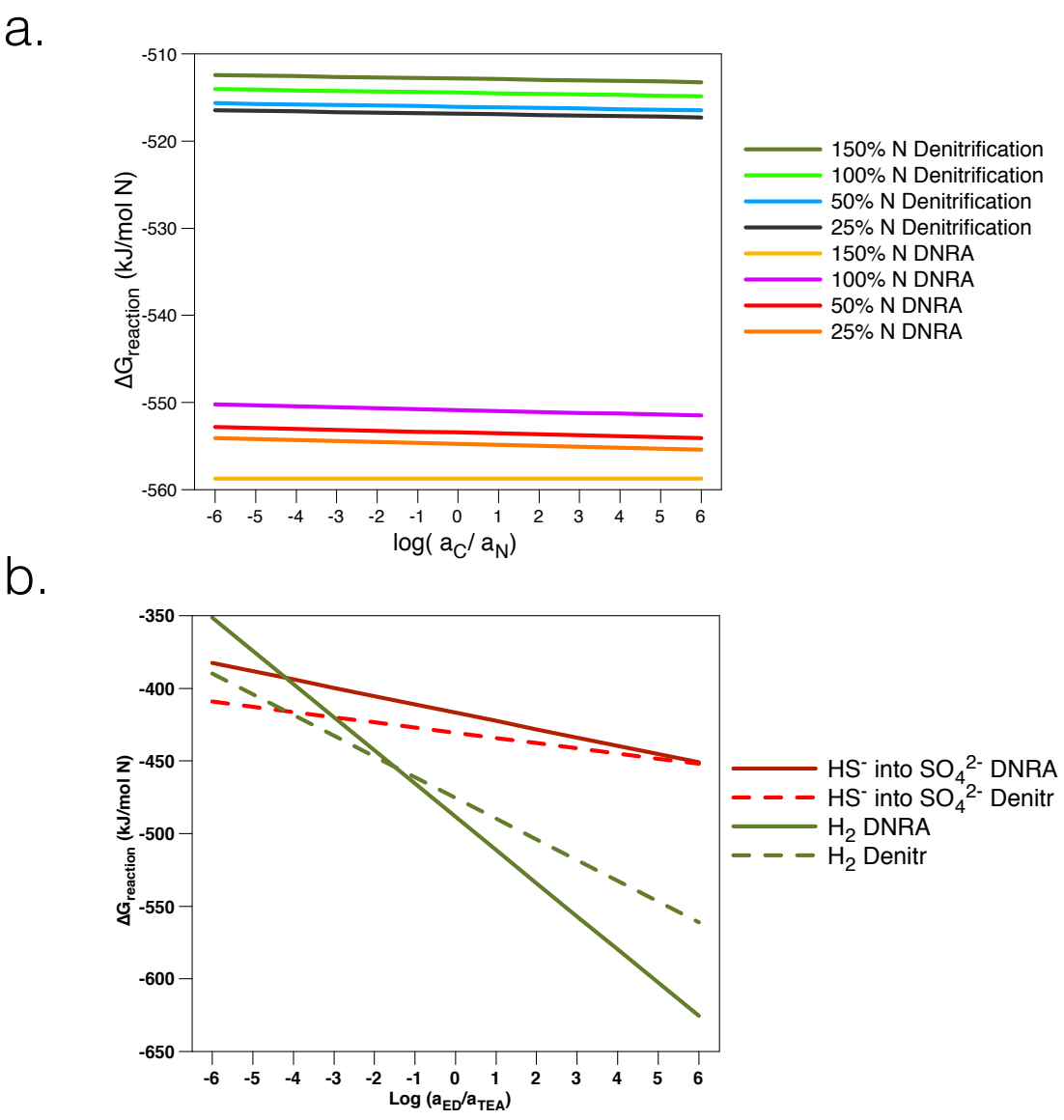

Figure 1.5: *$\Delta G_{reaction}$ in function of the logarithm of the activity (a) of the ED divided by the activity of the electron acceptor (NO_3^-)* a) With organic ED and varied N-content b) With inorganic electron donors, HS^- and H_2

1.5 Distributed metabolisms and the N-cycle

The N-cycle is composed of a set of reactions performed (Fig. 1.1) by a wide array of microorganisms (Fig. 1.2). The study of the genes and enzymes involved in the N-cycle is complex, as several enzymes are sometimes capable of catalyzing the same reaction and the diversity of the microorganisms involved is broad. Most studies investigating microbial communties in the environment often offer an overview of the entire community, without deciphering which taxa are potentially involved in specific pathways (for example: [120]). Investigating which taxa are involded in the metabolic pathways of N-cycling, however, would facilitate the determination of ecophysiological information, and thus improve the specificity of models for N-cycling. Furthermore, knowing which taxa are involved will make this information generally extensible to other environments where pathways of N-cycling are supported by similar key-players. Such studies have started to emerge, however, thanks to the advances in high-throughput sequencing and computing power. For example, Hawley et al. (2014)[33] describe the key-players involved in N-cycling for an anoxic fjord (Saanich Inlet, BC, Canada) based on meta'omic data (Fig. 1.2c) –metagenomic, metatranscriptomics and proteomics; this conceptual model highlighted the involvment of SUP05 as a main player in partial denitrification, *Ca.* Scalindua (from the Planctomycetes phylum) as the key-player for the anammox pathway, and finally the archaea Thaumarchaeota and bacteria Nitrospira sp.were implicated in nitrification. The information generated for the inlet is generally extensible to OMZs as the same taxa can be found in OMZs as well (e.g. [18, 121]), and thus, if rates and pathways of N-cycling are measured in the inlet, they can also be compared to rates measured in other low oxygen zones with the same supporting microbial populations. Thus, Saanich Inlet can be considered as a model ecosystem for the metabolic activities found in OMZs. In this section, we highlight more generally the main genes and enzymes reported in the literature for N-fixation, nitrification, denitrification, DNRA and anammox.

N-fixation is carried out by the enzyme nitrogenase. Three versions of nitrogenase exist, requiring different metal-cofactors such as Molybdenum (Mo), Iron (Fe) and Vanadium (Va) [122]. There are thus 3 different genes of interest: *nif*, *anf* and *vnf*, requiring one of the three different co-factors, respectively (Fig. 1.1 and table 1.3). In the modern ocean and in terrestrial settings,

Table 1.3: Main genes and enzymes involved in the N-cycle, based on Kuypers et al. (2018) [3] and references therein. The subunits for the genes are not specified here.

Gene abbr.	Enzyme	Processes associated	Reaction
nif	Mo-Nitrogenase	N-fixation	$N_2 + 8e^- + 8H^+ + 6ATP \Rightarrow 2NH_3 + H_2 + 16ADP + 16P_i$
anf	Va-Nitrogenase	N-fixation	See above
vnf	Fe-Nitrogenase	N-fixation	See above
amo	Ammonia monooxygenase	Nitrification	$NH_4^+ + O_2 + 2e^- + H^+ \Rightarrow NH_2OH + H_2O$
hao	Hydroxylamine oxidoreductase	Nitrification	$NH_2OH \Rightarrow NO + 3e^- + 3H^+$
nxr	Nitrite oxidoreductase	Nitrification	$NO_2^- + H_2O \Rightarrow NO_3^- + 2e^- + 2H^+$
nar/nap	Cytoplasmic/ Periplasmic Nitrate reductase	DNRN	$NO_3^- + 2e^- + 2H^+ \Rightarrow NO_2^- + H_2O$
*nir**	*Cu-Nitrite reductase	Denitrification/PDNO/Anammox?	$NO_2^- + e^- + 2H^+ \Rightarrow NO + H_2O$
*nir***	**Assimilatory nitrite reductase	Fermentative DNRA	$NO_2^- + 6e^- + 8H^+ \Rightarrow NH_4^+ + 2\ H_2O$
nor	Nitric oxide reductase	Denitrification/PDNO	$2\ NO + 2e^- + 2H^+ \Rightarrow N_2\ O + H_2O$
nos	Nitrous oxide reductase	Complete denitrification	$N_2O + 2e^- + 2H^+ \Rightarrow N_2 + H_2O$
nrf	NADH-dependent nitrite reductase	DNRA	$NO_2^- + 6e^- + 8H^+ \Rightarrow NH_4^+ + 2\ H_2O$
hzs	Hydrazine synthase	Anammox	$NO + NH_4^+ + 3e^- + 2H^+ \Rightarrow N_2H4 + H_2O$
hzo/hdh	Hydrazine oxidoreductase or hydrazine dehydrogenase	Anammox	$N_2H4 \Rightarrow N_2 + 4e^- + 4H^+$
otr	Octaheme tetrathionate reductase	DNRA?	$NO_2^- + 6e^- + 8H^+ \Rightarrow NH_4^+ + 2\ H_2O$
onr	Octaheme nitrite reductase	DNRA?	$NO_2^- + 6e^- + 8H^+ \Rightarrow NH_4^+ + 2\ H_2O$

Fe and Mo are often scarce, respectively, and is therefore a source of limitation for N-fixation [123]. Further, nitrogenases operate under anoxic conditions [124]. Therefore, microorganisms evolved mechanisms to protect the enzyme from oxygen with, for example, spatial separation of oxygenic photosynthesis and N-fixation in a nitrogenase-containing heterocyst or temporal separation of both processes [124]. Nitrogenases likely evolved during the early proliferation of life on Earth when N became limiting, and this is supported by the fact that it contains oxygen-sensitive co-factors that would have been widely available in the anoxic oceans of the Precambrian and thus became distributed across prokaryotes [30, 31] . Indeed, both archaea and bacteria possess the ability to fix N. The genes for N-fixation have been found in both photosynthetic and non-photosynthetic organisms, such as *Trichodesmium* spp. [124], UCYN-A in the oceans [125] and members of the Planctomycetes and Proteobacteria phyla [126], as well as members of the Rhizobiales order in terrestrial settings [127]. In particular, the nif gene was found in 189 different taxa [128]. These microorganisms sometimes live in symbiosis with eukaryotes, providing the N necessary for their growth.

Nitrification has historically been divided in to a two-step reaction (Fig. 1.1), with phyloge-

netically separated microorganisms performing the distinct steps of the process. The first step involves the oxidation of NH_4^+ to hydroxylamine with ammonium oxidase enzyme (AMO), a reaction that is endergonic (Table 1.3) [129]. The energy is then conserved through the oxidation of hydroxylamine to NO or directly to NO_2^- using the octaheme hydroxylamine oxidoreductase (HAO) (Table 1.3). This step is conducted by either so-called ammonium-oxidizing bacteria (AOB), such as Beta- and Gammaproteobacteria, Nitrosomas, or Nitrospira, or by ammonium oxidizing archaea (AOA) such as Thaumarcheaota [130], although the gene for the archaeal *hao* remains elusive, to date [131]. A recent discovery, however, showed that a Nitrospira sp. possess all the genes necessary for the whole reaction and is able to perform the entire nitrification process [132]. This complete nitrification was dubbed Comammox for complete ammonia oxidation [132]. This discovery confirms previous hypotheses based on the complete energetic yield (ΔG° = -349kJ $(\text{mol}\, NH_4^+)^{-1}$) which is greater than performing the 2 steps separately (ΔG° = -275kJ $(\text{mol}\, NH_4^+)^{-1}$ and ΔG° = -74kJ $(\text{mol}\, NO_2^-)^{-1}$). The second step of nitrification, NO_2^- oxidation of NO_3^-, is conducted using the enzyme nitrite oxidoreductase (NXR) (Table 1.3) [133]. This enzyme can be found across bacterial phyla, with members in Alpha-, Beta-, Gammaproteobacteria, Chloroflexi, Nitrospinae and Nitrospirae, in anoxygenic photosynthetic organisms such as *Thioploca* sp. KS1 and in anammox bacteria (Kuypers et al. (2018) [3] and references therein).

Similar to nitrification, denitrification is a multi-step reaction and it is usually distributed across multiple phylogenetic groups, although certain microorganisms possess the suite of enzymes needed to perform the entire process. NO_3^- reduction to NO_2^- is performed under low oxygen conditions where NO_3^- is available, with either a periplasmic or membrane-bound enzyme (NAP or NAR Fig. 1.1 and Table 1.3) [134]. Many organisms perform only this step, such as the members of the SAR11 clade, microorganisms that comprise up to half of the total microbial cells found in oxic marine waters and seem also to be ecologically relevant in OMZs [135]. For other microorganisms, like *Parococcus denitrificans* and *Beggiatoa* sp., this first step is followed by further reactions including NO_2^- reduction to NO, N_2O, or N_2, or to NH_4^+ [134, 136]. NO_2^- reduction to NO is conducted via nitrite reductases (NIR) that can either be heme-containing or Cu-containing enzymes [137]. The genes coding for these enzymes (*nirK* and *nirS*) are usually used as marker genes for canonical denitrifiers. However, they are present in many other organisms, and are

widespread in bacteria and archaea [138]. Nitric oxide reductase, an enzyme that catalyzes the reduction of NO to N_2O, refers to a suite of enzymes, from flavoproteins to haem copper-oxidases (NOR), that are distributed throughout the tree of life [3]. The enzymes are used either for detoxification of NO or for respiration and have special environmental relevance, as they are responsible for the production of the greenhouse gas N_2O. The final step for complete denitrification involves two versions of nitrous oxide reductases (NOS), one typical and another called atypical found in soil bacteria [139]. Generally, the genes coding for the enzymes were found in diverse bacterial phyla such as members of the Proteobacteria, Bacteroidetes and Chlorobi, as well as archaeal phyla such as Crenarcheota and Halobacteria [3]. As denitrification is a multistep reaction, with each step distributed across multiple diverse taxa, the interactions between these different taxa can control the balance between sources and sinks of N_2O in the environment.

Dissimilatory nitrite reduction to ammonium (DNRA) is a fermentative or respiratory pathway that uses either a cytoplasmic nitrite reductase (NIR) [140] or a periplasmic cytochrome c nitrite reductase (NRF) [141], respectively. The latter enzyme is the most studied and the most used as a marker gene for DNRA [141]. It has also been hypothesized that DNRA might also be conducted by octaheme nitrite reductase (ONR) or the octaheme tetrathionate reductase (OTR). Indeed, these two enzymes (ONR and OTR) have been shown to be closely related to the cytochrome c nitrite reductase as it has a similar active sites [142]. Hydroxylamine appears to be produced as an intermediate of the reaction when catalyzed by the cytochrome c enzyme, however, it does not accumulate [143]. This process can be carried out by most bacterial lineages (e.g. Bacteroidetes, Firmicutes, Proteobacteria, Planctomycetes - [144]), some archaea, diatoms and fungi, making this reaction widespread, phylogenetically [3].

The anammox reaction is biochemically challenging to conduct as it produces hydrazine (N_2H_4-rocket fuel) as an intermediate [61]. This intermediate molecule needs to be contained as it can be highly reactive and toxic. Anammox bacteria have thus evolved a specialized intracytoplasmic compartment called the anammoxosome in order to enclose hydrazine [61, 145]. Due to this highly specific function, anammox appears to be confined to bacteria from 5 generas of the phylum Planctomycetes [61, 62]. Three enzymes are involved in the multiple step reaction. An unknown nitrite reductase (NIR) transforms NO_2^- to NO, similar to the enzyme in denitrification [146].

Then, a hydrazine synthase (HZS) combines NO and NH_4^+ into hydrazine [147]. Hydrazine is subsequently transformed to N_2 using hydrazine dehydrogenase (HDH or HZO) [148]. Thus, anammox is a very specialized process with the use of hydrazine as an intermediate, and the confinement of this process to one phylum only is highly uncommon in the N-cycle.

Metabolic reactions of the N-cycle are widely distributed across the 3 domains and across multiple phyla in each domain. Mainly, microorganisms involved in the N-cycle seem to have developed specific niches and have crafted complex interactions between functional metabolic groups in order to recycle N. Despite the complexity of the N-cycle apparent from existing knowledge, the true complexity may be much greater given that most of this knowledge comes from lab cultures, whereas the vast majority of microbial diversity remains uncultivated [3]. It is thus likely that we are missing much of the metabolic and taxonomic diversity connected to the N-cycle, and there is appreciable scope for the discovery of novel taxa, and perhaps genes and enzymes that catalyze N-species transformations.

1.6 Problem statement

Models of N-cycling fall short of making robust and explicit predictions of future N-cycling or reconstructions of the past. This is, in part, due to lack of constraints on the factors that regulate the partitioning between denitrification, anammox and DNRA, as well as a lack of information on the ecophysiology describing the relevant microorganisms. Indeed, with a small fraction of microorganisms cultured to date, model parameters are mostly set with information from lab cultures with limited extensibility to the environment. Direct ecophysiological information comes through process rate measurements, yet these generally lack coupled information on microbial community composition, thereby limiting their extensibility across multiple environments. Furthermore, information from key environments, like those with ferruginous conditions similar to the Precambrian oceans, is almost entirely lacking. Quantitative information on dynamics of rates and pathways of N-cycling that is accompanied by relevant information on microbial community dynamics and ecophysiologies is thus needed across diverse environments to improve reconstructions of the N-cycle in the past and make better predictions of the N-cycle in the future.

1.7 Dissertation overview

The overall goal of my thesis is to generate new information on the rates and pathways of N-cycling under low-oxygen conditions that can be used to improve models of once and future N-cycling. More specifically I aim to determine:

i the rates and pathways of pelagic N-cycling under ferruginous conditions extensible to the Precambrian oceans.

I also aim to:

ii quantitavely describe rates and pathways of N-cycling in modern anoxic marine environments and:

iii investigate dynamics in the microbial community structure and their metabolic potential that are relevant to N-cycling

This information will be incorporated into:

iv quantitative models that will enable reconstructions of past N-cycling and reproduction of rates and pathways of modern N-cycling.

These aims are achieved in the following chapters:

Chapter 2: Iron-dependent nitrogen cycling in a ferruginous lake and the nutrient status of Proterozoic oceans

This chapter elucidates (i) the rates and pathways of Fe-dependent NO_3^- reduction in a ferruginous pelagic environment. It then takes the *in-situ* process rates measurements and (iv) integrates these results in a box-model for the Proterozoic oceans to study how these processes impact cycling of N and biological productivity during the Proterozoic Eon.

Chapter 3: Rates and pathways of N_2 production in sulphidic Saanich Inlet

Chapter 3 presents a detailed investigation of (ii) the environmental factors that influence the partitioning of N-loss between anammox and denitrification for an anoxic and sulphidic fjord, Saanich Inlet (BC), with a year-long time-series of process rate measurements. (iv) A kinetic model was also built to study the competition between anammox and complete denitrification for NO_2^- based on the rates obtained in the study. Finally, (iii) the vertical and temporal changes in microbial community composition were shown to confirm the conceptual model of distributed metabolism in SI previously built in Hawley et al. 2014.

Chapter 4: Combining microbiological and geochemical information to constrain energy flow through the marine N-cycle

In chapter 4, I further address the partitioning of N-cycling through anammox, denitrification and DNRA in an anoxic fjord (Saanich Inlet, BC), and link the dynamics in anaerobic N-metabolisms to renewal in the inlet. We show that higher energy fluxes are coupled with higher rates of DNRA and with changes to the microbial community structure and metabolic potential. I thus combined here (ii) process rate measurements and (iii) metagenomic analysis of the microbial community composition and structure, as well as metabolic potential, in order to study the changes in substrate supply rates in SI and the associated changes in the microbial communities and their metabolic activities.

Chapter 5: Conclusions

This chapter addresses the current and future challenges to the study of the N-cycle and the distribution of the metabolisms involved, as well as to the integration of the newly produced knowledge into informative and quantitative models for the past and future N-cycle.

Chapter 2

Iron-dependent nitrogen cycling in a ferruginous lake and the nutrient status of Proterozoic oceans

Nitrogen limitation during the Proterozoic has been inferred from the great expanse of ocean anoxia under low-O_2 atmospheres, which could have promoted NO_3^- reduction to N_2 and fixed N loss from the ocean. The deep oceans were Fe rich (ferruginous) during much of this time, yet the dynamics of N cycling under such conditions remain entirely conceptual, as analogue environments are rare today. Here we use incubation experiments to show that a modern ferruginous basin, Kabuno Bay in East Africa, supports high rates of NO_3^- reduction. Although 60% of this NO_3^- is reduced to N_2 through canonical denitrification, a large fraction (40%) is reduced to NH_4^+, leading to N retention rather than loss. We also find that NO_3^- reduction is Fe dependent, demonstrating that such reactions occur in natural ferruginous water columns. Numerical modelling of ferruginous upwelling systems, informed by our results from Kabuno Bay, demonstrates that NO_3^- reduction to NH_4^+ could have enhanced biological production, fuelling sulfate reduction and the development of mid-water euxinia overlying ferruginous deep oceans. This reduction to NH_4^+ could also have partly offset a negative feedback on biological production that accompanies oxygenation of the surface ocean. Our results indicate that N loss in ferruginous upwelling systems may not have kept pace with global N fixation at marine phosphorous concentrations (0.04–0.13 μM) indicated by the rock record. We therefore suggest that global marine biological production under ferruginous ocean conditions in the Proterozoic eon may thus have been P not N limited.

2.1 Introduction

As an element essential to life, nitrogen (N) often limits biological production [19]. N is made available to life through microbial fixation of atmospheric N_2. This N is liberated as NH_4^+ from decaying biomass, and oxidized to NO_3^- in the presence of oxygen. N is returned to the atmosphere through NO_3^- reduction to N_2 under low O_2 conditions. Two microbial processes are responsible for N_2 production; denitrification, which reduces NO_3^- through a series of intermediates to N_2, and anammox, which forms N_2 by directly coupling NO_2 with NH_4^+. Organisms responsible for denitrification and anammox proliferate in O_2 minimum zones (OMZs) of the modern oceans, which support 20-40% of global fixed N loss to the atmosphere [63].

Under the well-oxygenated modern atmosphere, OMZs ($O_2 < 20\mu$M) comprise 7% by volume of the global ocean [149], and their anoxic cores, which sustain most fixed N loss, occupy only 0.1% [63]. During the Proterozoic eon, however, atmospheric O_2 levels were lower than today and vast regions of the ocean were anoxic [45]. Loss of fixed N is predicted under ocean anoxia and such expansive anoxia could have led to extreme N limitation [39]. N isotope distributions from Palaeoproterozoic upwelling systems, however, imply relatively little fixed N loss [42]. This suggests either modest rates of denitrification or N retention, possibly through reduction of NO_3^- to NH_4^+ [42]. Notably, anoxia and a supply of NO_3^- will not support fixed N loss without electron donors to drive denitrification, or NH_4^+ to support anammox. In the modern ocean, denitrification is fuelled through both organic electron donors and H_2S [18, 60]. Organic electron donors may have been scarce under the generally low productivity of Proterozoic oceans [39], and H_2S would have been scarce except during episodic euxinic periods that punctuate the Proterozoic geologic record [42, 47–49, 55]. Ferruginous conditions were much more prevalent than euxinia, dominating ocean chemistry throughout the Proterozoic [150]. Ferrous Fe (Fe(II)) is known to support NO_3^- reduction in laboratory experiments [58, 59] but the environmental operation, significance and pathways of Fe-dependent NO_3^- reduction remain untested in natural ferruginous water columns.

2.2 Methods

Physico-chemical parameters as well as ^{15}N-labelled incubations were performed during a sampling expedition to Kabuno Bay (Lake Kivu, East Africa – 1.58°to 1.70°S, 29.01°to 29.09°E) in February 2012. *In situ* vertical conductivity - temperature - depth (CTD) profiles were collected via two multi-parameter probes (Hydrolab DS5, OTT Hydromet; and Sea&Sun CTD90, Sea and Sun Technology). NO_2^- and NH_4^+ concentrations were measured spectrophotometrically [151]. Additionally, NO_3^- concentrations were determined by subtracting NO_2^- from the NOx (NO_3^- and NO_2^-) measurements (via chemiluminescence [152]). Fe speciation was measured according to Viollier et al. 2000 [153]. H_2S and SO_4^{2-} concentrations were determined using the Cline method [151] and ion chromatography (Dionex), respectively. ^{15}N-labelled incubations were performed in duplicate in 12ml Exetainers, allowing water to be incubated under anoxic conditions. Microbial activity was arrested with $ZnCl_2$ at several time points for each experiment. The $^{15}N-N_2$ and $^{15}N-NH_4^+$ produced was quantified with isotopic ratio mass spectrometry. Rates of DNRA, denitrification and anammox were determined according to Thamdrup et al. 2006 [154]. Rates were calculated on the basis of linear regressions with the least-squares method over the most linear data intervals (24 or 48h). The structure of the box model set-up here is the same as that developed in Canfield et al. 2006 [5] and adapted for the Proterozoic eon in Boyle et al. 2013 [44]. Details on model parameters can be found in Appendix B.

2.3 Results and discussion

Kabuno Bay (KB) is a ferruginous sub-basin of Lake Kivu, which straddles the border of Rwanda and the Democratic Republic of Congo, East Africa [50]. Saline springs feed KB causing permanent stratification, anoxia below 10m (Fig. 2.1 a and b), and Fe(II)-rich deep waters (500 μM – Fig. 2.1d). Such ferruginous conditions are analogous to those that prevailed through much of the Proterozoic eon [50]. A strong gradient of NH_4^+ between 10 and 11.5m depth (Fig. 2.1c) indicates high rates of NH_4^+ oxidation to NO_3^- and NO_2 within this depth interval. Since KB's oxic surface waters are devoid of NO_3^- and NO_2^- (concentrations$<1\mu$M), NO_3^- and NO_2 produced through NH_4^+ oxidation are advected to the main basin, assimilated, or rapidly reduced.

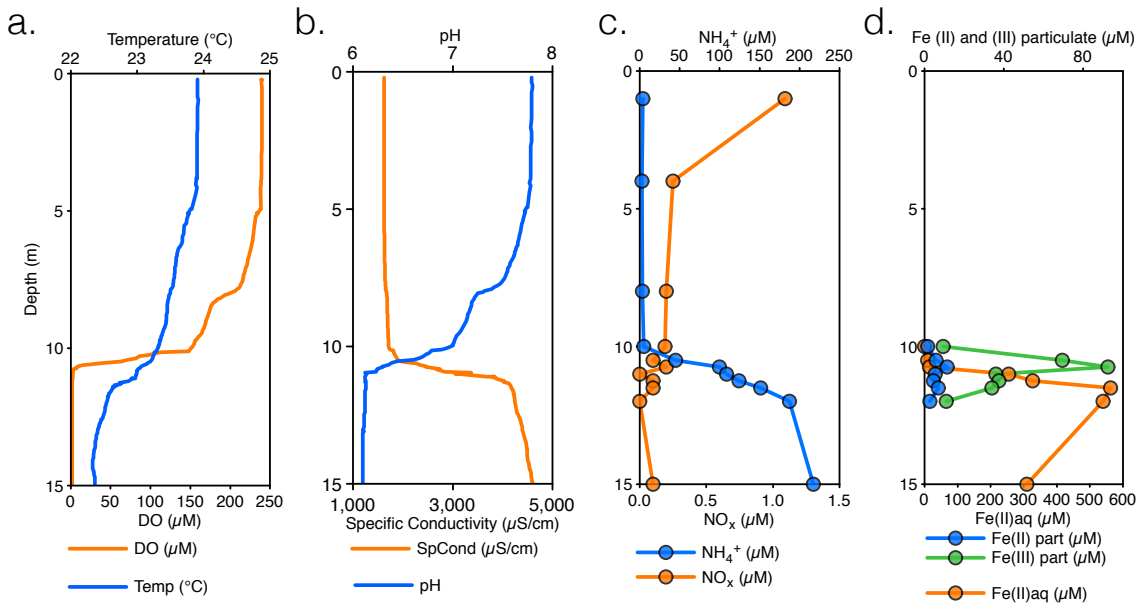

Figure 2.1: *Vertical distribution of selected physical and chemical properties of Kabuno Bay for February 2012.* a) Dissolved O_2 (DO) concentration (μM) and temperature (°C). b) pH and specific conductivity (SpCond, μS cm^{-1}). c) NH_4^+ and NOx concentration (μM). d) Fe(II)aq, Fe(II)part and Fe(III)part concentrations (μM)

We determined rates and pathways of microbial N transfomations in KB using incubations with ^{15}N-labelled NO_3^-. Both denitrification and dissimilatory nitrate reduction to ammonium (DNRA) occur between 11 and 11.5 m, but anammox was below our limit of detection (6nmol N l^{-1} d^{-1}). Rates of denitrification and DNRA were up to 80 $\pm$ 10 and 50 $\pm$ 10nmol N l^{-1} d^{-1}, respectively (Fig. 2.2a,b and Fig. B.3), exceeding those typically found in marine OMZs [60, 67] but similar to coastal marine anoxic basins such as the Baltic Sea [56]. While 60% of NO_3^- reduced is lost from the KB through denitrification, 40% is retained as NH_4^+ through DNRA. Substantial NO_3^- recycling to NH_4^+ has also been periodically observed in the Peruvian and Omani OMZs [65, 67], but such a high fraction appears to be unusual for modern pelagic marine environments [60, 98]. Our observations imply that some biogeochemical feature of KB favours DNRA compared with other environments studied to date. Fe(II), which is unusually abundant in KB, indeed promotes DNRA in estuarine sediments [155], and may also do so in KB.

To test for such Fe dependency, we amended a subset of our ^{15}N incubations with 40 μM Fe(II). We found that Fe(II) addition considerably enhanced both denitrification and DNRA to 230 $\pm$ 40

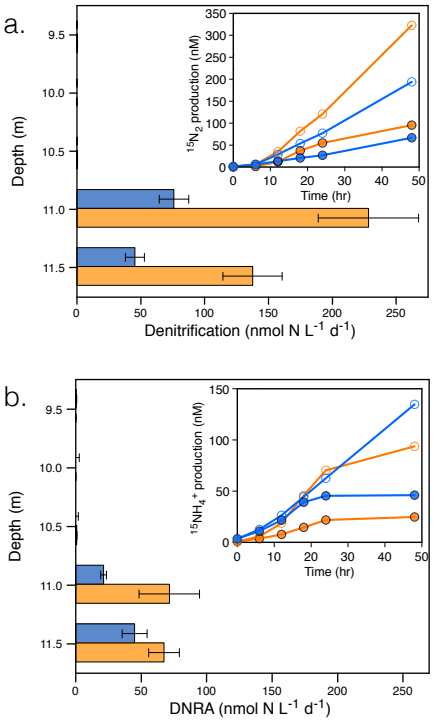

Figure 2.2: *Rates and pathways in Kabuno Bay for February 2012* a&b Denitrification (a) and DNRA (b) in Kabuno Bay water column. Samples were collected in February 2012, with (in orange) or without (in blue) addition of the electron donor Fe(II) to the incubations. Insets show time-course evolution of 15N-labelled metabolic products. Rates were calculated on the basis of linear regressions over the linear data intervals (24 or 48h). Table B.3 contains the detailed rates and associated errors. The error on the rate is the standard error of the slope for the linear regression.

and 70 $\pm$ 20nmol N l^{-1} d^{-1}, respectively (Fig. 2.2a,b and Table B.3), suggesting a role for Fe(II) in NO_3^- reduction. Our results support measurements from estuarine sediments, which invoke microbial mediation [155], but the nearly equivalent stimulation between both NO_3^- reduction to NH_4^+ and denitrification provides no evidence that Fe(II) favours DNRA and instead may indicate that Fe(II) enhances the reduction of an intermediate (for example, NO_2^-) common to both reactions.Thermodynamic considerations reveal that reduction of NO_3^-, and a number of intermediate N species, by Fe(II) is energetically favourable in KB (see Appendix B) yielding sufficient free energy for microbial growth. While the precise pathway remains unresolved, Fe(II) clearly plays a role in NO_3^- reduction in KB.

To assess the biogeochemical role of Fe-dependent NO_3^- reduction in KB, we compared rates

of NO_3^- reduction with other key processes [50]. While Fe(II) supports NO_3^- reduction, the corresponding Fe(II) oxidation rates of 1,700nmol Fe l^{-1} d^{-1} (based on stoichiometry) are only a minor fraction (1%) of the observed phototrophic Fe(II) oxidation in the KB chemocline [50]. By comparison, NO_3^- reduction rates are an order of magnitude lower than SO_4^{2-} reduction rates, which are up to 410nmol S l^{-1} d^{-1} [50]. We also compared rates of NO_3^- reduction with dark carbon fixation, and on the basis of growth yields for chemoautotrophic NO_3^- reduction (see Appendix B), this comparison suggests that NO_3^--driven chemoautotrophy could support up to 2% of the total dark carbon fixation in KB's water column [50]. The overall contribution of NO_3^- reduction to biogeochemical cycling, therefore, is largely to regulate recycling and loss of fixed N from KB, and here, the partitioning of NO_3^- reduction between DNRA and denitrification is key.

We have shown that NO_3^- reduction both to N_2 and NH_4^+ takes place at relatively high rates under ferruginous conditions, and further, that this NO_3^- reduction is partly coupled to the oxidation of Fe(II). By extension, the ferruginous oceans of the Proterozoic eon could also have supported large-scale NO_3^- reduction, possibly through both denitrification and DNRA, and with Fe(II) as the electron donor [39, 156]. To quantitatively link our observations in KB to possible biogeochemical cycling under ancient marine ferruginous conditions, we set up a box model for N cycling in ocean upwelling systems [44, 156]. Our model describes mass balances for C, N, S, O and Fe species and their biogeochemical reactions (see Fig. 2.3a and full description in Appendix B). NH_4^+ and Fe were supplied through upwelling, and these, along with nutrient recycling, ultimately controlled primary production in the overlying surface waters. Production in the surface waters is sustained exclusively through upwelled N with no productivity by local N fixation. Settling of organic matter generated through primary production drives respiration and nutrient recycling in intermediate waters. Chemotrophic processes such as nitrification, and Fe-dependent denitrification and DNRA were included (Fig. 2.3a). Our model is based on previous studies[44, 156], but we considered a ferruginous system where N cycling was driven first by Fe-dependent NO_3^- reduction, with the remaining NO_3^- reduced by organic matter originating through primary production (Fig. 2.3a). We also included DNRA, in accordance with our results from KB, to evaluate its impact on coupled C, N, Fe and S cycling under ferruginous conditions. Without explicit constraints on the fraction of NO_3^- reduced to NH_4^+ versus N_2 in

ferruginous oceans, we varied its contribution from 0 to 40%, with the balance occurring through denitrification.

Deep-ocean Fe(II) and NH_4^+ concentrations throughout the Proterozoic eon are uncertain. If global N-fixation is limited by phosphorous supply according to the Redfield ratio (16N:1P; [157]), we can set deep-ocean NH_4^+ concentrations in our model at 16 times the phosphorous concentration (0.04–0.13 μM) of Proterozoic seawater [158] (see Appendix B), which yields up to 2 μM NH_4^+. To validate this assumption, we excluded DNRA and ran our model with different ratios of N/P in deep waters. When deep ocean NH_4^+ is greater than 13 μM, sulfidic conditions develop without DNRA or N fixation under all reasonable upwelling rates [156] (Fig. 2.3e). Thus, if deep-ocean NH_4^+ concentrations were more than 13 μM, sulfidic conditions would have been widespread during the Proterozoic eon. Such widespread euxinia is not supported by the geologic record [150], indicating that NH_4^+ concentrations were generally less than 13 μM in the deep ocean. We thus chose 2 μM NH_4^+ as the benchmark for our modelling, but also explored a concentration range from 0.6 through to 13 μM. In line with considerations for both siderite solubility [46] and nutrient dynamics that permit marine oxygenic photosynthesis [158] we chose 42 μM as our benchmark Fe(II) concentration (see Appendix B). We also considered a broader range of Fe(II) concentrations (see Appendix B), which may be possible if siderite formation was kinetically inhibited [159].

Our model shows that in ferruginous upwelling systems the balance between DNRA and denitrification strongly influences coupled C, N, S and Fe cycling with enhanced primary production when DNRA is an appreciable NO_3^- reduction pathway. Indeed, when 40% of NO_3^- reduction is channelled through DNRA, primary production rates increase by up to 170% (Fig. 2.3b,c). A notable effect of this enhanced primary production is greatly increased H_2S production. This occurs even in the absence of N fixation as DNRA provides the nitrogen to stimulate additional organic matter production, which ultimately fuels microbial sulfate reduction (see Appendix B). At 40% DNRA, strong upwelling leads to sulfate reduction and pyrite deposition at rates sufficient to yield sediment iron speciation (Fe_{py}/Fe_{HR}) that indicates possible water column euxinia. Such Fe_{py}/Fe_{HR} values (>0.7) exist in Proterozoic sedimentary rocks [42, 47–49, 55], which could thus record a contribution of DNRA to NO_3^- reduction at this time.

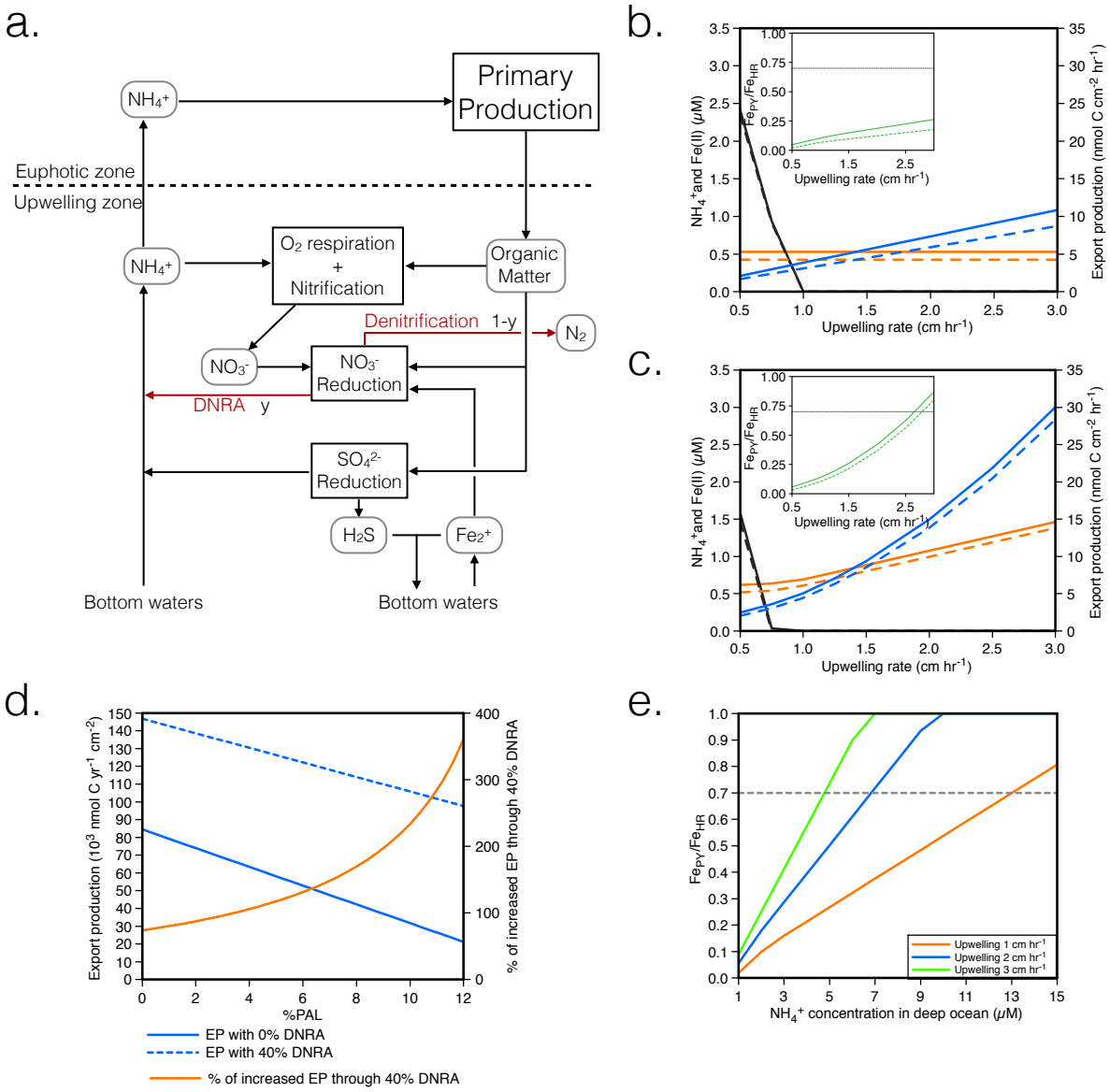

Figure 2.3: *Model outputs describing coupled C, N, S and Fe cycling in an idealized Proterozoic upwelling system.* a) Model structure illustrating reactions included and their reactants and products. b&c) Model runs with 0% (b) and 40% NO_3^- reduction (c) through DNRA. The solid lines represent model runs with the surface water oxygen concentrations of 3.8% PAL, whereas the dashed lines represent runs at 6.2% PAL (blue, export production; orange, NH_4^+ concentrations in the upwelling zone; black, Fe(II) concentrations in the upwelling zone; the insets show the Fe pyrite to highly reactive Fe ratio (Fe_{py}/Fe_{HR}) where the grey line delineates plausible euxinic conditions [150]). d, Yearly export production (EP) for 0% and 40% DNRA for a range of surface waters oxygen concentrations (from 0 to 12% PAL) at an upwelling rate of 2 cm h^{-1}. At 0% PAL, nitrification is not present in our model; however, NO_3^- is still supplied from the intermediate waters through advection and diffusion, therefore feeding NO_3^- reduction through DNRA and denitrification (see Appendix B). e, Fe_{py}/Fe_{HR} ratios for a range of deep-ocean NH_4^+ concentrations at 0% DNRA for three different upwelling rates at 3.8% PAL (the grey dashed line delineates plausible euxinic conditions[150]). See Appendix B for details.

Our model also reveals a negative feedback between primary production and surface ocean oxygen. This negative feedback develops when N loss increases in response to enhanced NO_3^- supply due to stimulation of nitrification by O_2. An increase from 3.8% to 6.2% PAL (present atmospheric level) O_2, values thought possible for the Mesoproterozoic [160] (values as low as 0.1% PAL have been proposed [161]), reduces primary production by up to 20% when NO_3^- reduction occurs exclusively through denitrification. This effect is muted by DNRA (Fig. 2.3b and c), which can play an increasingly important role in supplying N for primary production with the progressive oxygenation of the surface ocean (Fig. 2.3d).

It is widely assumed that the Proterozoic oceans were N limited due to massive N loss [39]. While the euphotic waters directly overlying upwelling systems can be locally N–limited due to N–loss from below, the global expression of N limitation ultimately depends on the balance between the geographic expansiveness of upwelling systems, and ocean-wide N fixation. We extrapolated N loss from our model to an area equivalent to upwelling regions in the modern ocean ($0.36\ 10^{12}$ m^2 – [162]) yielding a modelled global N-loss from Proterozoic oceans of up to 1.6 Tg N yr^{-1} (see Appendix B). By comparison, Proterozoic phosphorous concentrations [158] could have supported 4.8 Tg of N fixation per year based on an equivalent ratio of N fixed to deep ocean phosphorous as in the modern ocean [157] (see Appendix B). It has also been proposed that molybdenum (Mo) limited N fixation due to its scavenging from seawater as sulfide minerals [163]. Mo limitation seems unlikely, as Mo scavenging from seawater generally requires strong euxinia (see Appendix B), which as we show here, would not likely have developed in Proterozoic upwelling systems. To balance global N fixation with N loss in the Proterozoic eon, an upwelling area three times that of the modern ocean would have been needed. This suggests that N limitation in the Proterozoic was unlikely and that productivity would, instead, have been limited by phosphorous. Our modelling results are well supported by the Palaeoproterozoic rock record [42], which implies upwelling systems with euxinic conditions (possibly supported by DNRA) that induce little fixed N loss (also possibly the result of DNRA). The operation of these processes throughout the Proterozoic eon can be further tested through an expansion of the N isotope record, and through simulations in global biogeochemical models informed by our data.

Chapter 3

Rates and pathways of N_2 production in sulphidic Saanich Inlet

Marine oxygen minimum zones (OMZs) support 30-50% of global fixed-nitrogen (N) loss but comprise only 7% of total ocean volume. This N-loss is driven by canonical denitrification and anaerobic ammonium oxidation (anammox), and the distribution and activity of these two processes vary greatly in space and time. Factors that regulate N-loss processes are complex, including organic matter availability, oxygen concentrations, and NO_2^- and NH_4^+ concentrations. While both denitrification and anammox produce N_2, the overall geochemical outcome of these processes are different, as incomplete denitrification, for example, produces N_2O, which is a potent greenhouse gas. Information on rates of anammox and denitrification and more detailed ecophysiological knowledge of the microorganisms catalyzing these processes are needed to develop more robust models of N-loss in OMZs. To this end, we conducted monthly incubations with ^{15}N-labeled N under anoxic conditions and during a deep-water renewal cycle in Saanich Inlet, British Columbia, a persistently anoxic fjord. Both denitrification and anammox operated throughout the low oxygen water column with depth integrated rates of anammox and denitrification ranging from 0.15$\pm$0.03 to 3.4$\pm$0.3 and 0.02$\pm$0.006 to 14$\pm$2 mmol N_2 m^{-2} d^{-1}, respectively. Most N_2 production in Saanich Inlet was driven by denitrification, with high rates developing in response to enhanced substrate supply from deep water renewal. Dynamics in rates of denitrification were linked to shifts in microbial community composition. Notably, periods of intense denitrification were accompanied by blooms in an *Arcobacter* population against a background community dominated by SUP05 and Marinimicrobia. Rates of N_2 production through denitrification and anammox, and their dynamics, were then explored through flux-balance modeling with higher rates of denitrification

linked to the physiology of substrate uptake. Overall, both denitrification and anammox operated throughout the year, contributing to an annual N-loss of $2 \cdot 10^{-3}$ Tg N_2 yr^{-1}, 37% of which we attribute to anammox and 63% to complete denitrification. Extrapolating these rates from Saanich Inlet to all similar coastal inlets in BC (2478 km^2), we estimate that these inlets contribute 0.1% to global pelagic N-loss.

3.1 Introduction

Nitrogen (N) is an essential element to life and it is used as a building block for proteins and nucleic acids in all terrestrial and marine organisms. The bioavailability of N, therefore, can limit primary production in both terrestrial and aquatic compartments of the biosphere [8, 32]. The largest pool of N at the Earths surface is N_2 in the atmosphere and this N_2 is made available to life mostly through energetically expensive microbial N-fixation [2]. The abundance of fixed-N in the oceans is governed by the balance between this N-fixation into biomass, biomass deposition and ultimate burial in marine sediments, and the return of fixed-N to the atmosphere through a suite of redox reactions that ultimately lead to anaerobic N_2 production [9]. The processes that comprise the N-cycle are spatially decoupled with most N-fixation occurring in the euphotic surface ocean [164], the oxidative components distributed throughout much of the ocean, and anaerobic N_2 production partitioned between the low oxygen waters (30-50%) that typically develop at intermediate water depths and in eutrophic coastal regions, as well as in bottom sediments (50-70%) [165]. The availability of N to marine life, therefore, depends on the relative rates of N-fixation versus N-loss, and N-loss is expected to scale with the extent and intensity of low oxygen marine waters, which are currently expanding with unconstrained feedbacks on marine N inventories [72, 166, 167].

Under low oxygen conditions (<20 μM O_2 concentration), NO_3^- is used as an electron acceptor in anaerobic microbial energy transduction leading, in part, to N_2 production and closure of the N- cycle. Such low oxygen conditions commonly develop in the open ocean at intermediate water depths, in restricted basins, and in eutrophic coastal regions, when respiratory oxygen consumption outpaces physical mixing and oxygenic photosynthesis. Low oxygen marine waters

are commonly referred to as Oxygen Minimum Zones (OMZs), and are pervasive features of the modern oceans comprising 7% of their total volume (with $O_2 < 20\mu$M) [149]. The anoxic cores of OMZs, which contain oxygen concentrations below the limit of detection of oxygen sensors generally used in oceanographic research ($<5\mu$M, but as low as 1nM), constitute only 0.1% of the oceans total volume [63, 121]. Despite their relatively low volumes, OMZs play an outsized role in N biogeochemistry sustaining up to 50% of global marine fixed N-loss with an annual N-sink of 150 Tg of N [165].

N_2 production and thus N-loss in OMZs is driven by two entirely different microbial metabolisms: canonical denitrification and anaerobic ammonium oxidation (anammox). In denitrification a suite of either inorganic [sulphide (HS^-), ferrous iron (Fe(II))] or organic electron donors is used to reduce NO_3^- through a series of intermediates; NO_2^-, NO, and N_2O to ultimately produce N_2 (see Eqs. 3.1 and 3.2).

Organotrotrophic denitrification [168]:

$$84.8NO_3^- + (CH_2O)_{106}(NH_3)_{16}H_3PO_4 \Rightarrow 42.4N_2 + 106HCO_3^- + 42.4H_2O + HPO_4^{2-} + 16NH_4^+ + 7.2H^+ \quad (3.1)$$

$$\text{Chemotrophic denitrification: } 8NO_3^- + 5HS^- + 3H^+ \Rightarrow 4N_2 + 5SO_4^{2-} + 4H_2O \quad (3.2)$$

Anammox directly couples NO_2^- reduction to the oxidation of NH_4^+ through hydroxylamine and hydrazine intermediates to produce N_2 (Eq. 3.3).

$$\text{Anammox: } NO_2^- + NH_4^+ \Rightarrow N_2 + 2H_2O \quad (3.3)$$

Both pathways are fuelled, in part, by relatively oxidized N species and yield N_2 as their ultimate metabolic products, and they thus occupy overlapping niches. Denitrification and anammox, however, diverge in both their ecophysiology and their biogeochemical outcomes including possible leakages of intermediate N species and their overall influence on the carbon (C) cycling [169]. Denitrification, for example, can either consume or produce CO_2 depending on the

electron donor used, as denitrifiers can be heterotrophic or autotrophic. Anammox, on the other hand, is considered exclusively autotrophic and only consumes CO_2. Denitrification, furthermore, yields N_2O as an intermediate, a potent greenhouse gas, that may accumulate during partial denitrification and play a role in global climate forcing [170]. The differing ecophysiologies of the organisms conducting denitrification and anammox are thus expected to interact with one another in different ways across a spectrum of anaerobic conditions. These differences confound attempts to model N-cycle dynamics and its interactions with other cycles, without explicit descriptions for both anammox and denitrification and their regulation.

Process rate measurements are beginning to define the relationships between anammox, denitrification and the N-cycle. In OMZs globally, anammox appears to support most N_2 production [18, 60, 65–67, 84, 98, 154], while denitrification may dominate ephemerally [69, 105, 171, 172]. In open ocean OMZs, the relative contributions of anammox and denitrification to N_2 production are theoretically constrained by the stoichiometry of settling organic matter and the NH_4^+ supply from remineralization of organic matter to anammox [63, 105, 173–175]. This constraint develops when anammox is limited by NH_4^+ supplied through ammonification of organic N during heterotrophic NO_3^- respiration (organotrophic denitrification). In this case, N_2 production should occur 71% through denitrification and 29% through anammox based on Redfieldian organic matter stoichiometry of 106C:16N (Eq. 3.4) [100, 173, 175].

Coupling of organotrophic denitrification and anammox in open ocean OMZ:

$$94.4NO_3^- + (CH_2O)_{106}(NH_3)_{16}H_3PO_4 \Rightarrow 55.2N_2 + 106HCO_3^- + 71.2H_2O + HPO_4^{2-} + 13.6H^+ \quad (3.4)$$

Here, denitrification produces 16 moles of NH_4^+ and 16 moles of NO_2^- that fuels anammox, producing 16 moles out of a total 55.2 moles N_2, hence 29% of the total N_2 production (Eqs. 3.5

3.6).

Denitrification products fuel anammox entirely through organic matter degradation:

$$94.4NO_3^- + (CH_2O)_{106}(NH_3)_{16}H_3PO_4 \Rightarrow 39.2N_2 + 106HCO_3^- + 39.2H_2O + HPO_4^{2-} + 16NH_4^+ + 16NO_2^- + 13.6H^+ \quad (3.5)$$

Anammox consumes NH_4^+ and NO_2^- from denitrification:

$$16NH_4^+ + 16NO_2^- \Rightarrow 16N_2 \quad (3.6)$$

This expected ratio between anammox and denitrification, however, is rarely observed in the ocean and deviations from the ratio can be at least partially explained through variability in organic matter composition and departures from the Redfield ratio [105]. While this stoichiometric variability appears to account for differences observed in the role of anammox in N_2 production in open ocean OMZs, it remains unclear to what extent organic matter stoichiometry can explain the apparently outsized role of anammox in global N_2 production, more generally. Denitrification is commonly undetected in many OMZs, and this then raises the question as to what supplies NH_4^+ to anammox when denitrification appears absent. One possibility is microbial NO_3^- reduction to NH_4^+ (DNRA), which has been detected in the Peruvian OMZ and above the Omani shelf, and could be partially responsible for directly supplying NH_4^+ to anammox [65, 67]. While DNRA could provide NH_4^+ for anammox in some cases, it is unlikely the universal source as the rates of DNRA measured are generally insufficient to fully support the NH_4^+ requirements of concurrent anammox [67]. Other possible sources of NH_4^+ include remineralization of organic matter through NO_3^- reduction to NO_2^-, microaerobic respiration, and sulphate reduction [18], and in certain shallow settings, benthic release of NH_4^+ [60, 67]. While we are gaining a clearer picture of the controls on rates of anammox and denitrification in OMZs, there remain no universal rules that allow quantitative prediction of the partitioning between these two pathways.

Beyond observations from canonical OMZs, anammox and denitrification have been reported from other anoxic environments, including marine sediments, anoxic fjords and lakes, and

wastewater treatment facilities. In marine sediments for example, it has been shown that the relative contribution of anammox to N_2 production increases dramatically with both distance from the coast and water depth [83, 90] with anammox comprising up to 80% of the total N-loss at 700m depth [176]. This trend may be attributed to decreased organic matter content in deeper sediments [90]. Indeed, availability of organic matter, rather than its reactivity or quality, appears to regulate the relative importance of denitrification and anammox in estuarine sediments [112]. The relative contribution of anammox to sediment N_2 production also appears to increase when NO_3^- concentrations are persistently high in overlying waters [112, 177]. Notably, in sediments underlying low oxygen marine waters, nearly all N_2 production was supported by anammox [64]. In these sediments, NH_4^+ was supplied to anammox through DNRA. This implies then that the relative importance of anammox to sediment N_2 production may in part depend on the activity of DNRA. HS^- may also play a role in regulating anammox and denitrification. While HS^- is a common electron donor and thus a suitable substrate for denitrification, it has been shown to inhibit anammox at micromolar levels, possibly through toxicity [56]. This is consistent with the distribution of anammox, which appears to operate above the sulphidic zone in the Black Sea [114]. Likewise, anammox contributes up to 30% of the N_2 production in lacustrine water columns, but the highest rates of anammox occur in nearly HS^- free waters [107]. In contrast, anammox appears entirely excluded from very iron-rich lake waters and sediments [111, 178], and ferruginous estuarine sediments [97, 155]. Taken together, the emerging picture suggests that the regulation of the relative importance of anammox and denitrification to total N_2 production is convoluted and development of predictive knowledge will require comprehensive and detailed studies across the broad range of systems where these processes are known to operate.

We have conducted a time-series study of the rates of denitrification and anammox and their relative contribution to N_2 production in Saanich Inlet (SI). SI is a persistently anoxic fjord that provides a tractable ecosystem in which to study anaerobic microbial metabolisms relevant and extensible to low oxygen environments globally (Fig. 3.1 a and b). The choice to use the word "persistent" for SI is recent, however, as only partial renewals have been recorded between 2014 and 2019. Part of the water column therefore remains anoxic throughout the year. Biogeochemical research has been conducted in SI since 1965 [179] and has culminated with instrumented real-time

monitoring and a more than 10 year continuous time-series experiment [180–183], making it one of the best studied anoxic fjords on Earth. The inlet is situated on the southern tip of Vancouver Island (Fig. 3.1a) and is up to 228m deep with a 75m deep sill at its entrance that restricts hydrological connection to the Strait of Georgia and the mixing of waters in its deep basin. Similar to OMZs, aerobic respiration in SI water column outpaces O_2 supply through physical water mixing and photosynthesis in the surface waters, rendering low oxygen conditions for most of the year below 100m for most of the year (Fig. 3.1b). In contrast to most open ocean OMZs, however, sulphidic conditions develop in the bottom waters of SI as a result of either sulphate reduction in the water column [184] and/or sulphide efflux from the underlying sediments [185]. Most years, SI stagnant deep waters transition from sulphidic to oxic at the end of the summer (late August - early September) in response to upwelling off the coast of Vancouver Island that forces dense well-oxygenated waters into the Strait of Georgia and over the sill into the inlet [184], in connection to weak tidal currents [186]. The inlet thus exists in two main states during the year if renewal occurs: a state of stagnation referring to low oxygen concentrations in the deep-waters and a state of renewal when oxygenated waters penetrate the inlet and mix with low oxygen deep-waters. These physical-chemical characteristics combine to support microbial communities with anaerobic metabolisms that couple the C, N and S-cycles and are broadly analogous to those we expect to find in other low oxygen and anoxic marine waters globally [104].

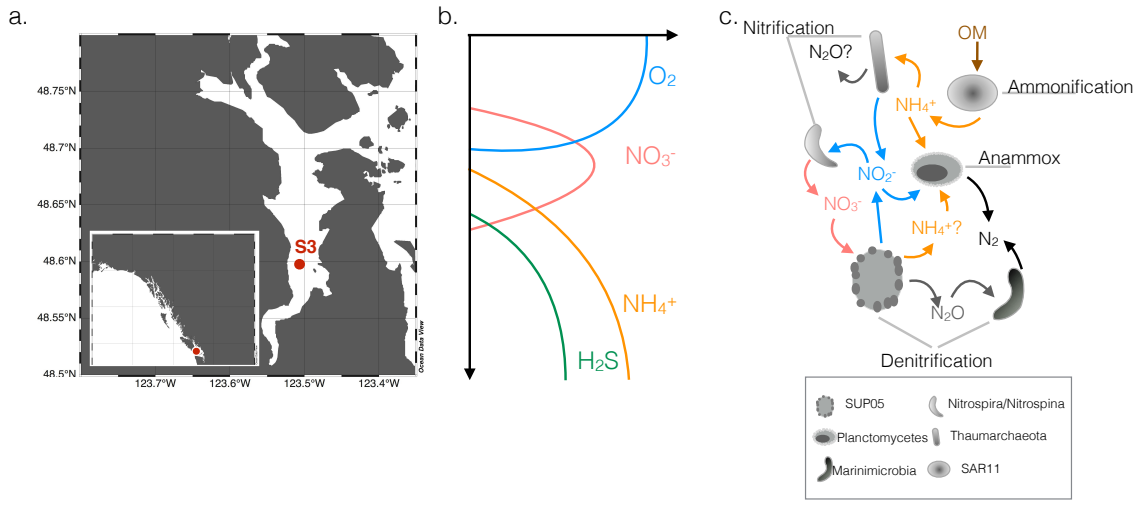

Figure 3.1: *Saanich Inlet (SI), a model ecosystem for the study of microbial metabolisms in OMZs* a) Sampling of Station S3 in Saanich Inlet, on Vancouver Island, British Columbia (Canada). Sampling of S3 happened once a month within a historic time series data collection. b) Typical redox gradients found in SI. These gradients move vertically depending on the season. c) Active microbial metabolisms of the N-cycle present along the redox gradients of SI.

N-cycling and its interactions with the other cycles in SI have been previously interrogated using a variety of geochemical and microbiological analyses. Geochemical data indirectly imply that SI supports relatively high rates of both pelagic and benthic N-loss that vary seasonally, with the highest rates in the winter (December to February, 8.1 mmol m^{-2} d^{-1}) and lowest in the summer (May to August, 1.7 mmol m^{-2} d^{-1}) [186]. Multi-omic analyses revealed that microbial communities in SI harbour the metabolic potential to catalyze many components of the N-cycle and to link it to cycling of C and S [33, 182, 187]. These metabolic pathway reconstructions have led to a conceptual model describing the microbial interactions that underpin N-cycling in SI, and

low oxygen waters more broadly (Fig. 3.1c). Specifically, this model (reproduced in Fig. 3.1c from [33]) proposes that Thaumarchaeota are responsible for the first step of nitrification (NH_4^+ to NO_2^-) and that two different species of bacteria, *Nitrospina gracilis* and *Nitrospira defluvii*, oxidize NO_2^- to NO_3^-. Along with nitrification, the SAR11 are the most abundant aerobic heterotrophs, and they are thought to degrade settling organic matter and release NH_4^+ to the oxic water column (Fig. 3.1c). Lower in the water column, the model suggests that Planctomycetes produce N_2 through the anammox process, while bacteria from the SUP05 clade (Gammaproteobacteria) were implicated in reducing NO_3^- to N_2O (Fig. 3.1c). The final step of denitrification remained more elusive but analyses of Single Cell Amplified Genomes (SAGs) reveal metabolic potential for N_2O reduction to N_2 in the Marinimicrobia ZA3312c-A and SHBH1141 (previously known as Marine Group-A) [187]. Notably, the taxonomic affiliations and genomic make-up of the key organisms that drive N-cycling in SI are closely related to those found across OMZs and other anoxic environments globally [104]. For example, the Gammaproteobacteria SUP05 – with a single cultivated member, *Ca.* T. autotrophicus strain EF1 [188] – appears to be a ubiquitous member of OMZ microbial communities with the metabolic potential for partial denitrification [33, 120, 182], along with bacteria from the group Marinimicrobia that reduce N_2O to N_2 [187] and are some of the most widely distributed and abundant taxa in marine OMZs.

The conceptual metabolic model for coupled C, N, and S cycling in OMZs was further expanded into a quantitative gene-centric model that integrates metabolic potential derived from multi-omic information with geochemical data to predict process rates [118]. Modeled rates were validated through direct measurements, but these rates were an order of magnitude lower than the rates needed to support previous geochemical data [186]. These observations highlight a discontinuity between current conceptual and quantitative models of the N-cycle in SI and a need for data that more fully capture and integrate the dynamics of N-cycling across multiple seasons.

Here, we used isotope labeling experiments to directly quantify rates and pathways of anaerobic N cycling in SI over an entire year. These measurements allowed us to calculate annual N-loss from Saanich inlet, determine the specific microbial pathways that are responsible, and to assess the biogeochemical controls on the rates and pathways of N-loss in the inlet. Overall, our data reveal that fixed N-loss from SI has strong seasonality and that periods of intense N-loss during

the summer are driven primarily through sulphide-dependent denitrification, which is likely fuelled by benthic sulphide supply and new input of NO_3^- from a partial renewal of the water column. Anammox also contributed to N-loss at relatively constant rates throughout the year.

3.2 Methods

3.2.1 Study site and sampling

Saanich Inlet (SI) is a marine fjord located on the West Coast of Vancouver Island, British Columbia, Canada (Fig. 3.1). We conducted a monthly time series experiment between January and December 2015 (Table 3.1) and sampled at station S3 (Fig. 3.1a 48 ° 35.5 N and 123° 30.3 W, 227m deep). A standard profile of 16 depths was sampled every month with 12L GO-FLO bottles attached in-series to a steel cable (10, 20, 40, 60, 75, 85, 90, 97, 100, 110, 120, 135, 150, 165, 185 and 200m). Depths were set using a metered winch cable with a precision of plus or minus 0.5m and the accuracy of the depth reached was checked with the CTD depth profile. CTD profiles [pressure (SBE 29), conductivity (SBE 4C), temperature (SBE 3F), and oxygen (SBE 43)] were obtained with the SBE25 Sealogger CTD (SBE). Oxygen concentrations measured with the SBE 43 sensor were calibrated monthly against Winkler titrations [151] and its limit of detection is $<1\mu$M. The CTD, attached at the end of the winch cable, and the bottles were lowered to their final depths and left there to equilibrate with surrounding water for at least a minute before closing.

Samples for nutrient concentration measurements were immediately filtered and put on ice for later analysis. Samples for sulfide analyses were fixed in 0.5% Zinc Acetate final concentration without prior filtration and frozen at -20°C for later analysis. 250mL serum bottles destined for incubations were overfilled 3 times with water from 7 depths (90m, 100m, 120m, 135m, 150m, 165m and 200m). The overfilling of the bottle as well as capping with blue halobutyl stoppers (Bellco, UK) minimized oxygen contamination (De Brabandere et al., 2012). Samples for chlorophyll *a* determination were collected in carboys from four depths corresponding to 100%, 50%, 15% and 1% of the surface incident irradiance as measured by the PAR sensor on the CTD. Carboys were kept cool and dark until further subsampling back in the lab. 500 mL subsamples from each carboy were filtered for phytoplankton biomass (chl *a*). Filters were kept frozen at -20°C until

Table 3.1: Addition of labeled N-species and electron donors to incubations in 2015.

	Exact date of sampling	Type of ^{15}N labeled-incubation
January 2015	14 January 2015	$^{15}NO_3^-$ (10µM), $^{15}NH_4^+$ & $^{14}NO_3^-$ (10µM&10µM)
February 2015	11 February 2015	/
March 2015	11 March 2015	$^{15}NO_3^-$ (10µM), $^{15}NH_4^+$ & $^{14}NO_3^-$ (10µM&10µM)
April 2015	8 April 2015	$^{15}NO_3^-$ (10µM), $^{15}NH_4^+$ & $^{14}NO_3^-$ (10µM&10µM)
May 2015	13 May 2015	$^{15}NO_3^-$ (10µM), $^{15}NH_4^+$ & $^{14}NO_3^-$ (10µM&10µM)
June 2015	3 June 2015	$^{15}NO_3^-$ (10µM), $^{15}NH_4^+$ & $^{14}NO_3^-$ (10µM&10µM), $^{15}NO_3^-$ (10µM) & HS^- (1, 5, 10, 15, 20µM)
July 2015	8 July 2015	$^{15}NO_3^-$ (10µM), $^{15}NH_4^+$ & $^{14}NO_3^-$ (10µM&10µM)
August 2015	12 August 2015	$^{15}NO_3^-$ (2.5, 5, 10, 15, 25µM), $^{15}NH_4^+$ & $^{14}NO_3^-$ (10µM&10µM)
September 2015	9 September 2015	$^{15}NO_3^-$ (10µM), $^{15}NH_4^+$ & $^{14}NO_3^-$ (10µM&10µM)
October 2015	22 October 2015	$^{15}NO_3^-$ (10µM), $^{15}NH_4^+$ & $^{14}NO_3^-$ (10µM&10µM)
November 2015	18 November 2015	$^{15}NO_3^-$ (10µM), $^{15}NH_4^+$ & $^{14}NO_3^-$ (10µM&10µM)
December 2015	9 December 2015	$^{15}NO_3^-$ (10µM), $^{15}NH_4^+$ & $^{14}NO_3^-$ (10µM&10µM)

analysis.

3.2.2 Nutrient and process rate measurements

Samples for NO_2^-, NH_4^+ and HS^- determinations were thawed immediately prior to analysis and measured with spectrophotomectric assays: the Griess assay, the indophenol blue method, and the Cline assay, respectively [151]. NOx (NO_3^- and NO_2^-) was measured by chemiluminescence following reduction to NO with vanadium [189], and we subtracted NO_2^- from the total NOx concentrations to obtain NO_3^- concentrations (Antek instruments 745 and 1050, Houston TX). Chlorophyll *a* samples collected on filters (0.7m nominal porosity) were extracted for 24 hours with 90% acetone at -20C, and the extracted chlorophyll a measured in a Turner Designs 10AU fluorometer, using an acidification method and corrected for phaeopigment interference [190]. DIN deficit (DIN_{def}) was calculated according to Bourbonnais et al. (2013) [191] and corrected for the release and dissolution of iron and manganese oxyhydroxide-bound PO_4^{3-} under anoxic conditions.

Dark Carbon fixation rates were measured by overfilling 60mL serum bottles 3 times to minimize O_2 contamination and ammending $^{14}C-HCO_3$ to the incubation bottles following the JGOFS protocol [192].

The protocol used for measuring rates of denitrification and anammox was modified from

[110]. In an attempt to minimize bottle effects arising from the use of small sample volumes, we incubated the water in 250mL serum bottles closed with blue butyl rubber stoppers. At the start of the incubation, we inserted a 20mL oxygen scrubbed helium headspace into the bottle and then added the ^{15}N labeled N-species and electron donors to the bottles according to table 3.1. Gas entering the serum bottle was passed through an oxygen scrubber (Cu-CuO, Glasgertebau Ochs - Germany) to limit O_2 introduction to incubations of anoxic water to below our detection limit measured with flow-through cell oxygen sensor ($<0.2\mu$mol L^{-1}, Pyroscience). For incubations of oxygen contaminated water, adding a 20 mL headspace decreases the amount of oxygen in the seawater by about 30 times due to preferential partitioning of O_2 into the headspace gas. In contrast, given the distribution of sulphide between aqueous and gaseous species in seawater, less than 2% of the total sulphide in our incubation vessels resides in the headspace. Samples were taken approximately every 6, 12, 24 and 48 hours during the incubations to both allow maximum sensitivity and capture intervals with constant rates. In between time points, incubations were kept in the dark at 15°C. To determine the time-course of ^{15}N labeled-N_2 production, gas samples were taken with a 1 mL gas-tight syringe (Hamilton) previously flushed with He and then with the headspace gas. Gas samples were stored in 3mL exetainers previously filled with milliQ water. Liquid samples were taken to follow the production or consumption of NO_2^-, NO_3^-, or NH_4^+. Liquid samples were taken with a plastic 5 mL syringe previously flushed with He, filtered and then stored at -20°C for later analysis. The ^{15}N content of N_2 was determined in gas samples collected during the incubations on an Isotope-Ratio Mass Spectrometer (Delta V with continuous flow inlet, thermoscientific). Concentrations of N_2 were calibrated with standards by injecting different amounts of gas from N_2 flushed Exetainer vials at 1 atmosphere. The excess $^{14}N^{15}N$ and $^{15}N^{15}N$ in the gas samples was calculated as described by [193]. Then, rates were calculated through least squares fitting of the slope of ^{15}N accumulation versus time for the linear region of ^{15}N excess ingrowth (i.e. constant rates), correcting for the ^{15}N labelling percentages of the initial substrate pool and accounting for the initial pool of substrate present. Rates were determined to be significant if the slope of the linear regression was considered different from 0 ($p_i0.05$). Denitrification rates were determined from the accumulation of $^{30}N_2$ in the bottle headspace from the $^{15}NO_3^-$ additions, and anammox rates were calculated from the accumulation of $^{29}N_2$ from the

$^{15}NH_4^+$+$^{14}NO_3^-$ additions according to [154] with modifications and compared to the accumulation of $^{29}N_2$ from the $^{15}NO_3^-$ additions. The detection limit on these rates were calculated as the median of the standard error on the slope used to calculate all significant rates [98, 106] and was determined to be 0.04 nM h^{-1} and 0.4 nM h^{-1} for anammox and denitrification, respectively. To produce integrated rates of denitrification and anammox for each month, we first scaled potential rates (R_{pot}) to in situ rates or corrected rates (R_{cor}) by using Michaelis-Menten half saturation constants K_m and in situ substrate concentrations for each process, respectively (Eq. 3.7).

$$R_{cor} = \frac{[S]}{[S] + K_m} * R_{pot} \tag{3.7}$$

For denitrification, we used K_m determined through the addition of different $^{15}NO_3^-$ concentrations in the incubations (Fig. 3.4a and table 3.1). For anammox, we used a K_m from the literature [109]. Then, we integrated the corrected rates over the sampling depth intervals to attain area specific process rates.

3.2.3 Microbial community profiling

Six different depths (10, 100, 120, 135, 150, and 200m) were sampled for microbial community profiling and water from these depths was returned to the lab for same-day filtering. 10L of water was filtered onto Sterivex 0.22μm (Millipore) filters with a 2.7μm glass fiber pre-filter. Filtered biomass was soaked in lysis buffer then frozen immediately in liquid nitrogen. Filters were stored at -80C until further analysis. DNA was extracted according to [194]. Extracted DNA was quantified using the picogreen assay (Invitrogen) and checked for amplification of the small subunit ribosomal RNA (SSU or 16S rRNA) gene using universal primers targeting the V4-V5 region of the bacterial and archaeal 16S rRNA gene (515F-Y and 926R) [195]. DNA was sent to the Joint Genome Institute (California, USA) for 16S rRNA amplicon sequencing on the Illumina MiSeq platform (https://jgi.doe.gov/wp-content/uploads/2016/06/DOE-JGI-iTagger-methods.pdf).

Once sequenced, amplicons were quality filtered using the JGI "itaggerReadQC" pipeline (source: `https://bitbucket.org/berkeleylab/jgi_itagger/` and `https://jgi.doe.gov/wp-content/uploads/2016/06/DOE-JGI-iTagger-methods.pdf`). Quality filtered reads were run through USE-

ARCH [196] and QIIME [197]. First, we identified chimeras using UCHIME [196]. We then picked OTUs de novo with the sumaclust method at 97% OTU threshold [198]. We filtered singletons from the OTU table and then assigned taxonomy to a representative set of sequences with rdp classifier using the QIIME release Silva database V128 [199]. Chao1 diversity index was calculated with R. Clustering of the samples was also performed in R based on a dissimilarity matrix with Euclidean method (`https://uc-r.github.io/hc_clustering`).

We also quantified total bacterial and archaeal 16S rRNA genes present in our samples via qPCR by targeting the region V1-V3 regions of the bacterial and archaeal 16S rRNA genes with the primers 27F/20F (5'-AGAGTTTGATCCTGGCTCAG, 5'-TTCCGGTTGATCCYGCCRG) and DW519R (5'-GNTTTACCGCGGCKGCTG) [183]. Standards used for total bacteria and total archaea quantification were obtained from SSU rRNA gene clone libraries as described in [183]. qPCR program was as followed: (1) 95°C for 3 minutes, (2) 95°C for 20 seconds, (3) 55°C for 30 seconds, (4) plate read, repeat (2) to (4) 44 times, obtain melting curve by incrementing 0.5°C from 55°C to 95°C every second. qPCR reactions were performed in low-profile PCR 96 well-plates (BioRad) in a 20μl reaction volume on a CFX Connect Real-Time thermocycler (BioRad). Results can be found in Appendix C.

3.2.4 Flux balance modeling

Flux balance modeling was conducted to describe rates of anammox, NO_3^- reduction to NO_2^- and complete denitrification (NO_2^- to N_2) based on cell abundance, input fluxes of substrates, and kinetic descriptions of these processes. The script for the simulation was written in Matlab (version R2015b) and can be found in the Appendix C. More details can be found in the discussion section that follows as well as in Appendix C.

3.3 Results

3.3.1 General water column physical, chemical, and biological properties

A salinity profile (Fig. 3.2a), shows relatively uniform bottom waters with monthly variability in the surface waters. Figure 3.2b shows the relatively homogeneous temperature in the SI

water column with a warming in the surface waters during the summer (June to September 2015) and the extension of this warming to deeper water depths in the following months. The chlorophyll *a* data (Fig. 3.2c) shows peaks of fluorescence in the surface waters in March, May, and September 2015 with the highest peak, at 43.82 μg L^{-1} chlorophyll *a* in March just below the surface. O_2 concentration profiles (Fig. 3.2d) were also determined with the CTD probe, revealing O_2 depletion at depth to less than the sensor limit of detection ($<1\mu$M) for all of 2015. The upper boundary of the oxycline (depths where there is a sharp gradient in oxygen concentration) is generally around 80m and oxygen penetrates at least to 120m, though penetration can be as deep as 150m, as seen in July and September. Low O_2 concentrations and anoxia thus characterize the deeper waters of SI (>120m depth) throughout 2015. NO_3^- concentrations (Fig. 3.2e) are high in surface waters (up to 32μM) and generally decline with increasing depth within the oxycline and often remain detectable in deeper low-oxygen waters. A peak in NO_2^- concentrations (Fig. 3.2f) can be detected sporadically in both the surface waters and/or around 120m-135m depth where it can reach concentrations as high as 2.5μM. Surface waters are largely devoid of any NH_4^+ (Fig. 3.2g), which tends to accumulate below 140m in anoxic waters and reaches the highest measured concentrations (up to 32μM) by 200m. Sulphide (HS^-) was only present in bottom waters, reaching concentrations up to 41μM in February 2015, and was generally detected at 135m and below (Fig. 3.2h). In figure 3.2i, we show DIN deficit [191] calculated for the year 2015 with values varying from 0 in the surface waters to 60 in the bottom waters for February 2015. Overall, values reflected a DIN deficit in the anoxic waters and increased with depth (Fig. 3.2i).

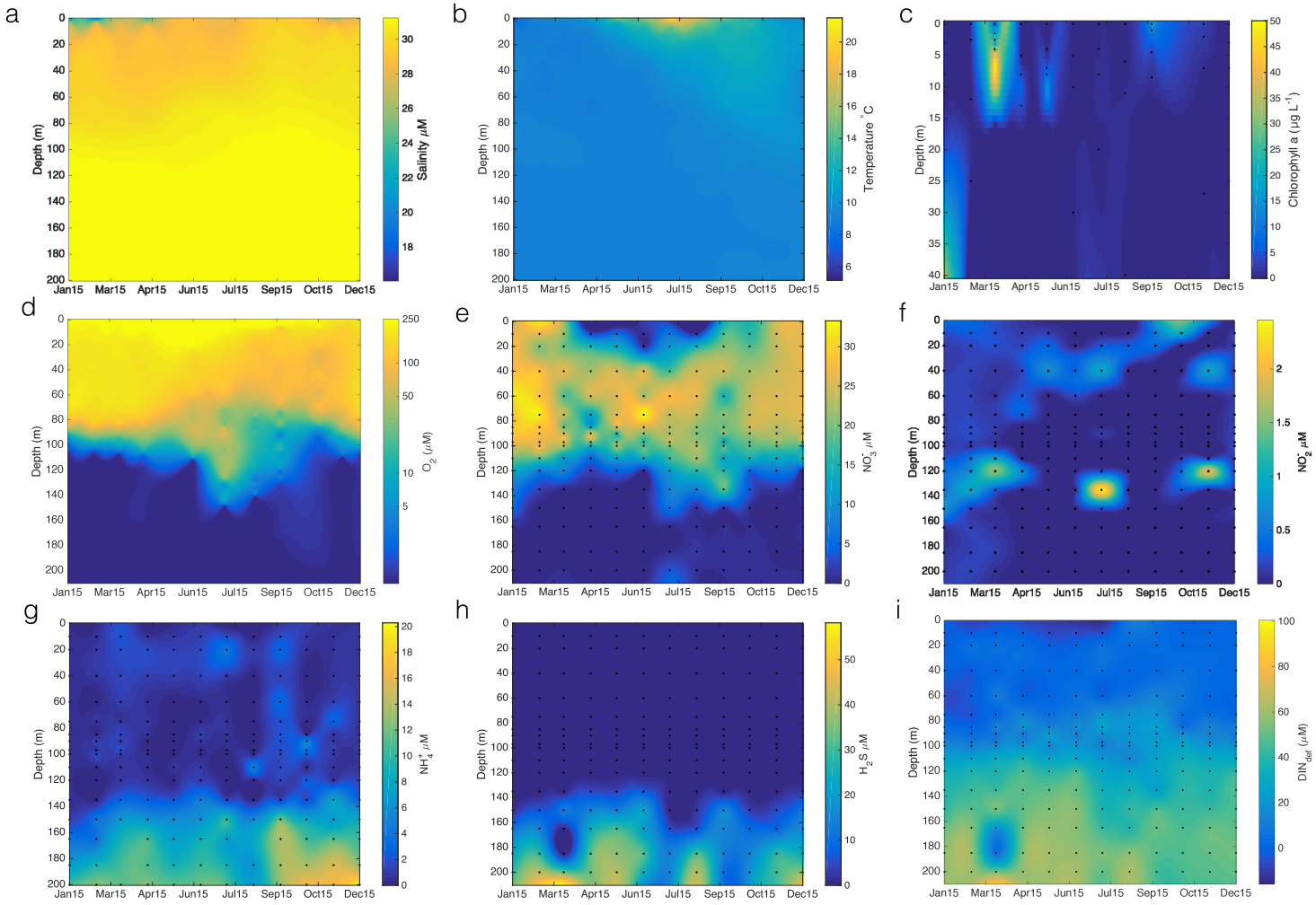

Figure 3.2: *Geochemical profiles for SI, 2015* a) Salinity (g kg-1); b) Temperature (C); c) Chlorophyll *a* μg L^{-1}) d) Oxygen profiles (μM); e) NO_3^- concentrations (μM); f) NO_2^- concentrations (μM); g) NH_4^+ concentrations (μM); h) HS^- concentrations (μM) i) calculated DIN deficit values (see methods in main text) for Saanich Inlet during the year 2015 at station S3. a, b and d values have been obtained from the CTD profiles monthly. Intermediate values have been interpolated in matlab using the gridfit function (specifically the nearest neighbor). c, d-g values were obtained from discrete sampled depths as indicated by black dots on graphs and interpolated interpolated in matlab using the gridfit function (specifically the nearest neighbor). Note that Fig. 3.2c only goes down to 100m depth as the values obtained for the chlorophyll *a* profile were sampled mostly above 50m.

3.3.2 Rates of denitrification, anammox, and dark carbon fixation

Both anammox and denitrification were active throughout the year in the low oxygen waters where we conducted ^{15}N-labeled incubations. Rates of denitrification, corrected for *in situ* substrate concentrations, varied between 0.28±0.03 and 140±14 nM hr^{-1} (Fig. 3.3b) based on the accumulation of $^{30}N_2$ in $^{15}NO_3^-$ amended incubations (Table 3.1). Similarly, rates of anammox varied throughout the year, between 0.07±0.01 and 13.2±0.4 nM hr^{-1} (Fig. 3.3c) based on the accumulation of $^{29}N_2$ in $^{15}NH_4^+$ + $^{14}NO_3^-$ amended incubations. We also compared rates of anammox obtained through the accumulation of $^{29}N_2$ with the addition of $^{15}NO_3^-$ and found that they were of the same order of magnitude as the rates obtained from $^{15}NH_4^+$+$^{14}NO_3^-$ incubations (Fig. 3.3a). Overall, rates of denitrification, when detected, were equal to or higher than rates of anammox, although anammox dominated N_2 production in 55% of the measurements made. However, the fact that rates of denitrification were generally higher, when detected, led to a higher annual proportion of N_2 production through denitrification (see section 2.3.4: depth-integrated rates of N-loss). Dark carbon fixation rates were measured for most of the water column and ranged between 0.24 to 400 nmoles C L^{-1} hr^{-1} (Fig. 3.3d).

3.3.3 Response of denitrification and anammox to amendments

Between 1 and 20μM $^{15}NO_3^-$ was amended to seawater collected from 165 m depth in August 2015. This depth contained 1 μM NO_3^- *in situ* and was therefore at the lower end of NO_3^- concentrations found within Saanich inlet's anoxic waters. Hence, NO_3^- concentrations may be expected to limit denitrification, NO_3^- reduction to NO_2^-, and anammox at this depth. Rates of dentirification, based on the accumulation of $^{30}N_2$, increased with increasing NO_3^- concentrations up to 20μM (Fig. 3.4a), and the relationship between rates and NO_3^- concentration could be modeled with a Michaelis-Menten formulation. Our data could be described with a maximum rate of denitrification (V_{max}) and a half-saturation constant, K_m, for NO_3^- of 112 nmol L^{-1} hr^{-1} and 5μM (Fig. 3.4d and f, table 3.2), respectively. The rate of denitrification found at 20μM NO_3^-, however, is lower than for 15 μM and did not follow predictions from the Michaelis-Menten model in Figure 3.4e and f. Anammox was not detected. We also determined changes in the concentrations of NOx and NH_4^+ when we

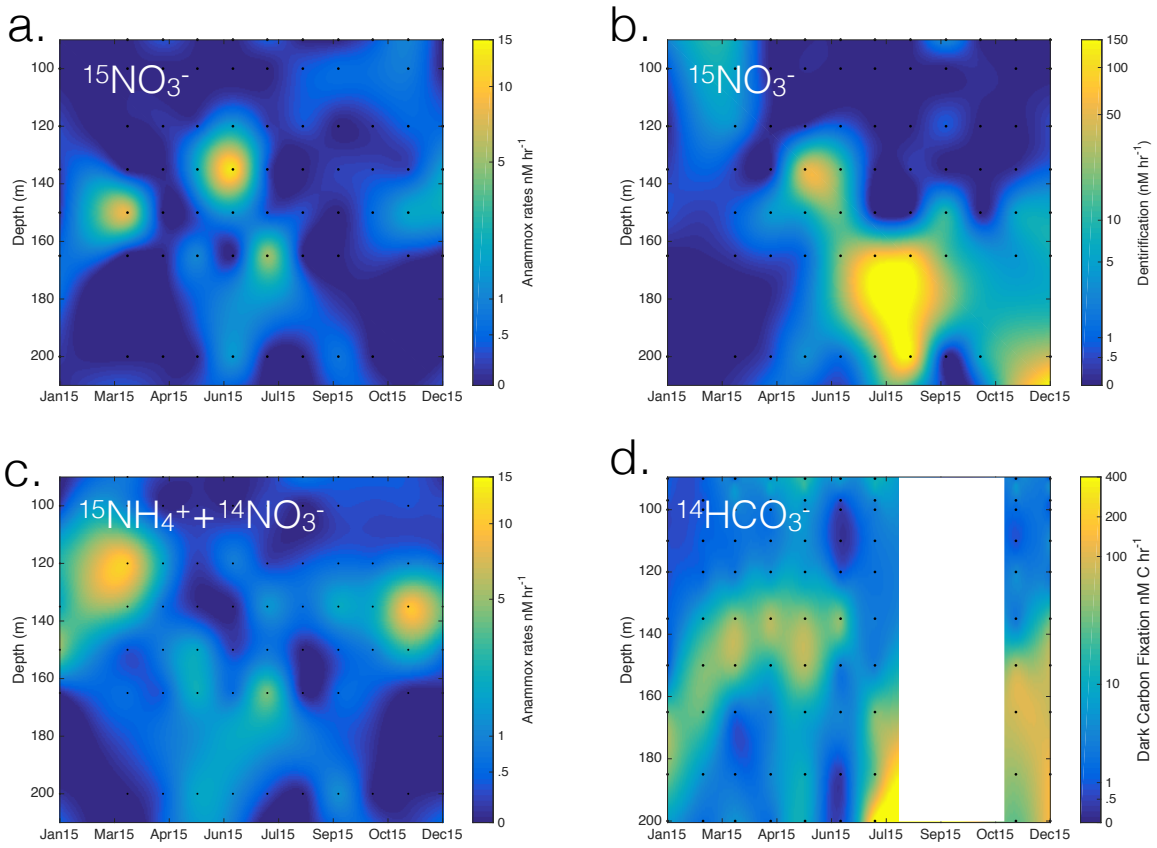

Figure 3.3: *Process rate measurements for SI, 2015* Potential rates of a) anammox (nM hr^{-1}) and b) denitrification (nM hr^{-1}) calculated from the incubated samples with $^{15}NO_3^-$ for the year 2015 at station S3. c) shows potential rates of anammox of samples incubated with $^{15}NH_4^+$ + $^{14}NO_3^-$. In d), graph shows rates of dark carbon fixation from incubation with H14CO3- in nM hr^{-1}. The scale bar is in log scale.

added different $15NO_3^-$ concentrations (Fig. 3.4a and b). We observed that NO_2^- accumulates with concentrations reaching a maximum of 9μM when 20 μM $^{15}NO_3^-$ was added. NH_4^+ concentrations, on the other hand, remain relatively constant between 8 and 12μM. Rates of NO_3^- reduction varied, between 0 and 430 nM hr^{-1}, and rates of NO_2^- accumulation varied between 0 and 286 nM hr^{-1} (Fig. 3.4e). The latter rates combined with the rates of denitrification are enough to explain the rates of NO_3^- reduction and thus no accumulation of other intermediates such as N_2O is required or expected.

We also amended seawater collected from 120m depth in June 2015 with HS^- ranging from 1 to 10μM, in addition to 10μM $^{15}NO_3^-$ to examine the influence of HS^- on rates of denitrification

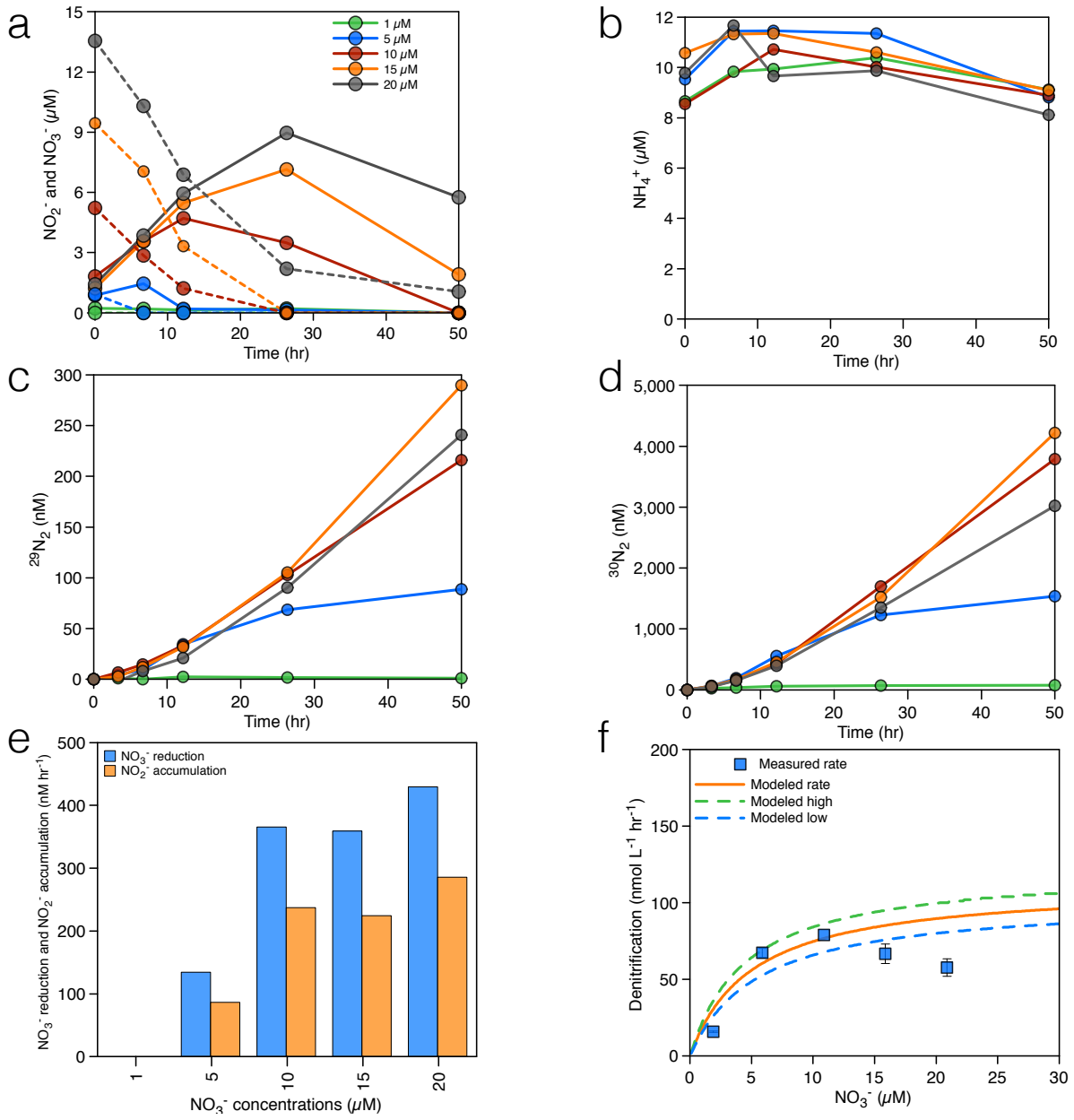

Figure 3.4: *NO_3^- dependency in SI.* a) NOx accumulation/consumption over time with the addition of different NO_3^- concentrations NO_3^- concentrations in dashed lines, NO_2^- concentrations in solid lines b) NH_4^+ accumulation/consumption over time with the addition of different NO_3^- concentrations. c) Production of $^{29}N_2$ in the incubations (nM) d) Production of $^{30}N_2$ in the incubations (nmol), e) rates of NO_3^- reduction and NO_2^- accumulation (nM hr^{-1}) f) Michaelis Menten curve and measured denitrification rates for different NO_3^- concentrations in August 2015, see table 3.2 for details on the Michaelis Menten parameters used in f)

Table 3.2: Michaelis-Menten parameters, K_m (μM) and V_{max} (nmol L^{-1} hr^{-1}) for NO_3^- dependency of denitrification at 165m in August 2015. Note that anammox kinetics are not following Michaelis-Menten model in this case

	Denitrification
K_m (μM)	5 ± 0.5
V_{max} (nmol L^{-1} hr^{-1})	112 ± 10

and anammox. This depth was chosen because it does not contain any detectable sulphide *in situ*. Instead, it immediately overlies the sulphidic deep waters and thus likely receives a flux of HS^- from below that fails to accumulate to detectable concentrations at 120m depth and signifies sulfide oxidation. Results show an increase in denitrification rates with increasing HS^- concentrations (Fig. 3.5d and f) above an apparent threshold of 2.5 μM HS^-. These experiments reveal a seemingly linear trend, but scarcity in data precludes the delineation of a definitive relationship (Fig. 3.5e and f). Anammox occurs (Fig. 3.5c and e) with 1 and 2.5μM HS^- amendments but was not detected with 5 and 10μM HS^- amendments. NOx concentrations were constant over time in these experiments except for the highest HS^- concentrations (Fig. 3.5a) and NH_4^+ concentrations decreased over time (Fig. 3.5b).

3.3.4 Depth-Integrated rates of N-loss

Depth-integrated rates of N_2 production varied over the year, with a greater contribution from denitrification (63%) than anammox (37%) (Fig. 3.6). Rates of denitrification ranged between 0.02±0.006 to 14±2 mmol m^{-2} d^{-1} (Fig. 3.6), with the highest rates following renewal in July and August. Anammox rates, on the other hand, were comparatively constant throughout the year, and varied between 0.15±0.03 and 3.4±0.3 mmol m^{-2} d^{-1} (Fig. 3.6). Anammox dominated N_2 production in January, April, May, June, October and November (>50% of N_2 production). Nevertheless, results show that denitrification overall dominates the yearly N_2 production in the water column (Fig. 3.6).

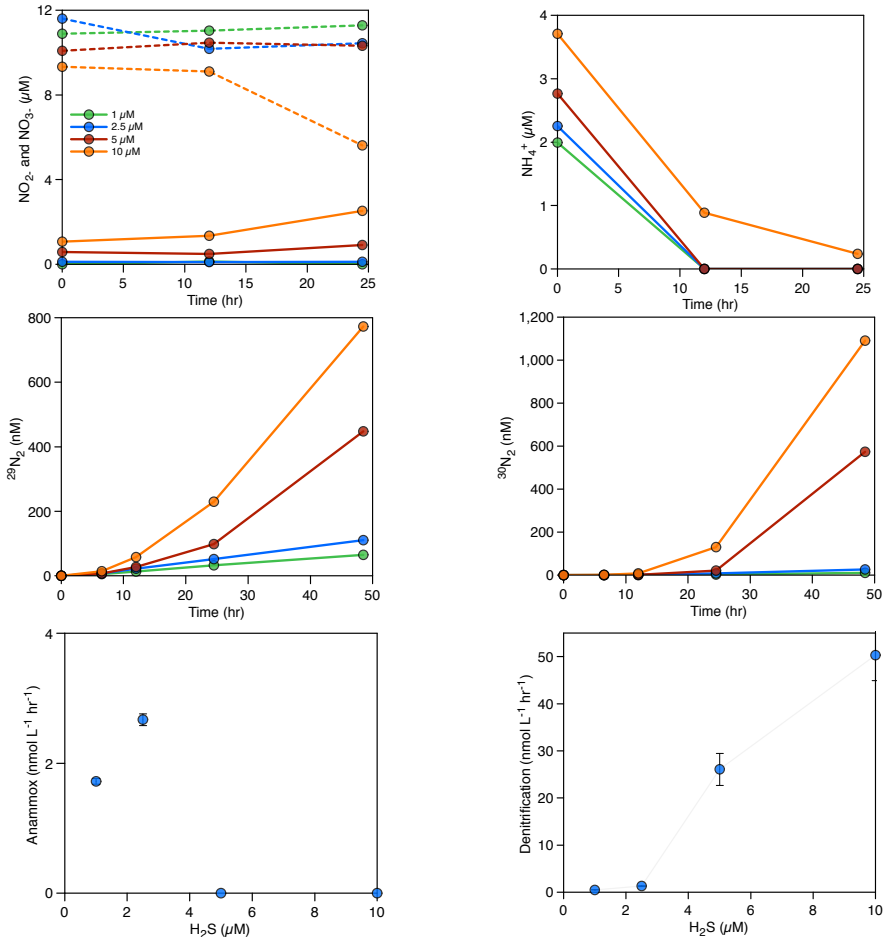

Figure 3.5: *HS^- dependency in SI* a) NOx accumulation/consumption over time with the addition of different HS^- concentrations NO_3^- concentrations in dashed lines, NO_2^- concentrations in solid lines b) NH_4^+ accumulation/consumption over time with the addition of different HS^- concentrations. c) Production of $^{29}N_2$ in the incubations (nM) d) Production of $^{30}N_2$ in the incubations (nM) e) measured anammox rates for different HS^- concentrations in June 2015 f) measured denitrification rates for different HS^- concentrations in June 2015

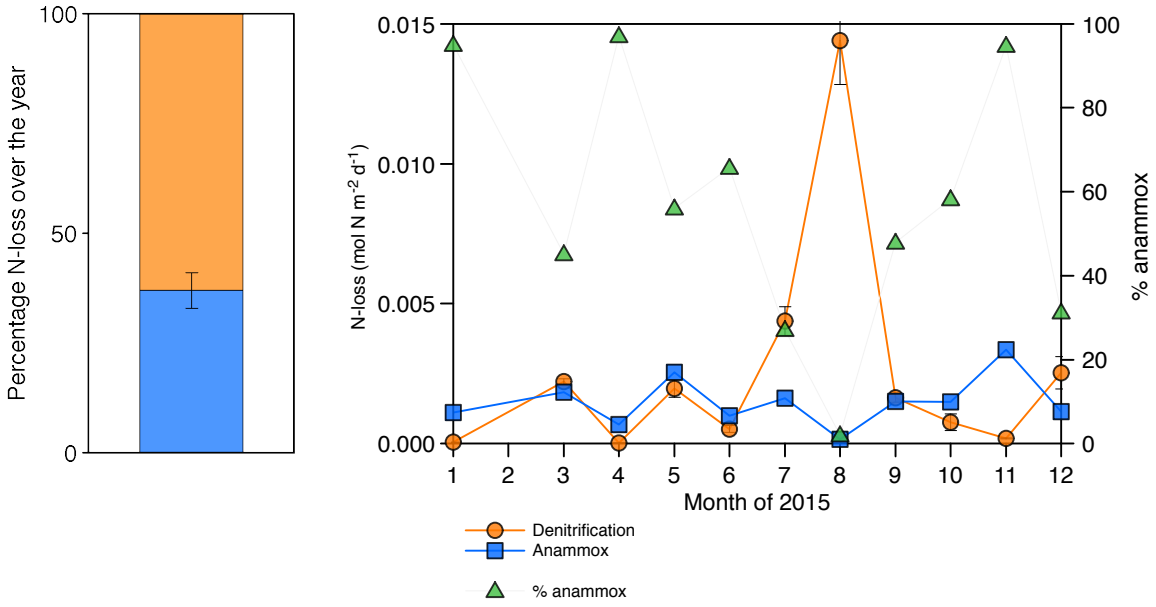

Figure 3.6: *Depth Integrated N-loss.* Depth Integrated N-loss rates over the year through denitrification in orange and through anammox in blue. The black dotted line represents the percentage of N-loss occurring through anammox (in %). The stacked bar represents the averaged N-loss over the entire year.

3.3.5 Microbial community composition

From a total of 6,889,880 sequences quality filtered by the JGI, 0.3% of the reads were discarded because they were too short or too long and 2% of the sequences were identified as chimeras and discarded. The final read count per sample can be found in table C.1. After clustering at the 97% identify threshold, 28,947 OTUs were resolved across 72 samples. The estimated community diversity (chao1) was low and variable in the surface waters and comparably higher and more stable at deeper depths. These results are summarized in figure C.1 and table C.1 of the Appendix C.

The microbial community in SI is vertically stratified with strong shifts in community compositions apparent between the surface waters (10m) and the deeper waters (100m and below) (Figs. 3.7 and 3.8). In particular, there is a shift between high relative abundances of Alphaproteobacteria and Bacteroidetes (together, 42 to 85.3%) in the surface to a higher relative abundance of Gammaproteobacteria (23.4 to 68.5%) in the deeper waters (between 100 and 200m) (Fig.

3.7). In the surface waters, Alphaproteobacteria were mainly comprised of the SAR11 clade and Bacteroidetes of the Flavobacteriales. The cyanobacterial population present early in the year decreases to <1% during the spring bloom (April, May, June), along with a sharp increase in Flavobacteriales for these 3 months (Fig. 3.7 and 3.8). In the deeper waters, the overwhelming majority of the Gammaproteobacteria are associated with two OTUs belonging to the SUP05 cluster (Oceanospiralles clade) (Figs. 3.7 and 3.9, and Appendix C). This trend was constant throughout the year. Another Gammaproteobacterial group Ectothiorhospiraceae (purple sulfur bacteria) were present throughout the year as well in the deeper waters (100 to 200m), with one OTU present between 1 and 30% (Fig. C.3). Thaumarcheotal (Marine Group 1) relative abundance was generally low in the surface waters and increased up to 28% at 100m where NO_3^- concentrations generally peak (Figs. 3.7, C.2 and C.3). In the deeper waters (100 to 200m), the Marinimicrobia clade totalled a few percent throughout the year and increased to up to 12% in November at 135m. Epsilonbacteria were mostly comprised of an OTU from the genus *Arcobacter*, which reached up to 30% at 200m in July 2015 during deep water renewal and remained present at relatively high abundances until September (Figs. 3.7, 3.9 and C.3). Several OTUs from the genera *Ca.* Scalindua (Planctomycetes) were present throughout the water column with a total up to 5.7% at 100m in December 2015 (Figs. 3.7 and 3.9). Members of the Woesearcheota phylum were most abundant at depths from 100 to 200m (0.3% to 12.2%). These results indicate a strong vertical stratification of the water column microbial community and relative consistency in this stratified community throughout the year, with notable exceptions (Fig. 3.8). Surface waters, for example, exhibited considerable dynamics in microbial communities during the spring blooms (April to June), and deeper waters shifted composition following renewal in July (Fig. 3.8).

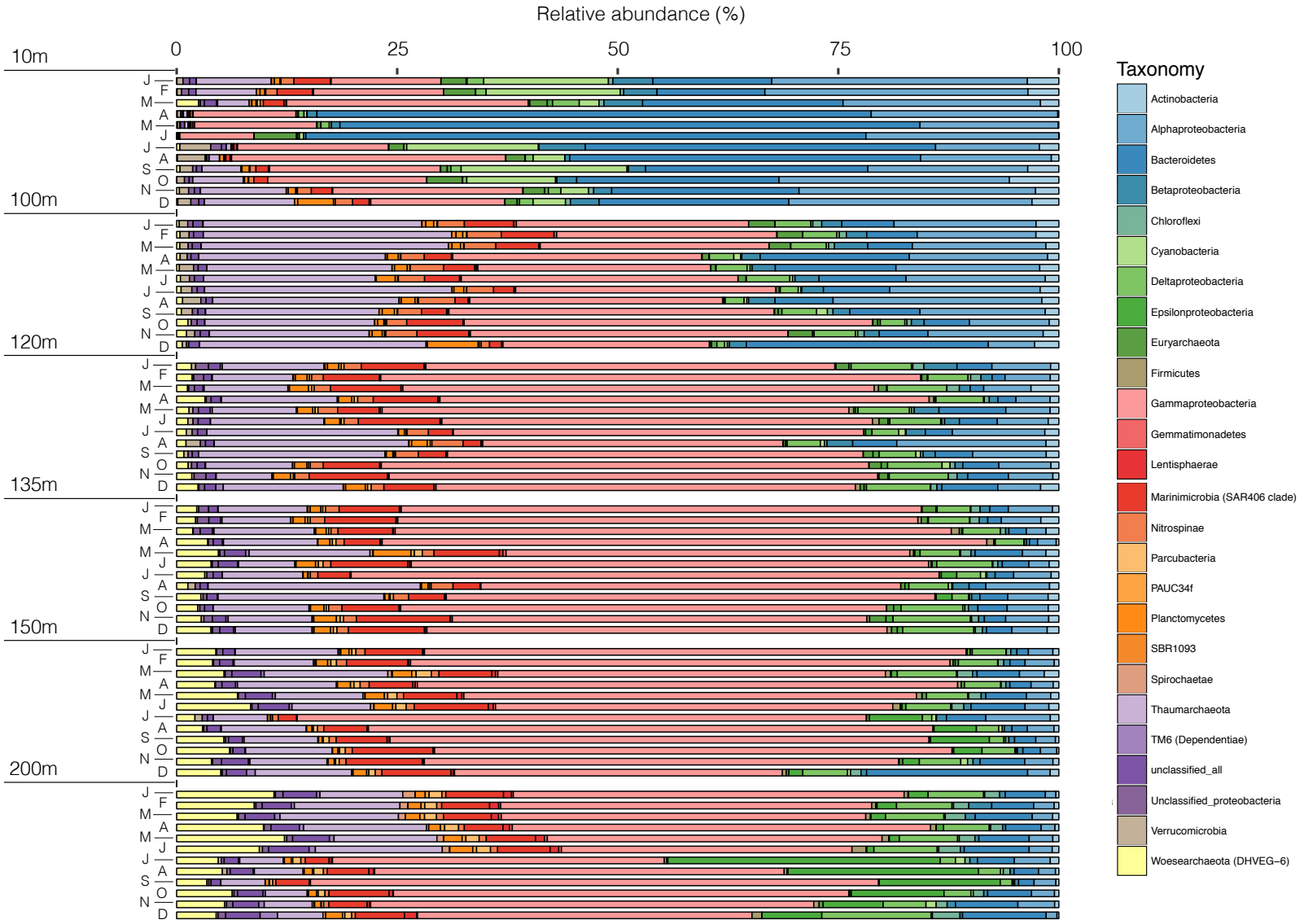

Figure 3.7: *Microbial communities in SI from 16S rRNA gene sequencing.* Microbial communities composition of SI in 2015 for 6 depths (10, 100, 120, 135, 150 and 200m) at the phylum level in relative abundance.

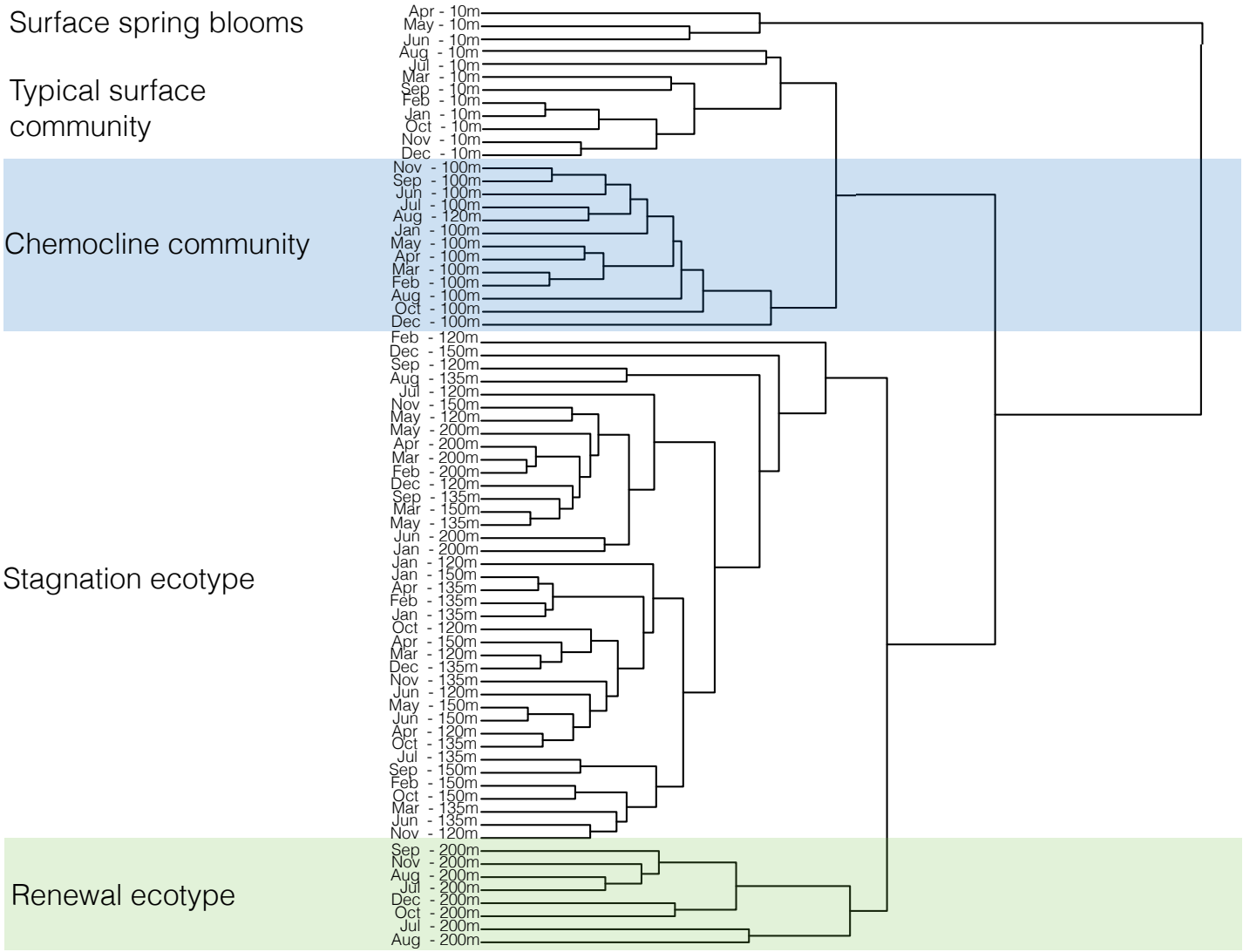

Figure 3.8: *Clustering of the microbial community composition of SI in 2015.* Clustering of the microbial community composition of SI in 2015 for 6 depths (10, 100, 120, 135, 150 and 200m) and 12 months. Dissimilarities between samples is shown by the height of the fusion of the dendrogram: the higher the fusion, the more dissimilar samples are between each other. Clustering of samples was performed in R with the Euclidean method.

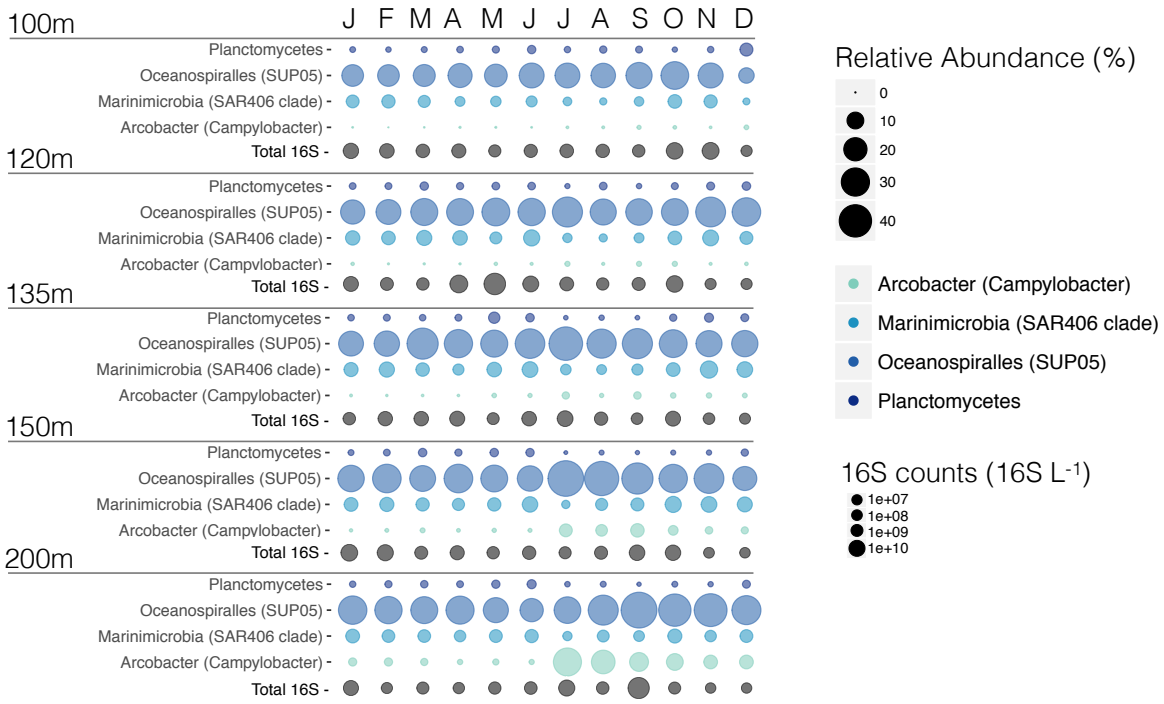

Figure 3.9: *Relative abundance of Planctmycetes, SUP05, Marinimicrobia and Arcobacter.* Comparison of the relative abundance of Planctomycetes, SUP05 cluster Marinimicrobia, and newly highlighted *Arcobacter* bacteria. In addition to the relative abundance of these clades, we added total 16S counts (16S L^{-1}) for each of these samples.

3.4 Discussion

3.4.1 Partitioning of N-loss in SI, and the seasonality of anammox and denitrification

^{15}N-labeled incubations indicate that both anammox and denitrification operated simultaneously throughout the year in the anoxic water column of SI. Although anammox dominated (responsible for >50% N-loss) in 55% of the measurements in which N_2 production was detected (Fig. 3.3a, b and c), depth-integrated rates of denitrification show that it accounts for up to 63% of the total N-loss from SI (Fig. 3.6). Overall, depth-integrated rates of denitrification and anammox ranged between 0.02 to 14.4 mmol m^{-2} d^{-1} and 0.15 and 3.36 mmol m^{-2} d^{-1}, respectively (Fig. 3.6). These integrated rate measurements agree well with rates previously reported based solely

on geochemical measurements [186], which imply N-loss of between 1.7 to 8.1 mmol m^{-2} d^{-1}. Annual N-loss for the inlet was calculated from these measurements by taking the average of the depth-integrated rates, and multiplying these by the surface area of the anoxic basin of SI (33 km^2). Annual N-loss totalled 0.002 Tg N yr^{-1} in 2015. Given that 50% of the N-loss previously reported is from benthic N_2 production, the rates that we measure here, that only capture pelagic N-loss, appear appreciably higher and may thus suggest inter-annual variability in N_2 production rates. Rates of denitrification and anammox were previously reported for 2 months during peak stagnation in SI in 2010 [118] and while these are at the lower end of the range of rates measured here, they generally agree with the rates we detect during peak stagnation.

The monthly variability in rates of N-loss from Saanich inlet are driven through dynamics in rates of both anammox and denitrification. Thus, knowledge on the regulation of both anammox and denitrification is key to knowing how N-budgets in Saanich inlet, and by extension, other anoxic fjords, vary. Partitioning of N-loss between these pathways for the entire year reveals 63% denitrification and 37% anammox. This ratio is close to the theoretical ratio calculated for the partitioning of N-loss in the open ocean through anammox and denitrification (29 to 71% ratio anammox/denitrification ratio). This ratio applies when substrate (NH_4^+) supply rates for anammox are constrained by the stoichiometry of settling organic matter [63, 105, 173–175]. Excursions beyond this ratio might indicate additional sources of NH_4^+, such as sulphate reduction, and/or an input of NH_4^+ from the underlying sediments. Excursion below this ratio more likely signals competition for nitrite or chemoautotrophic denitrification, which would not liberate NH_4^+. In July and December of 2015, N-loss was close to the theoretical ratio (27 and 31%, respectively), which is consistent with the canonical scenario in which heterotrophic denitrification supplies anammox with NH_4^+. The ratio deviates from this throughout much of the rest of the year, with generally higher proportions of anammox (40% and beyond), implying that an additional supply of NH_4^+, beyond that supplied through heterotrophic denitrification, is needed.

Rates of denitrification and anammox are expected to respond to the rates of supply of the principal substrates: NO_3^-, organic matter or HS^- for denitrification, and NH_4^+ and NO_2^- for anammox; as well as possible inhibitors like HS^- for anammox and O_2 for both anammox and denitrification. In July 2015, O_2 and NO_3^- both penetrate to 150m (Fig. 3.2d and e) signalling the

intrusion of oxygenated NO_3^- rich waters to intermediate depths in SI, and although devoid of O_2, deep waters (185 and 200m) contain detectable NO_3^-. These observations indicate intermediate- and deep-water renewal in July. Although our monthly nutrient profiles do not record a strong deep-water renewal that would have oxygenated the deep waters, we do observe changes in nutrient concentrations, which coincide with higher rates of denitrification in July and August (Fig. 3.6). Thus, the regulation of denitrification in SI appears linked to renewal, and is further enhanced by the accumulation of HS^- in August.

A dramatic increase in deep water NH_4^+ concentrations is reflected by relatively high rates of anammox recorded in September, October and November (Fig. 3.6), along with lower concentrations of HS^-, implying that increased deep-water NH_4^+ leads to higher rates of anammox. The NH_4^+ in the deep waters could originate from the remineralization of sinking organic matter supplied through primary production in the surface waters. Chlorophyll *a* peaks in the surface waters of SI, a proxy for the abundance of photosynthetic organisms, vary over the year, and increases during the spring/early summer (Fig. 3.2c). Organic matter from primary production is exported to the deep waters and sediments as particles and fecal pellets. Given that both particles and fecal pellets would sediment to the deep waters in less than a week [200], we expect deep water NH_4^+ concentrations to respond to blooms in the surface waters within 15 days. As we sampled approximately every 4 weeks, it is possible that we lacked the temporal resolution to capture intense degradation activity following a bloom. However, as blooms are a common occurrence during the summer months [33, 201, 202], the increase in the deep-water NH_4^+ concentrations in September (Fig. 3.2g) likely originates from a corresponding increase in surface water primary production. Therefore, the combination of relatively high productivity in surface water and the ensuing high NH_4^+ concentrations in the deep waters likely support relatively high rates of anammox towards the end of the summer.

Though ultimately sourced from primary production, the detailed biogeochemical pathways through which NH_4^+ is made available to anammox can vary. These pathways include: ammonification due to organotrophic denitrification; DNRA; ammonification associated with sulphate reduction; or benthic NH_4^+ efflux. We thus consider these possible sources and their relative fluxes in relation to rates of anammox. Rates of denitrification measured in SI could have supplied

25% of the NH_4^+ needed to support co-occuring anammox on average, assuming Redfieldian OM stoichiometry and 100% organotrophic denitrification (in August 2015, Fig. 3.6). This is unlikely as HS^- clearly influences rates of denitrification, and is consistent with previously reported genomic information [33, 182], which implies chemoautotrophic denitrification in SI. Another source of NH_4^+ could be organotrophic NO_3^- reduction to NO_2^-.

We calculate that the highest potential rates of NO_3^- reduction to NO_2^- recorded in August 2015 (Fig. 3.4e, 400nM N hr^{-1} for 20μM NO_3^- addition), are sufficiently high such that all of the NH_4^+ needed to support the highest rates of anammox found could come from this reaction (13.7 nM hr^{-1}). However, *in situ* NO_3^- concentrations are generally not as high as the concentrations in these amended incubations, and thus rates of NO_3^- reduction to NO_2^- might not supply all the NH_4^+. Remineralization of organic matter through partial or complete denitrification is thus likely only partly responsible for the NH_4^+ supply to anammox. Similarly, SO_4^{2-} reduction could also produce NH_4^+ through remineralization of organic matter in the water column. In SI, however, sulfate reduction remains unmeasured through direct process rate experiments but functional markers for canonical sulfate reduction were found in the metaproteomes generated to date for SUP05 [33]. DNRA can also supply NH_4^+ to anammox, as it does in the Peruvian OMZ [67]. A DNRA catalyzing-like protein, hydroxylamine-oxidoreductase, was recovered in metaproteomes and appears to be associated with the dentrifier SUP05 [33]. DNRA, however, has not been detected in SI to date, though modeling predicts appreciable DNRA for September 2009, and DNRA, if operating in SI, could thus contribute to dynamics in anammox activity [118]. Given that the pelagic pathways for NH_4^+ delivery to annamox appear insufficient to support the measured rates, we consider the possibility that NH_4^+ efflux from the bottom sediments also contributes NH_4^+ to anammox. Indeed, high rates of organic matter remineralization through SO_4^{2-} reduction characterize SI sediments [185]. Some of the NH_4^+ liberated in the process would diffuse from the sediment and could advect upwards to fuel anammox in the overlying water. Based on our calculations (see Appendix C), NH_4^+ fluxes from the sediment in SI could fuel 88 to 100% of the NH_4^+ required to support anammox. We thus expect a combination of these multiple NH_4^+ sources fuels anammox and contributions to its variability throughout the year.

3.4.2 Kinetics of denitrification and anammox

External forcing by substrate supply rates places overall constraints on material fluxes and thus microbial community metabolism, but microbial community structure and function also depend on the specific ecophysiologies of relevant organisms, such as an organisms ability to take up and metabolize a given substrate. We showed that denitrification in SI appears to depend on NO_3^- concentrations (Fig. 3.4c and table 3.2), and the K_m for NO_3^- obtained at 165m in August 2015 was 5 μM and in the same range as earlier reports from both environmental measurements and cultured denitrifiers (1.7 to 10μM) [56]. These prior kinetic constants come from pure cultures of organotrophic denitrifiers [203, 204], sediment microbial communities [110, 205], and an anoxic sulfidic fjord [56]. When NO_3^- concentrations exceeded 15μM, however, the rates of complete denitrification decreased (Fig. 3.4f). This is in line with the observation that denitrifiers tend to favor the first step of denitrification, NO_3^- reduction to NO_2^-, over complete NO_3^- reduction to N_2, when NO_3^- concentrations are high. Similar observations were made previously in Mariager fjord [56] where NO_3^- reduction to NO_2^- took over when NO_3^- concentrations exceeded 5μM.

Rates of denitrification and anammox in SI are sensitive to the HS^- concentrations present. When seawater from 120m depth (June 2015) was amended with HS^-, rates of denitrification increased with respect to HS^- concentrations (Fig. 3.5) for HS^- concentrations higher than 2.5μM. The rates then seemed to exhibit a linear response, possibly because the enzyme saturation for sulphide oxidation is much higher [56]. This, observation is similar to reports of a linear dependency of denitrification on HS^- concentrations, with no sign of saturation, up to 40μM HS^- in Mariager Fjord, Denmark [56]. Measurements of NO_3^- and NO_2^- indicate low or no NO_2^- accumulation during these incubations and, given the low rates of denitrification for 2.5μM HS^-, this implies a shunting of the NO_2^- produced to anammox. Indeed, anammox occurs with HS^- amendment (Fig. 3.5d). Anammox occurrence at low HS^- concentrations was observed previously in a sulphidic alpine lake [107], in contrast with most previous marine observations, which found that anammox was inhibited by HS^- at concentrations as low as 1.6μM [100, 114]. The stimulation of anammox with low HS^- concentrations in SI may reflect the production of NO_2^- through partial denitrification (when the relevant substrates such as HS^- are abundantly available) and

the bypass of complete denitrification due to a higher affinity of anammox bacteria for NO_2^- [110]. This is supported by the fact that NO_2^- did not accumulate during these incubations (Fig. 3.5a), implying that sulfide dependent partial denitrification (NO_3^- to NO_2^-) underpins nitrite leakage to anammox in SI.

As rates of anammox appear to be sensitive to higher fluxes of NH_4^+ in the water column (see above), we plotted the rates of anammox obtained for the whole year vs. the *in situ* NH_4^+ concentrations (Fig. 3.10). However, the lack of a coherent positive relationship between rates of anammox and NH_4^+ concentrations generally implies insensitivity of anammox to NH_4^+ concentrations higher than 2μM. These results could indicate that the K_m for NH_4^+ of anammox bacteria is lower than the *in situ* NH_4^+ concentrations. Alternatively, this could also indicate that anammox bacteria could obtain the NH_4^+ needed through tight coupling between anammox and DNRA [64] or through ammonification in particle-associated processes [206], which would not be specifically recorded in the ambient NH_4^+ concentrations in SI.

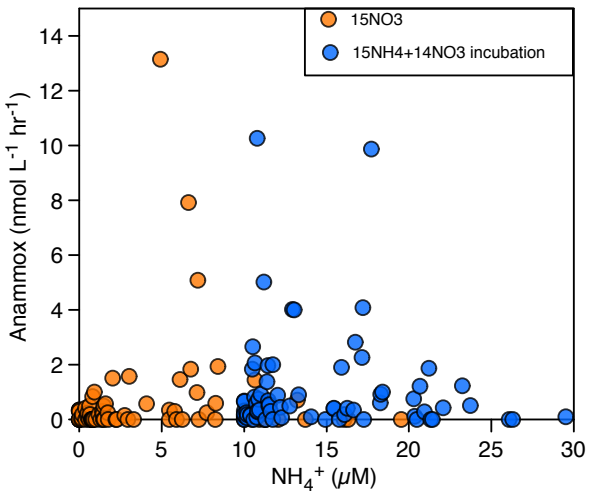

Figure 3.10: Comparison of anammox rates vs *in situ* NO_3^- concentrations (μM)

3.4.3 Vertical partitioning of the microbial communities in SI

The strongest difference in microbial community composition was between the surface waters at 10m depth and deep waters below 100m depth (Fig. 3.8), while temporal variations were most

notable in the surface waters (Fig. 3.8). Variation in community composition between 120 and 200m depth was comparatively small as were dynamics in deep water community composition throughout the year, with the exception of OTUs assigned to the Epsilonproteobacterium, *Arcobacter* (Fig. 3.7). Such vertical stratification in microbial community composition is typical for aquatic ecosystems including OMZs [104, 120, 207], and has been previously observed in SI [33, 183] . Indeed, niche partitioning along redox gradients is generally expected [104]. A conceptual model previously developed [33] describes microbial community structure and function in SI and provides a benchmark framework through which to view temporal and vertical dynamics in microbial community composition (Figs. 3.1c, 3.7 and 3.8 , 3.9, C.2 and C.3). The key taxa that comprise this model, including SUP05, Marinimicrobia, Thaumarcheota, SAR11, and Planctomycetes were prevalent community members throughout SI in 2015. Thamarcheaota and SAR11 were the most abundant at 100m and SUP05 increasing in abundance with depth. Planctomycetes were low in the surface water and increased to a few percent in the deeper waters, similar to Marinimicrobia. In addition to these taxa, our community profiles reveal dynamics in relatively abundant Bacteroidetes, which increase in the surface waters during the spring bloom (from 20% to 65% in April, May and June) and *Arcobacter* that appears to bloom in the deep waters (from $<$1% up to 30% at 200m) in association with renewal in July and subsequently decreases in relative abundance in the following month.

A closer analysis of microbial community dynamics in the surface waters reveals that of the 15 most abundant OTUs, there were high relative abundances of 3 OTUs of the Flavobacteriaceae and 1 OTU of the Rhodobacterales family in April, May and June, and correspondingly low abundances of an OTU belonging to the SAR11 clade (Fig. C.3). This particular microbial community composition appears contemporaneous with photosynthetic blooms. Flavobacteriaceae and Rhodobacterales are generally considered participants in biomass degradation [208] and their relatively high abundance in the spring may thus be a response to relatively strong photosynthetic activity (Fig. 3.2c). While photosynthetic blooms are evident from pigment distributions (Fig. 3.2c), we did not observe correspondingly high relative abundances of photosynthetic bacterial taxa (cyanobacteria) at this time. This likely indicates that cyanobacteria play a limited role in this bloom, which instead is the response of diatom growth, as previously reported [200]. Diatom

blooms in April, May, and June thus appear to stimulate a number of microbial taxa linked to organic matter degradation in the surface waters, while cyanobacterial contributions to microbial community composition are marginalized at this time.

One of the most abundant OTUs present throughout the water column was assigned to the SUP05 cluster (C.3), which varied between a few percent in the surface water to a maximum of 48% in July and September at 150 and 200m, respectively (Figs. 3.9 and C.3). Based on its metabolic potential to couple sulphide oxidation to NO_2^- reduction to N_2O and its relatively high abundance, SUP05 has been implicated as a key-player in coupled C, N and S cycling and N-loss from SI [33, 182], and more broadly throughout low oxygen marine waters globally [209–211]. Consistent with this, we find that N_2 production through denitrification was active throughout the year when SUP05 was a ubiquitously abundant community member (Figs. 3.7, 3.9 and C.3). Likewise, water in collected from 120m in June had a microbial community composition with 28% SUP05, and rates of denitrification in this water increased in response to HS^- addition, indirectly linking SUP05 to sulphide dependent denitrification. However, N_2O did not accumulate in our incubations, and we thus suspect that other taxa also play a role in denitrification, by reducing N_2O to N_2.

Some Marinimicrobia clades indeed possess the *nosZ* gene and have the metabolic potential to perform this last step in dentrification [187]. Like SUP05, Marinimicrobia were relatively abundant in the deep waters where they comprised 4 different OTUs that together comprise up to 12% of the total microbial community at 135m in November 2015 (Figs. 3.7, 3.9, 3.11a and C.3). These 4 OTUs were phylogenetically compared to previously identified Marinimicrobia genome bins and SAGs (Fig. 3.11b, [187]) and were found to be affiliated to 4 different clades: 3 SI clones (SHBH1141, SHBH319 and SHAN400) as well as an Arctic clone (Arctic96B-7). Interestingly, only SHBH1141 appear to carry the *nosZ* gene [187], making it the most likely microorganism in SI to reduce N_2O to N_2 coupled to HS^- oxidation [33]. The SHBH1141 clade increased with depth, with the overall highest relative abundance at 150m (Fig. 3.11a). However, SHBH1141s relative abundance decreased in July, in association with the renewal. Comparatively, SHAN400 clade stays relatively constant between 100 and 200m and both Arctic96B-7 and SHBH391 have higher relative abundance at 120m than at 100m and remain constant down to 200m. From SAGs,

SHAN400 and Arctic96B-7 were shown to carry NO_3^- reduction to NO coupled to HS^- oxidation, thus participating to partial denitrification, whereas no genes involved in the N-cycle was found for SHBH391 [187].

Anammox was also operative throughout the entire year in 2015, and accordingly, we found members of the Planctomycetes phylum present at up to 5% in the water column (Figs. 3.7,3.8 and 3.9). Indeed, Planctomycetes is the only phylum known to contain bacteria that perform anammox. The metabolic potential for anammox is restricted in the Planctomycetes to the order Brocadiales [62]. SI hosts mainly *Ca.* Scalindua, a well-known marine anammox bacterium which comprised up to 2.6% of the community at 135m in May (Fig. 3.9). Altogether, microbial community profiling reveals that the key taxa that comprise previous conceptual models for coupled microbial C, N, and S cycling in SI are present and relatively abundant at depths between 100 and 200m throughout the year. At the community level, these taxa collectively underpin N cycling and loss from Saanich inlet, which we demonstrate through contemporaneous process rate measurements.

In addition to the taxa discussed above, it appears that an OTU assigned to the Epsilonproteobacteria *Arcobacter* increases dramatically in relative abundance in the deep waters, notably at 200m where it goes from $<$1% in June to 30% in July, becoming one of the 15 most abundant OTUs in SI, and then drops to 20% in August (Fig. 3.9a and Fig. 3.11a). This increase in relative abundance appears to be a response to deep water renewal and is strongly correlated with the enhanced rates of denitrification found in July and August, relative to the rest of the year, as well as the highest rates of dark carbon fixation (Fig. 3.3d). Indeed, a number of *Arcobacter* isolates are known to perform complete denitrification (NO_3^- to N_2) [212], as well as sulphide oxidation [213]. The high relative abundances of *Arcobacter* in July and the fact that Marinimicrobia OTUs decreased at the same time posits an important role for *Arcobacter* in the SI N-cycle (Fig. 3.9).

Considering our observations of microbial community and biogeochemical dynamics across the year, we suggest that the inlet exists in two principle biogeochemical states: throughout much of the year, the inlet is relatively stagnant, anaerobic N_2 production is distributed between anammox and denitrification and we suggest that *Ca.* Scalindua, SUP05, and Marinimicrobia are the key taxa responsible; during the summer renewal the input of NO_3^- to deep sulphide-rich waters stimulates the growth of *Arcobacter*, which drives most N_2 production through

denitrification marginalizing anammox. These two states thus define microbial community phenotypes representing background or stagnation periods and renewal periods, respectively.

Shifts between stagnation and renewal phenotypes imply that the relevant community members possess differing ecophysiology. In particular, the bloom in *Arcobacter* in response to renewal implies that these organisms have higher maximum cell specific growth rates and/or lower biomass yield than the combination of SUP05 and Marinimicrobia. Without any existing information on biomass yield, we thus estimated cell-specific rates of N_2 production through denitrification during stagnation and renewal periods. We expect for the combined Marinimicrobia/SUP05 population to have lower cell specific rates in comparison to the *Arcobacter* population, which produces N_2 at higher rates for similar cell abundance. For the stagnation phenotype we used an average cell abundance of $1.64 \cdot 10^9$ cells L^{-1} for the combined abundance of Marinimicrobia and SUP05, which we estimated by combining qPCR of the bacterial 16S rRNA gene as a proxy for total community size with the relative Marinimicrobia/SUP05 abundance from our amplicon sequence data. Marinimicrobia, in association with SUP05, are likely responsible for the production of N_2 throughout most of the year, and we used the lowest and highest rates of denitrification in the stagnant period (0.01 – 38.45 nM hr^{-1}) to come up with a range of cell specific denitrification rates for Marinimicrobia/SUP05 between 0.0001 – 0.6 fmol N_2 $cell^{-1}$ d^{-1}.

To compare against the renewal phenotype, we estimated *Arcobacter* cell abundance (based on total bacterial 16S rRNA gene copies for July at 200m, $3.05 \cdot 10^9$ cells L^{-1} combined with the relative abundance of *Arcobacter* from our amplicon sequence data) and with the corresponding rates of denitrification obtained cell-specific rates of 1.08 fmol N_2 $cell^{-1}$ d^{-1} for *Arcobacter*. The cell-specific rates for Marinimicrobia are therefore lower than the cell-specific rate calculated for *Arcobacter*. Thus, it is likely that SUP05/Marinimicrobia population has a higher growth yield to *Arcobacter*, shown by similar cell abundance but lower cell-specific rate for the former.

The low relative abundance of Planctomycetes associated with lower N_2 production rates indicate that the anammox bacteria present in SI have a high cell-specific growth rate with a low growth yield. Again, based on the 16S abundance obtained from qPCR analysis applied to the average relative abundance of anammox bacteria, cell-specific rates for anammox vary between 0.02 and 6.72 fmoles NH_4^+ $cell^{-1}$ d^{-1}, using an average cell counts for anammox for the

year ($2.3 \cdot 10^7$ anammox cells L^{-1}) and the highest and lowest rates measured in SI in 2015. Our measured rates encompass the cell specific rates obtained from the Namibian OMZ [4.5 fmol NH_4^+ $cell^{-1}$ d^{-1}, [66]], the Black Sea [3-4. fmol NH_4^+ $cell^{-1}$ d^{-1}, [114]], and diverse bioreactors [2-20 fmol NH_4^+ $cell^{-1}$ d^{-1}, [61]]. The lower end of our measured rates might be explained by small fractions of active versus total anammox bacteria present, which would increase the cell-specific rates calculated here. This highlights that, even though anammox bacteria are generally present in at lower relative abundances than denitrifiers (SUP05, Marinimicrobia and/or *Arcobacter*), they play a similar role in N-species transformations and N_2 production as well as overall energy transduction in low-oxygen and anoxic marine waters.

3.4.4 Model of NO_2^- competition between anammox and complete denitrification

Based on the results described above, we built a flux balance model to study the competition for NO_2^- between anammox and complete denitrification, testing if we could reproduce the rates corresponding to the two community phenotypes proposed (high or low N_2 production). Lower rates of denitrification are attributed to a stagnation phenotype, whereas higher rates of denitrification correspond to a renewal phenotype (Fig. 3.12). The rates of anammox, NO_3^- reduction to NO_2^-, and complete denitrification (NO_2^- to N_2), are described through Michaelis-Menten equations, depending on both substrates (electron donors and electron acceptors), their respective kinetic parameters (k_m and V_{max}) for each of these substrates, cell abundance and biomass yield (Y) (see Appendix C for a complete description of the model). Both NO_3^- reduction to NO_2^-, and complete denitrification are sulphide-dependent. Nutrient concentrations of interest (NO_3^-, NO_2^-, NH_4^+ and HS^-) are calculated based on the rates of anammox, NO_3^- reduction to NO_2^-, and complete denitrification, as well as fixed input fluxes of the substrates through possible advection and diffusion (see Appendix C). These fluxes, however, are fixed throughout the simulation and do not reflect the highly dynamic nature of the nutrient fluxes found in SI, specifically through a renewal event. This model has thus been built to represent the two phenotypes introduced in the previous section in a steady-state scenario.

The stagnation phenotype represents the background state and characterizes the inlet throughout most of the year, with limited input of NO_3^- and higher fluxes of NH_4^+ and HS^- coming from

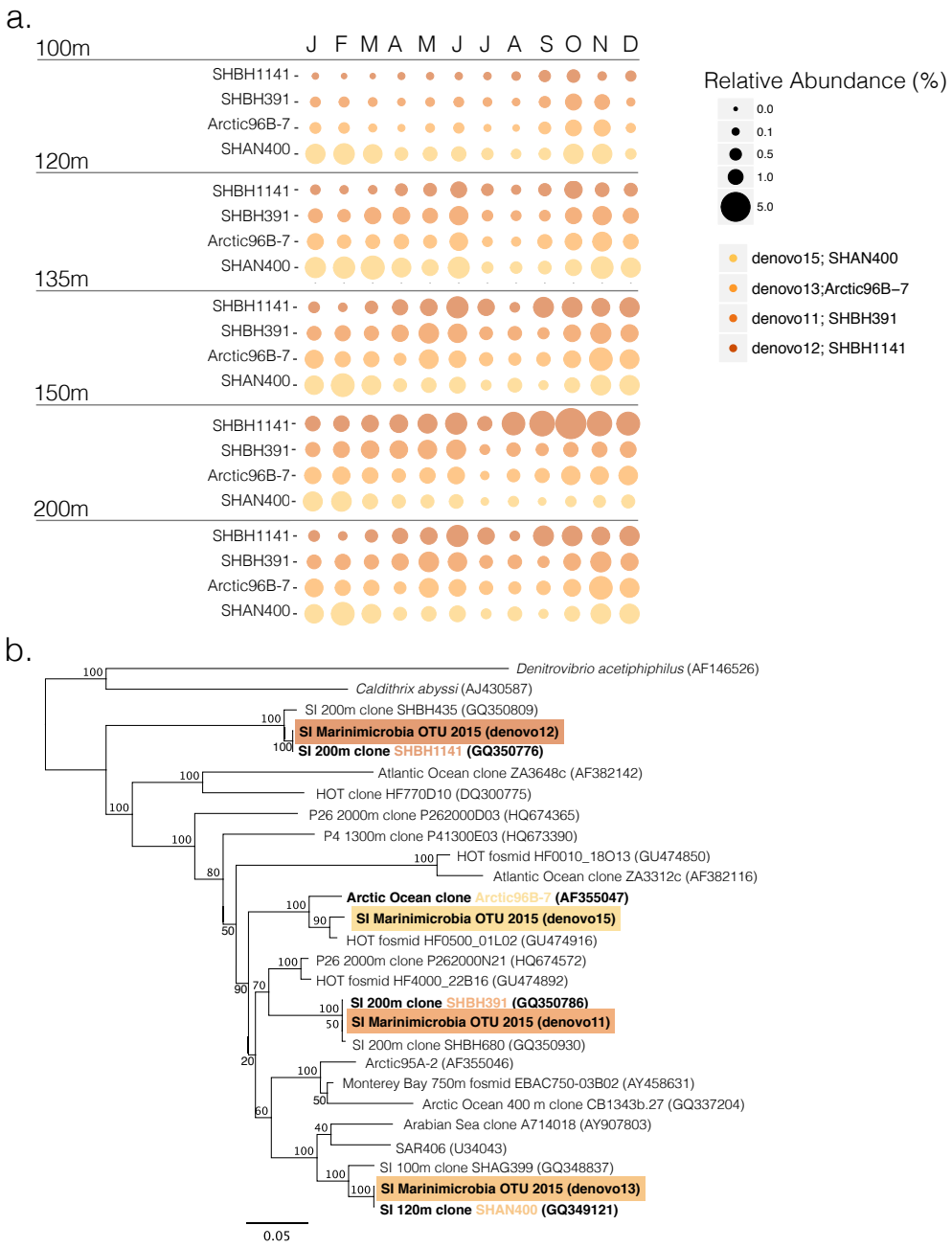

Figure 3.11: *Marinimicrobia OTUs in SI, 2015* OTUs from the Marinimicrobia phylum in SI. (a) Relative abundance of the 4 most abundant OTUs of the Marinimicrobia phylum in SI plotted by depths and months (b) maximum-likelihood phylogenetic tree of the small subunit rRNA for sequences of the Marinimicrobia clade (ML implemented with RaxML, 100 bootstraps). OTUs identified in this study are highlighted in a colored box. Previously identified SAGs or genome bins are in bold. The bar represents 5% estimated sequence divergence. Bootstrap value at the branch node indicate the robustness of the branching of the tree

the sediments underlying the anoxic water. To mimic this situation, we thus chose lower input flux of NO_3^- in comparison to NH_4^+ and HS^- (Fig. 3.12 and table 3.3). Kinetic parameters (K_m and V_{max}) for anammox bacteria were taken from the literature [109]. Kinetic parameters measured for denitrification in SI were determined during the renewal phenotype (August 2015, 165m) and therefore, the stagnation pehnotype kinetic parameters remained unconstrained. Thus, kinetic parameters for the SUP05/Marinimicrobia consortium (or stagnation phenotype) were fit to yield rates of the same order of magnitude for denitrification as those measured in SI during stagnation (Fig. 3.12, table 3.3 and Appendix C). However, cell-specific growth rates (V_{max}) and growth yield (Y) were estimated based on rates of denitrification and cell abundance (see above). With nutrient fluxes appropriate for the stagnation period and reasonable physiological parameters for the relevant organisms, we find that rates of both denitrification and anammox are similar, and fall within the range observed in SI outside of a renewal period (Fig. 3.12a, Fig. 3.3). The dominance of one pathway over another could be inverted by changing the relative K_m values for denitrification and anammox, as these appear to be similar to one another in the stagnation period (see Appendix C). Modeled abundances of anammox bacteria were similar to those observed in SI ($2.3*10^7$ anammox cells L^{-1}) as well as the modeled abundances of complete denitrifiers than observed in SI (cell abundance of Marinimicrobia/SUP05=10^9 cells L^{-1}). Therefore, we could reproduce with a simple flux balance model rates of the same order of magnitude for anammox and complete denitrification measured during the year 2015 during peak stagnation in SI.

Deep water renewal in SI introduces oxygenated water to the deep basin, where NO_3^- is produced through rapid nitrification, and the NO_3^- produced is in turn lost through anaerobic NO_3^- reduction and N_2 production following renewal. The renewal event is thus far away from steady-state, and we therefore tried to reproduce the high rates of denitrification in 60 days of the simulation, corresponding to the approximate duration of the event based on the geochemical profiles and rate measurements. The kinetic parameters for anammox parameters were identical to simulations of the stagnant phenotype, however, we changed the kinetic parameters for denitrification to represent *Arcobacter* in the renewal phenotype. As NO_3^- dependency was measured in August 2015, corresponding to higher rates of N_2 production, we chose to use the Michaelis-Menten constants modeled from this data to describe complete denitrification (NO_3^- to

N_2) (tables 3.2 and 3.3). We also chose a higher cell-specific growth rate than in the 'background' phenotype (table 3.3), as it appears that the *Arcobacter* population grows rapidly from <1% to 30% of relative abundance within a months time (table 3.3). The simulation reveals that under the conditions described here (Fig. 3.12b and table 3.3), rates of denitrification reach 10^{-6} N_2 M d^{-1}, which corresponds to the highest rates measured in July 2015 at 200m (Fig. 3.3). Rates of anammox remain similar to the rates that can be found after renewal in SI (Figs. 3.3 and 3.11b). The abundance of complete denitrifiers reaches 10^9 cells L^{-1} after only 15 days of simulation, which is again similar to abundances observed in SI during renewal. However, to fully mimic the input fluxes in SI, the model would need to have dynamic fluxes that can be changed over time. In addition to dynamic fluxes, competition between two different population of complete denitrifiers should be implemented to fully study the transition between one phenotype to the other.

3.4.5 SI as a model ecosystem for coastal OMZs

We have extrapolated the annual N-loss calculated for SI (33 km^2) to all similar coastal inlets in BC (2478 km^2) in order to estimate the possible importance of BC coastal fjords to N-loss from the North Eastern Sub-Arctic Pacific Ocean. We estimate that these inlets could contribute up to 0.12 Tg N yr-1, which constitutes 0.1 % to global pelagic N-loss [165] if they are all anoxic and similar to SI. On an area-specific basis this is extremely high in comparison to the ETSP, for example, which has a surface area of $1.2 \cdot 10^6$ km^2 and supports up to 10 Tg N yr^{-1} [60]. This highlights that coastal OMZs are hotspots for N-loss and could also, in the near future, be subject to changes due to increased anthropogenic influence.

The low oxygen conditions in SI support pelagic anaerobic microbial metabolisms including denitrification and anammox that co-occur and underpin high rates of N-loss from the water column. We showed that denitrification is the most important contributor to N_2 production and its rates and the organisms responsible vary seasonally. Rates of anammox, in contrast, are relatively constant throughout the year, contributing 37% of the N-loss from SI. Anammox is often reported as the primary pathway of N-loss from OMZs [18, 60, 65–67, 84, 98, 154], and our time-series observations from SI may be more broadly extensible to low oxygen marine waters globally. In SI, rates and pathways of N-loss and the responsible microbial taxa are dynamic

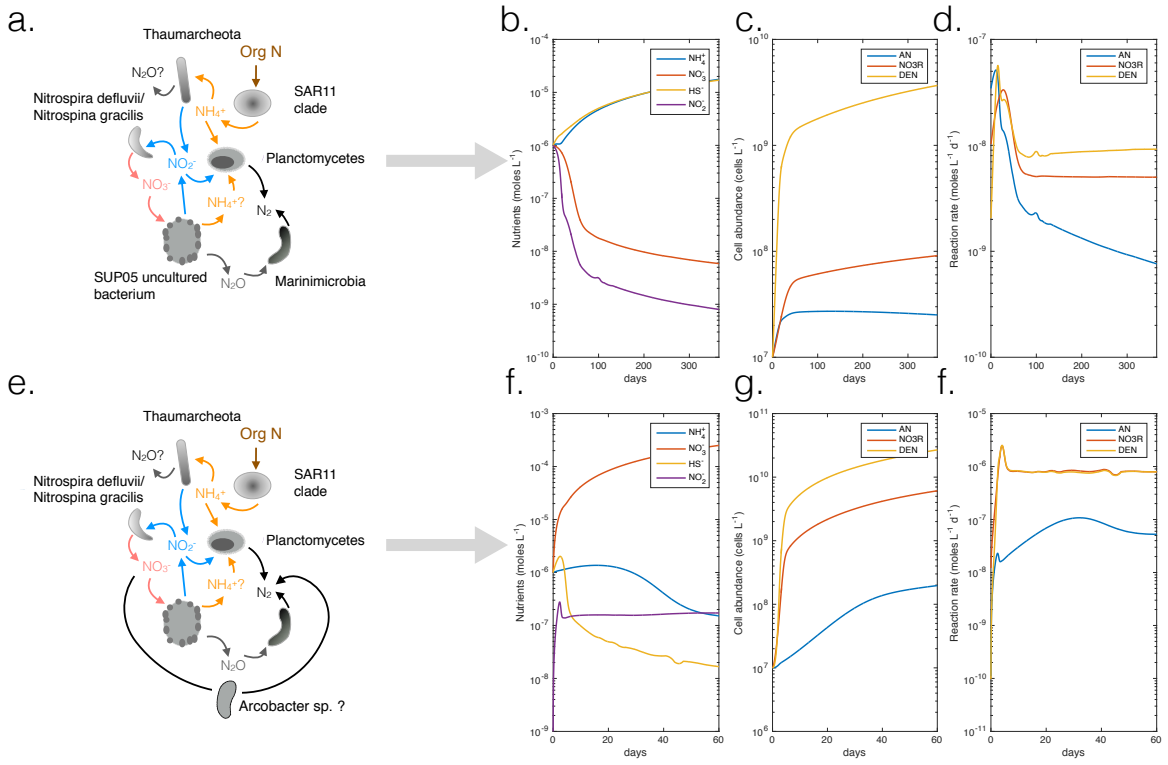

Figure 3.12: *Model of NO_2^- competition between anammox and complete denitrification* model of NO_2^- competition between anammox and complete denitrification for the 2 phenotypes found in SI, stagnation phenotype and renewal phenotype. a) represents the phenotype found in SI during stagnant periods of time. (b, c and d) shows a simulation of the model that tested to see if the phenotype of the phenotype could be reproduced through modeling. Parameters used to model this simulation can be found in table 3.3. c) represents the second phenotype found in SI during renewal event, leading to higher N_2 production (d, e and f) shows that the model reproduced higher rates of N_2 production. Parameters used in this simulation can be found in table 3.3.

Table 3.3: Parameters used in model for competition of NO_2^- between anammox and complete denitrification (Fig. 3.12)

Ecotype	Parameters	Value & units	Reference
'Stagnation'	R_{NO3}	$5x10^{-9}$ moles L^{-1} d^{-1}	State of stagnation in SI
	R_{NO2}	$5x10^{-9}$ moles L^{-1} d^{-1}	"
	R_{NH4}	$5x10^{-8}$ moles L^{-1} d^{-1}	"
	R_{HS}	$5x10^{-8}$ moles L^{-1} d^{-1}	"
	K_{m_AN} for NH_4^+	3 µM	Awata et al. 2013
	K_{m_AN} for NO_2^-	0.45 µM	Awata et al. 2013
	$K_{m\_DEN\ \&\ NO3R}$ for HS^-	10 µM	Jensen et al. 2009 and this paper
	$K_{m\_DEN\ \&\ NO3R}$ for NO_2^- or NO_3^-	1 µM and 5 µM	Fit the rates in SI
	V_{max} (AN, NO3R)	$2x10^{-14}$ moles N_2 $cell^{-1}$ d^{-1}	Strous et al. 1999
	V_{max} (DEN)	$2x10^{-15}$ moles N_2 $cell^{-1}$ d^{-1}	Fit the rates in SI
	Y_{AN}	$5x10^{13}$ cell (moles ED)$^{-1}$	Louca et al. 2016
	Y_{NO3R}	$5x10^{14}$ cell (moles ED)$^{-1}$	Fit the rates in SI
	Y_{DEN}	$5x10^{15}$ cell (moles ED)$^{-1}$	"
'Renewal'	R_{NO3}	$5x10^{-6}$ moles L^{-1} d^{-1}	After renewal in SI
	R_{NO2}	$5x10^{-8}$ moles L^{-1} d^{-1}	"
	R_{NH4}	$5x10^{-7}$ moles L^{-1} d^{-1}	"
	R_{HS}	$5x10^{-8}$ moles L^{-1} d^{-1}	"
	K_{m_AN} for NH_4^+	3 µM	Awata et al. 2013
	K_{m_AN} for NO_2^-	0.45 µM	Awata et al. 2013
	$K_{m\_DEN\ \&\ NO3R}$ for HS^-	10 µM	Jensen et al. 2009 and this paper
	$K_{m\_DEN\ \&\ NO3R}$ for NO_2^- or NO_3^-	5 µM	This paper, August 2015 (165m)
	V_{max} (AN, NO3R)	$2x10^{-14}$ moles N_2 $cell^{-1}$ d^{-1}	Strous et al. 1999
	V_{max} (DEN)	$2x10^{-13}$ moles N_2 $cell^{-1}$ d^{-1}	Fit the rates in SI
	Y_{AN}	$5x10^{13}$ cell (moles ED)$^{-1}$	Louca et al. 2016
	Y_{NO3R}	$5x10^{14}$ cell (moles ED)$^{-1}$	Fit the rates in SI
	Y_{DEN}	$1.5x10^{15}$ cell (moles ED)$^{-1}$	"

responding to substrate fluxes driven by physical forcings. Analogous dynamics in upwelling and horizontal transport or large-scale eddies in open ocean OMZs may also lead to strong microbial responses with corresponding biogeochemical outcomes [103, 214]. While sulphidic conditions that characterize SI are rare in modern open ocean OMZs, they could become prevalent with progressive ocean deoxygenation [121, 210]. Information on microbial responses to system dynamics and on the ecophysiology the underpins coupled C, N, and S cycling in Saanich Inlet and other experimentally tractable coastal ecosystems is key for predicting broader global responses to ocean deoxygenation and the expansion of marine anoxia.

Chapter 4

Combining microbiological and geochemical information to constrain energy flow through the marine N-cycle

Modern oceans contain large volumes of anoxic water that are currently expanding due to anthropogenic activities. Importantly, high rates of anaerobic N-metabolisms characterize these anoxic waters, resulting in intense cycling of N through microbial metabolisms. This can either lead to N-loss or N-retention, depending on the partitioning of N-reduction across denitrification, anammox, and dissimilatory NO_3^- reduction to NH_4^+ (DNRA). The outcome therefore influences marine N-budgets and thus can impact biological production, the marine C-cycle, and climate. While substrate supply rates are a first order control on the rates of N-reduction, the controls on partitioning across the different pathways remain uncertain and this confounds efforts to predict the response of the marine N-cycle to deoxygenation. Here we show that DNRA dominates N-reduction on an annual basis in Saanich Inlet, a persistently anoxic fjord that serves as an analogue for anaerobic marine microbial metabolisms. While anammox and denitrification play an important role throughout most of the year, high rates of DNRA develop following introduction of new oxidants and substrates to the anoxic deep-waters during renewal events. These events provided enhanced energy fluxes, or power supply, that fueled higher rates of N-reduction and altered the microbial community structure and metabolic potential. Notably, changes in microbial community abundance, structure and metabolic potential did not scale with corresponding metabolic rates, and this undermines attempts to model biogeochemical cycling with gene-centric modeling theory, which inherently relies on such scaling. The observation that

DNRA emerges transiently, to dominate N-reduction, in response to physical perturbations that enhance power supply, suggests that N-recycling should be considered in models that aim to predict biogeochemical responses to ocean deoxygenation.

4.1 Introduction

Nitrogen (N) is an essential nutrient for life and thus often limits primary production in the oceans. The marine N-cycle, therefore, is tightly coupled to biological CO_2 sequestration, creating feedbacks between N biogeochemistry and climate [9, 215] – dynamics in ocean N-inventories can thus have large-scale effects on the Earth system [157]. Ocean N-inventories are primarily set by the balance between fixation of atmospheric N_2, largely by photosynthetic microorganisms inhabiting the sunlit surface ocean [9], NO_3^--supply via terrestrial runoff, and removal by N_2 producing organisms in anoxic regions of the oceans and coastal sediments [9, 216]. N-scarcity in the oceans develops when biological N-fixation and terrestrial nitrate runoff is outpaced by N_2 production, which can happen when marine anoxic water masses expand [16, 217]. N-loss under anoxic conditions, however, can be short-circuited by dissimilatory nitrate reduction to ammonium (DNRA), or counteracted by enhanced N-fixation within or beyond the euphotic zone. Dynamics between these interacting processes ultimately control ocean N-inventories impacting primary production and climate [42, 44, 178].

Connections between ocean N-inventories, marine anoxia, N-fixation, anaerobic N-metabolisms, primary production, and climate are evident throughout Earth's history, with notable examples during the Paleoproterozoic [2.5 – 1.6 Ga ago, [16, 39, 44, 178, 217, 218]] and during Phanerozoic Oceanic Anoxic events (OAEs)[219]. Indeed, N-scarcity may have characterized much of the Paleoproterozoic due to a combination of appreciable nitrification, supported by oxygen in the surface ocean, and volumetrically expansive masses of underlying anoxic ocean waters supporting denitrification and possibly anammox [16, 39, 217, 218]. Such N-scarcity could have limited global biological productivity, influencing atmospheric chemistry and climate [16, 217, 218]. Other N-metabolisms, such as N-fixation or DNRA however, likely counteracted N-loss to maintain N availability in the oceans during specific intervals [39, 44, 178], and can lead to changes in

ocean chemistry, from ferruginous to euxinic conditions. Maintenance of N availability, in light of strong N-sinks, would have been essential to supporting biological production with corresponding influences on ocean chemistry, atmospheric oxygen concentrations [178], and the strength of the marine C-sink [8, 39]. In the Phanerozoic eon, by contrast, abundantly available N may have driven intervals with elevated primary production, which in turn contributed to ocean deoxygenation, and the onset of Oceanic Anoxic Events, along with biological crises [219–221]. The modern oceans are also losing oxygen, which is the combined result of anthropogenic climate warming and ocean nutrient loading [72]. As anoxic water masses expand, so too may the strength of marine N_2 production with corresponding implications for ocean N inventories, primary production, and climate. If deoxygenation favored DNRA and N-retention, however, it could instead lead to positive feedbacks on primary production and ocean deoxygenation. In addition to driving marine deoxygenation, both climate warming and nutrient loading thus influence the distribution of N in the oceans. In the absence of predictive models that accurately diagnose the response of the N-cycle to ocean deoxygenation, however, predictions of future N inventories and the corresponding feedbacks on biological production and climate remain unconstrained.

Anoxic and low oxygen marine waters are characterized by high rates of anaerobic N-metabolisms, and the partitioning of these metabolisms between anammox, denitrification and DNRA dictates N-loss versus N-retention, and influences oceanic N-inventories. N-loss, through N_2 production, is the result of NO_3^- and NO_2^- reduction through the microbial metabolisms denitrification and anammox. NO_3^- and NO_2^- reduction can also be channeled through DNRA, which short-circuits N_2 production and retains fixed N in the ocean. Denitrification and anammox reactions and corresponding N_2 production, are widespread throughout marine oxygen minimum zones (OMZs) and in coastal shelf sediments. Rates of these microbial metabolisms have been extensively determined [18, 56, 60, 65–67, 84, 85, 98, 100, 154, 171, 222], and together with measurements of N-fixation as well as models of the distribution of nutrients (for example: [223]), form the basis for current ocean N-budgets [1, 2, 63]. Despite the wealth of information on rates of denitrification and anammox, the controls on partitioning between these metabolisms, remain uncertain. Measurements of DNRA, by contrast, are sparse, although it has been transiently detected in OMZs [60, 65, 67, 224] and it can be an important pathway in N-cycling in estuarine

sediments [225]. While all three of these NO_3^- /NO_2- reduction pathways can be simultaneously studied using ^{15}N-labeling experiments, there remains insufficient ecophysiological information on the relevant organisms with which to build predictive models that would inform the response of the marine N-cycle to ocean deoxygenation. Acquiring this ecophysiological information is becoming possible using new meta'omic information coupled with process rate measurements, and their collective integration into gene-centric modeling frameworks [118, 119]. Even with these approaches, determining the ecophysiologies of the relevant microorganisms, however, is confounded by the diversity and complexity of marine microbial communities, and their corresponding interactions with the surrounding environment.

Substrate availability is a key constraint of rates of microbial metabolism and this likely plays a role in governing the relative importance of the different anaerobic N-metabolisms [60, 67, 105]. Conventional approaches often consider the interaction between microorganisms and their substrates in terms of free energy availability [105, 108, 226], and enzyme-kinetics [227]. Classical studies, for example, predict the cascade of terminal electron acceptor use in redox stratified environments based on the successive use of the electron acceptor yielding the most free energy upon reaction with a given electron donor [104, 216]. However, the rate at which this energy can be supplied – rather than its potential availability – also places constraints on microbial growth [228, 229]. The rate of energy supply, in essence the power supply [228, 229], can be calculated as the product of free energy yields and corresponding reaction rates [228, 229]. Notably, since power supply depends on the rate at which a reaction substrate is supplied, it also depends on physical transport as well as ambient substrate concentrations. Power supply rates can thus be inferred by combining geochemical information to estimate free energy yields with measurements of metabolic reaction rates [228, 229] that through mass balance necessarily reflect rates of substrate supply. Organic matter degradation rates, for example, have been combined with free energy yields for specific metabolic reactions that occur in marine sediments [228] to infer the power supply in the marine subsurface. Power supply, however, has rarely been explored more broadly as a large-scale regulator of biogeochemical processes and microbial ecology in the oceans.

We have used a time-series experiment in Saanich Inlet (SI) to determine the response of the

N-cycle and its underlying microbial catalysts to dynamics in power supply induced by ocean currents. SI is an anoxic fjord on the east coast of Vancouver Island, Canada, that undergoes partial renewals of its water column due to a combination of weak tidal action and upwelling of dense water into the Strait of Georgia [179]. SI represents an experimentally tractable ecosystem in which to study biogeochemical processes and microbial ecology more broadly extensible to low oxygen marine waters in the global ocean. Multi-omic sequencing approaches have been used to develop qualitative models that describe the microbial N metabolisms that underpin the N-cycle in SI [33]. These qualitative models have been extended to a quantitative reaction-transport and gene-centric modeling approach that couples multi-omic sequence information with geochemistry to link gene abundances to key microbial metabolic pathways and their rates under steady-state conditions [118]. More recent studies, however, imply year-long dynamics in SI with strong variation in the rates and pathways of N_2 production associated with renewal events ([186, 230] and chapter 3) and these cannot be addressed through the existing gene-centric framework. Prior studies in SI, furthermore, have overlooked the potential role of DNRA, and while its operation was not evident through gene-centric modeling [118], proteins related to cytochromes that confer metabolic potential for DNRA have been detected in SI, implying a possible role for DNRA [33]. We measured rates and pathways of NO_x (NO_3^- and NO_2^-) reduction through DNRA, denitrification and anammox monthly in the water column of SI across two consecutive years, through stagnation periods and renewal events. We combined geochemical profiles, thermodynamic calculations, process rate measurements, and analyses of the metabolic potential of microbial communities using metagenomics to determine how N-metabolisms respond to dynamics in substrate supply regimes. We show that DNRA becomes the dominant NO_3^- reduction pathway and mode of energy transduction following renewal events. These renewal events were also followed by increase in power supply, linking power supply to the outcome of networked microbial N-metabolisms. Our results, therefore, suggest that dynamics in power supply influence microbial community metabolisms with consequences for N-budgets and elemental cycles more broadly.

4.2 Methods

4.2.1 Study site and sample collection

Sampling took place in Saanich Inlet (BC, Canada) at Station 3 (48° 35.5 N and 123° 30.3 W, 227m deep). The study was spanned from February 2015 to January 2017, with the exception of January 2016. Exact dates of sampling can be found in Appendix D (table C.4). For each month, a CTD profile was taken for the following parameters with the corresponding sensors in parentheses: pressure (SBE 29), conductivity (SBE 4C), temperature (SBE 3F), and oxygen (SBE 43). Samples for chemical analyses were obtained from 16 depths (10, 20, 40, 60, 75, 85, 90, 97, 100, 110, 120, 135, 150, 165, 185 and 200m) as described in chapter 3 [230], for NO_3^-, NO_2^-, NH_4^+ and HS^-. Nutrient samples for NO_3^-, NO_2^- and NH_4^+ were filtered through a 0.2μm filter and the HS^- samples were fixed in 0.5% ZnAc final concentration. Both sets of samples were then frozen until analysis. Water samples for DNA filtration were taken from 6 depths (10, 100, 120, 135, 150 and 200m) with a volume of 10L and were filtered back in the lab the night after the sampling. The filtration apparatus consists of a pre-filter (glass fiber filter 2μm pore size) and a 0.2μm sterivex filter (Millipore Sigma). Both filters were then filled with lysis buffer and frozen immediately in liquid nitrogen and kept at -80°C. Samples for process rate measurements were collected from 7 depths (90, 100, 120, 135, 150, 165 and 200m) in 250mL serum glass bottles, overflowed 3 times, and closed without any air bubble with blue butyl rubber stoppers (Bellco glass). The bottles were put on ice before processing in the lab the night of the sampling.

4.2.2 Nutrient analyses

Samples for NO_2^-, NH_4^+ and HS^- were thawed before analysis and measured according to the following spectrophotometric assays: the Griess assay, the indophenol blue method and the Cline assay, respectively [151]. NO_x (NO_2^- and NO_3^-) concentrations were measured by chemiluminescence following reduction with vanadium [189], and NO_3^- concentrations were obtained by subtracting NO_2^- from the total NO_x concentrations.

4.2.3 Process rate measurements

^{15}N-labeling incubations were performed according to chapter 3 [230]. Rates of anammox were calculated from the net accumulation of $^{29}N_2$ in the headspace of the samples, with addition of $^{15}NH_4^+$ + $^{14}NO_3^-$ or with addition of $^{15}NO_3^-$ [83]. Rates of denitrification were calculated from the net accumulation of $^{30}N_2$ in the headspace of the samples, with addition of $^{15}NO_3^-$. Rates of DNRA were calculated based on the net accumulation of $^{15}NH_4^+$ in the liquid samples from $^{15}NO_x$ labeled incubation, after transformation of $^{15}NH_4^+$ to $^{15}N_2$ [231]. The excess of $^{14}N^{15}N$ and $^{15}N^{15}N$ in the samples were measured by Isotope-Ratio Mass Spectrometry (Delta V, thermoscientific). Concentrations of $^{29}N_2$ and $^{30}N_2$ were determined according to chapter 3 [230] and Thamdrup et al. (2006)[154]. Rates of the processes were calculated based on least squares fitting of the slope of ^{15}N accumulation, correcting for the initial $^{15}N_2$ present and accounting for the initial pool of unlabelled substrates present (chapter 3 and [230]). A detailed table of the incubations can be found in Appendix D (Table D.4).

4.2.4 DNA extraction, qPCR and absolute cell abundance

DNA was extracted from sterivex filters following Wright et al. (2009) [194] for 4 months in 2016 (April, August, September and October). Once extracted, DNA was checked for quality and sent for high-throughput metagenomic sequencing at the Joint Genome Institute (Walnut Creek, California). We also quantified total bacterial and archaeal 16S rRNA genes (or SSU rRNA gene) via qPCR by targeting the bacterial and archaeal 16S rRNA genes with the primers 27F/20F (5'-AGAGTTTGATCCTGGCTCAG, 5'-TTCCGGTTGATCCYGCCRG) and DW519R (5'-GNTTTACCGCGGCKGCTG) [183], respectively. Standards used for total bacteria and total archaea quantification were obtained from a SSU rRNA gene clone libraries as described in Zaikova et al. (2010) [183]. qPCR program was as follows: (1) 95°C for 3 minutes, (2) 95°C for 20 seconds, (3) 55°C for 30 seconds, (4) read, repeat (2) to (4) 44 times, obtain melting curve by incrementing 0.5°C from 55°C to 95°C every second. qPCR reactions were performed in low-profile PCR 96 well-plates (BioRad) in 20μl volume reaction on a CFX Connect Real-Time thermocycler (BioRad). 16S rRNA gene abundance (16S rRNA gene L^{-1}) was multiplied by the

average number of 16S rRNA gene copies found in bacterial genomes (4.2) [232] and was used as a proxy for absolute cell abundance (cell L^{-1}).

4.2.5 Metagenome sequencing and assembly

Twenty samples (4 months and 5 depths) were used to generate metagenomic datasets at the DOE-JGI (Walnut Creek, California) following the protocols for library production and sequencing on the Illumina HiSeq platform and the accession numbers can be found in Table D.5. The sequences were first trimmed and filtered using Trimmomatic (Bolger et al., 2014). Adapters supplied in the Illumina TruSeq3 adapter sequence file were removed by Trimmomatic's ILLUMINACLIP command. Next, the first three and last three nucleotides were removed from each read if below a quality threshold, and a sliding window of four nucleotides was checked based on average Phred score (Qscore). Nucleotides within these windows were removed until the average Qscore across the window was >15. Finally, the sequence reads with <36 bp were removed, along with their mate-pair reads. Paired-end sequencing reads were assembled into contigs using Megahit [233], with default settings. Open Reading Frames (ORFs) were predicted using Prodigal v2.0 (`https://github.com/hyattpd/prodigal/wiki`), based on a minimum nucleotide length of 60 as implemented in MetaPathways 2.5 [234] and `https://github.com/hallamlab/metapathways2/wiki`). Metagenomic data sets are accessible through the JGI IMG/M portal (`https://img.jgi.doe.gov/cgi-bin/m/main.cgi`) under the study name 'Mapping the global Methanome' (project ID 503042) and raw reads at the NCBI Sequence Read Archive numbers for all the samples can be found in the Appendix D.

4.2.6 Taxonomy of of the microbial community recovered through metagenomic analyses

16S rRNA gene sequences were retrieved from metagenomic datasets (trimmed reads) using EMIRGE [235]. We then used the retrieved 16S rRNA gene sequences to reconstruct the taxonomic composition of the microbial community. The sequences were aligned and classified using the latest SILVA database at a 90% identity cut-off.

4.2.7 Quantification of functional genes

Curated reference sequences for genes involved in nitrogen cycling were downloaded from FunGene (`http://fungene.cme.msu.edu/`) except for *hzs*, *hao* and *hzo* [236]. The other genes were downloaded from GenBank and manually curated based on sequence length, annotations, and phylogeny [237]. A complete list of the genes studied in this paper can be found in Appendix D (Table D.3). Chosen functional genes were quantified using TreeSAPP, a phylogenetic-based protein profiling software (available at `https://github.com/hallamlab/TreeSAPP`). TreeSAPP was used to both build the reference trees and map putative protein sequences to these trees for functional classification and quantification. Specifically, the script create_treesapp_ref_data.py was used to cluster the reference protein sequences with UCLUST at some percent similarity such that trees contained between 150 and 600 sequences [238]; this range balanced highly accurate taxonomic annotations and reasonable compute time to determine the optimal sequence placements in the phylogenetic trees. Following clustering, MAFFT version 7.294b was used with the –maxiterate 1000 and –localpair settings to generate a multiple sequence alignment and trimAl version 1.4.rev15 was used to remove non-conserved positions [239, 240]. RAxML version 8.2.0 was used to build the reference trees with the'–autoMRE' to decide when to quit bootstrapping before 1000 replicates have been performed and PROTGAMMAAUTO to select the optimal protein model [241][242].

TreeSAPP's treesapp.py was then used to map the query sequences (protein sequences from called genes in contigs) onto these reference trees using the following procedure: Proteins were predicted using Prodigal version 2.50 from the assembled metagenomic contigs [243]. Open-reading frame (ORF) protein sequences were aligned to HMMs using hmmsearch and the aligned regions were extracted [244]. hmmalign was used to include the new query sequences in the reference multiple alignment and then trimAl removed the unconserved positions from the alignment file [239]. RAxML was used to classify the query sequences using thorough sequence insertions [245]. Quality-controlled reads provided by the JGI were aligned to the nucleotide ORFs using BWA MEM [246]. An executable that calculates reads per kilobase per million mappable reads (RPKM) from a SAM file was used to generate these normalized abundance values for each

predicted protein.

4.3 Results and discussion

4.3.1 Dynamics in rates and pathways of N-cycling

During most of the year, the water column in SI is stagnant, with O_2 and NO_3^- abundant in the surface waters and scarce at depth. Below ∼100-110m, water in SI is usually devoid of O_2 and NO_3^-. In the bottom waters, NH_4^+ and HS^- accumulate (Fig. D.1), likely diffusing out of the underlying sediments [185]. Geochemical dynamics within the water column, however, are induced transiently by renewal events in intermediate and deep-waters (100 to 200m). These renewal events result from the input of dense water from outside of the inlet that spills over the sill at the inlets entrance and settles to depths of equal density (isopycnals) [184]. This new mass of water introduces O_2 and NO_3^- that can accumulate to detectable concentrations depending on the flux of renewal water, its mixing with deep water, and the rate, abiotic or biologically catalyzed, at which O_2 and NO_3^- react with reducing agents like HS^- and NH_4^+. Monthly profiles of O_2 and NO_3^- concentrations reveal 6 renewal events between 2015 and 2016 (Fig. 4.1 - grey shading, and Fig. D.1). These renewal events were marked by increases in concentrations of O_2 and/or NO_3^- in intermediate or deep-waters relative to previous months. The strongest renewal over this period developed in September 2016 where high O_2 and NO_3^- concentrations were recorded in deep-waters (50μM and 12μM, respectively). During some events, O_2 remained undetectable in deep and intermediate waters and yet NO_3^- accumulated, for example in July of 2015, revealing renewal, nonetheless (Fig. D.1). Renewal events thus often occurred at the end of the summer, such as in 2015. Several renewal events, however, were recorded throughout 2016 and the inlet went through several cycles of renewal/stagnation (at least 6 detected) over the 2 years studied here.

To test the responses of anaerobic N-metabolisms to renewal-induced physical-chemical dynamics, we measured rates and pathways of microbial N-metabolisms, specifically anammox, denitrification, and DNRA. Rates of anammox, denitrification and DNRA, integrated over the depth of the anoxic water column (Fig. 4.1b and c), change in response to renewal, revealing

dynamics in the partitioning of NO_x (NO_3^- /NO_2^-) reduction between these processes with implications for N-loss and retention. Overall, total NO_x reduction (through DNRA, denitrification and anammox) varies between $7 \cdot 10^{-4}$ and 1.4 moles N m^{-2} d^{-1}, spanning several orders of magnitude over the two-year period. The highest rates of NO_x reduction followed renewal events. Five of the six renewal events were, indeed, followed by elevated rates of NO_x reduction and also corresponded to very high rates of DNRA (Fig. 4.1a and b – August and November 2015, February, May, October 2016). The single other renewal event, by contrast, was dominated by high rates of denitrification (Fig. 4.1a and b – August 2016). NO_x reduction rates following renewal were several orders of magnitude higher than those measured in stagnation periods (e.g. June and December 2015, Fig. 4.1b), and developed in association with a large advective supply of new oxidants, mainly O_2 (Fig. 4.1a), which likely fueled nitrification. Nitrification, in turn, supplied oxidized N-species (NO_x) needed to support higher rates of anaerobic N-metabolisms. Rates of nitrification were previously shown to increase after renewal [247] and the rates measured in the low oxygen waters would have been sufficient to support the highest volumetric rates of anaerobic N-metabolisms measured in this study.

The distribution of NO_x reduction across the 3 pathways varies strongly over time. Shifts in anaerobic N-metabolisms were shown to occur, specifically between a regime of fixed N-retention through DNRA following renewal (e.g. August 2015 and October 2016 in Fig. 4.1b) and one of N-loss driven mainly through denitrification and to a lesser extent, anammox (e.g. March and July 2016 in Fig. 4.1b and c). N-retention through DNRA totaled 58% of the total NO_x reduction when integrated over the two years studied, making DNRA the dominant pathway for NO_x reduction in SI. Few previous studies have observed DNRA in such a prominent role in N-cycling with notable exceptions in estuarine and coastal margin sediments [91, 225]. Appreciable DNRA has also been detected in the Peruvian OMZ [67], but there, DNRA represented a minor fraction (<12%) of the total NO_x reduction. Our results thus reveal strong dynamics in the rates and pathways of anaerobic N-metabolisms in SI, with a notable rise of DNRA to prominence in response to renewal events. These dynamics in anaerobic N-metabolisms are the likely phenotypic expression of changes in the underlying microbial community structure and function, which we explore below.

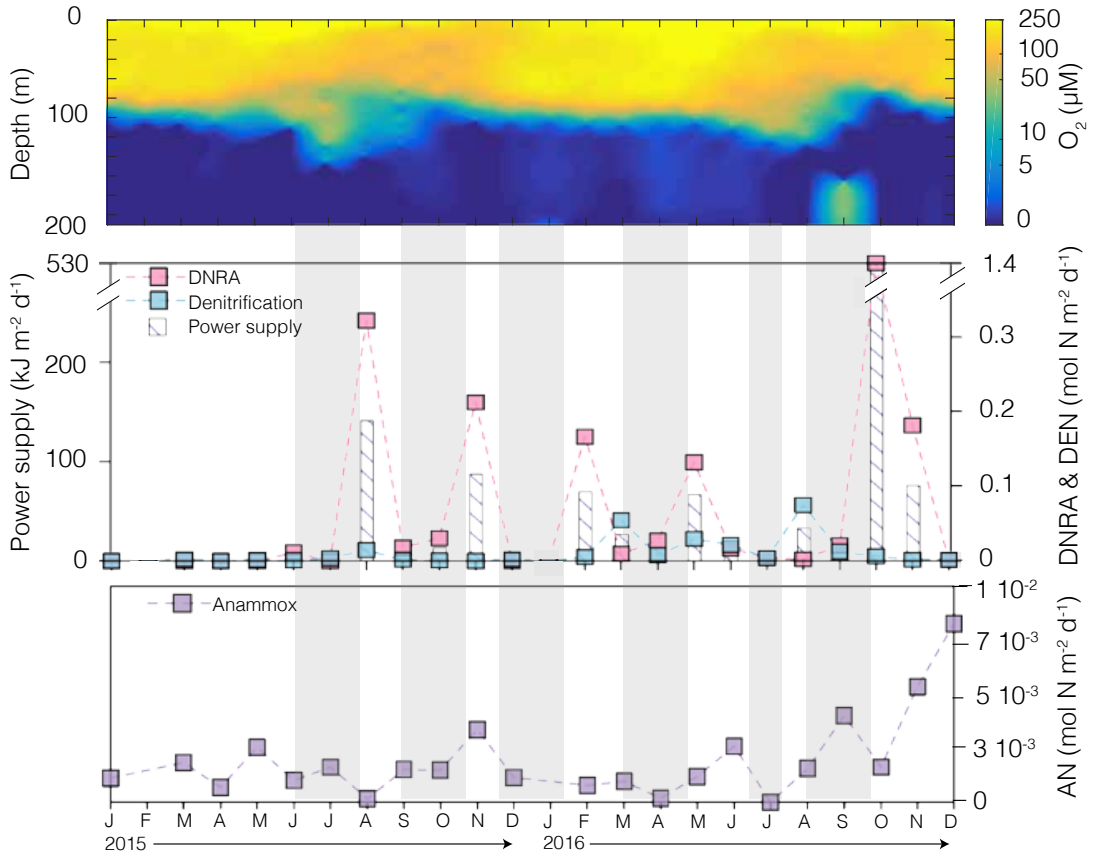

Figure 4.1: *Rates and pathways of anaerobic N-metabolisms.* (a) Oxygen concentrations (μM) and (b) Depth-integrated rates of denitrification (blue) and DNRA (pink) in moles N $m^{-2}\,d^{-1}$, as well as power supply (kJ $m^{-2}\,d^{-1}$) plotted as histograms (c) depth integrated rates of anammox (purple) in moles N $m^{-2}\,d^{-1}$. Standard error on the depth-integrated rates were compiled in table D.1 of Appendix D, and were not depicted in this figure as they were smaller than the square depicting the data point.

4.3.2 Dynamics of the microbial community in response to physical perturbations

We find that microbial community composition and structure changes in response to renewal. Environmental disturbances have previously been linked both to increased [248] and decreased [249] microbial community diversity, as well as to changes in activity. Here we observe that the diversity of the microbial community decreased following renewal events. Changes in diversity were evident in both the number of observed species as well as in diversity indices (Figs. 4.2 and 4.3e). We note that the decrease in diversity was also accompanied by an increase in cell abundance (see methods for description of cell abundance). Such an increase in cell abundance and a decrease in diversity, in less than a month, suggests that only a few specific taxa have grown following enhanced substrate supply rates – mainly O_2 and NO_x – and the decrease in diversity is the likely result of a few blooming taxa. The taxon *Arcobacter*, of the Epsilonproteobacteria which are commonly known as blooming organisms [250] for example, increased in absolute abundance after renewal (Figs. 4.2 and 4.3 and see methods for absolute cell abundance), and could be partially responsible for the decrease in diversity. Taken together these observations suggest that renewal induces growth of blooming organisms and this occurs in association with increased rates of N-metabolisms such as denitrification or DNRA. This may thus imply that microbial growth is stimulated by enhanced N-supply and linked to specific N-metabolisms.

Figure 4.2: *Taxonomic composition of the microbial community.* The taxonomic composition of the microbial communities is plotted at the phylum level, and was obtained from 16S rRNA gene extraction via EMIRGE from metagenomic samples for 4 months and 5 depths (100, 120, 135, 150 and 200m).

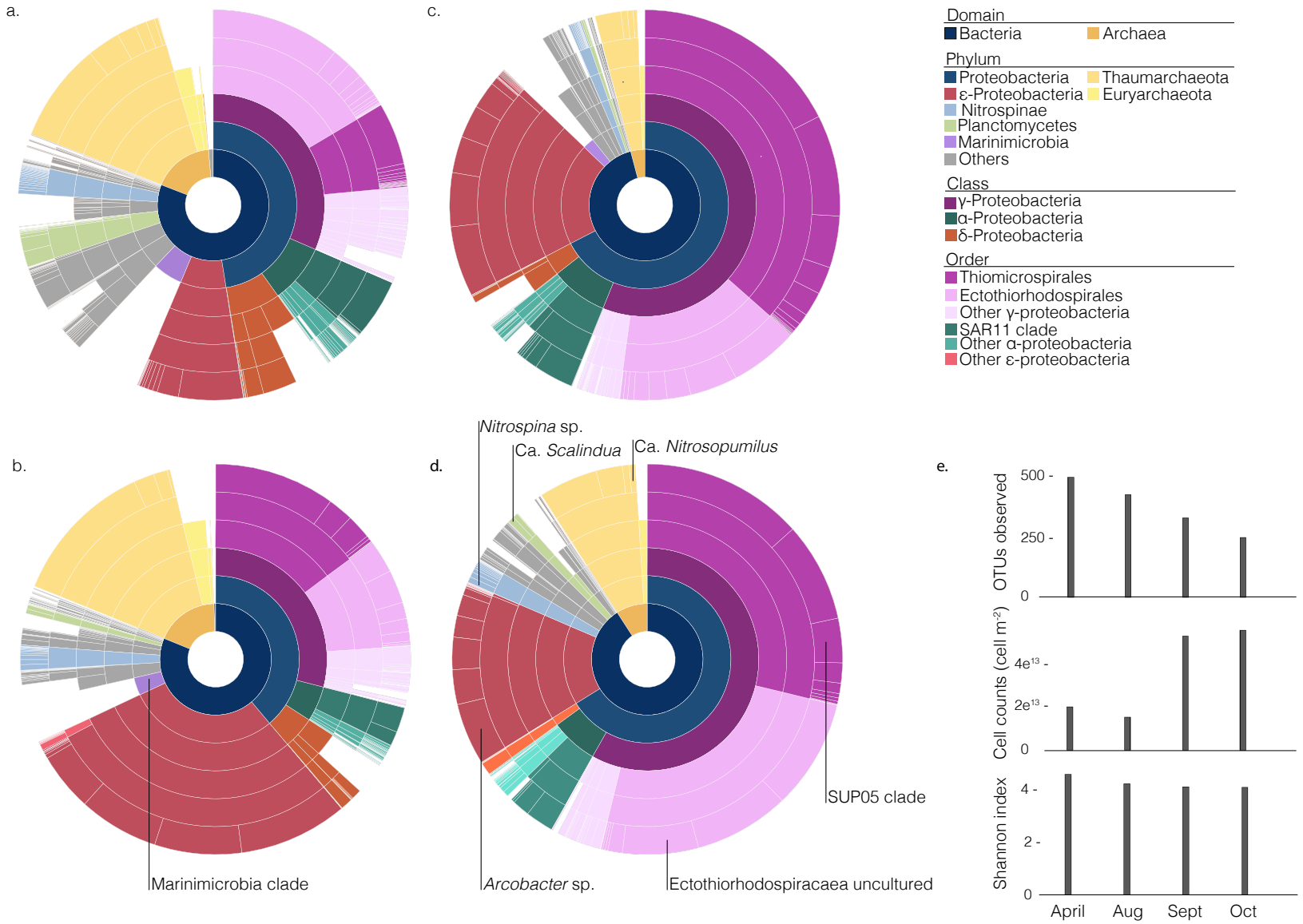

Figure 4.3: *Depth-integrated taxonomic composition of microbial communities.* The taxonomic composition of the microbial communities is plotted at the OTU level (97% similarity), and was obtained from 16S rRNA gene extraction via EMIRGE from metagenomic samples for 4 months (a=April, b=August, c=September, d=October) and 5 depths (100, 120, 135, 150 and 200m). The absolute abundance (see methods) for each sequence was integrated over the 5 depths mentioned here. Each concentric circle represents a taxonomic level. e) shows OTUs observed during the 4 months (April, August, September and October) cell abundances, and the alpha-diversity index – Shannon.

Emerging gene-centric modeling approaches imply that rates of biogeochemical reactions scale with the abundance of genes that code for enzymes involved in that pathway and thus, based on these approaches we might expect a direct link between dynamics in organismal and gene abundances, substrate supplies, and metabolic rates [118, 119]. In gene-centric modeling approaches, biogeochemical reaction rates are tied to the growth rates and abundances of the organisms that host relevant genes and pathways. While it is often assumed that rates of gene transcription better reflect microbial activity than gene or organism abundances [251], multi-omic modeling implied that, in anaerobic marine environmental systems, the time-scales of microbial growth and biogeochemical reaction rates were similar and thus best linked through gene and organism abundances [118]. It follows then that the dynamics we observe in rates and pathways of anaerobic N-metabolisms in SI should be tied to changes in the abundances of genes and their host organisms involved in these pathways. Renewal events indeed induce both microbial community growth (Figs. 4.2 and 4.3) and cause enhanced rates of anaerobic N-metabolisms (Fig. 4.1), implying a connection between growth and biogeochemical reaction rates in SI. It may be possible, therefore, to connect the abundance of taxa involved in N-cycling to the reaction rates, in line with multi-omic modeling theory [118, 119]. Previous studies identified key-taxa that support N-cycling in SI [33, 187], and provide a benchmark against which to evaluate microbial community dynamics in response to perturbation and test the idea that biogeochemical reaction rates scale with the abundance of relevant genes and organisms.

SUP05 is a prominent member of the microbial community throughout the period of observation and its abundance does not vary strongly despite dynamics in the rates and pathways of anaerobic N-metabolisms (Fig.4.4). SUP05 has been implicated in partial denitrification, in essence NO_3^- reduction to N_2O, in SI and other low oxygen marine waters, globally [18, 33, 121]. According to gene-centric models, we might thus have expected the abundances of SUP05 to scale with rates of denitrification. While rates of denitrification vary over nearly 3 orders of magnitude (Fig. 4.1b), the abundance of SUP05 changes less than 10's of percent over the same time period (Figs. 4.2 and 4.3). The relationship between SUP05 and the rates of denitrification may be confounded by several factors. Notably, SUP05 in SI may operate in partnership with Marinimicrobia to achieve complete reduction from N_2O to N_2 [187] and thus partial denitrification may obscure

the relationship between rates of denitrification and SUP05 abundances. We note, however, that N_2O did not accumulate to appreciable concentrations during our experiments implying that denitrification, when operative, was complete. Marinimicrobia abundances, furthermore, are negatively correlated with rates of denitrification (Fig. 4.3). These observations, therefore, suggest that there is a decoupling between the rates of denitrification and the abundances of SUP05 and Marinimicrobia, and barring strong transcriptional regulation, this instead may suggest a likely role for other taxa in denitrification or that growth of SUP05 and Marinimicrobia is sustained through alternative metabolisms, such as aerobic respiration and/or sulfur oxidation [187, 188]. Other taxa implicated in denitrification, for example, include *Arcobacter* (chapter 3 and [230]), which is highest in abundance in August when rates of denitrification are highest (Figs. 4.2 and 4.3), but otherwise *Arcobacter* abundance does not scale with rates of denitrification over the 4 months of observation. We also note relatively high abundances of Ectothiorhodospiraceae (Gammaproteobacteria, Fig. 4.3), which has previously been linked to HS^- oxidation and denitrification in other environments [252] and may thus also contribute to denitrification in SI. Collectively, these observations suggest that some of the most abundant and conspicuous taxa in SI are decoupled from rates of the pathways that putatively support their growth based on prior analyses. Other factors thus likely contribute both to controlling organism abundance and rates of denitrification.

The abundances of the genes involved in denitrification, like the corresponding organisms, did not scale with the rates of denitrification. This suggests a decoupling of gene abundances from rates of biogeochemical reactions and is inconsistent with gene-centric modeling theory. Indeed, we find that the denitrification gene pool (*nirS*, *norB* and *C*, and *nosZ*) more than tripled between August and September (Figs. 4.4 and 4.5), achieving the highest gene abundances a month after the highest rates of denitrification. This increase in the gene abundances also matched an increase in overall cell abundance for the same month, indicating microbial growth when renewal occurred (Figs. 4.2 and 4.3). In contrast, the rates of denitrification detected in September, after renewal (Figs. 4.1 and 4.5), were an order of magnitude lower than the highest rates detected in August. Therefore, the growth of the denitrifying population, based on the gene abundances, did not scale with the rates of denitrification. This may further imply that other pathways are used to

generate growth of the microbial populations containing denitrification genes, as suggested above. Alternatively, a switch between the activity of multiple populations of denitrifying bacteria with distinctive physiologies causing variable cell-specific rates and biomass yields could lead to either high gene abundance at low denitrification rates or low gene abundance and high denitrification rates (Fig. 4.5). The discrepancy between the dynamics in the rates and the abundances of the genes underpinning denitrification therefore suggests that gene abundance is not always a good predictor of biogeochemical activity.

The abundances of anammox bacteria and their functional genes both remained relatively constant and did not follow the dynamics in the rates of anammox. Anammox is restricted to the phylum Planctomycetes, and *Ca.* Scalindua was previously implicated in anammox in SI [33] and more globally in OMZs [66, 120, 121, 253]. In the 4 months studied here, *Ca.* Scalindua only comprised a few percent of the microbial community and varied less than an order of magnitude in absolute abundance (Figs. 4.2 and 4.3) despite an order of magnitude change in the rates of anammox (Fig. 4.5). Similarly, the anammox gene pool (*hzs* and *hzo* – hydrazine synthase and hydrazine oxidoreductase) remained constant, within the same order of magnitude (Figs. 4.4 and 4.5). Thus, like denitrification, rates of anammox did not scale with respective gene and cell abundances. The variations in the rates of anammox, however, are relatively small compared to those of denitrification, with no appreciable changes in the abundance of anammox bacteria (Fig. 4.5). The factors responsible for the inconsistency between the rates of anammox and their gene and cell abundances are likely different from denitrification. While taxa involved in denitrification can grow facultatively through other metabolisms, *Ca.* Scalindua is only known to grow through the anammox pathway [62] and therefore, the decoupling between abundances and rates is not the likely result of growth of *Ca.* Scalindua through alternative metabolisms. Also, while the capacity for denitrification is distributed across many taxa and thus conducted through different physiologies, the anammox metabolism is restricted to Planctomycetes [254] and it is unlikely to be conducted by other taxa with different physiologies. The combined results for denitrification and anammox thus show that the relationships between metabolic rates and gene and organism abundances appear more complex than currently accounted for in gene-centric modeling and that these relationships further diverge across pathways and organisms.

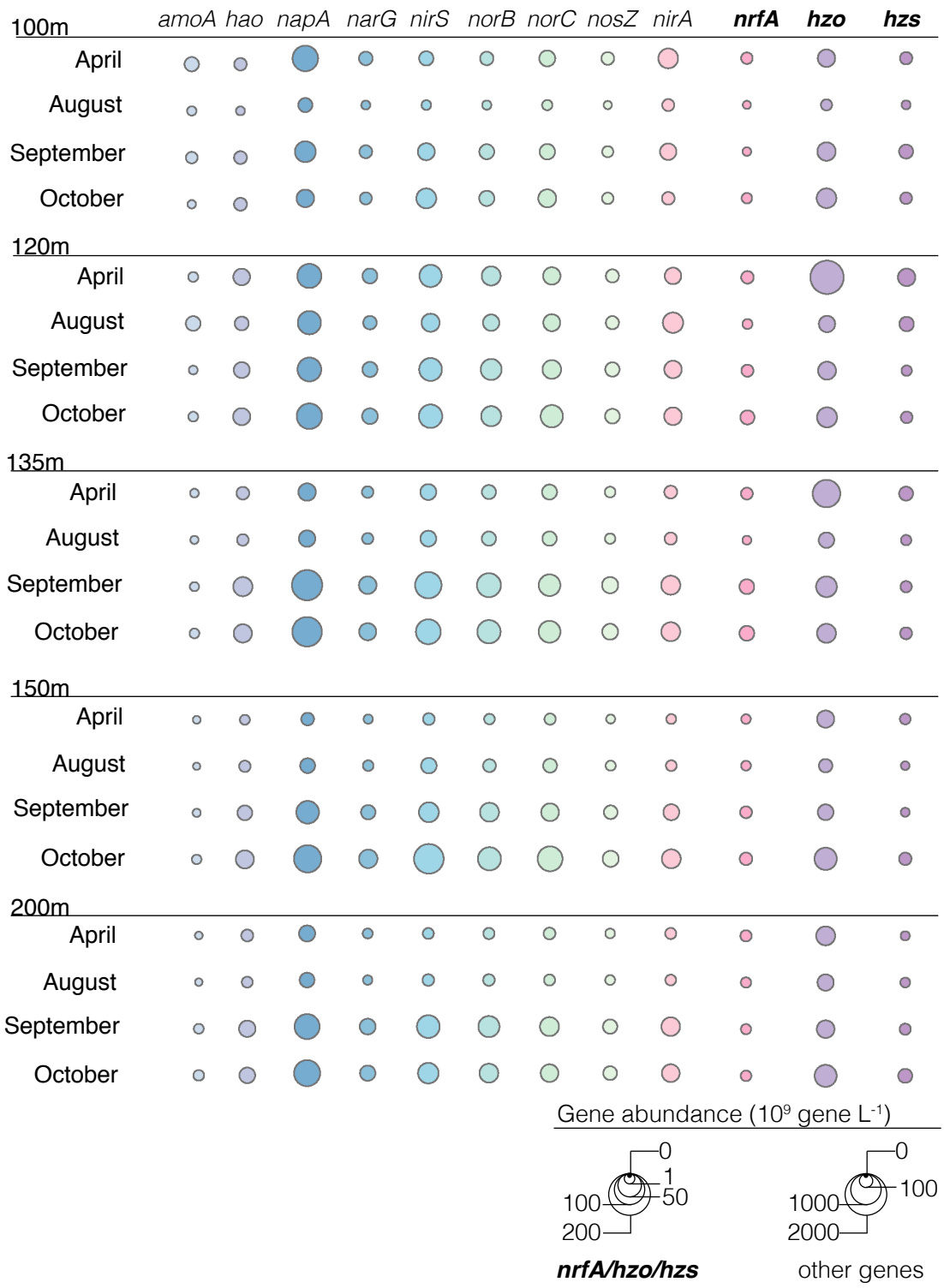

Figure 4.4: *Functional gene abundances of anaerobic N-metabolisms.* Gene abundances (gene L^{-1}) for the following pathways and associated genes: nitrification (*pmo/amoA*=ammonia monooxygenase, *hao*=hydroxylamine oxidoreductase), anammox (*hzo*=hydrazine dehydrogenase, *hzs*=hydrazine synthase), NO_3^- reduction (*napA*=periplasmic dissimilatory nitrate reductase, *narG*=membrane-bound dissimilatory reductase), denitrification (*nirS*=nitrite reductase, *norBC*=nitric oxide reductase, *nosZ*=nitrous oxide reductase), DNRA (*nrfA*=dissimilatory periplasmic cytochrome c nitrite reductase, *nirA*=assimilatory nitrite reductase). Of note, the different scales for *hzo*, *hzs* and *nrfA* than for the other genes.

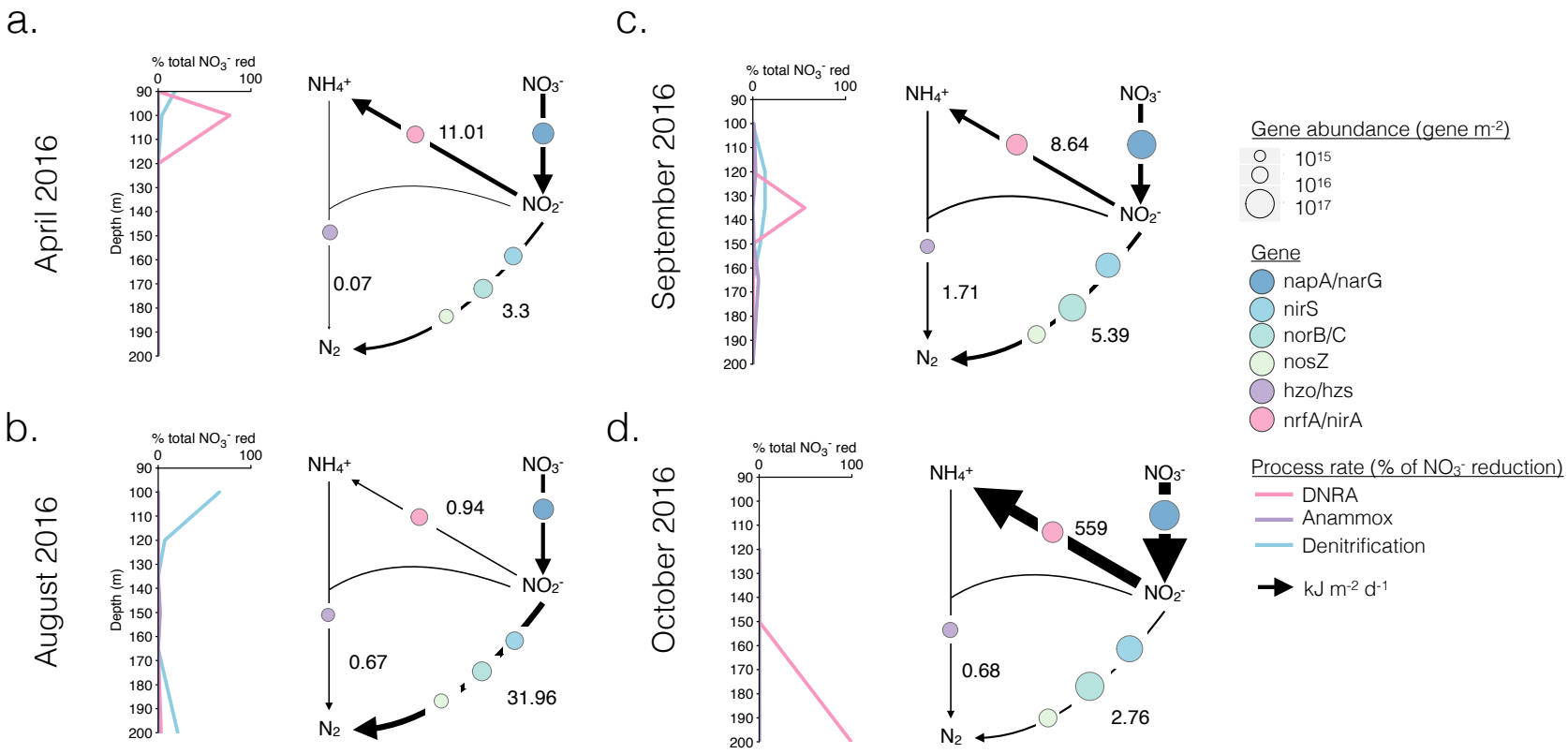

Figure 4.5: *Re-networking of anaerobic N-metabolisms linked to power supply.* Depth-integrated rates of power supply associated with DNRA, denitrification and anammox (black arrows, in kJ m^{-2} d^{-1}) with depth-integrated gene abundances (in genes m^{-2}) associated with these rates (in bubble). The insets on the left of each conceptual model shows where most of the NO_x reduction occurs in the water column and through which process (blue for denitrification, pink for DNRA, purple for anammox).

In addition to denitrification and anammox, both of which are implicated conceptually and quantitatively in N-cycling in SI, we also found that DNRA contributed appreciably to the N-cycle following renewal, and like denitrification and anammox, genes involved in DNRA did not scale with rates of DNRA. While the taxa that conduct DNRA in SI remain unknown, SUP05 has been tentatively linked to DNRA through the discovery of *nrfA* homologues in a SUP05 affiliated open reading frame. The abundances of the genes involved in DNRA (*nrfA* and *nirA*, [3]) tripled between August and September, following renewal (Fig. 4.4), but remained constant between September and October despite two orders of magnitude increase in the rates of DNRA (Figs. 4.1 and 4.5). The disconnect between DNRA rates and gene abundances, like denitrification, probably reflect both the distribution of DNRA across multiple organisms as well as growth of *nrfA*/*nirA* genes through metabolisms apart from DNRA. Connecting rates of DNRA to gene abundances is further confounded by both uncertainty in the taxa that conduct DNRA and their underlying genes. Indeed, DNRA may be achieved through enzymatic pathways that do not contain *nrfA* and may instead be catalyzed by other enzymes encoded by other genes [3, 224, 255]. Again, it is difficult to reconcile rates of DNRA with corresponding gene abundances as required in gene-centric modeling frameworks.

Nitrifying bacteria and Archaea as well as the nitrification gene pool respond to renewal in likely connection to elevated nitrification rates. Key organisms implicated in nitrification including, *Nitrospina* sp. as well as Thaumarchaeota [33], along with the genes encoding enzymes that catalyze key steps in nitrification (*amoA* and *hao* – ammonia oxidase and hydroxylamine oxidoreductase), appear to increase following renewal. Specifically, we find an increase in the abundance of organisms belonging to these clades at the depths where renewal was observed (135m in August and 200m in September/October - Fig. 4.4). The genes *amoA* and *hao* also exhibited similar increases in abundance at the same depths at the same time. Although we did not measure rates of nitrification, it was previously detected in the low-oxygen waters of SI and shown to increase in rate following renewal in 2008 [247]. It is therefore likely that rates of nitrification increased in response to the new input of oxygenated waters in SI following the September 2016 renewal as well (Fig. 4.1a) and so did the nitrifying population according to the abundance of key nitrifying organisms and the abundance of nitrifying genes. However, we

cannot confirm whether the rates and nitrifying microbial population growth scale as we are lacking rates of nitrification for the period studied.

4.3.3 Power supply and ecophysiology of anaerobic N-metabolisms

We often think about microbial communities in redox stratified environments in terms of energy available or free energy yield (ΔG). However, microbial communities can be limited by the rate at which this energy is made available, or in other words, by the power supply [228, 229]. We determined the power supply in the water column of SI for the anaerobic N-metabolisms denitrification, anammox, and DNRA. This was accomplished by multiplying reaction rates by the corresponding free energy yield at that depth and these were integrated over the depth of the anoxic water column (see Appendix D for more details on the power supply calculations). We also use reaction rates as a proxy for the substrate supply rate. This works because substrates did not accumulate and thus reaction rates place maximum values on the supply rate. Likewise, reaction rates place minimum values on substrate supply rates because mass balance precludes reaction rates that exceed substrate supply rates. We show that the power supply spans several orders of magnitude and is higher following renewal (Figs. 4.1a, b, and 4.5). Power supply in SI varied between 0.3 and 560 kJ m^{-2} d^{-1} and was the highest in October 2016 (Fig. 4.1b). The dynamics in power supply were mainly driven by changes in substrate supply rates rather than the changes in free energy yield that accompany changes in substrate and metabolite concentrations, which remain within an order of magnitude despite relatively small changes in substrate concentrations (Table D.3). Dynamics in power supply thus appear to be the result of changes in the input of oxidants to anoxic waters during renewal, which fuels nitrification and in turn supports higher rates of anaerobic N-metabolisms.

Changes in power supply are tightly coupled to changes in N-metabolisms. This has the effect of changing the overall outcome of reductive N-metabolisms, switching between N-loss and N-retention in connection to the substrate supply rate. Following renewal, the increase in power supply was reflected mainly as enhanced rates of DNRA, which causes N-retention in the inlet instead of N-loss through denitrification and anammox (Table D.1). A shift between N_2 production and N-retention through denitrification/anammox or DNRA, respectively, therefore

has important consequences for nutrient budgets in SI. The connection between this shift in pathways and dynamics in power supply implies that changes in power supply may play an important role in controlling the biogeochemistry of systems above and beyond simple regulation of the rates at which reactions take place. In this case, it appears to cause a re-networking of the N-cycle, by diverting the rate at which the energy is processed from one pathway to another, here from anammox and denitrification, to DNRA.

Power is used by organisms to maintain biomass, respond to environmental stressors, and if sufficient, fuel growth [228, 229]. Here we partitioned energy flow between different metabolic pathways in the N-cycle and compared these to functional gene abundances, as a proxy for microbial abundances (Fig. 4.5). Gene-centric modeling theory is based on scaling between reaction rates and functional gene abundances. In SI, however, changes in functional gene abundances associated with renewal did not scale to corresponding changes in rates. Since dynamics in power supply in SI are mostly driven by substrate supply rates, functional gene abundances also do not scale with power supply (Figs. 4.4 and 4.5). Therefore, because power is at least partly decoupled from microbial growth based on the results presented here, it must be dissipated through other mechanisms. These can include but are not limited to: extracellular secretions; energy spilling reactions (i.e. heat loss); defense against chemical stresses; cell motility; and proofreading and synthesis of macromolecules, such as RNA and proteins [229]. The power used in these processes could be referred to as maintenance energy and seems to vary between taxa and with growth conditions [256–259]. Thus, if the maintenance energy is low, there is generally more energy available to fuel growth that could support higher biomass yield. Here, anammox bacteria appear to have higher maintenance energy requirements, as we did not observe substantial changes in the relevant gene abundances despite changes in the rates of anammox, and this further implies a low biomass yield and this is consistent with previous observations from wastewater treatment plants [62]. Conversely, gene abundances for denitrification and DNRA changed substantially after renewal, although these did not scale with the corresponding increase in rates of these reactions. This therefore suggests lower maintenance energy requirements for the organisms involved in denitrification and DNRA, as well as relatively higher biomass yields. The lack of consistent relationship between gene abundances, relevant organisms and

rates imply that maintenance energy requirements and biomass yield are variable and depend on growth conditions. Beyond the complexities apparently associated with the relationship between growth and reaction rate, differentials in taxon-specific death rates would further confound these relationships. These observations demonstrate a need for more information on biomass yield, maintenance energy requirements and taxon-specific death rates. Such information should be generated for key-relevant taxa and appropriate model organisms that would enable predictive biogeochemical modeling that includes information on microbial ecology under dynamic (non-steady state) conditions.

4.4 Implications and extensions

DNRA was the dominant pathway of NO_x reduction in SI when summed over the year, with seasonal shifts between denitrification and anammox, and DNRA. This is notable as such a predominance of DNRA has rarely been observed in marine settings – and to date, only in some coastal and estuarine sediments [64, 93, 97, 155, 225]. Nevertheless, DNRA has previously been detected in pelagic settings, where it appeared to play a relatively minor role, such as in the Peruvian OMZ and the Baltic Sea [67, 106]. In SI, our time-series observations allowed us to capture large-scale dynamics in anaerobic N-metabolisms, and these observations reveal temporal shifts in denitrification and anammox, and DNRA that, when integrated annually, have important implications for N budgets in SI. The extent to which such large temporal variations in rates and pathways occur more broadly in coastal and open ocean low oxygen marine waters remains unknown, but should be evaluated in future studies.

Physical dynamics in the ocean influence power supply and, as we show here, can be accompanied by changes in the rates and pathways of microbial metabolism, with consequences for biogeochemical cycles and ocean chemistry. Models predict that current trends in climate will lead to increased frequencies of meso-scale eddies as well as increased upwelling, both of which have the potential to enhance the supply of oxidants and oxidized N-substrates to low oxygen marine waters [214, 260–263]. This enhanced supply of oxidants and N-substrates can lead to enhanced power supply, and, given that enhanced power supply appears linked to a shift in anaerobic

N-metabolisms to DNRA, we suggest that predicted changes in ocean circulation may influence N-inventories by promoting N-retention at the expense of N-loss. Anecdotally, detection of DNRA in the Peruvian upwelling system [67], which is currently characterized by frequent meso-scale eddies, supports this idea. If DNRA were to become the dominant anaerobic N-metabolism in the future oceans, it would dramatically influence global N-budgets and likely support a positive feedback on ocean deoxygenation.

Given the connection between power supply, physical dynamics and ocean circulation, and pathways of anaerobic N-metabolisms, there may be evidence in the geologic record that supports the positive feedbacks we propose here and their influence on the Earth system. For example, the oceans transiently became anoxic during Oceanic Anoxic Events, in the Cretaceous period [219], with links to changes in ocean circulation and enhanced primary productivity [219, 264, 265]. N-retention through DNRA, in response to enhanced power supply triggered by changes in ocean circulation, provides a means to initiate a positive feedback on ocean deoxygenation that could drive the expansive ocean anoxia during OAEs. At even larger scales, the oceans have changed from ferruginous (iron-rich) to euxinic (sulphide-rich) conditions during intervals in the late Archean and throughout the Proterozoic eons [42, 47–49, 55]. N-retention through DNRA versus loss through denitrification provides a means of sustaining euxinia under the widespread ocean anoxia that characterized the Precambrian eons and indeed, the N-isotope record implies basin scale DNRA during some intervals [42]. The reasons for widespread DNRA in the Precambrian oceans are necessarily uncertain at this time but by analogy, we suggest that variations in power supply linked to physical or chemical dynamics in the oceans could be responsible for changes between DNRA dominated and denitrification dominated anaerobic N-metabolisms. Changes in ocean circulation in response to deglaciation events in the Late Proterozoic eon have indeed been linked to the development of euxinia [266]. Taken together, we suggest that power supply dynamics can cause changes to the N-cycle that impact ocean nutrient status and can have large-scale effects on ocean chemistry, biological production, and the Earth system. Analogous changes in ocean circulation and power supply could mirror these events of deoxygenation in the future, and this deoxygenation could possibly lead to the development of widespread euxinia in the oceans with potential to induce biological crises of similar scale to the Cretaceous OAEs.

Chapter 5

Conclusions

This dissertation provides new knowledge about the dynamics in rates and pathways of both ancient and modern marine N-cycling, through the combination of information from geochemical profiles, process rate measurements, and analysis of microbial community composition, structure and function. This new knowledge was then integrated into models to study the effect of these rates on the nutrient status of the ancient oceans, the competition between metabolic pathways of interest leading to N_2 production, and the bioenergetics of anammox, denitrification and DNRA. This chapter synthesizes the dissertation's findings and concludes with a discussion on the future challenges related to the N-cycle and corresponding modeling efforts.

5.1 Dynamics in rates and pathways of anaerobic N-cycling

This dissertation describes rates and pathways of anaerobic N-metabolisms across different pelagic environments, which expands current knowledge on the factors that control the partitioning of these pathways. Prior to this work, the drivers of the partitioning were underexplored and remained unconstrained. In Chapter 2, we show the presence of Fe-dependent NO_3^- reduction – through DNRA and denitrification – under pelagic ferruginous conditions, which can serve as an analogue environment extensible to the Proterozoic oceans. The fact that these pathways are active under these analogous conditions to the ancient ocean can inform on ancient marine N-cycling and gives us further insight, when combined with the geologic record, on how anaerobic N-metabolisms would have been active. In Chapter 3 we study the variations in rates and pathways of anaerobic N-metabolisms with fine-scale temporal and spatial resolution in an anoxic fjord. This reveals rate variations of previously unappreciated magnitude, in addition to temporal changes in the partitioning of the pathways that responds to physical perturbations in the inlet. Most

studies are currently limited, both temporally and spatially, therefore overlooking these changing environmental conditions and corresponding dynamics in rates and pathways of N-cycling. In Chapter 4, we also show that DNRA is a dominant pathway of NO_x reduction, challenging current assumptions that DNRA constitutes a minor process under OMZ-like conditions. Rates of DNRA are regulated nearly exclusively by substrate supply rates, which changes the paradigm of how we think about controls on rates and partitioning of these pathways. Rather than measuring the state of physico-chemical conditions at a singular time-point (presence or absence of substrates, inhibitors, e.g.) – which is the currently accepted approach to studying these pathways – we show it can instead be the rate of change in these conditions that regulates the rates and pathways of anaerobic N-metabolisms.

5.2 Integrated approach for better modeling of biogeochemical cycling

New knowledge on the connection between rates and pathways of anaerobic N-cycling and corresponding environmental conditions presented in this thesis, promotes more thorough N-cycle models. In Chapter 2, the presence of DNRA under ferruginous conditions was tested in a reaction-transport model for a coastal upwelling set for the Proterozoic oceans. This allowed us to study the potential impact of DNRA on the nutrient status of the ancient ocean, as well as its influence on biological production, and ocean and atmospheric chemistry. Ultimately, these changes can be found in the rock record, but the study of a modern analogue can give more insight on the microbial mechanisms that could have occurred under similar conditions in the ancient oceans. In Chapter 3, we reproduce the variations in rates and pathways in a simple flux-balance model mimicking the competition between anammox and denitrification, while using kinetic parameters measured *in situ*, or inferred when the parameters were not available. Even though the model was straightforward in its structure, it generated similar rates of N-cycling and similar growth rates of relevant cell populations to those observed in Saanich Inlet. Thus, by combining geochemical (substrate concentrations) and microbiological (process rate measurements and microbial community composition) information, we are able to broadly reconstruct the rates

and pathways observed in the water column. In Chapter 4, we show that DNRA is an important N-cycle pathway in Saanich Inlet and should be considered both in conceptual and gene-centric modeling. We further show that, under dynamic (non-steady state) conditions, rates of anaerobic N-metabolisms and corresponding gene abundances, used as a proxy for microbial populations responsible for the pathways, did not scale uniformly, contradicting the current framework of gene-centric modeling.

5.3 Looking ahead

The extent to which temporal and spatial variations in rates and pathways of N-metabolisms occur in marine systems needs to be further studied globally. Indeed, it is unclear whether N-budgets are currently balanced (see Chapter 1), due to uncertainties in estimates of the N-budgets and rates of N-transformations [2]. Most studies that measure rates and pathways of N-transformations in OMZs, for example, are limited to a singular time-point, and remain relatively localized spatially (e.g. [18, 65, 67, 98, 100]). It is therefore possible that changing environmental conditions influencing changes in rates and pathways are not captured by current spatial and temporal resolution of most studies. In Chapters 3 and 4, we show that rates of denitrification and DNRA vary over several orders of magnitude on an annual basis in a coastal anoxic fjord, Saanich Inlet. These variations were linked to environmental perturbations of the inlet, which were coupled with higher substrate supply rates and thus higher energy brought to the system. Environmental perturbations can also occur in the coastal and open oceans. These can be large and meso-scale eddies [260], for example, or increased upwelling currents due to increased winds that are a consequence of climate change [263]. These changes have rarely been studied in combination with process rate measurements [103, 214] and lack altogether microbial community analysis. Thus, these observations call for a broadening of the research to rates and pathways of anaerobic N-cycling in OMZs under dynamic conditions. This would in turn allow for more accurate estimates of marine N-budgets, and further, better inform biogeochemical modeling efforts.

Biogeochemical models of N-cycling should consider DNRA as an important pathway of NO_x reduction for the reconstruction of rates and pathways of past, present and future N-cycling. In

current approaches, however, DNRA is often overlooked [5, 39, 44], and considered insignificant to global N-budgets. While DNRA is not a primary source of fixed-N, the activity of DNRA can impact biological productivity by mitigating N-loss, through anammox and denitrification, by diverting the products of NO_x reduction to NH_4^+ rather than to N_2, with the retained N being upwelled to surface waters and feeding primary production. In Chapters 2 and 4, we indeed determine that DNRA plays an important role in NO_x reduction, more than previously thought, both in ferruginous conditions that are analogous to the Proterozoic oceans, as well as in a modern coastal anoxic fjord. Furthermore, in Chapter 2, a higher partitioning of NO_x reduction through DNRA was shown through modeling to lead to higher rates of primary production in the surface waters of the Proterozoic oceans, with corresponding impact on ocean and atmosphere chemistry. To confirm the activity of DNRA in the ancient oceans, it would be essential to test whether the N-isotope fractionation found in the rock record can be reproduced when adding DNRA to the pathways considered in models such as the one in Boyle et al. (2013) [44]. N-isotope fractionation through DNRA remains, however, poorly constrained so far [64], unlike denitrification and anammox, and further research is needed, both in natural and laboratory cultured settings to observe the fractionation associated with DNRA. Results in Chapter 4 also shows that rates of DNRA vary greatly in range, responding to physical perturbations in the system, and if found at larger scale in the modern oceans, could have similar effect on biological productivity and ocean chemistry. This switch between denitrification and DNRA in response to dynamic conditions should also be considered in current modeling efforts, in light of deoxygenation of the modern oceans [72] and changes in ocean circulation due to climate change [262, 263] . Together, these results call for the consideration of DNRA in models for the past, and reconstruction of present and future conditions.

Key-players involved in anaerobic N-cycling in Saanich Inlet remain elusive, and their corresponding ecophysiological information unknown, and this information is key to refining current models. These key-players found in Saanich Inlet are likely extensible to other parts of the oceans, and could greatly impact N-cycling under specific environmental conditions. The ecophysiological information associated with the key-players is difficult to constrain, however, due to the complexity of the microbial community involved in these pathways. In Chapter 3, we identified two differing

denitrifying populations – SUP05 and Marinimicrobia versus *Arcobacter* – and these populations were linked to changes in rates of N_2 production, with either low or high rates of N_2-production, respectively. Although SUP05 and Marinimicrobia were previously recognized as key-players in Saanich Inlet [33, 187], the involvement of *Arcobacter* needs to be further confirmed through meta'omic analysis that can be used to test its potential and expressed metabolic activities. In Chapter 4, we also detected genes involved in DNRA, which was previously omitted in the conceptual metabolic model developed for Saanich Inlet [33]. The taxonomic identification of key-players involved in DNRA remains unknown so far and thus, missing taxa have yet to be uncovered for Saanich Inlet. This information will allow us to improve existing conceptual models of N-cycling, and likely add relevant key-players involved in NO_x reduction. Another notable finding from this thesis is that the gene-centric modeling approach, which states that changes in rates scale with changes in the abundance of the genes that code for the enzyme conducting the metabolic pathway [118, 119], is not applicable under dynamic (non-steady state) conditions. This therefore asks for further details on ecophysiological parameters such as biomass yields of relevant taxa changing with different growth conditions, as well as taxon-specific growth and death rates. To do so, new information could be produced through cultivation of relevant taxa in the lab. The culture of these taxa might not be feasible, as is the case for many environmental taxa (e.g. anammox bacteria), but other techniques could be used to measure taxon-specific growth and death rates in the environment, for example through stable isotope probing techniques [267]. The fact that we cannot model rates and pathways of anaerobic N-cycling under dynamic conditions underscores the lack of knowledge on the metabolic and growth parameters of relevant taxa.

5.4 Closing

Over the span of $\sim$4 billion years, the Earth's surface redox state has been drastically altered through coupling of geologic and microbial metabolic processes. The interactions between these processes are extremely complex and require both in-depth knowledge of the micro-scale as well as the global system in order to model the multiple feedback loops that constitute these interactions. This dissertation developed a more informed modeling framework for ancient

and contemporaneous N-cycle predictions that incorporates geochemical and microbiological information. By using an integrated approach in a specific environment to develop new knowledge, resulting models can be made extensible to other environments. As the Earth is entering the Anthropocene, a new geologic epoch where humankind is the main driver in changing the redox state of the Earth's surface, unprecedented alterations to the environment and climate are occurring. These alterations will be disruptors of current biogeochemical cycling and predictions of the feedbacks from microbial processes that will arise from it are largely unconstrained. Collaboration between fields, from climate modeling to environmental microbiology, will therefore be necessary in order to tackle future changes. By being able to predict what the future will look like given the current path that we are headed, this will allow us to plan how humankind needs to bio/geoengineer changes in order to keep a life-sustainable planet.

Bibliography

[1] N. Gruber and J. N. Galloway. An earth-system perspective of the global nitrogen cycle. *Nature*, 451:293, 01/16/online 2008.

[2] D. E. Canfield, A. N. Glazer, and P. G. Falkowski. The evolution and future of earth's nitrogen cycle. *Science*, 330(6001):192–6, Oct 8 2010. Canfield, Donald E Glazer, Alexander N Falkowski, Paul G eng Research Support, Non-U.S. Gov't Research Support, U.S. Gov't, Non-P.H.S. Review New York, N.Y. 2010/10/12 06:00 Science. 2010 Oct 8;330(6001):192-6. doi: 10.1126/science.1186120.

[3] M. M. M. Kuypers, H. K. Marchant, and B. Kartal. The microbial nitrogen-cycling network. *Nature Reviews Microbiology*, 16:263, 02/05/online 2018.

[4] D. E. Canfield, E. Kristensen, and B. Thamdrup. Aquatic geomicrobiology. *Adv Mar Biol*, 48:1–599, 2005. Canfield, Donald E Kristensen, Erik Thamdrup, Bo eng Review Adv Mar Biol. 2005;48:1-599. doi: 10.1016/S0065-2881(05)48017-7.

[5] D. E. Canfield. Models of oxic respiration, denitrification and sulfate reduction in zones of coastal upwelling. *Geochimica Et Cosmochimica Acta*, 70(23):5753–5765, Dec 1 2006.

[6] Sterner, Robert, and Elser. *Ecological Stoichiometry: The Biology of Elements From Molecules to The Biosphere*. 2002.

[7] H. Bothe, O. Schmitz, M. G. Yates, and W. E. Newton. Nitrogen fixation and hydrogen metabolism in cyanobacteria. *Microbiology and Molecular Biology Reviews : MMBR*, 74(4):529–551, 2010.

[8] P. G. Falkowski. Evolution of the nitrogen cycle and its influence on the biological sequestration of co2 in the ocean. *Nature*, 387(6630):272–275, May 15 1997.

[9] N. Gruber. The dynamics of the marine nitrogen cycle and its influence on atmospheric co2 variations. In M. Follows and T. Oguz, editors, *The Ocean Carbon Cycle and Climate*, pages 97–148. Kluwer Academic, Dordrecht, 2004.

[10] P. A. Schroeder and A. A. McLain. Illite-smectites and the influence of burial diagenesis on the geochemical cycling of nitrogen. *Clay Minerals*, 33(4):539–546, // 1998.

[11] V. Busigny, P. Cartigny, and P. Philippot. Nitrogen isotopes in ophiolitic metagabbros: A re-evaluation of modern nitrogen fluxes in subduction zones and implication for the early earth atmosphere. *Geochimica et Cosmochimica Acta*, 75(23):7502–7521, 2011.

[12] B. Johnson and C. Goldblatt. The nitrogen budget of earth. *Earth-Science Reviews*, 148:150–173, 2015/09/01/ 2015.

[13] R. A. Berner. Geological nitrogen cycle and atmospheric n2 over phanerozoic time. *Geology*, 34(5):413–415, 2006.

[14] C. Goldblatt, M. W. Claire, T. M. Lenton, *et al.* Nitrogen-enhanced greenhouse warming on early earth. *Nature Geoscience*, 2:891, 11/15/online 2009.

[15] J. M. Klingler, R. L. Mancinelli, and M. R. White. Biological nitrogen fixation under primordial martian partial pressures of dinitrogen. *Advances in Space Research*, 9(6):173–176, 1989/01/01/ 1989.

[16] A. L. Zerkle, S. W. Poulton, R. J. Newton, *et al.* Onset of the aerobic nitrogen cycle during the great oxidation event. *Nature*, 542:465, 02/06/online 2017.

[17] B. W. Johnson and C. Goldblatt. A secular increase in continental crust nitrogen during the precambrian. *Geochemical Perspectives Letters*, 4:24–28, 2017.

[18] D. E. Canfield, F. J. Stewart, B. Thamdrup, *et al.* A cryptic sulfur cycle in oxygen-minimum-zone waters off the chilean coast. *Science*, 330(6009):1375–1378, Dec 3 2010.

[19] P. M. Vitousek. Human domination of earth's ecosystems (vol 277, pg 494, 1997). *Science*, 278(5335):21–21, Oct 3 1997.

[20] E. A. Bell, P. Boehnke, T. M. Harrison, and W. L. Mao. Potentially biogenic carbon preserved in a 4.1 billion-year-old zircon. *Proceedings of the National Academy of Sciences*, 112(47):14518–14521, 2015.

[21] D. L. Pinti and K. Hashizume. 15n-depleted nitrogen in early archean kerogens: clues on ancient marine chemosynthetic-based ecosystems?: A comment to beaumont, v., robert, f., 1999. precambrian res. 96, 6282. *Precambrian Research*, 105(1):85–88, 2001.

[22] V. Beaumont and F. Robert. Nitrogen isotope ratios of kerogens in precambrian cherts: a record of the evolution of atmosphere chemistry? *Precambrian Research*, 96(1):63–82, 1999/06/15/ 1999.

[23] W. L. Chameides and J. C. G. Walker. Rates of fixation by lightning of carbon and nitrogen in possible primitive atmospheres. *Origins of life*, 11(4):291–302, 1981/12/01 1981.

[24] J. F. Kasting. Stability of ammonia in the primitive terrestrial atmosphere. *Journal of Geophysical Research-Oceans and Atmospheres*, 87(Nc4):3091–3098, 1982.

[25] J. F. Kasting. Bolide impacts and the oxidation state of carbon in the earth's early atmosphere. *Origins of life and evolution of the biosphere*, 20(3):199–231, 1990/05/01 1990.

[26] J.F. Kasting and J. C. G. Walker. Limits on oxygen concentration in the prebiological atmosphere and the rate of abiotic fixation of nitrogen. *Journal of Geophysical Research: Oceans*, 86(C2):1147–1158, 1981.

[27] D. P. Summers and B. Khare. Nitrogen fixation on early mars and other terrestrial planets: Experimental demonstration of abiotic fixation reactions to nitrite and nitrate. *Astrobiology*, 7(2):333–341, 2007/04/01 2007.

[28] J. A. Brandes, R. M. Hazen, and H. S. Yoder. Inorganic nitrogen reduction and stability under simulated hydrothermal conditions. *Astrobiology*, 8(6):1113–1126, 2008/12/01 2008.

[29] A. Smirnov, D. Hausner, R. Laffers, D. R. Strongin, and M. A. A. Schoonen. Abiotic ammonium formation in the presence of ni-fe metals and alloys and its implications for the hadean nitrogen cycle. *Geochemical Transactions*, 9:5–5, 05/19 10/02/received 05/19/accepted 2008.

[30] A. L. Zerkle, C. K. Junium, D. E. Canfield, and C. H. House. Production of 15ndepleted biomass during cyanobacterial n2fixation at high fe concentrations. *Journal of Geophysical Research: Biogeosciences*, 113(G3), 2008.

[31] J. B. Glass, F. Wolfe-Simon, and A. D. Anbar. Coevolution of metal availability and nitrogen assimilation in cyanobacteria and algae. *Geobiology*, 7(2):100–23, Mar 2009.

[32] P. G. Falkowski, T. Fenchel, and E. F. Delong. The microbial engines that drive earth's biogeochemical cycles. *Science*, 320(5879):1034–1039, May 23 2008.

[33] A. K. Hawley, H. M. Brewer, A. D. Norbeck, L. Pasa-Tolic, and S. J. Hallam. Metaproteomics reveals differential modes of metabolic coupling among ubiquitous oxygen minimum zone microbes. *Proc Natl Acad Sci U S A*, 111(31):11395–400, Aug 05 2014.

[34] R. Buick. When did oxygenic photosynthesis evolve? *Philosophical Transactions of the Royal Society B: Biological Sciences*, 363(1504):2731–2743, 05/09 2008.

[35] S. A. Crowe, L. N. Dssing, N. J. Beukes, *et al.* Atmospheric oxygenation three billion years ago. *Nature*, 501:535, 09/25/online 2013.

[36] M. T. Rosing and R. Frei. U-rich archaean sea-floor sediments from greenland indications of ¿3700 ma oxygenic photosynthesis. *Earth and Planetary Science Letters*, 217(3):237–244, 2004/01/15/ 2004.

[37] C. Magnabosco, K. R. Moore, J. M. Wolfe, and G. P. Fournier. Dating phototrophic microbial lineages with reticulate gene histories. *Geobiology*, 16(2):179–189, Mar 2018.

[38] S. L. Olson, L. R. Kump, and J. F. Kasting. Quantifying the areal extent and dissolved oxygen concentrations of archean oxygen oases. *Chemical Geology*, 362:35 – 43, 2013. Special Issue dedicated to H.D. Holland: Evolution of the atmosphere and ocean through time.

[39] K. Fennel, M. Follows, and P. G. Falkowski. The co-evolution of the nitrogen, carbon and oxygen cycles in the proterozoic ocean. *American Journal of Science*, 305(6-8):526–545, 2005.

[40] L. V. Godfrey and P. G. Falkowski. The cycling and redox state of nitrogen in the archaean ocean. *Nature Geoscience*, 2:725, 09/13/online 2009.

[41] A. L. Zerkle and S. Mikhail. The geobiological nitrogen cycle: From microbes to the mantle. *Geobiology*, 15(3):343–352, 2017.

[42] L. V. Godfrey, S. W. Poulton, G. E. Bebout, and P. W. Fralick. Stability of the nitrogen cycle during development of sulfidic water in the redox-stratified late paleoproterozoic ocean. *Geology*, 41(6):655, 2013.

[43] C. Thomazo, D. L. Pinti, V. Busigny, *et al.* Biological activity and the earth's surface evolution: Insights from carbon, sulfur, nitrogen and iron stable isotopes in the rock record. *Comptes Rendus Palevol*, 8(7):665–678, 2009/10/01/ 2009.

[44] R. A. Boyle, J. R. Clark, S. W. Poulton, *et al.* Nitrogen cycle feedbacks as a control on euxinia in the mid-proterozoic ocean. *Nature Communications*, 4, Feb 2013.

[45] D. E. Canfield. A new model for proterozoic ocean chemistry. *Nature*, 396(6710):450–453, Dec 3 1998.

[46] H. D. Holland. *The Chemical Evolution of the Atmosphere and Oceans*. Princeton University Press, 1984.

[47] D. T. Johnston, S. W. Poulton, C. Dehler, *et al.* An emerging picture of neoproterozoic ocean chemistry: Insights from the chuar group, grand canyon, usa. *Earth and Planetary Science Letters*, 290(1-2):64–73, Feb 15 2010.

[48] C. Li, G. D. Love, T. W. Lyons, *et al.* A stratified redox model for the ediacaran ocean. *Science*, 328(5974):80–83, Apr 2 2010.

[49] C. T. Reinhard, R. Raiswell, C. Scott, A. D. Anbar, and T. W. Lyons. A late archean sulfidic sea stimulated by early oxidative weathering of the continents. *Science*, 326(5953):713–716, Oct 30 2009.

[50] M. Lliros, T. Garcia-Armisen, F. Darchambeau, *et al.* Pelagic photoferrotrophy and iron cycling in a modern ferruginous basin. *Sci Rep*, 5:13803, 2015.

[51] X. A. Walter, A. Picazo, M. R. Miracle, *et al.* Phototrophic fe(ii)-oxidation in the chemocline of a ferruginous meromictic lake. *Frontiers in Microbiology*, 5:713, 12/08 09/08/received 11/30/accepted 2014.

[52] A-C. Lehours, I. Batisson, A. Guedon, G. Mailhot, and G. Fonty. Diversity of culturable bacteria, from the anaerobic zone of the meromictic lake pavin, able to perform dissimilatory-iron reduction in different in vitro conditions. *Geomicrobiology Journal*, 26(3):212–223, 2009/03/13 2009.

[53] M. A. Lazzaretti, K. W. Hanselmann, H. Brandl, D. Span, and R. Bachofen. *The role of sediments in the phosphorus cycle in Lake Lugano. II. Seasonal and spatial variability of microbiological processes at the sediment-water interface*, volume 54. 1992.

[54] S. A. Crowe, J. A. Maresca, C. Jones, *et al.* Deep-water anoxygenic photosythesis in a ferruginous chemocline. *Geobiology*, 12(4):322–39, Jul 2014.

[55] S. W. Poulton, P. W. Fralick, and D. E. Canfield. Spatial variability in oceanic redox structure 1.8 billion years ago. *Nature Geoscience*, 3(7):486–490, Jul 2010.

[56] M. M. Jensen, J. Petersen, T. Dalsgaard, and B. Thamdrup. Pathways, rates, and regulation of n-2 production in the chemocline of an anoxic basin, mariager fjord, denmark. *Marine Chemistry*, 113(1-2):102–113, Jan 30 2009.

[57] Frost and McDowell. The dissociation energy of the nitrogen molecule. *Proceedings of the Royal Society of London. Series A. Mathematical and Physical Sciences*, 236(1205):278, 1956.

[58] K. L. Straub, M. Benz, B. Schink, and F. Widdel. Anaerobic, nitrate-dependent microbial oxidation of ferrous iron. *Appl Environ Microbiol*, 62(4):1458–60, Apr 1996.

[59] K. A. Weber, M. M. Urrutia, P. F. Churchill, R. K. Kukkadapu, and E. E. Roden. Anaerobic redox cycling of iron by freshwater sediment microorganisms. *Environmental Microbiology*, 8(1):100–113, Jan 2006.

[60] T. Kalvelage, G. Lavik, P. Lam, *et al.* Nitrogen cycling driven by organic matter export in the south pacific oxygen minimum zone. *Nature Geoscience*, 6(3):228–234, Mar 2013.

[61] M. Strous, J. A. Fuerst, E. H. M. Kramer, *et al.* Missing lithotroph identified as new planctomycete. *Nature*, 400(6743):446–449, 07/29/print 1999.

[62] B. Kartal, N. M. de Almeida, W. J. Maalcke, *et al.* How to make a living from anaerobic ammonium oxidation. *Fems Microbiology Reviews*, 37(3):428–461, May 2013. 123cb Times Cited:98 Cited References Count:201.

[63] L. A. Codispoti, J. A. Brandes, J. P. Christensen, *et al.* The oceanic fixed nitrogen and nitrous oxide budgets: Moving targets as we enter the anthropocene? *Scientia Marina*, 65:85–105, Sep 2001.

[64] M. G. Prokopenko, M. B. Hirst, L. De Brabandere, *et al.* Nitrogen losses in anoxic marine sediments driven by thioploca-anammox bacterial consortia. *Nature*, 500(7461):194–8, Aug 8 2013. Prokopenko, M G Hirst, M B De Brabandere, L Lawrence, D J P Berelson, W M Granger, J Chang, B X Dawson, S Crane, E J 3rd Chong, L Thamdrup, B Townsend-Small, A Sigman, D M eng Research Support, U.S. Gov't, Non-P.H.S. England 2013/08/09 06:00 Nature. 2013 Aug 8;500(7461):194-8. doi: 10.1038/nature12365.

[65] M. M. Jensen, P. Lam, N. P. Revsbech, *et al.* Intensive nitrogen loss over the omani shelf due to anammox coupled with dissimilatory nitrite reduction to ammonium. *Isme Journal*, 5(10):1660–1670, Oct 2011.

[66] M. M. M. Kuypers, G. Lavik, D. Woebken, *et al.* Massive nitrogen loss from the benguela upwelling system through anaerobic ammonium oxidation. *Proceedings of the National Academy of Sciences of the United States of America*, 102(18):6478–6483, 2005.

[67] P. Lam, G. Lavik, M. M. Jensen, *et al.* Revising the nitrogen cycle in the peruvian oxygen minimum zone. *Proceedings of the National Academy of Sciences of the United States of America*, 106(12):4752–4757, Mar 24 2009.

[68] Ph. Lam and M. M. M. Kuypers. Microbial nitrogen cycling processes in oxygen minimum zones. *Annual Review of Marine Science*, 3(1):317–345, 2011/01/15 2010.

[69] B. B. Ward, A. H. Devol, J. J. Rich, *et al.* Denitrification as the dominant nitrogen loss process in the arabian sea. *Nature*, 461(7260):78–81, 09/03/print 2009.

[70] T. Ohde, H. Siegel, J. Reimann, and M. Gerth. Identification and investigation of sulphur plumes along the namibian coast using the meris sensor. *Continental Shelf Research*, 27(6):744–756, 2007/03/15/ 2007.

[71] S. J. Weeks, B. Currie, A. Bakun, and K. R. Peard. Hydrogen sulphide eruptions in the atlantic ocean off southern africa: implications of a new view based on seawifs satellite imagery. *Deep Sea Research Part I: Oceanographic Research Papers*, 51(2):153–172, 2004/02/01/ 2004.

[72] D. Breitburg, L. A. Levin, A. Oschlies, *et al.* Declining oxygen in the global ocean and coastal waters. *Science*, 359(6371), 2018.

[73] L. P. Nielsen. Denitrification in sediment determined from nitrogen isotope pairing. *FEMS Microbiology Letters*, 86(4):357–362, 1992.

[74] M. Holtappels, G. Lavik, M. M. Jensen, and M. M. Kuypers. 15n-labeling experiments to dissect the contributions of heterotrophic denitrification and anammox to nitrogen removal in the omz waters of the ocean. *Methods Enzymol*, 486:223–51, 2011.

[75] J. Meija, B. Coplen Tyler, M. Berglund, *et al.* Atomic weights of the elements 2013 (iupac technical report), 2016.

[76] E.A. Paul, J. Melillo, R. Knowles, and H. Blackburn. *Nitrogen Isotope Techniques*. Elsevier Science, 2012.

[77] B. Eyre, S. Rysgaard, T. Dalsgaard, and P. Christensen. *Comparison of isotope pairing and N2:Ar methods for measuring sediment denitrificationAssumption, modifications, and implications*, volume 25. 2002.

[78] J. Brandes. *Isotopic effects of denitrification in the marine environment*. 1996.

[79] T. Yoshinari and R. Knowles. Acetylene inhibition of nitrous oxide reduction by denitrifying bacteria. *Biochemical and Biophysical Research Communications*, 69(3):705–710, 1976/04/05/ 1976.

[80] A. C. Redfield. The biological control of chemical factors in the environment. *American Scientist*, 46(3):230A–221, 1958.

[81] N. Gruber. *The Marine Nitrogen Cycle: Overview and Challenges*. 2008.

[82] A. Mulder, A. A. Vandegraaf, L. A. Robertson, and J. G. Kuenen. Anaerobic ammonium oxidation discovered in a denitrifying fluidized-bed reactor. *Fems Microbiology Ecology*, 16(3):177–183, Mar 1995. Qn679 Times Cited:512 Cited References Count:21.

[83] B. Thamdrup and T. Dalsgaard. Production of n(2) through anaerobic ammonium oxidation coupled to nitrate reduction in marine sediments. *Appl Environ Microbiol*, 68(3):1312–8, Mar 2002.

[84] M. R. Hamersley, G. Lavik, D. Woebken, *et al.* Anaerobic ammonium oxidation in the peruvian oxygen minimum zone. *Limnology and Oceanography*, 52(3):923–933, 2007.

[85] M. M. Kuypers, A. O. Sliekers, G. Lavik, *et al.* Anaerobic ammonium oxidation by anammox bacteria in the black sea. *Nature*, 422(6932):608–11, Apr 10 2003.

[86] K.C. Cameron, H.J. Di, and J.L. Moir. Nitrogen losses from the soil/plant system: a review. *Annals of Applied Biology*, 162(2):145–173, 2013.

[87] S. Humbert, S. Tarnawski, N. Fromin, *et al.* Molecular detection of anammox bacteria in terrestrial ecosystems: distribution and diversity. *The Isme Journal*, 4:450, 12/10/online 2009.

[88] T. Rtting, P. Boeckx, C. Mller, and L. Klemedtsson. Assessment of the importance of dissimilatory nitrate reduction to ammonium for the terrestrial nitrogen cycle. *Biogeosciences*, 8:1779–1791, 2011.

[89] B. Romain, P. W. Leadley, and B. A. Hungate. Global change, nitrification, and denitrification: A review. *Global Biogeochemical Cycles*, 19(1), 2005.

[90] M. Trimmer and J. C. Nicholls. Production of nitrogen gas via anammox and denitrification in intact sediment cores along a continental shelf to slope transect in the north atlantic. *Limnology and Oceanography*, 54(2):577–589, Mar 2009.

[91] L. F. Dong, M. N. Sobey, C. J. Smith, *et al.* Dissimilatory reduction of nitrate to ammonium, not denitrification or anammox, dominates benthic nitrate reduction in tropical estuaries. *Limnology and Oceanography*, 56(1):279–291, 2011.

[92] W. P. Porubsky, N. B. Weston, and S. B. Joye. Benthic metabolism and the fate of dissolved inorganic nitrogen in intertidal sediments. *Estuarine, Coastal and Shelf Science*, 83(4):392–402, 2009/08/01/ 2009.

[93] G. D. Song, S. M. Liu, H. Marchant, M. M. M. Kuypers, and G. Lavik. Anammox, denitrification and dissimilatory nitrate reduction to ammonium in the east china sea sediment. *Biogeosciences*, 10(11):6851–6864, 2013.

[94] S. Rysgaard and R. N. Glud. Anaerobic n2 production in arctic sea ice. *Limnology and Oceanography*, 49(1):86–94, 2004.

[95] L. Bohlen, A. Dale, S. Sommer, *et al. Benthic nitrogen cycling traversing the Peruvian oxygen minimum zone*, volume 75. 2011.

[96] K. L. Roberts, V. M. Eate, B. D. Eyre, D. P. Holland, and P. L. M. Cook. Hypoxic events stimulate nitrogen recycling in a shallow saltwedge estuary: The yarra river estuary, australia. *Limnology and Oceanography*, 57(5):1427–1442, 2012.

[97] K. L. Roberts, A. J. Kessler, M. R. Grace, and P. L. M. Cook. Increased rates of dissimilatory nitrate reduction to ammonium (dnra) under oxic conditions in a periodically hypoxic estuary. *Geochimica Et Cosmochimica Acta*, 133:313–324, May 15 2014.

[98] L. De Brabandere, D. E. Canfield, T. Dalsgaard, *et al.* Vertical partitioning of nitrogen-loss processes across the oxic-anoxic interface of an oceanic oxygen minimum zone. *Environ Microbiol*, 16(10):3041–54, Oct 2014.

[99] A. Burgin, S. Hamilton, S. E. Jones, and J. Lennon. *Denitrification by sulfur-oxidizing bacteria in a eutrophic lake*, volume 66. 2012.

[100] T. Dalsgaard, D. E. Canfield, J. Petersen, B. Thamdrup, and J. Acuna-Gonzalez. N2 production by the anammox reaction in the anoxic water column of golfo dulce, costa rica. *Nature*, 422(6932):606–8, Apr 10 2003.

[101] A. Bourbonnais, M. F. Lehmann, David A. Butterfield, and S. Kim Juniper. Subseafloor nitrogen transformations in diffuse hydrothermal vent fluids of the juan de fuca ridge evidenced by the isotopic composition of nitrate and ammonium. *Geochemistry, Geophysics, Geosystems*, 13(2), 2012.

[102] H. Schunck, G. Lavik, D. K. Desai, *et al.* Giant hydrogen sulfide plume in the oxygen minimum zone off peru supports chemolithoautotrophy. *Plos One*, 8(8), Aug 21 2013. 218YW Times Cited:1 Cited References Count:113.

[103] A. Bourbonnais, M. A. Altabet, C. N. Charoenpong, *et al.* N-loss isotope effects in the peru oxygen minimum zone studied using a mesoscale eddy as a natural tracer experiment. *Global Biogeochemical Cycles*, 29(6):793–811, 2015/06/01 2015.

[104] J. J. Wright, K. M. Konwar, and S. J. Hallam. Microbial ecology of expanding oxygen minimum zones. *Nature Reviews Microbiology*, 10(6):381, 2012.

[105] A. R. Babbin, R. G. Keil, A. H. Devol, and B. B. Ward. Organic matter stoichiometry, flux, and oxygen control nitrogen loss in the ocean. *Science*, 344(6182):406–408, Apr 25 2014.

[106] S. Bonaglia, I. Klawonn, L. De Brabandere, *et al.* Denitrification and dnra at the baltic sea oxic–anoxic interface: Substrate spectrum and kinetics. *Limnology and Oceanography*, 61(5):1900–1915, 2016/09/01 2016.

[107] C. B. Wenk, J. Blees, J. Zopfi, *et al.* Anaerobic ammonium oxidation (anammox) bacteria and sulfide-dependent denitrifiers coexist in the water column of a meromictic south-alpine lake. *Limnology and Oceanography*, 58(1):1–12, Jan 2013.

[108] D. E. LaRowe and P. Van Cappellen. Degradation of natural organic matter: A thermodynamic analysis. *Geochimica Et Cosmochimica Acta*, 75(8):2030–2042, Apr 15 2011. 796EJ Times Cited:11 Cited References Count:92.

[109] T. Awata, M. Oshiki, T. Kindaichi, *et al.* Physiological characterization of an anaerobic ammonium-oxidizing bacterium belonging to the "candidatus scalindua" group. *Applied and Environmental Microbiology*, 79(13):4145–4148, Jul 2013.

[110] T. Dalsgaard and B. Thamdrup. Factors controlling anaerobic ammonium oxidation with nitrite in marine sediments. *Appl Environ Microbiol*, 68(8):3802–8, Aug 2002.

[111] E. K. Robertson and B. Thamdrup. The fate of nitrogen is linked to iron(ii) availability in a freshwater lake sediment. *Geochimica et Cosmochimica Acta*, 205:84–99, 5/15/ 2017.

[112] J. C. Nicholls and M. Trimmer. Widespread occurrence of the anammox reaction in estuarine sediments. *Aquatic Microbial Ecology*, 55(2):105–113, 2009.

[113] R. C. Brunet and L. J. GarciaGil. Sulfide–induced dissimilatory nitrate reduction to ammonia in anaerobic freshwater sediments. *FEMS Microbiology Ecology*, 21(2):131–138, 1996/10/01 1996.

[114] M. M. Jensen, M. M. M. Kuypers, L. Gaute, and B. Thamdrup. Rates and regulation of anaerobic ammonium oxidation and denitrification in the black sea. *Limnology and Oceanography*, 53(1):23–36, 2008.

[115] F. Lipschultz, S. C. Wofsy, B. B. Ward, *et al.* Bacterial transformations of inorganic nitrogen in the oxygen-deficient waters of the eastern tropical south pacific ocean. *Deep Sea Research Part A. Oceanographic Research Papers*, 37(10):1513–1541, 1990/10/01/ 1990.

[116] L. A. Bristow, T. Dalsgaard, L. Tiano, *et al.* Ammonium and nitrite oxidation at nanomolar oxygen concentrations in oxygen minimum zone waters. *Proceedings of the National Academy of Sciences*, 113(38):10601–10606, 2016.

[117] A. E. Giblin, N. B. Weston, G. T. Banta, J. Tucker, and C. S. Hopkinson. The effects of salinity on nitrogen losses from an oligohaline estuarine sediment. *Estuaries and Coasts*, 33(5):1054–1068, 2010/09/01 2010.

[118] S. Louca, A. K. Hawley, S. Katsev, *et al.* Integrating biogeochemistry with multiomic sequence information in a model oxygen minimum zone. *Proc Natl Acad Sci U S A*, 113(40):E5925–E5933, Oct 04 2016.

[119] D. C. Reed, C. K. Algar, J. A. Huber, and G. J. Dick. Gene-centric approach to integrating environmental genomics and biogeochemical models. *Proceedings of the National Academy of Sciences of the United States of America*, 111(5):1879–1884, Feb 4 2014.

[120] H. Stevens and O. Ulloa. Bacterial diversity in the oxygen minimum zone of the eastern tropical south pacific. (1462-2920 (Electronic)), 2008.

[121] O. Ulloa, D. E. Canfield, E. F. DeLong, R. M. Letelier, and F. J. Stewart. Microbial oceanography of anoxic oxygen minimum zones. *Proceedings of the National Academy of Sciences of the United States of America*, 109(40):15996–16003, Oct 2 2012.

[122] R. R Eady. Structure function relationships of alternative nitrogenases. *Chemical reviews*, 96(7):3013–3030, 1996.

[123] P. M. Vitousek and R. W. Howarth. Nitrogen limitation on land and in the sea: how can it occur? *Biogeochemistry*, 13(2):87–115, 1991.

[124] I. Berman-Frank, P. Lundgren, and P. Falkowski. Nitrogen fixation and photosynthetic oxygen evolution in cyanobacteria. *Res Microbiol*, 154(3):157–64, Apr 2003.

[125] A. W. Thompson, R. A. Foster, A. Krupke, *et al.* Unicellular cyanobacterium symbiotic with a single-celled eukaryotic alga. *Science*, 337(6101):1546–1550, 2012.

[126] T. O. Delmont, C. Quince, A. Shaiber, *et al.* Nitrogen-fixing populations of planctomycetes and proteobacteria are abundant in surface ocean metagenomes. *Nature Microbiology*, 3(7):804–813, 2018/07/01 2018.

[127] R. H. Burris. Biological nitrogen fixation. *Annual Review of Plant Physiology*, 17(1):155–184, 1966.

[128] E. S. Boyd, A. M. G. Costas, T. L. Hamilton, F. Mus, and J. W. Peters. Evolution of molybdenum nitrogenase during the transition from anaerobic to aerobic metabolism. *Journal of Bacteriology*, 197(9):1690–1699, May 1, 2015 2015.

[129] A. B. Hooper, T. Vannelli, D. J. Bergmann, and D. M. Arciero. Enzymology of the oxidation of ammonia to nitrite by bacteria. *Antonie van Leeuwenhoek*, 71(1-2):59–67, 1997.

[130] J. I. Prosser and G. W. Nicol. Relative contributions of archaea and bacteria to aerobic ammonia oxidation in the environment. *Environmental microbiology*, 10(11):2931–2941, 2008.

[131] J. Simon and M. G. Klotz. Diversity and evolution of bioenergetic systems involved in microbial nitrogen compound transformations. *Biochimica et Biophysica Acta (BBA)-Bioenergetics*, 1827(2):114–135, 2013.

[132] H. Daims, E. V. Lebedeva, P. Pjevac, *et al.* Complete nitrification by nitrospira bacteria. *Nature*, 528:504, 11/26/online 2015.

[133] H. Daims, S. Lcker, and M. Wagner. A new perspective on microbes formerly known as nitrite-oxidizing bacteria. *Trends in microbiology*, 24(9):699–712, 2016.

[134] C. Moreno-Vivian, P. Cabello, M. Martinez-Luque, R. Blasco, and F. Castillo. Prokaryotic nitrate reduction: molecular properties and functional distinction among bacterial nitrate reductases. *J Bacteriol*, 181(21):6573–84, Nov 1999.

[135] D. Tsementzi, J. Wu, S. Deutsch, *et al.* Sar11 bacteria linked to ocean anoxia and nitrogen loss. *Nature*, 536:179, 08/03/online 2016.

[136] A. Preisler, D. de Beer, A. Lichtschlag, *et al.* Biological and chemical sulfide oxidation in a beggiatoa inhabited marine sediment. *The Isme Journal*, 1:341, 06/28/online 2007.

[137] L. B. Maia and J. J. G. Moura. How biology handles nitrite. *Chemical Reviews*, 114(10):5273–5357, 2014/05/28 2014.

[138] D. R. H. Graf, C. M. Jones, and S. Hallin. Intergenomic comparisons highlight modularity of the denitrification pathway and underpin the importance of community structure for n2o emissions. *PloS one*, 9(12):e114118, 2014.

[139] R. A. Sanford, D. D. Wagner, Q. Wu, *et al.* Unexpected nondenitrifier nitrous oxide reductase gene diversity and abundance in soils. *Proc Natl Acad Sci U S A*, 109(48):19709–14, Nov 27 2012.

[140] J. A. Cole and C. M. Brown. Nitrite reduction to ammonia by fermentative bacteria: a short circuit in the biological nitrogen cycle. *FEMS Microbiology Letters*, 7:65–72, 1980.

[141] J. Simon. Enzymology and bioenergetics of respiratory nitrite ammonification. *FEMS Microbiol Rev*, 26(3):285–309, Aug 2002. Simon, Jorg eng Research Support, Non-U.S. Gov't Review Netherlands 2002/08/08 10:00 FEMS Microbiol Rev. 2002 Aug;26(3):285-309.

[142] M. G. Klotz, M. C. Schmid, M. Strous, *et al.* Evolution of an octahaem cytochrome c protein family that is key to aerobic and anaerobic ammonia oxidation by bacteria. *Environmental Microbiology*, 10(11):3150–3163, 2008.

[143] O. Einsle. Structure and function of formate-dependent cytochrome c nitrite reductase, nrfa. *Methods Enzymol*, 496:399–422, 2011.

[144] S. B. Mohan, M. Schmid, M. Jetten, and J. Cole. Detection and widespread distribution of the nrfa gene encoding nitrite reduction to ammonia, a short circuit in the biological nitrogen cycle that competes with denitrification. *FEMS Microbiol Ecol*, 49(3):433–43, Sep 1 2004. Mohan, Sudesh B Schmid, Markus Jetten, Mike Cole, Jeff eng Research Support, Non-U.S. Gov't England 2004/09/01 00:00 FEMS Microbiol Ecol. 2004 Sep 1;49(3):433-43. doi: 10.1016/j.femsec.2004.04.012.

[145] L. A. van Niftrik, J. A. Fuerst, J. S. S. Damst, *et al.* The anammoxosome: an intracytoplasmic compartment in anammox bacteria. *FEMS Microbiology Letters*, 233(1):7–13, 2004.

[146] R. Bartossek, G. W. Nicol, A. Lanzen, HP. Klenk, and C. Schleper. Homologues of nitrite reductases in ammoniaoxidizing archaea: diversity and genomic context. *Environmental microbiology*, 12(4):1075–1088, 2010.

[147] H. R. Harhangi, M. Le Roy, T. van Alen, *et al.* Hydrazine synthase, a unique phylomarker with which to study the presence and biodiversity of anammox bacteria. *Applied and environmental microbiology*, 78(3):752–758, 2012.

[148] B. Kartal, W. J. Maalcke, N. M. de Almeida, *et al.* Molecular mechanism of anaerobic ammonium oxidation. *Nature*, 479:127, 10/02/online 2011.

[149] A. Paulmier and D. Ruiz-Pino. Oxygen minimum zones (omzs) in the modern ocean. *Progress in Oceanography*, 80(34):113–128, 3// 2009.

[150] S. W. Poulton and D. E. Canfield. Ferruginous conditions: A dominant feature of the ocean through earth's history. *Elements*, 7(2):107–112, Apr 2011.

[151] K. Grasshoff, M. Ehrhardt, K. Kremling, and L. G. Anderson. *Methods of seawater analysis*. Wiley-VCH, Weinheim ; New York, 3rd, completely rev. and extended edition, 1999.

[152] A. Fontijn, A. J. Sabadell, and R. J. Ronco. Homogeneous chemiluminescent measurement of nitric oxide with ozone - implications for continuous selective monitoring of gaseous air pollutants. *Analytical Chemistry*, 42(6):575–&, 1970.

[153] E. Viollier, P. W. Inglett, K. Hunter, A. N. Roychoudhury, and P. Van Cappellen. The ferrozine method revisited: Fe(ii)/fe(iii) determination in natural waters. *Applied Geochemistry*, 15(6):785–790, Jul 2000.

[154] B. Thamdrup, T. Dalsgaard, M. M. Jensen, *et al.* Anaerobic ammonium oxidation in the oxygen-deficient waters off northern chile. *Limnology and Oceanography*, 51(5):2145–2156, 2006.

[155] E. K. Robertson, K. L. Roberts, L. D. W. Burdorf, P. Cook, and B. Thamdrup. Dissimilatory nitrate reduction to ammonium coupled to fe(ii) oxidation in sediments of a periodically hypoxic estuary. *Limnology and Oceanography*, 61(1):365–381, Jan 2016.

[156] D. E. Canfield, M. T. Rosing, and C. Bjerrum. Early anaerobic metabolisms. *Philosophical Transactions of the Royal Society B-Biological Sciences*, 361(1474):1819–1834, Oct 29 2006.

[157] T. Tyrrell. The relative influences of nitrogen and phosphorus on oceanic primary production. *Nature*, 400(6744):525–531, 08/05/print 1999.

[158] C. Jones, S. Nomosatryo, S. A. Crowe, C. J. Bjerrum, and D. E. Canfield. Iron oxides, divalent cations, silica, and the early earth phosphorus crisis. *Geology*, 43(2):135–138, Feb 2015.

[159] L. A. Derry. Causes and consequences of mid-proterozoic anoxia. *Geophysical Research Letters*, 42(20):8538–8546, Oct 28 2015.

[160] S. Zhang, X. Wang, H. Wang, *et al.* Sufficient oxygen for animal respiration 1,400 million years ago. *Proc Natl Acad Sci U S A*, 113(7):1731–6, Feb 16 2016.

[161] N. J. Planavsky, C. T. Reinhard, X. L. Wang, *et al.* Low mid-proterozoic atmospheric oxygen levels and the delayed rise of animals. *Science*, 346(6209):635–638, Oct 31 2014.

[162] J. H. Martin, G. A. Knauer, D. M. Karl, and W. W. Broenkow. Vertex - carbon cycling in the northeast pacific. *Deep-Sea Research Part a-Oceanographic Research Papers*, 34(2):267–285, Feb 1987.

[163] A. D. Anbar and A. H. Knoll. Proterozoic ocean chemistry and evolution: A bioinorganic bridge? *Science*, 297(5584):1137–1142, Aug 16 2002.

[164] D. G. Capone. Marine nitrogen fixation: what's the fuss? *Current Opinion in Microbiology*, 4(3):341–348, Jun 2001.

[165] L. A. Codispoti. An oceanic fixed nitrogen sink exceeding 400 tg na-1 vs the concept of homeostasis in the fixed-nitrogen inventory. *Biogeosciences*, 4(2):233–253, 2007.

[166] R. F. Keeling, A. Kortzinger, and N. Gruber. Ocean deoxygenation in a warming world. *Annual Review of Marine Science*, 2:199–229, 2010.

[167] S. Schmidtko, L. Stramma, and M. Visbeck. Decline in global oceanic oxygen content during the past five decades. *Nature*, 542:335, 02/15/online 2017.

[168] A. Mucci, B. Sundby, M. Gehlen, *et al.* The fate of carbon in continental shelf sediments of eastern canada: a case study. *Deep Sea Research Part II: Topical Studies in Oceanography*, 47(3):733–760, 2000/04/01/ 2000.

[169] M. Voss, H. W. Bange, J. W. Dippner, *et al.* The marine nitrogen cycle: recent discoveries, uncertainties and the potential relevance of climate change. *Philos Trans R Soc Lond B Biol Sci*, 368(1621):20130121, Jul 05 2013.

[170] D. Fowler, M. Coyle, U. Skiba, *et al.* The global nitrogen cycle in the twenty-first century. *Philosophical Transactions of the Royal Society B-Biological Sciences*, 368(1621), Jul 5 2013.

[171] S. E. Bulow, J. J. Rich, H. S. Naik, A. K. Pratihary, and B. B. Ward. Denitrification exceeds anammox as a nitrogen loss pathway in the arabian sea oxygen minimum zone. *Deep-Sea Research Part I-Oceanographic Research Papers*, 57(3):384–393, Mar 2010.

[172] T. Dalsgaard, B. Thamdrup, L. Farias, and N. P. Revsbech. Anammox and denitrification in the oxygen minimum zone of the eastern south pacific. *Limnology and Oceanography*, 57(5):1331–1346, Sep 2012.

[173] A. H. Devol. Nitrogen cycle: Solution to a marine mystery. *Nature*, 422(6932):575–576, 04/10/print 2003.

[174] W. Koeve and P. Khler. Heterotrophic denitrification vs. autotrophic anammox quantifying collateral effects on the oceanic carbon cycle. *Biogeosciences*, 7(8):2327–2337, 2010.

[175] B. A. S. Van Mooy, R. G. Keil, and A. H. Devol. Impact of suboxia on sinking particulate organic carbon: Enhanced carbon flux and preferential degradation of amino acids via denitrification. *Geochimica et Cosmochimica Acta*, 66(3):457–465, 2/1/ 2002.

[176] P. Engstrom, T. Dalsgaard, S. Hulth, and R. C. Aller. Anaerobic ammonium oxidation by nitrite (anammox): Implications for n-2 production in coastal marine sediments. *Geochimica Et Cosmochimica Acta*, 69(8):2057–2065, Apr 15 2005.

[177] J. J. Rich, O. R. Dale, B. Song, and B. B. Ward. Anaerobic ammonium oxidation (anammox) in chesapeake bay sediments. *Microb Ecol*, 55(2):311–20, Feb 2008.

[178] C. C. Michiels, F. Darchambeau, F. A. E. Roland, *et al.* Iron-dependent nitrogen cycling in a ferruginous lake and the nutrient status of proterozoic oceans. *Nature Geoscience*, 10(3):217–U176, Mar 2017.

[179] F. A. Richards. Anoxic basins and fjords. Academic press, 1965.

[180] A. K. Hawley, M. Torres-Beltrn, E. Zaikova, *et al.* A compendium of multi-omic sequence information from the saanich inlet water column. *Scientific Data*, 4:170160, 10/31/online 2017.

[181] M. Torres-Beltrn, A. K. Hawley, D. Capelle, *et al.* A compendium of geochemical information from the saanich inlet water column. *Scientific Data*, 4:170159, 10/31/online 2017.

[182] D. A. Walsh, E. Zaikova, C. G. Howes, *et al.* Metagenome of a versatile chemolithoautotroph from expanding oceanic dead zones. *Science*, 326(5952):578–82, Oct 23 2009.

[183] E. Zaikova, D. F. Walsh, Claire P. Stilwell, *et al.* Microbial community dynamics in a seasonally anoxic fjord: Saanich inlet, british columbia. *Environ Microbiol*, 12(1):172–91, 2010.

[184] J. J. Anderson and A. H. Devol. Deep water renewal in saanich inlet, an intermittently anoxic basin. *Estuarine and Coastal Marine Science*, 1(1):1–10, 1// 1973.

[185] A. H. Devol, J. J. Anderson, K. Kuivila, and J. W. Murray. A model for coupled sulfate reduction and methane oxidation in the sediments of saanich inlet. *Geochimica Et Cosmochimica Acta*, 48(5):993–1004, 1984.

[186] C. C. Manning, R. C. Hamme, and A. Bourbonnais. Impact of deep-water renewal events on fixed nitrogen loss from seasonally-anoxic saanich inlet. *Marine Chemistry*, 122(1-4):1–10, Oct 2010.

[187] A. K. Hawley, M. K. Nobu, J. J. Wright, *et al.* Diverse marinimicrobia bacteria may mediate coupled biogeochemical cycles along eco-thermodynamic gradients. *Nature Communications*, 8(1):1507, 2017/11/15 2017.

[188] V. Shah, B. X. Chang, and R. M. Morris. Cultivation of a chemoautotroph from the sup05 clade of marine bacteria that produces nitrite and consumes ammonium. *Isme Journal*, 11(1):263–271, Jan 2017.

[189] R. S. Braman and S. A. Hendrix. Nanogram nitrite and nitrate determination in environmental and biological materials by vanadium(iii) reduction with chemiluminescence detection. *Analytical Chemistry*, 61(24):2715–2718, 1989/12/01 1989.

[190] T. R. Parsons, Y. Maita, and C. M. Lalli. 4.3 - fluorometric determination of chlorophylls. In *A Manual of Chemical & Biological Methods for Seawater Analysis*, pages 107–109. Pergamon, Amsterdam, 1984.

[191] A. Bourbonnais, M. F. Lehmann, R. C. Hamme, C. C. Manning, and S. K. Juniper. Nitrate elimination and regeneration as evidenced by dissolved inorganic nitrogen isotopes in saanich inlet, a seasonally anoxic fjord. *Marine Chemistry*, 157:194–207, Dec 2013.

[192] A. H. Knap, A. Michaels, A. R. Close, H. Ducklow, and A. G. Dickson. Protocols for the joint global ocean flux study (jgofs) core measurements, 1996.

[193] B. Thamdrup and T. Dalsgaard. The fate of ammonium in anoxic manganese oxide-rich marine sediment. *Geochimica Et Cosmochimica Acta*, 64(24):4157–4164, Dec 2000.

[194] J. Wright, S. Lee, E. Zaikova, D. A. Walsh, and S. J. Hallam. *DNA Extraction from 0.22 M Sterivex Filters and Cesium Chloride Density Gradient Centrifugation*, volume 31. 2009.

[195] W. Walters, E. R. Hyde, D. Berg-Lyons, *et al.* Improved bacterial 16s rrna gene (v4 and v4-5) and fungal internal transcribed spacer marker gene primers for microbial community surveys. *mSystems*, 1(1):e00009–15, Jan-Feb 12/22 10/12/received 11/24/accepted 2016.

[196] R. C. Edgar, B. J. Haas, J. C. Clemente, C. Quince, and R. Knight. Uchime improves sensitivity and speed of chimera detection. *Bioinformatics*, 27(16):2194–2200, 2011.

[197] J. G. Caporaso, J. Kuczynski, J. Stombaugh, *et al.* Qiime allows analysis of high-throughput community sequencing data. *Nature Methods*, 7:335, 04/11/online 2010.

[198] E. Kopylova, J. A. Navas-Molina, C. Mercier, *et al.* Open-source sequence clustering methods improve the state of the art. *mSystems*, 1(1), Jan-Feb 2016.

[199] C. Quast, E. Pruesse, P. Yilmaz, *et al.* The silva ribosomal rna gene database project: improved data processing and web-based tools. *Nucleic Acids Research*, 41(D1):D590–D596, 2013.

[200] C. Sancetta and S. E. Calvert. The annual cycle of sedimentation in saanich inlet, british-columbia - implications for the interpretation of diatom fossil assemblages. *Deep-Sea Research Part a-Oceanographic Research Papers*, 35(1):71–90, Jan 1988.

[201] D. S. Grundle, D. A. Timothy, and D. E. Varela. Variations of phytoplankton productivity and biomass over an annual cycle in saanich inlet, a british columbia fjord. *Continental Shelf Research*, 29(19):2257–2269, Oct 30 2009.

[202] M. Takahashi, D. L. Seibert, and W. H. Thomas. Occasional blooms of phytoplankton during summer in saanich inlet, bc, canada. *Deep-Sea Research*, 24(8):775–&, 1977.

[203] S. Christensen and J. M. Tiedje. Sub-parts-per-billion nitrate method: Use of an n(2)o-producing denitrifier to convert no(3) or no(3) to n(2)o. *Appl Environ Microbiol*, 54(6):1409–13, Jun 1988.

[204] D. Parsonage, A. J. Greenfield, and S. J. Ferguson. The high affinity of paracoccus denitrificans cells for nitrate as an electron acceptor. analysis of possible mechanisms of nitrate and nitrite movement across the plasma membrane and the basis for inhibition by added nitrite of oxidase activity in permeabilised cells. *Biochimica et Biophysica Acta (BBA) - Bioenergetics*, 807(1):81–95, 1985/04/03 1985.

[205] R. E. Murray, L. L. Parsons, and M. S. Smith. Kinetics of nitrate utilization by mixed populations of denitrifying bacteria. *Appl Environ Microbiol*, 55(3):717–21, Mar 1989.

[206] S. Ganesh, D. J. Parris, E. F. DeLong, and F. J. Stewart. Metagenomic analysis of size-fractionated picoplankton in a marine oxygen minimum zone. *ISME J*, 8(1):187–211, Jan 2014. Ganesh, Sangita Parris, Darren J DeLong, Edward F Stewart, Frank J eng Research Support, Non-U.S. Gov't Research Support, U.S. Gov't, Non-P.H.S. England 2013/09/14 06:00 ISME J. 2014 Jan;8(1):187-211. doi: 10.1038/ismej.2013.144. Epub 2013 Sep 12.

[207] O Inceoglu, M. Llirs, T. Garca-Armisen, *et al.* Distribution of bacteria and archaea in meromictic tropical lake kivu (africa). *Aquatic Microbial Ecology*, 74(3):215–233, 2015.

[208] K. Bergauer, A. Fernandez-Guerra, J. A. L. Garcia, *et al.* Organic matter processing by microbial communities throughout the atlantic water column as revealed by metaproteomics. *Proceedings of the National Academy of Sciences*, 115(3):E400–E408, 2018.

[209] K. Anantharaman, J. A. Breier, C. S. Sheik, and G. J. Dick. Evidence for hydrogen oxidation and metabolic plasticity in widespread deep-sea sulfur-oxidizing bacteria. *Proceedings of the National Academy of Sciences*, 110(1):330–335, 2013.

[210] C. M. Callbeck, G. Lavik, T. G. Ferdelman, *et al.* Oxygen minimum zone cryptic sulfur cycling sustained by offshore transport of key sulfur oxidizing bacteria. *Nature Communications*, 9(1):1729, 2018/04/30 2018.

[211] Sa. Glaubitz, K. Kielich, C. Meeske, M. Labrenz, and K. Jrgens. Sup05 dominates the gammaproteobacterial sulfur oxidizer assemblages in pelagic redoxclines of the central baltic and black seas. *Applied and Environmental Microbiology*, 79(8):2767–2776, April 15, 2013 2013.

[212] A. Canion, O. Prakash, S. J. Green, *et al.* Isolation and physiological characterization of psychrophilic denitrifying bacteria from permanently cold arctic fjord sediments (svalbard, norway). *Environmental Microbiology*, 15(5):1606–1618, 2013.

[213] C. O. Wirsen, S. M. Sievert, C. M. Cavanaugh, *et al.* Characterization of an autotrophic sulfide-oxidizing marine arcobacter sp. that produces filamentous sulfur. *Applied and Environmental Microbiology*, 68(1):316–325, January 1, 2002 2002.

[214] M. A. Altabet, E. Ryabenko, L. Stramma, *et al.* An eddy-stimulated hotspot for fixed nitrogen-loss from the peru oxygen minimum zone. *Biogeosciences*, 9(12):4897–4908, 2012. BG.

[215] K. R. Arrigo. Marine microorganisms and global nutrient cycles. *Nature*, 437:349, 09/14/online 2004.

[216] P. Lam and M. M. Kuypers. Microbial nitrogen cycling processes in oxygen minimum zones. *Ann Rev Mar Sci*, 3:317–45, 2011. Lam, Phyllis Kuypers, Marcel M M eng Research Support, Non-U.S. Gov't Review 2011/02/19 06:00 Ann Rev Mar Sci. 2011;3:317-45.

[217] C. Thomazo and D. Papineau. Biogeochemical cycling of nitrogen on the early earth. *Elements*, 9(5):345–351, Oct 2013.

[218] C. Thomazo, M. Ader, and P. Philippot. *Extreme 15N-enrichments in 2.72-Gyr-old sediments: Evidence for a turning point in the nitrogen cycle*, volume 9. 2011.

[219] H. Strauss. Anoxia through time. In Lev N. Neretin, editor, *Past and Present Water Column Anoxia*, pages 3–19, Dordrecht, 2006// 2006. Springer Netherlands.

[220] H. C. Jenkyns, D. R. Grcke, and S. P. Hesselbo. Nitrogen isotope evidence for water mass denitrification during the early toarcian (jurassic) oceanic anoxic event. *Paleoceanography*, 16(6):593–603, 2001.

[221] M. B. Higgins, R. S. Robinson, J. M. Husson, S. J. Carter, and A. Pearson. Dominant eukaryotic export production during ocean anoxic events reflects the importance of recycled nh¡sub¿4¡/sub¿¡sup¿+¡/sup¿. *Proceedings of the National Academy of Sciences*, 109(7):2269–2274, 2012.

[222] M. Hannig, G. Lavik, M. M. M. Kuypers, *et al.* Shift from denitrification to anammox after inflow events in the central baltic sea. *Limnology and Oceanography*, 52(4):1336–1345, 2007/07/01 2007.

[223] C. Deutsch, J. L. Sarmiento, D. M. Sigman, N. Gruber, and J.P. Dunne. Spatial coupling of nitrogen inputs and losses in the ocean. *Nature*, 445:163, 01/11/online 2007.

[224] B. Kartal, M. M. Kuypers, G. Lavik, *et al.* Anammox bacteria disguised as denitrifiers: nitrate reduction to dinitrogen gas via nitrite and ammonium. *Environ Microbiol*, 9(3):635–42, Mar 2007. Kartal, Boran Kuypers, Marcel M M Lavik, Gaute Schalk, Jos Op den Camp, Huub J M Jetten, Mike S M Strous, Marc Journal Article Research Support, Non-U.S. Gov't England Environ Microbiol. 2007 Mar;9(3):635-42. doi: 10.1111/j.1462-2920.2006.01183.x.

[225] A. E. Giblin, C. R. Tobias, B. Song, *et al.* The importance of dissimilatory nitrate reduction to ammonium (dnra) in the nitrogen cycle of coastal ecosystems. *Oceanography*, 26(3):124–131, Sep 2013.

[226] E. E. Roden and Q. Jin. Thermodynamics of microbial growth coupled to metabolism of glucose, ethanol, short-chain organic acids, and hydrogen. *Applied and environmental microbiology*, 2011.

[227] D. K. Button. Kinetics of nutrient-limited transport and microbial growth. *Microbiological reviews*, 49(3):270–297, 1985. 3930934[pmid] PMC373036[pmcid] Microbiol Rev.

[228] D. E. LaRowe and J. P. Amend. Power limits for microbial life. *Frontiers in Microbiology*, 6:718, 07/15 01/30/received 06/30/accepted 2015. 26236299[pmid] Front Microbiol.

[229] D. E. LaRowe and J. P. Amend. Catabolic rates, population sizes and doubling/replacement times of microorganisms in natural settings. *American Journal of Science*, 315(3):167–203, March 1, 2015 2015.

[230] C. C. Michiels, J. A. Huggins, K. E. Giesbrecht, *et al.* Rates and pathways of n2 production in a persistently anoxic fjord: Saanich inlet, british columbia. *Frontiers in Marine Science*, 6:27, 2019.

[231] F. R. Warembourg. Nitrogen fixation in soil and plant systems, 1993.

[232] Tom Vtrovsk and Petr Baldrian. The variability of the 16s rrna gene in bacterial genomes and its consequences for bacterial community analyses. *PLOS ONE*, 8(2):1–10, 02 2013.

[233] D. Li, C. M. Liu, R. Luo, K. Sadakane, and T. W. Lam. Megahit: an ultra-fast single-node solution for large and complex metagenomics assembly via succinct de bruijn graph. *Bioinformatics*, 31(10):1674–6, May 15 2015.

[234] K. M. Konwar, N. W. Hanson, A. P. Pag, and S. J. Hallam. Metapathways: a modular pipeline for constructing pathway/genome databases from environmental sequence information. *BMC bioinformatics*, 14(1):202, 2013.

[235] C. S. Miller, B. J. Baker, B. C. Thomas, S. W. Singer, and J. F. Banfield. Emirge: reconstruction of full-length ribosomal genes from microbial community short read sequencing data. *Genome Biology*, 12(5):R44, 2011/05/19 2011.

[236] J. A. Fish, B. Chai, Q. Wang, *et al.* Fungene: the functional gene pipeline and repository. *Frontiers in microbiology*, 4:291, 2013.

[237] D. A. Benson, I. Karsch-Mizrachi, D. J. Lipman, J. Ostell, and D. L. Wheeler. Genbank. *Nucleic Acids Research*, 36(Database issue):D25–D30, 12/11 09/18/received 10/10/accepted 2008. 18073190[pmid] Nucleic Acids Res.

[238] R. C Edgar. Search and clustering orders of magnitude faster than blast. *Bioinformatics*, 26(19):2460–2461, 2010.

[239] S. Capella-Gutirrez, J. M. Silla-Martnez, and T. Gabaldn. trimal: a tool for automated alignment trimming in large-scale phylogenetic analyses. *Bioinformatics*, 25(15):1972–1973, 2009.

[240] K. Katoh and D. M. Standley. Mafft multiple sequence alignment software version 7: improvements in performance and usability. *Molecular biology and evolution*, 30(4):772–780, 2013.

[241] A. Stamatakis. Raxml-vi-hpc: maximum likelihood-based phylogenetic analyses with thousands of taxa and mixed models. *Bioinformatics*, 22(21):2688–2690, 2006.

[242] A. Stamatakis and J. Hoover, P.and Rougemont. A rapid bootstrap algorithm for the raxml web servers. *Systematic biology*, 57(5):758–771, 2008.

[243] D. Hyatt, G-L. Chen, P. F. LoCascio, *et al.* Prodigal: prokaryotic gene recognition and translation initiation site identification. *BMC bioinformatics*, 11(1):119, 2010.

[244] S. R. Eddy. Profile hidden markov models. *Bioinformatics (Oxford, England)*, 14(9):755–763, 1998.

[245] S. A. Berger, D. Krompass, and A. Stamatakis. Performance, accuracy, and web server for evolutionary placement of short sequence reads under maximum likelihood. *Systematic biology*, 60(3):291–302, 2011.

[246] H. Li. Aligning sequence reads, clone sequences and assembly contigs with bwa-mem. *arXiv preprint arXiv:1303.3997*, 2013.

[247] D. S. Grundle and S. K. Juniper. Nitrification from the lower euphotic zone to the sub-oxic waters of a highly productive british columbia fjord. *Marine Chemistry*, 126(1-4):173–181, Sep 2011.

[248] P. E. Galand, S. Lucas, S. K. Fagervold, *et al.* Disturbance increases microbial community diversity and production in marine sediments. *Frontiers in microbiology*, 7:1950–1950, 2016. 27994581[pmid] PMC5133735[pmcid] Front Microbiol.

[249] I. Ylla, H. Peter, A. M. Roman, and L. J. Tranvik. Different diversityfunctioning relationship in lake and stream bacterial communities. *FEMS Microbiology Ecology*, 85(1):95–103, 2013. 10.1111/1574-6941.12101.

[250] G. Lavik, T. Sthrmann, V. Brchert, *et al.* Detoxification of sulphidic african shelf waters by blooming chemolithotrophs. *Nature*, 457:581, 12/10/online 2008.

[251] M. A. Moran, B. Satinsky, S. M. Gifford, *et al.* Sizing up metatranscriptomics. *The Isme Journal*, 7:237, 08/30/online 2012.

[252] D. Y. Sorokin, T. N. Zhilina, A. M. Lysenko, T. P. Tourova, and E. M. Spiridonova. Metabolic versatility of haloalkaliphilic bacteria from soda lakes belonging to the alkalispirillumalkalilimnicola group. *Extremophiles*, 10(3):213–220, June 01 2006.

[253] L. Villanueva, D. R. Speth, T. van Alen, A. Hoischen, and M. S. M. Jetten. Shotgun metagenomic data reveals significant abundance but low diversity of "candidatus scalindua" marine anammox bacteria in the arabian sea oxygen minimum zone. *Frontiers in microbiology*, 5:31–31, 2014. 24550902[pmid] PMC3913995[pmcid] Front Microbiol.

[254] B. Kartal and J. T Keltjens. Anammox biochemistry: a tale of heme c proteins. *Trends in biochemical sciences*, 41(12):998–1011, 2016.

[255] D. Haase, B. Hermann, O. Einsle, and J. Simon. Epsilonproteobacterial hydroxylamine oxidoreductase (hao): characterization of a missing linkin the multihaem cytochrome c family. *Molecular microbiology*, 105(1):127–138, 2017.

[256] O. M. Neijssel and D. W. Tempest. Bioenergetic aspects of aerobic growth of klebsiella aerogenes nctc 418 in carbon-limited and carbon-sufficient chemostat culture. *Archives of Microbiology*, 107(2):215–221, 1976/03/01 1976.

[257] W. Chesbro, T. Evans, and R. Eifert. Very slow growth of escherichia coli. *Journal of Bacteriology*, 139(2):625, 1979.

[258] G. Goma, R. Moletta, and M. Novak. Comments on the maintenance coefficient changes during alcohol fermentation. *Biotechnology Letters*, 1(10):415–420, 1979/10/01 1979.

[259] W. Beyeler, P. L. Rogers, and A. Fiechter. A simple technique for the direct determination of maintenance energy coefficient: An example with zymomonas mobilis. *Applied Microbiology and Biotechnology*, 19(4):277–280, 1984/04/01 1984.

[260] P. G. Falkowski, D. Ziemann, Z. Kolber, and P. K. Bienfang. Role of eddy pumping in enhancing primary production in the ocean. *Nature*, 352:55, 07/04/online 1991.

[261] A. Oschlies and V. Garon. Eddy-induced enhancement of primary production in a model of the north atlantic ocean. *Nature*, 394:266, 07/16/online 1998.

[262] W. J. Sydeman, M. Garca-Reyes, D. S. Schoeman, *et al.* Climate change and wind intensification in coastal upwelling ecosystems. *Science*, 345(6192):77, 2014.

[263] P. Xiu, F. Chai, E. N. Curchitser, and F. S. Castruccio. Future changes in coastal upwelling ecosystems with global warming: The case of the california current system. *Scientific Reports*, 8(1):2866, 2018/02/12 2018.

[264] X-Y. Zheng, H. C. Jenkyns, A. S. Gale, D. J. Ward, and G. M. Henderson. Changing ocean circulation and hydrothermal inputs during ocean anoxic event 2 (cenomanianturonian): Evidence from nd-isotopes in the european shelf sea. *Earth and Planetary Science Letters*, 375:338–348, 2013/08/01/ 2013.

[265] H. C. Jenkyns. Transient cooling episodes during cretaceous oceanic anoxic events with special reference to oae 1a (early aptian). *Philos Trans A Math Phys Eng Sci*, 376(2130), Oct 13 2018. 1471-2962 Jenkyns, Hugh C ORCID: http://orcid.org/0000-0002-2728-0984 Journal Article Review England Philos Trans A Math Phys Eng Sci. 2018 Oct 13;376(2130). pii: rsta.2017.0073. doi: 10.1098/rsta.2017.0073.

[266] X. Lang, B. Shen, Y. Peng, *et al.* Transient marine euxinia at the end of the terminal cryogenian glaciation. *Nature Communications*, 9(1):3019, 2018/08/01 2018.

[267] B. J. Koch, T. A. McHugh, M. Hayer, *et al.* Estimating taxon-specific population dynamics in diverse microbial communities. *Ecosphere*, 9(1):e02090, 2018.

[268] K. Laufer, H. Roy, B. B. Jorgensen, and A. Kappler. Evidence for the existence of autotrophic nitrate-reducing fe(ii)-oxidizing bacteria in marine coastal sediment. *Appl Environ Microbiol*, 82(20):6120–6131, Oct 15 2016. Laufer, Katja Roy, Hans Jorgensen, Bo Barker Kappler, Andreas eng Appl Environ Microbiol. 2016 Sep 30;82(20):6120-6131. doi: 10.1128/AEM.01570-16. Print 2016 Oct 15.

[269] J. M. Klatt and L. Polerecky. Assessment of the stoichiometry and efficiency of co2 fixation coupled to reduced sulfur oxidation. *Front Microbiol*, 6:484, 2015. Klatt, Judith M Polerecky, Lubos eng Switzerland Front Microbiol. 2015 May 21;6:484. doi: 10.3389/fmicb.2015.00484. eCollection 2015.

[270] N. Gruber and J. L. Sarmiento. Global patterns of marine nitrogen fixation and denitrification. *Global Biogeochemical Cycles*, 11(2):235–266, Jun 1997. Xp160 Times Cited:551 Cited References Count:125.

[271] C. J. Bjerrum and D. E. Canfield. Ocean productivity before about 1.9 gyr ago limited by phosphorus adsorption onto iron oxides. *Nature*, 417(6885):159–62, May 9 2002. Bjerrum, Christian J Canfield, Donald E eng Research Support, Non-U.S. Gov't England Nature. 2002 May 9;417(6885):159-62. doi: 10.1038/417159a.

[272] C. Klein. Some precambrian banded iron-formations (bifs) from around the world: Their age, geologic setting, mineralogy, metamorphism, geochemistry, and origins. *American Mineralogist*, 90(10):1473, 2005.

[273] G.R. Helz, C.V. Miller, J.M. Charnock, *et al.* Mechanism of molybdenum removal from the sea and its concentration in black shales: Exafs evidence. *Geochimica et Cosmochimica Acta*, 60(19):3631 – 3642, 1996.

Appendix A

Chapter 1: supplemental material

A.1 Isotope pairing technique protocol

This method is used to measure the production of N_2 or NH_4^+ through the addition of ^{15}N-labeled species to measure the rates of denitrification, anammox and DNRA. The protocol was adapted from [74, 154] but scaled to bigger incubation vessels that allowed for less heterogeneity in the samples.

A.1.1 Sampling

From a Niskin bottle, overflow the 250mL serum bottle 3 times and close it with a blue stopper to avoid oxygen contamination. Do not seal the bottle and put it in the dark until the beginning of the experiment. Avoid any big temperature variation during transportation to the lab to prevent breaking the bottles.

A.1.2 Start of the incubation

Once back in the lab, start the incubations as soon as possible. First, add a 20mL Helium headspace (Helium 5.0 purity) at 1 atmosphere pressure. This can be achieved by having an outlet in the gas-line that is open to the atmosphere. After adding a headspace, the bottle can be sealed with a crimper. The liquid obtained from the 20mL headspace can be filtered (0.2m filter) and frozen at -20°C for later analysis of the nutrients in it. While the bottles equilibrate with their new headspace (shake gently for 15 minutes). Once equilibrated, add the ^{15}N-label to your bottles. The concentration added will depend on the environment considered. Typically, we add 50% of the ambient concentration of the N-species naturally present. It is essential to avoid any cross-contamination of the $^{15}NO_3^-$, $^{15}NO_2^-$ and $^{15}NH_4^+$ while using the syringes and needles.

A.1.3 Taking time points

Two types of samples are taken for each time point: a gas and a liquid sample. For the gas sample, a 1mL gas-tight syringe (Hamilton company) is flushed three times with Helium at 1 atmosphere. After flushing, 1mL of Helium is injected into the headspace of the serum bottle and 1mL of the headspace is taken up in the same syringe. This constitutes the gas sample and it will be preserved in a 3mL exetainer filled with ddi water. To do so, the 1mL of gas sample is inserted in the exetainer while having an output needle that expels 1mL of ddi water replaced by the gas. It is important to have a gas-tight syringe for each of the ^{15}N-labels used in the incubations in order to avoid cross-contamination that would lead to anammox producing $^{30}N_2$ gas. The liquid sample are taken by a flushed 5mL plastic syringe, 2mL of He are inserted, similarly to the gas sample, and 2mL of liquid are taken up in the syringe. The sample is then immediately frozen at -20°C for later analysis. Time points are usually taken at 0, 3, 6, 12 and 24 hours, depending on the activity of the microorganisms.

A.1.4 Analysis of samples

Gas samples are later analyzed on an Isotope Ratio Mass Spectrometer for the accumulation of $^{29}N_2$ and $^{30}N_2$ in the headspace. In the liquid samples, $^{15}NH_4^+$ is transformed into $^{15}-N_2$ following Warembourg et al. (year) and also analyzed on the IRMS. Total NO_2^- and NH_4^+ are analyzed spectrophotometrically

by the Griess and indophenol assay, respectively [151]. Total NOx (NO_2^- and NO_3^-) is measured via chemiluminescence [189].

A.2 Summary of pelagic and benthic rates of denitrification, anammox and DNRA

Table A.1: *Summary of benthic rates of denitrification, anammox and DNRA* The rates found in this table was summarized from the literature (see references column).

Place/Station	Conditions	Lat	Lon	DNRA		AN		DEN		Reference
Laguna Madre, Texas	Shallow estuary	27.279	-97.427	559.2	1843.2	0	0	256.8	902.4	(An and Gardner, 2002)
Venice Lagoon, Italy	Coastal seds	45.334	12.285	240	6600	0	0	240	6000	(Azzoni *et al.*, 2014)
Dorum, Denmark	Intertidal flats	53.736	-8.507		120	0	0		2160	(Behrendt *et al.*, 2013)
Aarhus Bight, Denmark	Coastal Bay	56.105	-10.463		120	0	0		1200	See above
Mississipi, USA	River delta	29.225	-83.453		240	0	0		2640	See above
Limfjord , Denmark	Shallow fjord	56.537	-9.370		120	0	0		1920	See above
Janssand, Denmark	Intertidal flats	53.735	-7.696	240	720	0	0		720	See above
Little Lagoon, Alabama	eutrophic estuary	30.237	-87.752	1089.6	3868.8	0	0	88.8	362.4	See above
Peruvian OMZ sediments	Sediments underlying OMZ	-11	-78.6	480	2930	280	430	200	2020	(Bohlen *et al.*, 2011)
Baltic Sea estuary	changes of oxygen conditions in sed, from hypoxia to oxidized	58.833	-17.666	0.24	720	12	48	48	408	(Bonaglia *et al.*, 2014)
Gulf of Bothnia	oligotrophic basin, cold, well-oxygenated	65.191	-23.395	10	275	10	65	50	300	(Bonaglia *et al.*, 2017).
Gulf of Mexico	hypoxic sediments	29.1	-89.3	ND	ND	ND	ND	1149.6	2594.4	(Childs *et al.*, 2002)
Western North American continental margin	continental shelf sediment	28	-113.5		2660	ND	ND	720	2680	(Chong *et al.*, 2012)
Lower St Lawrence Estuary	estuary sediments	48.700	-68.652		0.12		132		271.2	(Crowe *et al.*, 2011)
By Fjord (Sweden)	Hypoxic, euxinic sometimes basin sediements, reoxygenated	58.333	11.869	20	525	0	0	20	679	(De Brabandere *et al.*, 2015)
Mae Klong estuary (Thailand)	Tropical estuary	13.411	99.997	12000	720000	0	0	2400	216000	(Dong *et al.*, 2011)
Cisadane estuary (Indonesia)	Tropical estuary	-6.019	106.631	216000	24000000	0	0	24000	2400000	See above
Vunidawa-Rewa Estuary (Fiji)	Tropical estuary	-18.106	178.541	2400	288000	0	0	2400	72000	See above
Florida Bay	Eutrophic coastal sediments	25	-81	240	6000	ND	ND	120	4200	(Gardner and McCarthy, 2009)
Texas estuaries	Shallow estuaries	28.5	-98.520	384	2376	ND	ND	120	1128	(Gardner *et al.*, 2006)
Arctic Fjord sediments (Svalbard, Norway)	Arctic coastal sediments	79.700	11.086	ND	ND	10	26	34	294	(Gihring *et al.*, 2010)
Plum Island Sound Estuary (USA, MA)	salt marsh sediments	42.724	-70.831	100	2000	0	0	50	600	(Giblin *et al.*, 2010)
Gulf of Finland, Baltic Sea	Hypoxic basin	59.933	22.097	13	1060	0	0	38	1619	(Jantti and Hietanen, 2012)

Table A.2: *Summary of benthic rates of denitrification, anammox and DNRA, cont'd* The rates found in this table was summarized from the literature (see references column).

Lower Gt. Ouse (North Sea estuary)	temperate estuarine sediments	52.816	0.383	600	26400	ND	ND	168	5280	(Kelly-Gerreyn *et al.*, 2001)
Plum Island Sound Estuary (USA, MA)	salt marsh sediments	42.724	-70.831	93.6	585.6	0	0	428	7971	(Koop-Jakobsen and Giblin, 2010)
Ca'Stanga and Lago Verde	hypolimnetic sediments of lowland lake-mesotrophic	45.054	9.796	70	120	0	0	700	4100	(Nizzoli *et al.*, 2010)
Lake - Hoffman Metropark (Ohio)	Freshwater sediment - test of increase NO3 and bioturbation	39.013	-84.001	67.2	547.2	ND	ND	67.2	5512.8	(Nogaro and Burgin, 2014)
Colne estuary (UK)	estuary sediments	51.807	0.999	ND	ND	ND	ND	36	8848.8	(Ogilvie *et al.*, 1997)
Dover Bluff - Georgia (USA)	Coastal sediments	30.416	-81.5		912		1.2	12	6720	(Porubsky *et al.*, 2009)
Grave's Dock - South Carolina (USA)	Coastal sediments	32.333	-81.416		552		1.2	12.24	3984.96	See above
Gulf of Mexico seds	Hypoxic-sulfidic seds with Thioploca mats	25.5	-112	2500	3400		1600		1100	(Prokopenko *et al.*, 2013)
Yarra River estuary seds (Australia)	River seds	-37.843	145.116	480	14400	0	0	480	9600	(Roberts *et al.*, 2012)
Yarra River estuary seds (Australia)	River seds, under oxic and hypoxic conditions	-37.843	145.116	160.8	808.8	0	0	3720	17760	(Roberts *et al.*, 2014)
Arctic Sea ice - Young Sound	Artic sea ice	74.309	20.250	ND	ND	0	2.3	10	45	(Rysgaard and Glud, 2004)
Bassin d'Arcachon sediments (France)	Coastal lagoons sediments	44.699	-1.116	70	310	ND	ND	20	1010	(Rysgaard *et al.*, 1996)
East China Sea sediment	Shelf sediments	29.088	123.803	2600	9700	2000	5000	3000	18000	(Song *et al.*, 2013)
Banks of Weser river (Germany)	River sediments	52.994	9.004		52.8	ND	ND		1893.6	(Stief *et al.*, 2010)
Atlantic Ocean next to UK-Ireland	Continental slope	54.119	5.569		0.024		2.64		139.92	(Trimmer and Nicholls, 2009)
Atlantic Ocean next to UK-Ireland	Continental shelf	48.060	9.853		0.12		60.24		4.8	(Trimmer and Nicholls, 2009)
Lake Lugano (Switzerland)	Freshwater sediment	46.009	9.030	16.8	148.8	16.8	91.2	141.6	1372.8	(Wenk *et al.*, 2014)

Table A.3: *Summary of pelagic rates of denitrification, anammox and DNRA* The rates found in this table was summarized from the literature (see references column).

Place/Station	Conditions	Lat	Lon	DNRA		AN		DEN		Reference
ETSP Northern Chile	OMZ	-20.341	-70.561	ND	ND	2.5E-10	1.25E-09	5E-11	3E-10	(De Brabandere *et al.*, 2014)
Peruvian OMZ	OMZ	-12	-77.3	3E-09	2.2E-08	2E-08	2.50E-07	ND	ND	(Lam *et al.*, 2009)
ETSP	OMZ	-10	-80	4.8E-10	1.74E-09	2.84E-09	2.27E-07	2.21E-09	5.42E-09	(Kalvelage *et al.*, 2013)
Juan de Fuca Ridge	Sulfidic hydrothermal vents	45.92	-129.99	6E-09	1.51E-07	2E-09	5E-09	5E-09	9.77E-07	(Bourbonnais *et al.*, 2012)
Omani Shelf	OMZ	18	65	2E-08	3.70E-08	2E-09	2.5E-08	ND	ND	(Jensen *et al.*, 2011)
Mediterranean particles	Particles	43	5.5	5E-10	1.1E-08	ND	ND	2E-09	1.5E-07	(Michotey and Bonin, 1997)
Gotland Basin, Baltic Sea	anoxic, sulfidic basin	57.3	20.5	1E-08	1.5E-07	5E-09	5E-08	2.5E-07	2.7E-06	(Hannig *et al.*, 2007)
Gotland and Westerland basin, Baltic Sea	anoxic, sulfidic basin	58	18	3.6E-09	1.61E-08	1.68E-09	7.44E-09	5.52E-09	9.67E-07	(Bonaglia *et al.*, 2016b)
Wintergreen lake , MI , USA	Sulphidic Eutrophic lake	42.397	-85.386	1.2E-06	3.5E-06	ND*	ND	1E-06	1.7E-05	(Burgin *et al.*, 2012)
Rhone River	Plume water of the river	43.4667	4.833	7E-07	2.5E-06	ND	ND	1E-06	4.3E-06	(Omnes *et al.*, 1996)
Kabuno Bay, Lake Kivu (RDC)	Ferruginous conditions	-1.617	29.063	2.5E-08	4.8E-08	ND	ND	4.8E-08	7.5E-08	(Michiels *et al.*, 2017)
Benguela upwelling system (Namibian)	OMZ	-22.5	13.9			1E-08	1.7E-07	ND	ND	(Kuypers *et al.*, 2005)
ETSP	OMZ	-22	-73.5			9.6E-10	2.06E-08	2.64E-09	1.9E-07	(Dalsgaard *et al.*, 2012)
ETNP	OMZ	20.15	-106			5E-10	1.2E-08	1E-09	3E-08	(Babbin *et al.*, 2014)
ETSP Northern Chili	OMZ	-20.1	-70.317			3E-09	1.68E-08	ND	ND	(Thamdrup *et al.*, 2006)
Chilean OMZ	OMZ	-20.086	-70.336			6.96E-09	1.03E-08	1.01E-09	1.9 E-09	(Canfield *et al.*, 2010b)
Peruvian OMZ	OMZ	-12	-77.5			1.5E-09	3.84E-07	ND	ND	(Hamersley *et al.*, 2007)
Central Baltic Sea	OMZ	57.5	18.5			ND	ND	5.76E-09	3.816E-07	(Dalsgaard *et al.*, 2003)
Arabian Sea	OMZ	17.5	65			1.2E-10	4.32E-09	2.4E-10	2.54E-08	(Ward *et al.*, 2009)
Arabian Sea	OMZ	19	66				4.23E-09	1.00E-09	2.12E-08	(Bulow *et al.*, 2010)
Black sea	OMZ	42.512	30.245			7E-09	7E-09	ND	ND	(Kuypers *et al.*, 2003)
Golfo Dulce (Costa Rica)	Anoxic basin	8.570	83.245			1.2E-07	4.8E-07	7.2E-08	2.64E-06	(Dalsgaard *et al.*, 2003)
Golfo Dulce (Costa Rica)	Anoxic basin	8.6	83.267			1E-09	1.5E-08	ND	ND	Jensen, PhD thesis (2006)
Mariager Fjord	anoxic sulfidic basin	56.663	9.974			ND	ND		1.86E-05	(Jensen *et al.*, 2009)
Black Sea	anoxic sulfidic basin	43.233	34			1.7E-10	1.77E-08	ND	ND	(Jensen *et al.*, 2008)
Lugano Lake (Switzerland)	Sulfidic lake	46.009	9.031			1E-09	1.5E-08	3E-08	9E-08	(Wenk *et al.*, 2013)
Lake Cadagno (Switzerland)	Sulfidic lake	46.550	8.711			ND	ND	6.96E-08	7.92E-08	(Halm *et al.*, 2009)

Appendix B

Chapter 2: supplemental material

B.1 Fe-dependent NO_3^- reduction – thermodynamic considerations

In order to test the thermodynamic favourability of reactions involving the different possible intermediates in Fe-dependent NO_3^- reduction, we calculated the relevant Gibbs free energy yields (Table B.1). *In situ* concentrations for the different chemical species implicated are depicted in Table B.2. Temperature considered was 297°K (i.e., 23.85°C) and the gas constant (R) used was 0.008314 kJ K^{-1} mol^{-1}. Under Kabuno Bay conditions (Table B.2), all the reactions outlined in Table B.1 are thermodynamically favourable.

B.2 Denitrification and DNRA rates summary in Kabuno Bay

Rates of DNRA and denitrification have been calculated by linear-regressions with the least squares method over the time interval during which data are linear (24 or 48hrs) for $^{15}NH_4^+$ or $^{30}N_2$ production, respectively. The rates and the error associated are displayed in in Table B.3 .

B.3 Dark carbon fixation in Kabuno Bay

Recent literature described the carbon fixation efficiency of Fe(II) dependent NO_3^- reducers from coastal marine sediments as being 1 mole of CO_2 fixed per 26.5 moles of Fe oxidized [268]. The products of NO_3^- reduction were not fully known in this case but the authors hypothesized based on the reaction stoichiometry that it leads to N_2 production. Therefore, because 5 moles of Fe(II) are needed to reduce 1 mole of NO_3^-, the carbon fixation efficiency for denitrification would be 0.18 ($r_{C/Denitr}$). By applying a factor of 8/5 to $r_{C/Denitr}$, we hypothesize a ratio to DNRA ($r_{C/DNRA}$) of 0.3. These factors are similar to those described for sulphide dependent NO_3^- reducers by [269]. Indeed, ratios of CO_2 fixed per NO_3^- used through sulphide dependent denitrification (to N_2) vary from 0.13 to 0.36 [269]. By applying a factor of 8/5 to $r_{C/Denitri}$, we adapted the ratio to DNRA ($r_{C/DNRA}$), which then varies from 0.21 to 0.58. In practice, growth yields for DNRA may differ from denitrification, and this stands as an important opportunity for future research. With 40% DNRA and 60% denitrification, the contribution of NO_3^- reduction to total dark carbon fixation [50] is 2% (summarized in Table B.4) based on the ratio inferred from [268].

B.4 Box-model of C, N, S and Fe cycling for a hypothetical Proterozoic upwelling system

The model used in the present study is based on the model developed by [5] for a modern coastal upwelling system. It was previously adapted to a Proterozoic upwelling system by Boyle et al. 2013 showing that euxinia was only present when N_2-fixation occurred in the photic zone. The general structure of our 5 box model is briefly summarized in the main text, Figure B.1 as well as in Fig2.3a. We kept Canfield (2006)'s [5] model structure and dimensions (described in Fig.B.1), as well as most model parameters (described in Fig.B.1 and in Table B.5), but added DNRA as well as the Fe-cycle to our model. N-fixation was not considered here as the model sustains export production without its contribution, and N-fixation is commonly absent in modern upwelling systems. Upwelling rates are represented with the coefficient A and

B (cm hr^{-1}, see Fig.B.1 and in Table B.5) and vertical exchange between the different boxes is represented by the different K coefficients (cm hr^{-1}, see Fig.B.1 and in Table B.5). Upwelled waters bring nutrients to the euphotic zone (here NO_3^- and/or NH_4^+), settling rates of primary production are based on N limitation. Primary production, also called export production in Boyle et al. 2013 is described as follows (Eq.B.1):

$$EP = EP_{NO_3^-} + EP_{NH_4^+} = \frac{A + B + K_u}{r_{N:C}} * (NO_{3um} + NH_{4um}) \tag{B.1}$$

Primary production is exported through sedimentation to the intermediate box (UM), where microbial respiration occurs. In the UM box, part of sedimented organic matter is degraded through oxic respiration, which together with nitrification consumes oxygen. Nitrification, in turn, produces NO_3^-. Oxic respiration ($R_{aerobic}$) is limited by the oxygen diffusing from the surface waters (U box) into the UM box. Surface water oxygen was set assuming equilibrium with the atmosphere, and oxygen concentrations based on the reconstructions from the geologic record. We can calculate the rate of $R_{aerobic}$, which includes nitrification, based on the flux of oxygen entering the UM box, as shown in Eq.B.2.

$$R_{aerobic} = \frac{K_u * O_{2u} + (A + K_{um})O_{2D} + (K_I + B)O_{2I}}{r_{O_2:C}} \tag{B.2}$$

Considering that oxygen can only come from the U box, Eq.B.2 simplifies as:

$$R_{aerobic} = \frac{K_u * O_{2u}}{r_{O_2:C}} \tag{B.3}$$

All oxygen was consumed through combined respiration and nitrification directly in the UM box. NO_3^- reduction proceeds first using Fe(II) as an electron donor. For low upwelling rates, NO_3^- limits Fe-dependent NO_3^- reduction, and we can therefore calculate rates of NO_3^- reduction based on the supply of NO_3^- to the UM box as follows:

$$NO_3^- - limited : R_{NO_3^- Fe} = (A + K_{um}) * NO_{3D} + (B + K_I) * NO_{3I} + r_{N:C} * R_{aerobic} \tag{B.4}$$

NO_3^- is supplied through upwelling from intermediate waters and is also produced through nitrification in the UM box. Eq. B.4 implies that NO_3^- in the UM box is consumed entirely and is therefore zero. If Fe(II) is limiting (instead of NO_3^-), on the other hand, we can calculate rates of Fe-dependent NO_3^- reduction based on the supply of Fe(II) to the UM box instead of the supply of NO_3^-:

$$Fe - limited : R_{NO_3^- Fe} = ((A + K_u m) * Fe_D + (B + K_I) * Fe_I) * r_{NO3:Fe} \tag{B.5}$$

with $r_{NO3:Fe}$ defined in Eq.B.11 below.

In order to determine whether NO_3^- or Fe(II) is limiting, we compared the supply rates of both (Eqs.B.4B.5) and considered the lowest as the actual rate of Fe-dependent NO_3^- reduction (RNO_3^-Fe). If Fe(II) is limiting, there will be NO_3^- left in the UM box that then fuels organic matter oxidation. This yields both Fe and C-dependent NO_3^- reduction in the UM box. The NO_3^- allocated to C-dependent NO_3^- reduction (RNO_3^-C) can be calculated by subtracting Eq.B.4-Eq.B.5. Again, the NO_3^- concentration in the UM box is zero as it is all consumed through a combination of Fe and C-dependent NO_3^- reduction. In summary:

$$\text{Case 1: } NO_3^- \text{ limiting Fe-dependent } NO_3^- \text{ reduction } R_{NO3-tot} = R_{NO3-Fe} \tag{B.6}$$

$$\text{Case 2: Fe(II) limiting Fe-dependent } NO_3^- \text{ reduction } R_{NO3-tot} = R_{NO3-Fe} + R_{NO3-C} \tag{B.7}$$

As mentioned here above, we considered both DNRA and denitrification as part of NO_3^- reduction. By doing so, we are able to evaluate the effect of the partitioning between DNRA and denitrification on

primary production, sulphate reduction rates, and the accumulation of hydrogen sulphide. We therefore varied the relative contributions of DNRA and denitrification to overall NO_3^- reduction and this ultimately influences the loss of N from the system versus recycling to NH_4^+ through DNRA. In order to address this balance between the two pathways, we reformulated the description of NO_3^- reduced per molecule of electron donor consumed (Fe(II) or organic matter) so that it reflected the overall stoichiometry of combined DNRA and denitrification. Denitrification consumes 5 electrons per NO_3^- reduced versus the 8 electrons involved in DNRA. The half reactions for denitrification and DNRA are the following:

$$\text{Denitrification: } NO_3^- + 5e^- + 6H^+ \Rightarrow N_2 + 3H_2O \tag{B.8}$$

$$\text{DNRA: } NO_3^- + 8e^- + 10H^+ \Rightarrow NH_4^+ + 3H_2O \tag{B.9}$$

For Fe-dependent NO_3^- reduction, we considered the following half reaction:

$$Fe^{2+} + 3H_2O \Rightarrow Fe(OH)_3 + 1e^- + 3H^+ \tag{B.10}$$

With x being the contribution of DNRA to NO_3^- reduction and (1-x) the contribution of denitrification, we can define the number of moles of NO_3^- used per mole of Fe(II) in Eq.B.11.

$$r_{NO3:Fe} = \frac{x}{8} + \frac{(1-x)}{5} \tag{B.11}$$

We also can define the number of moles of NH_4^+ released per mole of Fe(II) in Eq.B.12.

$$r_{NH4:Fe} = \frac{x}{8} \tag{B.12}$$

Considering now C-dependent NO_3^- reduction, the half reaction of organic C oxidation used here is:

$$C_{106}H_{175}N_{16}O_{42}P + 280H_2O \Rightarrow 106HCO_3^- + 16NH_4^+ + HPO_4^{2-} + 564H^+ + 472e^- \tag{B.13}$$

Eq.B.14 shows the number of moles of NO_3^- consumed per mole of organic C with a varying contribution of DNRA and denitrification to NO_3^- reduction.

$$r_{NO3:C} = 472 * \frac{\frac{x}{8} + \frac{1-x}{5}}{106} \tag{B.14}$$

Finally, Eq.B.15 was modified from [44], so that $r_{NH4:C}$, accounted for both NH_4^+ released from remineralization of organic matter through NO_3^- reduction as well as the production of NH_4^+ through DNRA per mole of C oxidized. $r_{NH4:C}$ is therefore written as follows:

$$r_{NH4:C} = \frac{16 + (59 * x)}{106} \tag{B.15}$$

As NO_3^- in the UM box equals 0, the Eq.B.1 for export production can therefore be simplified to:

$$EP = \frac{(A + B + K_u) * NH_{4um}}{r_{N:C}} \tag{B.16}$$

With NH_{4UM} calculated in Eq.B.17, taking into account the ammonium released from NO_3^- reduction through DNRA (both Fe and C-dependent), we can therefore calculate Eq.B.16.

$$NH_{4um} = \frac{(A + K_{um}) * NH_{4D} + (B + K_I) * NH_{4I} + r_{NH4:Fe} * R_{NO3-Fe} + r_{NH4:C} * R_{NO3-C} - r_{N:C} * R_{aerobic}}{(K_{um} + K_I)} \tag{B.17}$$

If organic matter remains after exhausting NO_3^- in the UM box, the remaining amount can be oxidized through iron and sulphate reduction. Iron reduction was insignificant, and wasn't considered further. Sulfate reduction rates can be written as:

$$R_{SR} = EP - R_{aerobic} - \frac{R_{NO3-C}}{r_{NO3:C}} \tag{B.18}$$

The sulphide produced through RSR in the UM box being described in Eq.B.19:

$$H_2S_{um} = \frac{59}{106} * \frac{R_{SR}}{(A + B + K_I + K_{um} + K_u)} \tag{B.19}$$

With Eq.B.20 as the half reaction used for sulphate reduction

$$SO_4^{2-} + 8e^- + 10H^+ \Rightarrow H_2S + 4H_2O \tag{B.20}$$

Finally, based on the rate of highly reactive Fe entering the UM box and the rate of H_2S produced through sulphate reduction, we can then infer the ratio of Fe-pyrite to highly reactive Fe used in the rock record to distinguish euxinic from ferruginous conditions.

$$r_{Fe_{PY/HRFe}} = \frac{\frac{R_{SR}*59}{106}}{(2 * ((A + K_{um}) * Fe_D + (B + K_I) * Fe_I)} \tag{B.21}$$

Supplemental conditions from Fig.2.3b and c are displayed here below in Fig.B.2 for the Fe-pyrite to highly reactive Fe ratio under 2 atmospheric oxygen concentrations (3.8% and 6.2% PAL) and for higher contributions of DNRA to NO_3^- reduction. Results show that euxinic conditions are reached at upwelling rates lower than when the contribution of DNRA is smaller, and without the need of an increased ammonium supply from the deep ocean.

The main parameters are constrained in in Table B.5. These are the benchmark values used for the runs of the model of the main text, if not stated otherwise in the text or legends of the figures. We provide further explanation on how specific parameters were constrained below.

In the main text, we explored the influence of oxygen on the model outputs from 0% to 12% PAL (Fig. 2.3d in the main text). 0% PAL is a special case where oxygen is not available locally for nitrification in the upwelling zone. However, we maintained the supply of NO_3^- from intermediate waters, as non-local oxygen oases are plausible in the Archean ocean, even under an ostensibly anoxic atmosphere [38]. Therefore, these oxygen oases could have enabled the local production of NO_3^- through nitrification in other parts of the Archean ocean and supplied the NO_3^- to intermediate waters as considered in our box model. We also tested a broad range in deep ocean Fe(II) and NH_4^+ concentrations, as mentioned in the main text. Indeed, these parameters are poorly constrained in the literature and we therefore studied the influence of likely ranges on our model outputs. Fe(II) concentrations are commonly thought to be controlled by equilibrium with siderite ($FeCO_3$), which yields between 40 to 120μM deep ocean Fe(II) [46]. However, [159] suggests siderite formation was kinetically limited and Fe(II) concentrations may have been much higher ($<$ 3mM). Assuming upwelled P is needed to fuel oxygenic photosynthesis and sustain appreciable atmospheric O_2 in the Proterozoic Eon, Fe(II) concentrations must then have been less than 424 times deep water P concentrations [158]. Indeed, at Fe(II):P ratios greater than 424, upwelling P is consumed through photoferrotrophy and would therefore not reach the surface waters to support appreciable oxygenic photosynthesis. Based on these arguments, we chose an Fe(II) concentration 42μM (based on 424 x 0.1 μM P) for the benchmark in our model runs presented in the main text. However, we also tested a range of concentrations (from 10 to 500μM) that encompasses the values described by [46]. We focused on the role of Fe(II) concentrations in dictating the Fe_{PY}/Fe_{HR} ratio across a suite of different model conditions in Fig.B.3 (a-h). Overall, and as expected, without DNRA and at low deep ammonium concentrations (2μM, Fig. B.3 a to d), ferruginous conditions tend to prevail as Fe(II) concentrations increase. However, with DNRA and at 10μM Fe(II) (Fig. B.3 e), Fe(II) is limiting and euxinic conditions ($Fe_{PY}/Fe_{HR}>0.7$) develop at relatively low upwelling rates. Above 42μM on the other hand (Fig. B.3 b-d, f-h), with or without DNRA, Fe(II) is

supplied in excess and effectively titrates any sulphide produced through sulphate reduction, invariably yielding ferruginous conditions ($Fe_{PY}/Fe_{HR}<0.7$). Figure B.3 (j to l) depicts different concentrations of deep Fe(II) versus a wide range of deep NH_4^+ concentrations (between 0 and 15μM) without the contribution of DNRA (0% DNRA). This shows that euxinic conditions could also be reached without the contribution of DNRA, but mainly under low deep Fe(II) concentrations (between 10 and 42μM) and under relatively high NH_4^+ concentrations (>13μM), as mentioned in the main text. Our benchmark model runs described in the main text invariably consider NO_3^- to be present in the intermediate waters. We then assumed that these intermediate waters would be Fe(II) free as it would have been consumed through NO_3^- reduction. The opposite could be true, on the other hand, and so we also tested this here to evaluate the effect of Fe(II) bearing NO_3^- free intermediate waters. When intermediate waters contain Fe(II), we added equimolar NH_4^+ instead of NO_3^-, accordingly. Results of this test are depicted in Figure B.4 and show that, although export production is very high compared to the benchmark model scenarios, euxinic conditions ($Fe_{PY/FeHR}>0.7$) do not occur in the water column. Without a supply of NO_3^- through the intermediate waters, NO_3^- reduction is fuelled only through nitrification and therefore by the oxygen supply from the surface water (3.8% PAL in this test). This being minimal, NO_3^- reduction and N-loss are highly restricted.

B.5 Global N-fixation and N-loss in the Archean and Proterozoic

Annual rates of marine N-fixation for the Proterozoic Eon are estimated based on the modern rates described in [270]. In order to scale the modern rates to the Proterozoic Eon, we assumed that N-fixation was ultimately limited by P supply [157] and was therefore proportional to deep ocean P concentrations. We thus divided the modern rates of 135 50 Tg N yr^{-1} (encompassing both pelagic and benthic N-fixation) by the modern phosphorous concentration (2.3μM, [271]) in the deep ocean and multiplied this by the highest estimates for the phosphorous concentration (0.13μM) described for Paleoproterozoic oceans [158]. The 4.8 Tg N yr^{-1} we report in the main text is our lowest estimate if we consider the error on the N-fixation estimate. To assess the extent to which we could apply the 0.13 μM deep water P concentration from [158] across the Proterozoic Eon we took values of Fe/Si from the Rapitan iron-formation [272] and applied these to [158] model to infer phosphorous concentrations for the Neoproterozoic oceans. Values found for the Rapitan were within the range of those calculated by [158]. We also considered trace metal limitation of N-fixation very unlikely. The most likely metal to limit N-fixation in the Proterozoic is molybdenum [163]. However, [273] showed that high levels of sulphide (between 50 and 250μM) are necessary to effectively strip Mo from seawater under euxinia. Our model implies that under most reasonable scenarios sulphide concentrations do not exceed about 20μM and are therefore insufficient to trigger effective Mo removal. Conservative rates of global N-loss were inferred from our box-model when denitrification contributes 100% of NO_3^- reduction (no DNRA, therefore higher N-loss) under 6.2% PAL, low ammonium conditions (2μM) and deep ocean Fe(II) concentrations of 42μM. The highest rates of N-loss were found with the highest upwelling rate explored in this model (3 cm hr^{-1}). We then extrapolated N-loss from our model to an area equivalent to upwelling regions in the modern ocean (0.36 10^{12} m^2) as indicated in the main text. In comparison, rates of N-loss under the lowest upwelling rate considered in our model (0.5 cm hr^{-1}) are 4 times lower than with an upwelling rate of 3 cm hr^{-1}.

Table B.1: Free Gibbs Energy yield under standard conditions ($\triangle G^\circ$) and for Kabuno Bay concentrations ($\triangle G$). Values for $\triangle G^\circ$ can be found in [4]

Reactions	ΔG° (kJ /mol N)	ΔG (kJ /mol N)
$8\ Fe^{2+} + 21\ H_2O + \mathbf{NO_3^-} \Rightarrow \mathbf{NH_4^+} + 8\ Fe(OH)_3 + 14\ H^+$	51.67	-272.41
$5\ Fe^{2+} + 12\ H_2O + \mathbf{NO_3^-} \Rightarrow 0.5\ \mathbf{N_2} + 5\ Fe(OH)_3 + 9\ H^+$	-143.19	-336.97
$6\ Fe^{2+} + 16\ H_2O + \mathbf{NO_2^-} \Rightarrow \mathbf{NH_4^+} + 6\ Fe(OH)_3 + 10\ H^+$	31.93	-189.81
$3\ Fe^{2+} + 7\ H_2O + \mathbf{NO_2^-} \Rightarrow 0.5\ \mathbf{N_2} + 3\ Fe(OH)_3 + 7\ H^+$	-162.93	-328.28
$2\ Fe^{2+} + 4.5\ H_2O + \mathbf{NO_2^-} \Rightarrow 0.5\ \mathbf{N_2O} + 2\ Fe(OH)_3 + 3\ H^+$	-83.85	-137.86
$4\ Fe^{2+} + 11.5\ H_2O + 0.5\ \mathbf{N_2O} \Rightarrow \mathbf{NH_4^+} + 4\ Fe(OH)_3 + 7\ H^+$	115.78	-51.95
$Fe^{2+} + 2.5\ H_2O + 0.5\ \mathbf{N_2O} \Rightarrow 0.5\ \mathbf{N_2} + Fe(OH)_3 + 2\ H^+$	-158.16	-186.59
$2\ Fe^{2+} + 5\ H_2O + \mathbf{NO_3^-} \Rightarrow \mathbf{NO_2^-} + 2\ Fe(OH)_3 + 4\ H^+$	19.74	-82.60

Table B.2: Chemical species concentrations (in μM) representative for the chemocline in Kabuno Bay

Chemical species	Concentration (μM)
NO_3^-	1
NO_2^-	1
N_2O	0.01
NH_4^+	100
Fe (II)	100
$Fe(OH)_3$	10^6 activity=1 as a pure solid
pH	6.5

Table B.3: Summary of DNRA and denitrification rates for KBs water column. Rates were calculated over 48 hours unless stated otherwise next to the calculated rates.

Depth (m)	$^{30}N_2$ production (nmol N d^{-1})	$^{30}N_2$ production (nmol N d^{-1}) with Fe added	$^{15}NH_4^+$ production (nmol N d^{-1})	$^{15}NH_4^+$ production (nmol N d^{-1}) with Fe added
9.5	0 ± 0	0 ± 0	0 ± 0	0 ± 0
10	0 ± 0	0 ± 0	0 ± 0	0 ± 0
10.5	0 ± 0	0 ± 0	0 ± 0	0 ± 0
11	80 ± 10	230 ± 40	20 ± 0 (24h)	70 ± 20 (24h)
11.5	50 ± 10	140± 20	50 ± 10 (24h)	70 ± 10

Table B.4: Rates and ratio considered for calculations

Microbial process	Process rate measurements	Reference
Dark Carbon fixation	1.49µmol C L^{-1} d^{-1}	Lliros et al. 2015
DNRA	70 nmol N L^{-1} d^{-1}	This paper
Denitrification	230 nmol N L^{-1} d^{-1}	This paper

Table B.5: Description of the different parameters used in the current model

Parameters	Value/ Units	Description	Reference
K_{um}	0.2 cm h^{-1}	Vertical exchange	Canfield 2006
K_u	0.1 cm h^{-1}	Vertical exchange	Canfield 2006
K_i	0.4 cm h^{-1}	Vertical exchange	Canfield 2006
A	0 cm h^{-1}	Upwelling Rate	Canfield 2006
B	0.5-3 cm h^{-1}	Upwelling Rate	Canfield 2006
O_{2u}	9.5-15.5 µM (3.8% to 6.2% PAL)	O_2 concentration in U box	Zhang *et al*. 2016
O_{2D}	0 µM	O_2 concentration in D box	Boyle *et al.* 2013
O_{2I}	0 µM	O_2 concentration in I box	Boyle *et al.* 2013
$r_{O2:C}$	170/117	Ratio of molecule of O_2 consumed for 1 molecule of carbon oxidized	Boyle *et al.* 2013
$r_{N:C}$	16/106	Ratio based on Redfield ratio	Redfield, 1934
EP	nmol C cm^{-2} h^{-1}	Rate of export production	
$R_{aerobic}$	nmol C cm^{-2} h^{-1}	Rate of aerobic respiration	
$R_{NO3\text{-}tot}$	nmol N cm^{-2} h^{-1}	Rate of nitrate reduction through Fe dependent nitrate reduction (if case 1) or through Fe and C dependent NO_3^- reduction (if case 2)	
$R_{NO3\text{-}Fe}$	nmol N cm^{-2} h^{-1}	Rate of nitrate reduction through Fe dependent NO_3^- reduction	
$R_{NO3\text{-}C}$	nmol N cm^{-2} h^{-1}	Rate of nitrate reduction through C dependent NO_3^- reduction (only case 2)	
R_{SR}	nmol C cm^{-2} h^{-1}	Rate of sulphate reduction	
$R_{Fe\text{-}ox}$	nmol Fe cm^{-2} h^{-1}	Rate of Fe oxidation	
$NH4_{UM}$, $NH4_D$, $NH4_I$	TBD, 2, 0 µM	Ammonium concentration in UM, D, I box	Deep water concentrations based on Jones et al. 2015 Phosphorous concentration estimates.
$NO3_{UM}$, $NO3_D$, $NO3_I$	TBD, 0, 1 µM	Nitrate concentration in UM, D, I box	Deep water concentrations based on Jones et al. 2015 Phosphorous concentration estimates.
Fe_{UM}, Fe_D, Fe_I	TBD, 42, 0 µM	Iron (II) concentration in UM, D, I box	Deep water concentrations based on Jones et al. 2015 Phosphorous concentration estimates.
H_2S_{UM}	TBD µM	Sulfide concentration in UM box	

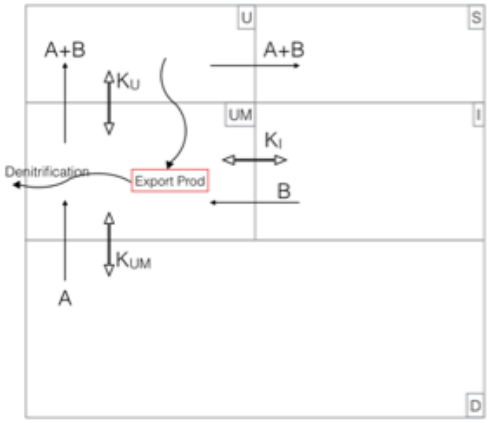

Figure B.1: *Box-model for C, N, S and Fe cycling in hypothetical Precambrian upwelling system adapted from [5]* Notation is as follows: Upwelling coefficients (A+B) from intermediate and deep waters (boxes I and D) as well as horizontal (KI) and vertical mixing (Ku and Kum) between the UM box and the other boxes considered (I, U and D respectively). Box S represents ocean surface waters away from the upwelling zone. The parameter values are listed in Table B.5. Organic matter produced in the euphotic zone (box U) as export production settles to box UM where it is partially (in [5]) or entirely ([44] and this paper) degraded. The order of the pathways through which it is degraded is oxic respiration, followed by nitrate reduction ([5] and [44]), and finally by sulphate reduction.

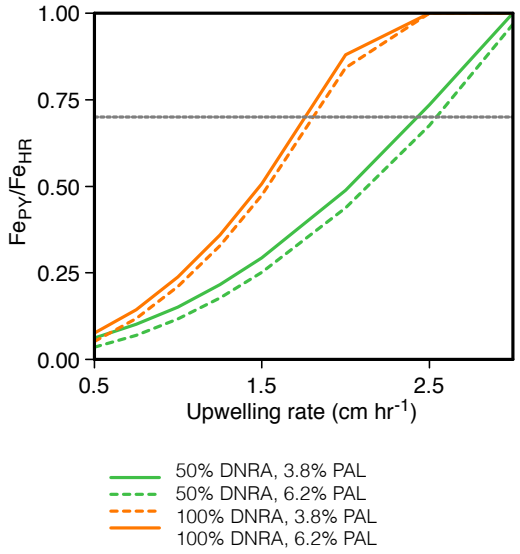

Figure B.2: *Fe-pyrite to highly reactive Fe ratio for 50 and 100% DNRA*$\mathrm{Fe_{PY/FeHR}}$ for 50 and 100% DNRA (in green and orange respectively) with varying surface waters oxygen (3.8% PAL in solid lines and 6.2%PAL in dashed lines) and for different upwelling rates. These model runs are for deep NH4+ concentrations of 2μM.

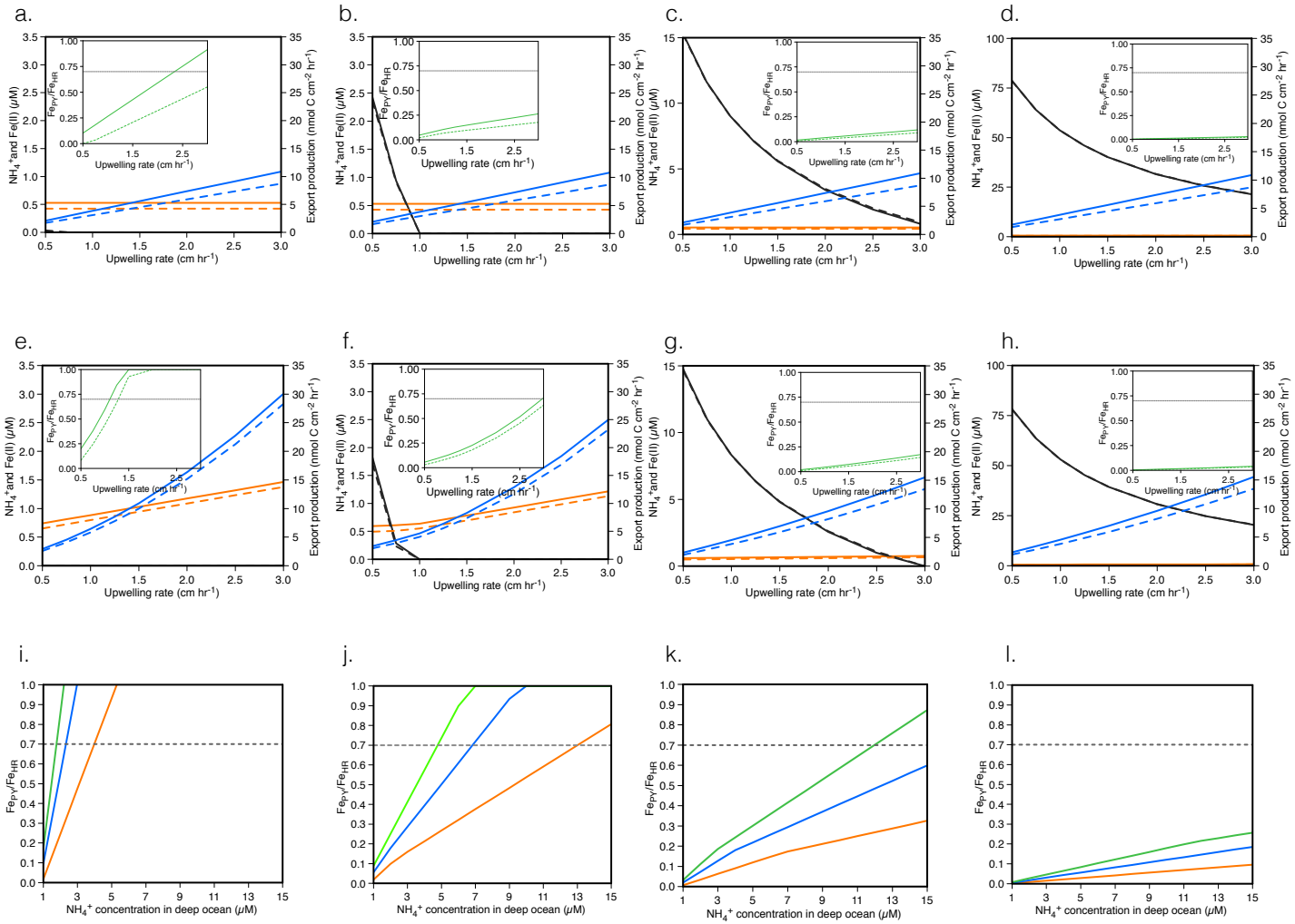

Figure B.3: *role of Fe(II) concentrations in dictating the FePY/FeHR ratio across a suite of different model conditions*Graphs (a-d) represents model runs with 0% DNRA; (e-h) represents model runs with 30% DNRA. Solid lines represent model runs with the surface water oxygen concentrations of 3.8% PAL, whereas dashed lines represent runs at 6.2% PAL [blue=export production, orange= NH_4^+ concentrations, and black=Fe(II) concentrations, insets show the Fe-pyrite to highly reactive Fe ratio ($Fe_{PY/FeHR}$) where the grey line delineates plausible euxinic conditions]; (i-l) represent model runs of $Fe_{PY/FeHR}$ ratios for a range of deep ocean NH_4^+ concentrations at 0% DNRA with surface water oxygen concentrations of 3.8% PAL (orange=upwelling rate of 1cm hr^{-1}, blue=upwelling rate of 2cm hr^{-1}, and green=upwelling rate of 3cm hr^{-1}). The first column of these graphs are for deep Fe(II) concentrations of 10μM, the second column is 42μM (as represented in the main text), the third is 120μM and the fourth is 500μM.

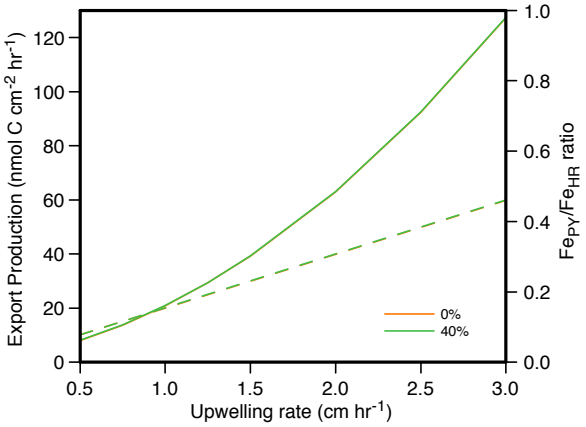

Figure B.4: *Run of the model with 20µM Fe(II) in the intermediate box (I) but no NO_3^-.* Instead, upwelled waters from box I are bringing 1μM of NH_4^+ to the upwelled zone. Deep waters are bringing 42μM Fe(II) and 2μM NH_4^+. Solid lines represent export production whereas dashed lines represent FePY/FeHR ratio. Case with 0% DNRA is in orange and case with 40%DNRA is in green, however, as the two cases yield very similar results, the orange case is hidden by the green.

Appendix C

Chapter 3: supplemental material

C.1 NH_4^+ sediment fluxes in Saanich

Based on the measured Sulphate Reduction rates (SRR) in SI [185], we considered SRR to be 2.97 to 10.44 mmol m^{-2} d^{-1}. We consider the ratio 53:16 to convert SRR into NH_4^+ release from carbon degradation, based on the Redfield Ratio. Therefore, when scaled to NH_4^+ release from sediments and a 50% desorption off the sediments, we obtain fluxes of NH_4^+ out of the sediments of 2.97 to 10.44 mmol N m^{-2} d^{-1}. Based on our depth-integrated rates, NH_4^+ requirements for anammox range between 0.15 to 3.36 m^{-2} d^{-1}. Therefore, NH_4^+ fluxes from the sediments in Saanich Inlet can support 90 to 100% of the NH_4^+ requirements for anammox.

C.2 Microbial communities in SI

Table C.1: Summary of samples and the number of sequences and OTUs observed in each sample, as well as bacterial small subunit ribosomal RNA (SSU or 16S rRNA) gene abundance obtained through qPCR. The chao diversity index was also calculated for each sample based on OTUs.

Sample	chao	Observed otus	# sequences	#16S L^{-1}
ALL	/	28946	6638571	/
JAN15.10m	7020	3303	73265	4.42E+09
JAN15.100m	8442	3816	111088	7.95E+09
JAN15.120m	8229	3935	132852	6.71E+09
JAN15.135m	5619	2540	92149	1.68E+09
JAN15.150m	4979	2218	84718	1.23E+10
JAN15.200m	6467	3032	67297	7.10E+09
FEB15.10m	5531	2491	55585	1.57E+10
FEB15.100m	6515	2951	71687	5.67E+09
FEB15.120m	6176	2769	106204	2.34E+09
FEB15.135m	5781	2775	87220	5.29E+09
FEB15.150m	6248	2673	97350	1.01E+10
FEB15.200m	7836	3437	85859	3.49E+08
MAR15.10m	4708	2248	35602	7.78E+08
MAR15.100m	6685	3090	81536	3.42E+09
MAR15.120m	5532	2283	78958	1.57E+09
MAR15.135m	6104	2898	104198	5.52E+09
MAR15.150m	6556	3137	94787	2.30E+09
MAR15.200m	7733	3418	87169	1.20E+09
APR15.10m	3799	2079	119314	8.06E+09
APR15.100m	6761	3314	86563	4.52E+09
APR15.120m	5342	2435	89452	1.68E+10
APR15.135m	3600	1665	70646	6.82E+09
APR15.150m	4408	1946	63358	4.56E+09
APR15.200m	6428	2986	76538	5.11E+08
MAY15.10m	2863	1660	81768	4.75E+09
MAY15.100m	7208	3245	71663	1.26E+09
MAY15.120m	7129	3504	88110	3.66E+10
MAY15.135m	7095	3157	92109	1.05E+09
MAY15.150m	8002	3756	102431	1.47E+09
MAY15.200m	8137	3900	116481	1.48E+09
JUN15.10m	1700	1110	102049	4.79E+08
JUN15.100m	7592	3648	95726	2.74E+09
JUN15.120m	6867	3191	98121	9.55E+09
JUN15.135m	6713	3038	102559	5.81E+09
JUN15.150m	9148	4140	111352	3.02E+09
JUN15.200m	7371	3682	91422	1.90E+09
JUL15.10m	4899	3506	100021	3.05E+09
JUL15.100m	7345	3647	95214	3.51E+09
JUL15.120m	5893	2731	75056	3.98E+09
JUL15.135m	4830	2257	80596	9.12E+09
JUL15.150m	5585	2517	91495	1.15E+09
JUL15.200m	5989	2720	83155	1.03E+10
AUG15.10m	3742	2043	74247	2.44E+10
AUG15.100m	8367	3472	103099	3.27E+09
AUG15.120m	7878	3438	99616	1.43E+09
AUG15.135m	5656	2607	94232	3.01E+09
AUG15.150m	5927	2548	100997	2.47E+09
AUG15.200m	6756	3097	110607	1.73E+09
SEP15.10m	7302	3612	93822	1.29E+08
SEP15.100m	9417	4110	105994	1.62E+09
SEP15.120m	6888	3093	114820	2.51E+09
SEP15.135m	4893	2335	72435	6.93E+08
SEP15.150m	5107	2360	81670	8.30E+09
SEP15.200m	4101	1942	99747	3.44E+10
OCT15.10m	5490	2856	84800	8.65E+08
OCT15.100m	4931	2389	76400	1.20E+10
OCT15.120m	5740	2657	90584	1.20E+10
OCT15.135m	5456	2525	92290	6.84E+09
OCT15.150m	4444	1986	96184	7.90E+09
OCT15.200m	6690	2866	89212	1.17E+09
NOV15.10m	8909	4599	111511	1.40E+10
NOV15.100m	8559	3973	117157	1.30E+10
NOV15.120m	6565	3075	119680	3.11E+08
NOV15.135m	6428	3107	117327	6.57E+08
NOV15.150m	7554	3638	88536	1.36E+08
NOV15.200m	7602	3499	108763	5.59E+07
DEC15.10m	9686	5304	125996	1.19E+09
DEC15.100m	5828	2974	76294	3.56E+08
DEC15.120m	4929	2359	81375	3.25E+08
DEC15.135m	5895	2569	81654	2.96E+08
DEC15.150m	6710	2982	97678	6.21E+07
DEC15.200m	5521	2864	99121	4.45E+07

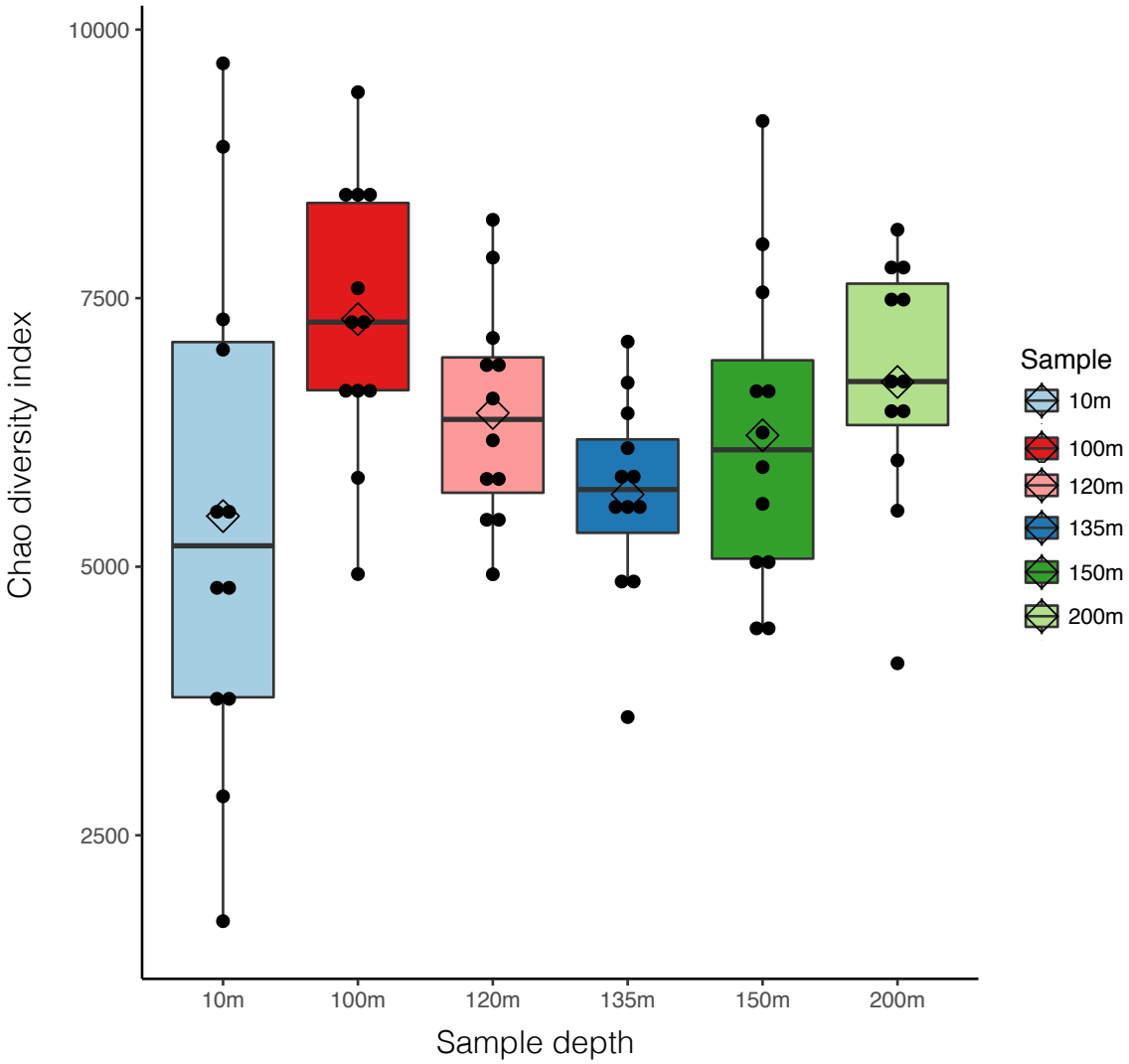

Figure C.1: Chao1 diversity index from iTags sequencing

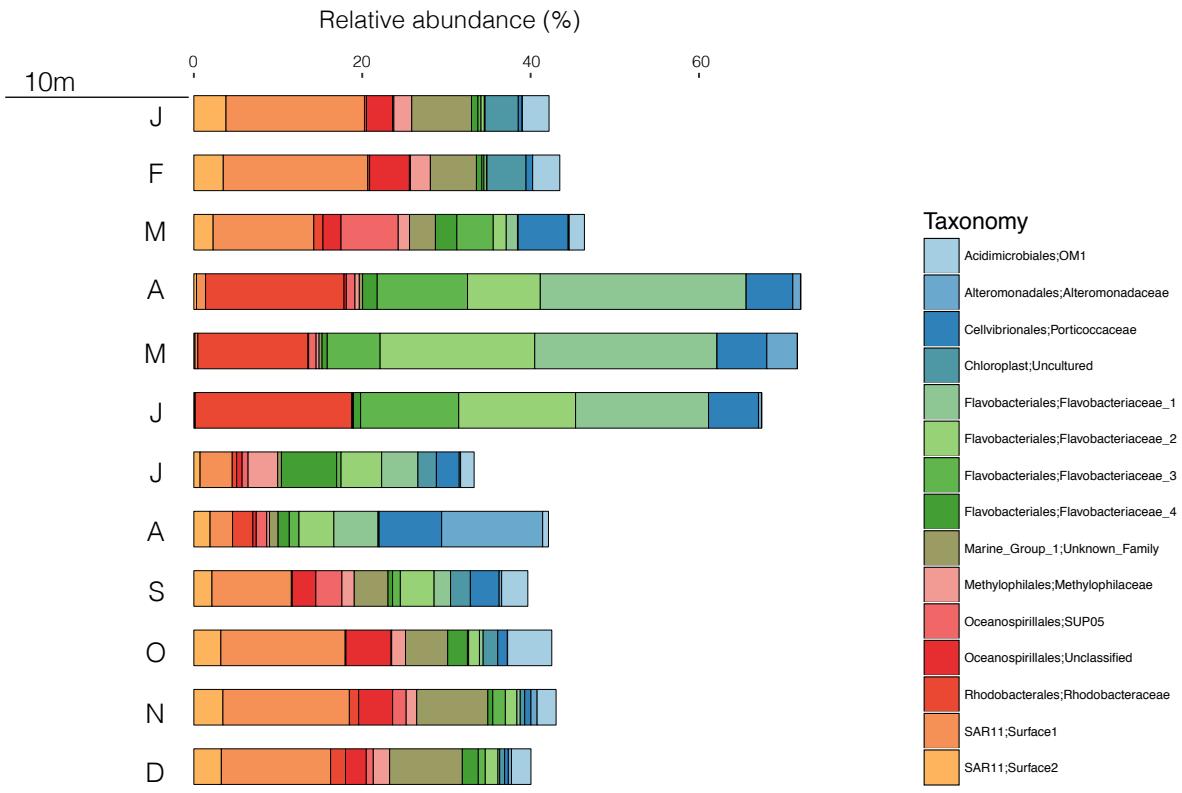

Figure C.2: Relative abundance of 15 most abundant taxa for the surface waters of SI in 2015 (10m). These taxa were the most abundant ones found in average throughout the samples.

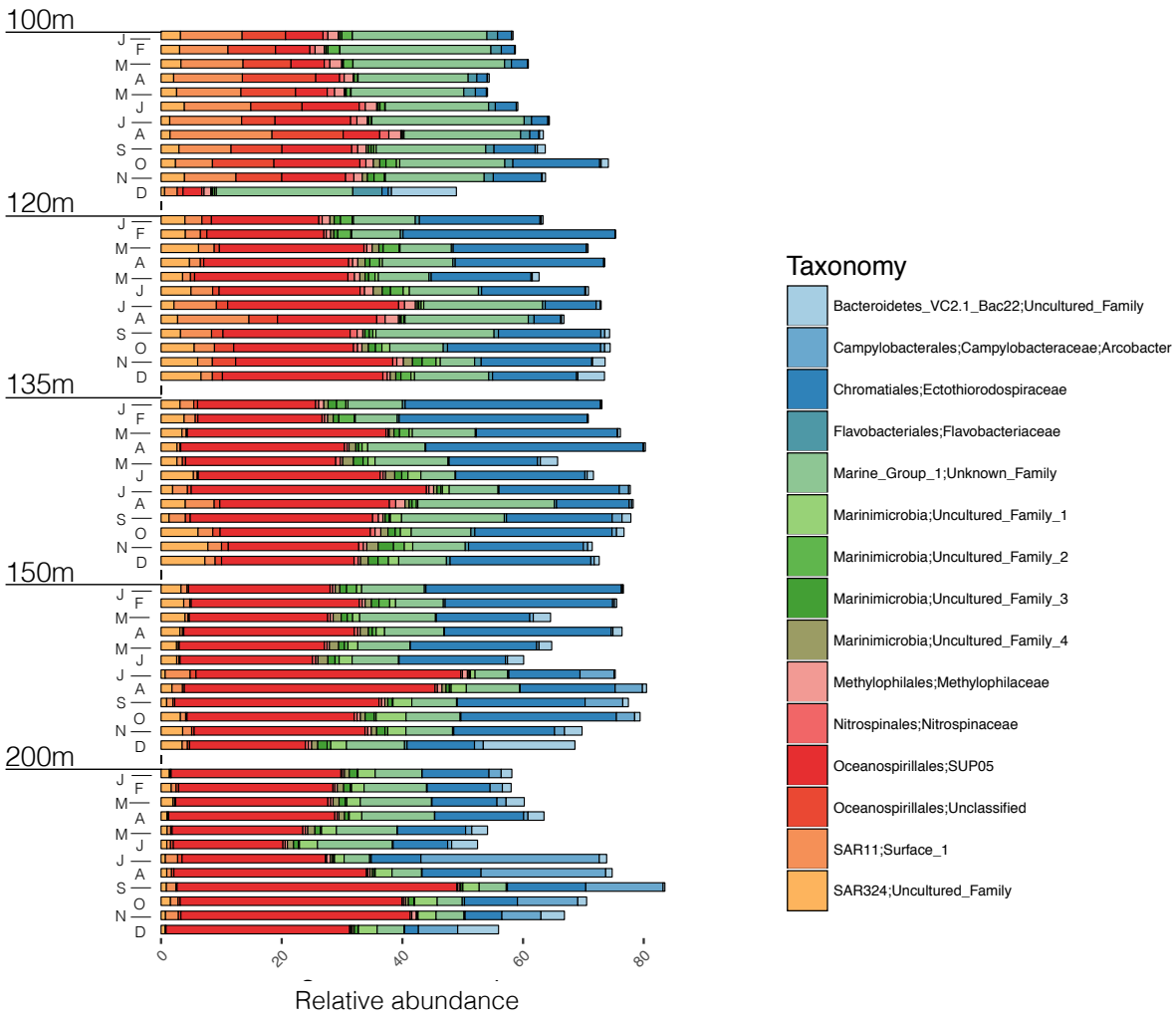

Figure C.3: Relative abundance of 15 most abundant taxa for the deeper waters of SI in 2015 (100, 120, 135, 150, 200m). These OTUs were the most abundant ones found in average throughout the samples.

C.3 Model of NO_2^- competition between anammox and complete denitrification

This model describes how anammox bacteria and denitrifiers compete against each other in response to varying metabolite input fluxes. The reaction rates are described using metabolite concentrations ([C]), cell abundance (X), as well as kinetic parameters (K_m and V_{max}) determined for microbial communities in Saanich Inlet (SI) or found in the literature when missing. In turn, metabolite concentrations (Eq. C.1) vary depending on the metabolite input fluxes (R_{in}) as well as the rates of metabolite consuming reactions described (Eqs. C.2 to C.7). Here, we choose 3 metabolic reactions: NO_3^- reduction to NO_2^- (NO3R, Eqs. C.2 and C.3), complete denitrification (DEN, NO_2^- to N_2, Eqs. C.4 and C.5) as well as anammox (AN, Eqs. C.6 and C.7). In this model, DEN and AN both compete for the NO_2^- produced through NO3R. We also consider both NO3R and DEN to use sulphide (HS^-) as an electron donor as implied from metagenomic information [33, 187] and our process rate measurements. The stoichiometric relationships for the 3 metabolic reactions and their metabolites are shown in Eqs. C.2 C.5 C.7 as well as in table C.2 and considered in the model on a per mole of electron donor (ED) basis.

$$\frac{d[C]}{dt} = R_{IN} - Rxn \tag{C.1}$$

$$NO_3^- \text{ reduction to } NO_2^- \text{ (NO3R): } 4NO_3^- + HS^- \Rightarrow 4NO_2^- + SO_4^{2-} + H^+ \tag{C.2}$$

$$NO3R = V_{max,NO3R} * X_{NO3R} * \frac{[HS^-]}{[HS^-] + K_{m,NO3R,HS}} * \frac{[NO_3^-]}{[NO_3^-] + K_{m,NO3R,NO3}} \tag{C.3}$$

$$\text{DEN: } 8/3NO_2^- + HS^- + 5/3H^+ \Rightarrow 4/3N_2 + SO_4^{2-} + 4/3H_2O \tag{C.4}$$

$$DEN = V_{max,DEN} * X_{DEN} * \frac{[NO_2^-]}{[NO_2^-] + K_{m,DEN,NO2}} * \frac{[HS^-]}{[HS^-] + K_{m,DEN,HS}} \tag{C.5}$$

$$\text{AN: } NH_4^+ + NO_2^- \Rightarrow N_2 + 2H_2O \tag{C.6}$$

$$AN = V_{max,AN} * X_{AN} * \frac{[NH_4^+]}{[NH_4^+] + K_{m,AN,NH4}} * \frac{[NO_2^-]}{[NO_2^-] + K_{m,AN,NO2}} \tag{C.7}$$

The change in metabolite concentrations is followed in our model for NH_4^+, NO_2^-, NO_3^- and HS^-, and depends on the input fluxes (R_{in}), as well as the production and consumption of the metabolites through

Table C.2: Stoichiometric coefficients for the metabolites considered in the model and their respective reactions.

M\RXN	AN	NO3R	DEN
NH_4^+	-1	0	0
NO_2^-	-1	+4	-8/3
NO_3^-	0	-4	0
HS^-	0	-1	-1

the reaction rates AN, DEN and/or NO3R. For example, NH_4^+ concentrations only depend on the input of NH_4^+ to the system and the consumption of NH_4^+ through AN. NO_2^- concentrations, on the other hand, depend on the input fluxes of NO_2^- and the production of NO_2^- through NO3R, as well as on consumption through AN and DEN. A stoichiometric coefficient is added in front of the reaction rate when needed as the reaction rates are described in [mol ED L^{-1} d^{-1}] (Eqs. C.8 to C.11).

$$\frac{d[NH_4^+]}{dt} = R_{NH4_iN} - AN \tag{C.8}$$

$$\frac{d[NO_2^-]}{dt} = R_{NO2_IN} - AN - (8/3)DEN + 4NO3R \tag{C.9}$$

$$\frac{d[NO_3^-]}{dt} = R_{NO3_iN} - 4NO3R + 4NO3R \tag{C.10}$$

$$\frac{d[HS^-]}{dt} = R_{HS_IN} - NO3R - DEN \tag{C.11}$$

Finally, the change in cell abundance (cell L^{-1}), described in Eqs. **??**, depends on the respective reaction rates (AN, DEN or NO3R), the biomass yield (Y [cells (moles of ED)$^{-1}$]), and the death rate ([d^{-1}]). It is important to note that we differentiate here between the growth of cells through NO3R and DEN as the energy yield can be different.

$$\frac{d[X_{AN}]}{dt} = AN * Y_{AN} - X_{AN} * \lambda_{AN} \tag{C.12}$$

$$\frac{d[X_{DEN}]}{dt} = DEN * Y_{DEN} - X_{DEN} * \lambda_{DEN} \tag{C.13}$$

$$\frac{d[X_{NO3R}]}{dt} = NO3R * Y_{NO3R} - X_{NO3R} * \lambda_{NO3R} \tag{C.14}$$

The biomass yield (Y) can be calculated according to Eq. C.15 and is based on the coefficient of the reaction (γ), the free gibbs energy (ΔG_r), and the quotient of the concentrations of the chemical species involved in the reaction (Qr, Eq. C.16). However, for the sake of simplifying this model and for easier comparison, we calculated this biomass yield and concluded that it ranges on the order of 10^{13} (cells mole ED)$^{-1}$. Changes of the biomass yield were tested below in this supplement.

$$Y = (2.08 * \gamma - 0.0211 * \Delta G_r) * \frac{1}{weight - of - 1 - cell} \text{ (Roden and Jin, 2011)} \tag{C.15}$$

$$\text{With: } \Delta G_r = \Delta G_r^\circ + RT * ln(Q_r) \tag{C.16}$$

We solved the multiple differential equations (Eqs. C.8 to C.14) numerically using Eulers technique with a step of 0.01 days (Eq. C.17) and build the equations in Matlab for the different simulations. We consider the model to have reached steady-state when the changes in metabolite concentrations, reaction rates and cell concentrations reaches an asymptote or a constant increase or decrease (see general remarks).

$$\text{If } \frac{dy}{dt} = f(y,t) \text{Then, } y_t = y_{t-1} + dt * f(y_{t-1}, t_{t-1}) \tag{C.17}$$

This model was created to test whether we could reproduce the stagnation phenotype with low N_2 production rates and the renewal phenotype with higher N_2 production rates. This was accomplished by varying the kinetic parameters of the underlying phenotypes and the input nutrient fluxes. While the main purpose of the model is highlighted developed in the main text, we also conducted a stability analysis of the model here in the supplement. We then looked at what controls the partitioning of N_2 production between

anammox and complete denitrification in a stagnation phenotype setting as the partitioning appear to vary throughout the year during this phenotype.

C.3.1 General remarks

- The code was developed in MATLAB (version R2015b) and is available online and in the supplement.below.
- All the rates reported for the model are in moles N L^{-1} d^{-1}.
- Nutrient concentration changes are not constrained by any output fluxes that would naturally occur in the environment such as advection and diffusion out of the depth studied. Therefore, if unused by the microbial reaction described in the mass balance of this model, nutrient can accumulate to unrealistic concentrations for SI. Also, because the model is dynamical, if a cell population was not sustained by the conditions set at the beginning of the stimulation, the cell population would decrease until reaching 0. Therefore, in these conditions, a constant development is reached but no so-called steady-state.
- Initial concentrations influenced how fast the model would get to a constant development. We thus chose cell abundance and nutrient concentrations that are closer to the end of the simulation.
- The figures for the model are constituted of 3 panels (figure C.4 to C.8). The first panel shows the evolution of the different substrates over the time of the simulation studied in the model in moles L^{-1} (NH_4^+, NO_3^-, NO_2^-, HS^-). The second panel shows the cell abundance of the three microbial populations studied in the model in cell L^{-1} (NO3R, DEN, and AN). The third panel shows the rates of NO_3^- reduction to NO_2^- (NO3R), anammox (AN) and complete denitrification (DEN) in moles N L^{-1} d^{-1}.

C.3.2 Stability of the model

The stability of the model was tested for a confined range of kinetic parameters, as these constants could be constrained through incubation experiments or taken out of the existing literature (i.e. anammox k_m constants were taken out of [109]). Therefore, we only varied the input nutrient fluxes to find the working limits of the model. The parameters used in the stability analysis can be found in table C.3. The lowest limit was determined by nutrient input fluxes that could not sustain any of the 3 microbial populations described in this model. Thus, we show the lower input nutrient fluxes to be of 10^{-11} moles of substrate L^{-1} d^{-1} (figure C.4). From the start of this stimulation (figure C.4), these microbial populations decrease to concentrations as low as 100 cells L^{-1} after running the model for 10 000 days. On the other side of the range, input nutrient fluxes of $5 \cdot 10^{-5}$ moles of substrate L^{-1} d^{-1} rendered the model to be unstable, with no solution found for the set conditions (table C.3). Thus, with input nutrient fluxes ranging between 10^{-11} and $5 \cdot 10^{-5}$ moles of substrate L^{-1} d^{-1}, it is possible to obtain a constant development from the model.

With this model, we could test whether we could reproduce two environmental phenotypes in SI (low N_2 production during stagnant phase of SI and high N_2 production Test 1 produces a first set of conditions that shows dominance of anammox in the system (figure C.4,tables C.3 and C.4). Among the model parameters, initial metabolite concentrations are low and metabolite input fluxes are stoichiometrically balanced aside from the NO_2^- input flux, which is 0. This was set based on the fact that NO_2^- concentrations are relatively low at all times in SI and therefore, input fluxes from below and above depths should be negligible. Most of the kinetic parameters were chosen from the literature (see table C.3) and some were determined here.

Table C.3: Kinetic parameters used in the stability analysis of the model.

Parameter	Value	Unit	Reference
$k_{m\_NH4\_AN}$	$3\ 10^{-6}$	Moles L^{-1}	(Thamdrup and Dalsgaard, 2002)
$k_{m\_NO2\_AN}$	$0.45\ 10^{-6}$	Moles L^{-1}	(Thamdrup and Dalsgaard, 2002)
$k_{m\_NO2\_DEN}$	$5\ 10^{-6}$	Moles L^{-1}	This paper and (Jensen *et al.*, 2009)
$k_{m\_NO3\_NO3R}$	$5\ 10^{-6}$	Moles L^{-1}	This paper and (Jensen *et al.*, 2009)
$k_{m\_HS\_DEN}$	$12\ 10^{-6}$	Moles L^{-1}	This paper
$k_{m\_HS\_NO3R}$	$12\ 10^{-6}$	Moles L^{-1}	This paper
V_{max_AN}, V_{max_DEN}, V_{max_NO3R}	$2\ 10^{-14}$	Moles $cell^{-1}$ d^{-1}	This parameter is based on cell specific rate for anammox and used at the same value for DEN and NO3R for comparison (Jensen *et al.*, 2008)
Y_{AN}	$1.5\ 10^{13}$	Moles ED $cell^{-1}$	Calculated from (Roden and Jin, 2011) and used as a reference.
Y_{DEN}, Y_{NO3R}	$1.5\ 10^{14}$	Moles ED $cell^{-1}$	Biomass yield for denitrifiers appear to be higher as they constitute a larger part of the microbial population with similar rates as anammox
d_{AN}, d_{DEN}, d_{NO3R}	0.001	d^{-1}	(Louca *et al.*, 2016; Whitman *et al.*, 1998)

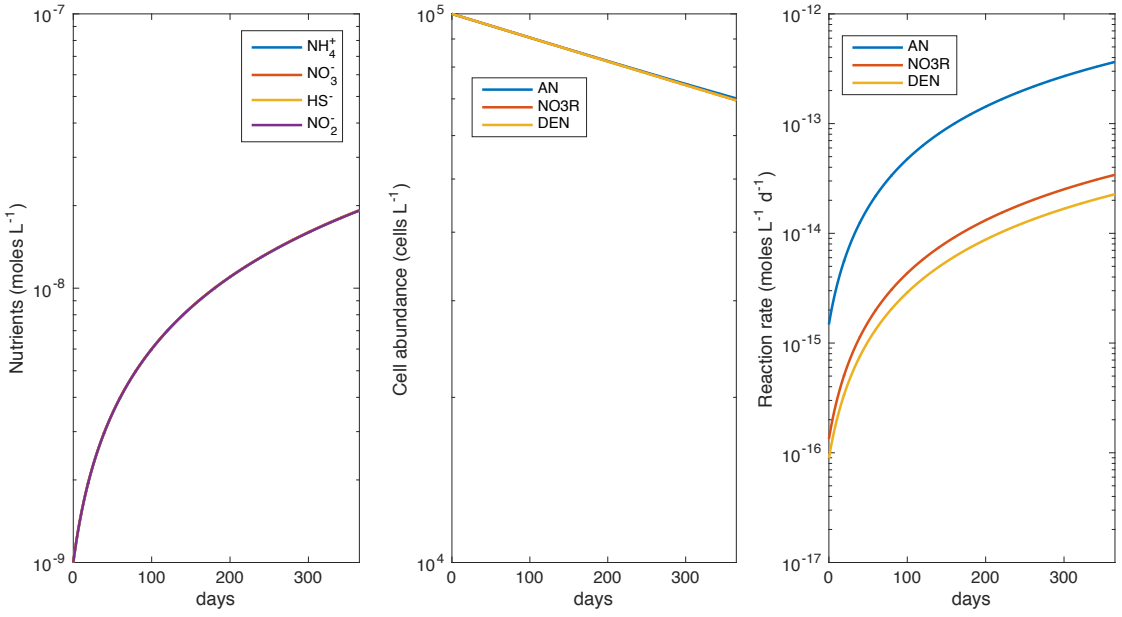

Figure C.4: Lower limit of the stability of the model for the set conditions found in table C.3.

C.3.3 Stagnation phenotype: partitioning of N_2 production through anammox and complete denitrification

Similar rates of anammox and denitrification were found in SI during most of the year, with a partitioning of N_2 production between anammox and denitrification close to 50% if the highest denitrification rates are excluded (during renewal phenotype). The alternation between the dominance of anammox or denitrification plausibly lies in slight changes in the capacity of the microbial populations to use the substrates (i.e. changes in kinetic parameters). Although input nutrient fluxes are also likely to influence the partitioning of N_2 production by limiting one process over the other, the inherent capacity of the microbial populations to process substrates more efficiently than others (based on their respective kinetic parameters) is likely to be the main determinant on the dominance of one process over the other.

Anammox was found to dominate N_2 production under the set conditions for the model found in table C.3 and with the following nutrient input fluxes: R_{NO3} and $R_{NO2} = 5 \cdot 10^{-9}$ moles L^{-1} d^{-1}, and R_{NH4} and $R_{HS} = 5 \cdot 10^{-8}$ moles L^{-1} d^{-1} (figure C.5). These nutrient input fluxes represent stagnation periods in SI, as described in the main text, with high NH_4^+ and HS^- fluxes coming from the sediments, and low NO_3^- and NO_2^- present in the anoxic water column. Indeed, the range of the rates of the described processes here correspond to those found in SI under the stagnation period. The high affinity of anammox for NO_2^- likely gave the advantage to anammox bacteria to process lower NO_2^- concentrations, despite complete denitrifiers possessing a higher biomass yield (table C.3). When the NO_2^- dependency constant was lowered for complete denitrifiers below 1.5μM ($k_{m,NO2,DEN}$), table C.4), the complete denitrifiers population appear to grow faster (figure C.6). After a stabilization period of 100 days in the simulation, the rates of denitrification were shown to be higher than those of anammox. Similarly, when the V_{max} or the biomass yield for complete denitrifiers was increased ($V_{max} \geq 6 \cdot 10^{-14}$ moles L^{-1} d^{-1} and $Y_{DEN} \geq 7 \cdot 10^{-14}$ cell (moles ED)$^{-1}$, table C.4), rates of denitrification also ended up higher than the rates of anammox (figures **??**) after a stabilization period of 100 days as well. Thus, within a same order of magnitude, variation in the kinetic parameters can highly influence the outcome of the partitioning of N_2 production between anammox and denitrification. It is thus highly relevant to constrain these parameters as well as identifying specific kinetic parameters for specific phenotypes in order to refine the modeling of the N-cycle.

Table C.4: Kinetic parameters for complete denitrifiers.

Parameter	Value	Simulation where tested	Unit
$k_{m\_NO2\_DEN}$	<1.5 10^{-6}	Figure S6	Moles L^{-1}
V_{max_DEN}	>6 10^{-14}	Figure S7	Moles cell^{-1} d^{-1}
Y_{DEN}	>7 10^{14}	Figure S8	Moles ED cell^{-1}

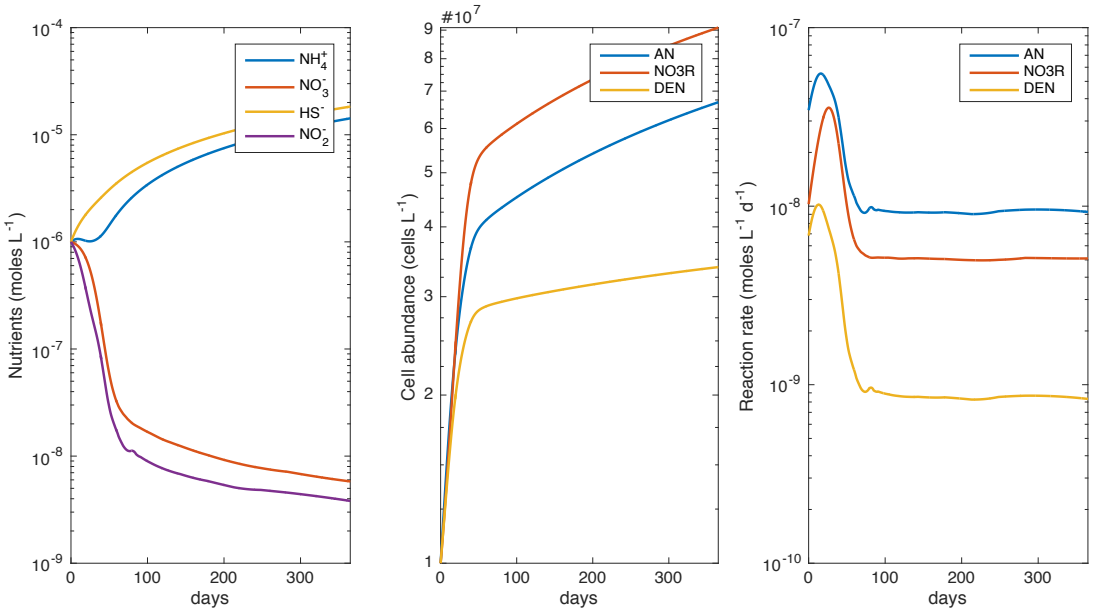

Figure C.5: Simulation of the model for a stagnation phenotype that shows anammox dominating N_2 production. See table C.3 for kinetic parameters used here.

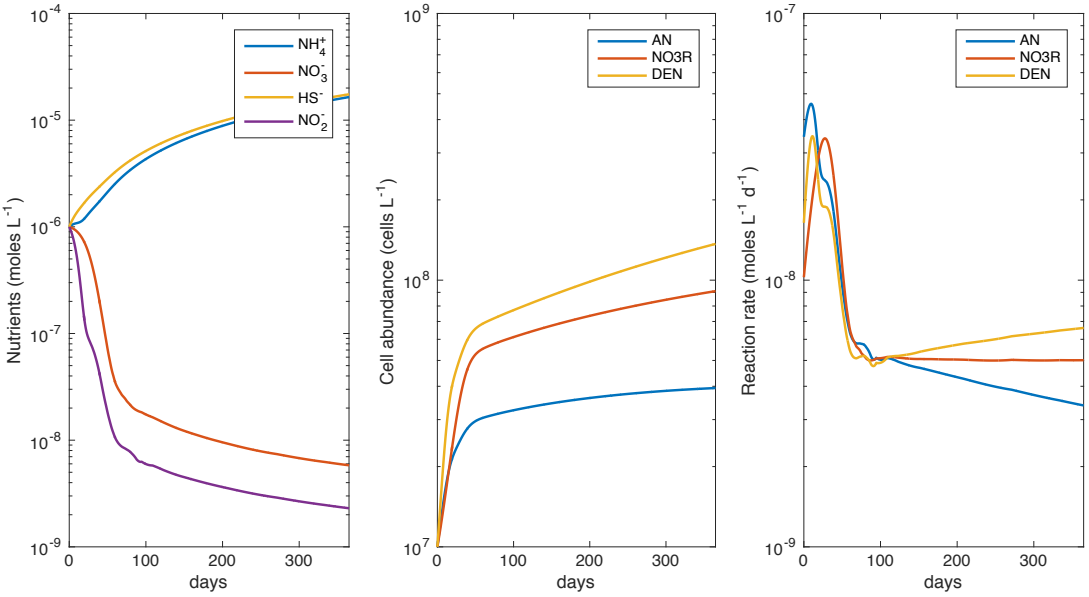

Figure C.6: Decrease of $k_{m,NO2}$ (see table C.4) for complete denitrification shows rates of denitrification dominating over anammox after 100 days.

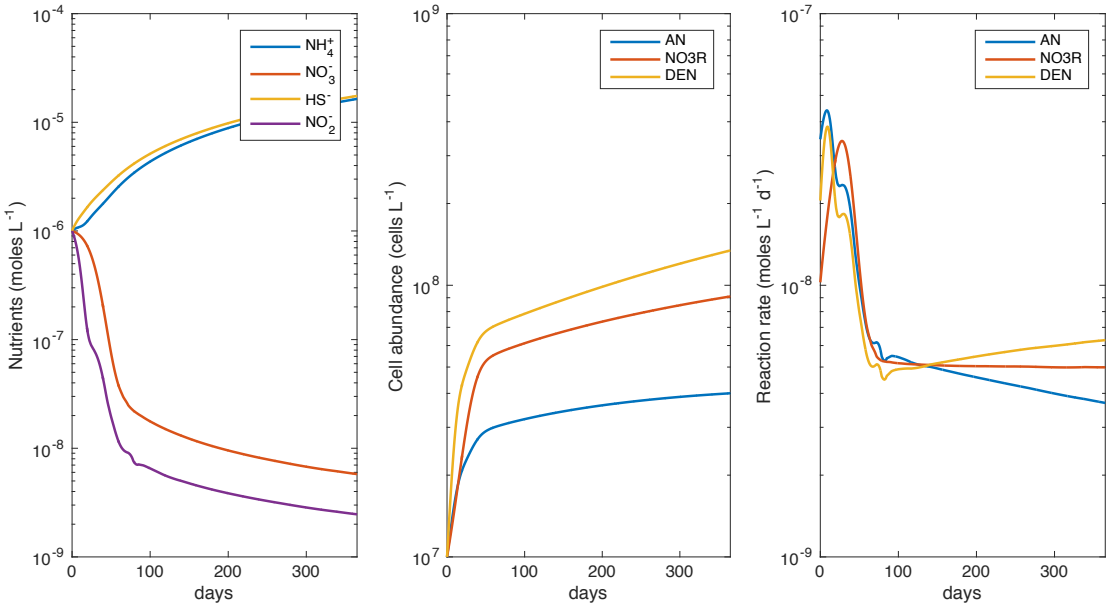

Figure C.7: Increase of $V_{max,DEN}$ (See table C.4) for complete denitrification shows rates of denitrification dominating over anammox after 100 days.

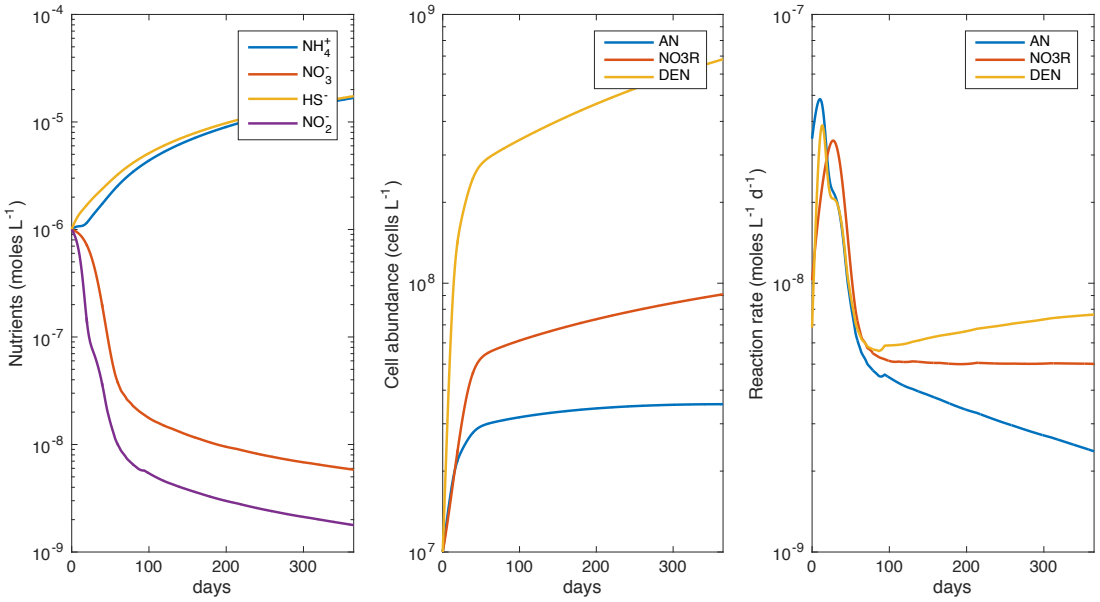

Figure C.8: Increase of Y_{DEN} (see table C.4) for complete denitrification shows rates of denitrification dominating over anammox after 100 days.

C.3.4 Matlab code for model NO_2^- competition

```
clc
clear all

%parameters used
%------------------------------

%nutrient fluxes in (moles L-1 d-1)

RNH4_IN=5*10^-8;
RNO3_IN=5*10^-6;
RHS_IN=5*10^-7;
RNO2_IN=5*10^-7;


%t0 input in ODE, 7 variables - nutrient concentrations (moles L-1) and
%cells concentrations (cells L-1)
%x(1)=NH4 x(2)=NO3 x(3)=HS x(4)=NO2 x(5)=X_AN x(6)=X_DEN x(7)=X_NO3R

x0=[10^-6 10^-6 10^-6 10^-9 10^7 10^7 10^7];
%time range
tspan=0:0.01:10000;

%death rate (d-1)

```

```
d_AN=0.001;
d_NO3R=0.001;
d_DEN=0.001;

%Km parameters (moles L-1)

km_NH4_AN=0.000003;
km_NO2_AN=0.00000045;
km_HS_DEN=0.00001;
km_NO2_DEN=0.000005;
km_HS_NO3R=0.00001;
km_NO3_NO3R=0.000005;

%Vmax (moles cells-1 d-1)

vm_AN=2*10^-14;
vm_DEN=2*10^-13;
vm_NO3R=2*10^-14;

%biomass yield (cell mol Electron Donor-1)

Y_AN=5*10^13;
Y_DEN=1.5*10^15;
Y_NO3R=5*10^14;




%f = system of equations to elucidate the following variables over time:
%x(1) = NH4
%x(2) = NO3
%x(3) = HS
%x(4) = NO2
%x(5) = AN_cells
%x(6) = DEN_cells
%x(7) = NO3R_cells


f= @(t,x) [RNH4_IN-(vm_AN*x(5)*x(1)*x(4)/((x(1)+km_NH4_AN)*(x(4)+km_NO2_AN)));
           RNO3_IN-4*(vm_NO3R*x(7)*x(2)*x(3)/((x(2)+km_NO3_NO3R)*(x(3)+km_HS_NO3R)));
           RHS_IN-(vm_NO3R*x(7)*x(2)*x(3)/((x(2)+km_NO3_NO3R)*(x(3)+km_HS_NO3R)))
                   -(vm_DEN*x(6)*x(4)*x(3)/((x(4)+km_NO2_DEN)*(x(3)+km_HS_DEN)));
           RNO2_IN-(vm_AN*x(5)*x(1)*x(4)/((x(1)+km_NH4_AN)*(x(4)+km_NO2_AN)))
                   -(8/3)*(vm_DEN*x(6)*x(4)*x(3)/((x(4)+km_NO2_DEN)*(x(3)+km_HS_DEN)))
                   +4*(vm_NO3R*x(7)*x(2)*x(3)/((x(2)+km_NO3_NO3R)*(x(3)+km_HS_NO3R)));

 ((vm_AN*x(5)*x(1)*x(4)/((x(1)+km_NH4_AN)*(x(4)+km_NO2_AN)))*Y_AN)-(x(5)*d_AN);
 ((vm_DEN*x(6)*x(4)*x(3)/((x(4)+km_NO2_DEN)*(x(3)+km_HS_DEN)))*Y_DEN)-(x(6)*d_DEN);
 ((vm_NO3R*x(7)*x(2)*x(3)/((x(2)+km_NO3_NO3R)*(x(3)+km_HS_NO3R)))*Y_NO3R)-(x(7)*d_NO3R);];


%solution for the 7 equations/variables with Euler s technique
options = odeset( NonNegative ,1);
[t,x] = ode15s(f,tspan,x0,options);


if(x<0)
```

```
  x=0;
end

%moles ED L-1 d-1, is in moles N L-1 d-1 already because it is anammox!
AN=vm_AN.*x(:,5).*x(:,1).*x(:,4)./((x(:,1)+km_NH4_AN).*(x(:,4)+km_NO2_AN));

%moles ED L-1 d-1
%DEN=vm_DEN.*x(:,6).*x(:,4).*x(:,3)./((x(:,4)+km_NO2_DEN).*(x(:,3)+km_HS_DEN));

%if needs to be in moles N L-1 d-1
DEN=(8/3)*vm_DEN.*x(:,6).*x(:,4).*x(:,3)./((x(:,4)+km_NO2_DEN).*(x(:,3)+km_HS_DEN));


%moles ED L-1 d-1
%NO3R=vm_NO3R.*x(:,7).*x(:,2).*x(:,3)./((x(:,2)+km_NO3_NO3R).*(x(:,3)+km_HS_NO3R));

%if needs to be in moles L-1 d-1
NO3R=4*vm_NO3R.*x(:,7).*x(:,2).*x(:,3)./((x(:,2)+km_NO3_NO3R).*(x(:,3)+km_HS_NO3R));



%plotting of solutions
figure
set(gcf,  Position , [100, 100, 800, 400])
subplot(1,3,1);

semilogy(t,x(:,1),t,x(:,2),t,x(:,3),t,x(:,4), LineWidth ,1.5);
xlabel( days );
ylabel( Nutrients (moles L^{-1}) );
legend( NH_{4}^{+} , NO_{3}^{-} , HS^{-} , NO_{2}^{-} );
%the following line can be commented so the figure shows time for 10000 days
%xlim([0 1000])


subplot(1,3,2);

semilogy(t,x(:,5),t,x(:,7),t,x(:,6), LineWidth ,1.5);
xlabel( days );
ylabel( Cell abundance (cells L^{-1}) );
legend( AN , NO3R , DEN );
%the following line can be commented so the figure shows time for 10000 days
%xlim([0 1000])


%plot reaction rates
subplot(1,3,3);

semilogy(t,AN,t,NO3R,t,DEN, LineWidth ,1.5);
legend( AN , NO3R , DEN );
xlabel( days );
ylabel( Reaction rate (moles L^{-1} d^{-1}) );
%the following line can be commented so the figure shows time for 10000 days
%xlim([0 1000])



figure
```

```
139 set(gcf,  Position , [100, 100, 800, 400])
140 subplot(1,3,1);
141
142 semilogy(t,x(:,1),t,x(:,2),t,x(:,3),t,x(:,4), LineWidth ,1.5);
143 xlabel( days );
144 ylabel( Nutrients (moles L^{-1}) );
145 legend( NH_{4}^{+} , NO_{3}^{-} , HS^{-} , NO_{2}^{-} );
146 %the following line can be commented so the figure shows time for 10000 days
147 xlim([0 60])
148
149
150 subplot(1,3,2);
151
152 semilogy(t,x(:,5),t,x(:,7),t,x(:,6), LineWidth ,1.5);
153 xlabel( days );
154 ylabel( Cell abundance (cells L^{-1}) );
155 legend( AN , NO3R , DEN );
156 %the following line can be commented so the figure shows time for 10000 days
157 xlim([0 60])
158
159
160 %plot reaction rates
161 subplot(1,3,3);
162
163 semilogy(t,AN,t,NO3R,t,DEN, LineWidth ,1.5);
164 legend( AN , NO3R , DEN );
165 xlabel( days );
166 ylabel( Reaction rate (moles L^{-1} d^{-1}) );
167 %the following line can be commented so the figure shows time for 10000 days
168 xlim([0 60])
169 %print( 5by3DimensionsFigure , -dpdf , -r0 )
```

Appendix D

Chapter 4: supplemental material

D.1 Geochemical profiles in Saanich Inlet (SI)

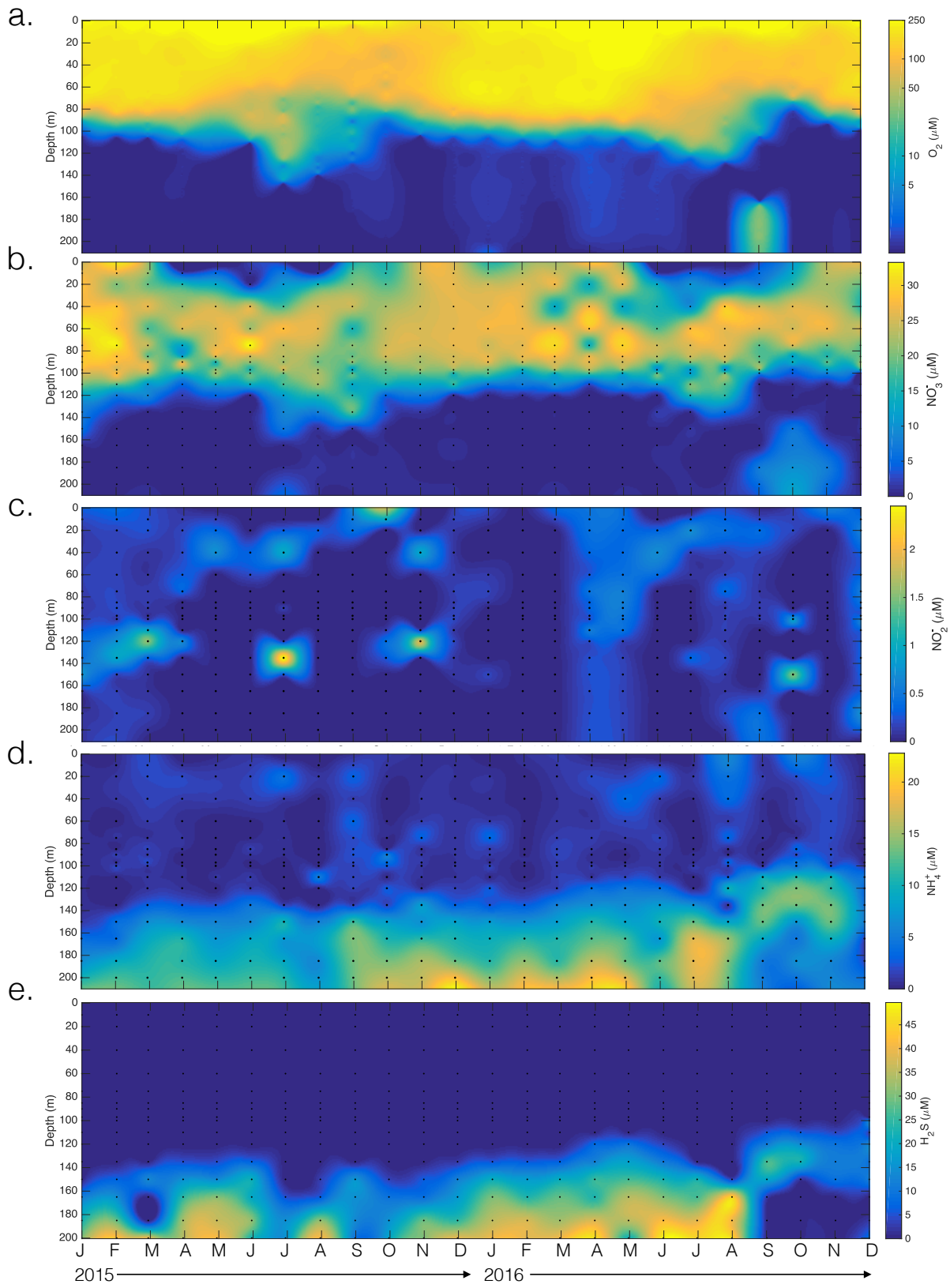

Figure D.1: *Nutrient concentrations in SI for the years 2015-2016 at station S3.* (a) O_2 concentrations (μM), (b) NO_3^- concentrations (μM), (c) NO_2^- concentrations (μM), (d) NH_4^+ concentrations (μM), (e) HS^- concentrations (μM).

D.2 Potential and scaled rates of anaerobic N-metabolisms

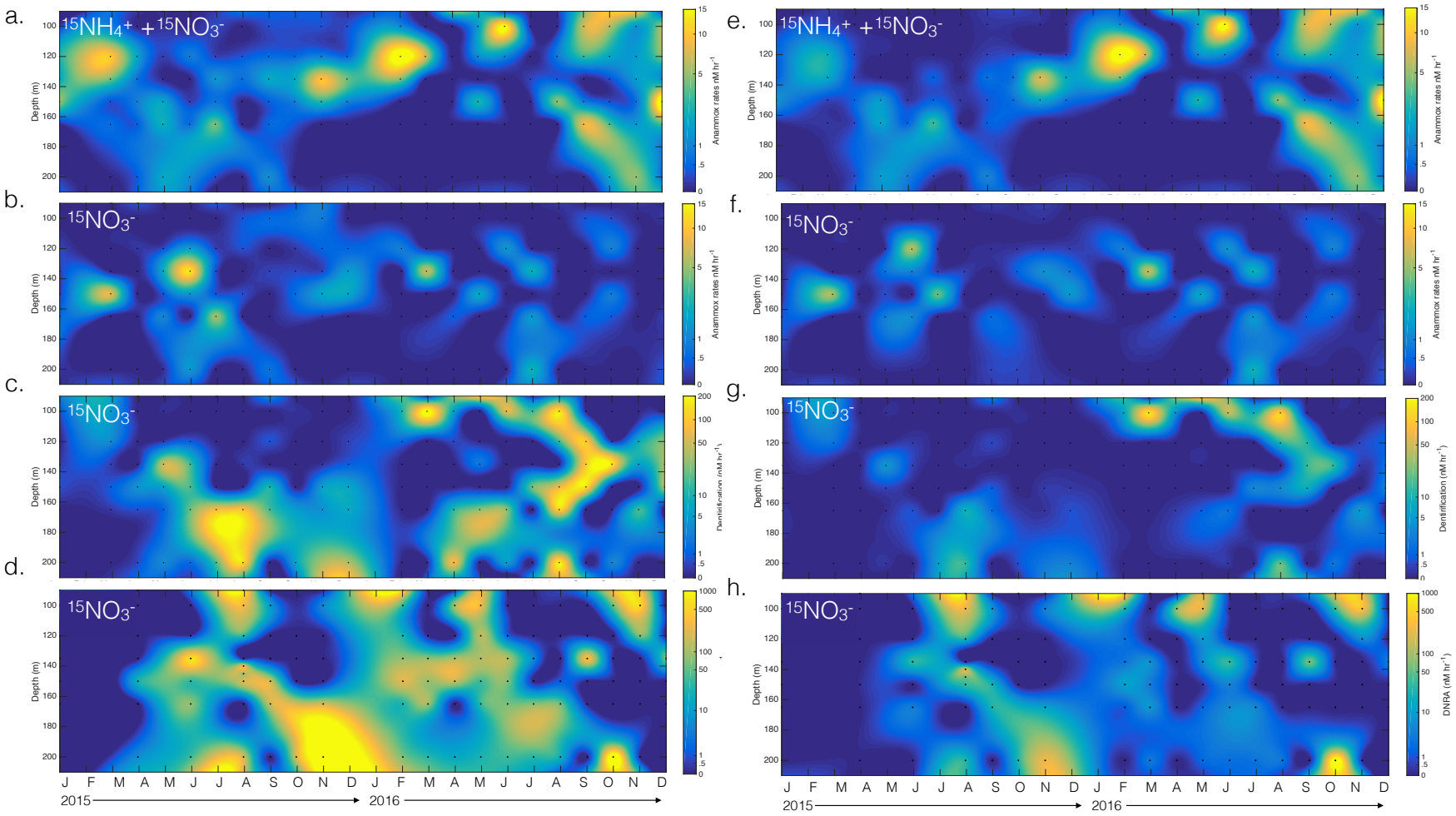

Figure D.2: *Potential and scaled rates of denitrification, anammox and DNRA.* (a) rates of anammox based on the accumulation of $^{29}N_2$ from $^{15}NH_4^+$ + $^{14}NO_3^-$ incubations (nM hr^{-1}), (b) rates of anammox based on the accumulation of $^{29}N_2$ from $^{15}NO_3^-$ incubations (nM hr^{-1}), (c) rates of denitrification based on the accumulation of $^{30}N_2$ from $^{15}NO_3^-$ incubations (nM hr^{-1}), (d) rates of denitrification based on the accumulation of $^{30}N_2$ from $^{15}NO_3^-$ incubations (nM hr^{-1}), (f-h) scaled rates

To produce depth-integrated rates of denitrification, anammox and DNRA (figure 1 in main text), the volumetric potential rates were scaled to *in situ* levels of NO_3^- for denitrification and DNRA or NH4+ for anammox, based on their half-saturation constant (k_m) found in Michiels et al. (2018, submitted) for anammox and denitrification and k_m=5μM for DNRA (data not shown). This was done according to Eq. D.1:

$$R_{scaled} = R_{pot} * \frac{[S]}{(k_m + [S])} \tag{D.1}$$

The scaled rates of denitrification, anammox and DNRA were then integrated over the anoxic water column (90m to 200m) and is summarized in table D.1.

Table D.1: *Partitioning of N-loss and N-retention through NO_x reduction in moles m^{-2} d^{-1}.*

Year	Month	DNRA	Denitrification	Anammox	Total N-loss	Total NOx reduction	% N-retention
2015	January	/	4E-05±1E-05	1.1E-03±2E-04	1.20E-03	/	/
2015	March	/	2.2E-03±1E-04	1.8E-03±1E-04	6.27E-03	/	/
2015	April	4.88E-05±0	2.1E-05±6E-06	6.9E-04±7E-05	7.28E-04	7.76E-04	6.29
2015	May	/	2.0E-03±3E-04	2.6E-03±1E-04	6.49E-03	/	/
2015	June	1.17E-02±2E-05	5E-04±1E-04	10.0E-04±7E-05	2.04E-03	1.37E-02	85.15
2015	July	/	4.4E-03±5E-04	1.6E-03±2E-04	1.04E-02	/	/
2015	August	3.23E-01±3E-03	1.4E-02±2E-03	1.5E-04±3E-05	2.90E-02	3.52E-01	91.77
2015	September	1.85E-02±5E-04	1.6E-03±2E-04	1.51E-03±9E-05	4.78E-03	2.33E-02	79.46
2015	October	3.09E-02±2E-04	8E-04±3E-04	1.5E-03±4E-04	3.02E-03	3.39E-02	91.09
2015	November	2.13E-01±4E-05	1.8E-04±2E-05	3.4E-03±3E-04	3.73E-03	2.17E-01	98.28
2015	December	/	2.5E-03±6E-04	1.2E-03±2E-04	6.21E-03	/	/
2016	February	1.67E-01±4E-03	5.6E-03±1E-04	8E-04±1E-04	1.20E-02	1.79E-01	93.26
2016	March	9.4E-03±1E-04	5.5E-02±6E-03	9.6E-04±6E-05	1.10E-01	1.19E-01	7.89
2016	April	2.71E-02±0	7.8E-03±3E-04	1.74E-04±4E-06	1.59E-02	4.29E-02	63.07
2016	May	1.33E-01±8E-04	3.0E-02±1E-03	1.20E-03±9E-05	6.07E-02	1.93E-01	68.58
2016	June	1.68E-02±1E-04	2.19E-02±3E-04	2.59E-03±0	4.64E-02	6.32E-02	26.53
2016	July	4.36E-03±0	4.13E-03±8E-04	4.0E-06±2E-07	8.27E-03	1.26E-02	34.53
2016	August	2.33E-03±3E-05	7.6E-02±3E-03	1.6E-03±1E-04	1.53E-01	1.55E-01	1.50
2016	September	2.11E-02±3E-04	1.3E-02±2E-03	4.0E-03±2E-04	2.93E-02	5.05E-02	41.86
2016	October	1.38E±0	6.49E-03±0	1.62E-03±0	1.46E-02	1.39E+00	98.95
2016	November	1.82E-01±1E-04	1.9E-03±6E-04	5.4E-03±2E-04	9.20E-03	1.92E-01	95.20
2016	December	1.22E-03±2E-06	1.7E-03±5E-04	8.3E-03±3E-04	1.17E-02	1.30E-02	9.44

D.3 Taxonomy and functional gene abundances

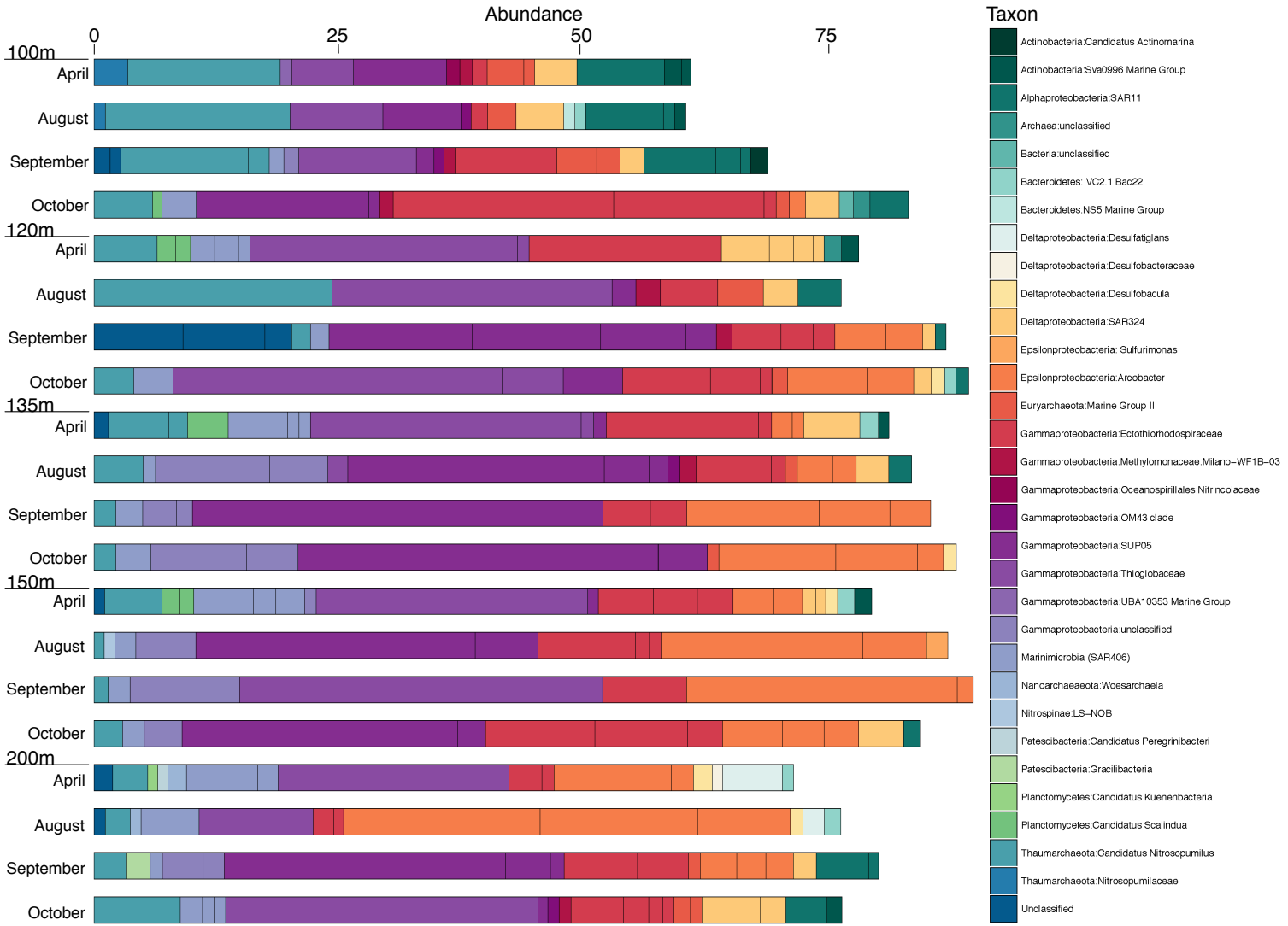

Figure D.3: *Taxonomic composition of microbial communities at the OTU level in SI.* Taxonomic composition of SIs microbial communities at the OTU level based on Metagenomic data, through EMIRGE analysis (extraction and reconstruction of 16S rRNA gene sequences out of metagenomes) and classified using the latest SILVA database (v132) - relative abundance (higher than 1%) of OTUs present in samples for SI at 5 depths and 4 months in 2016.

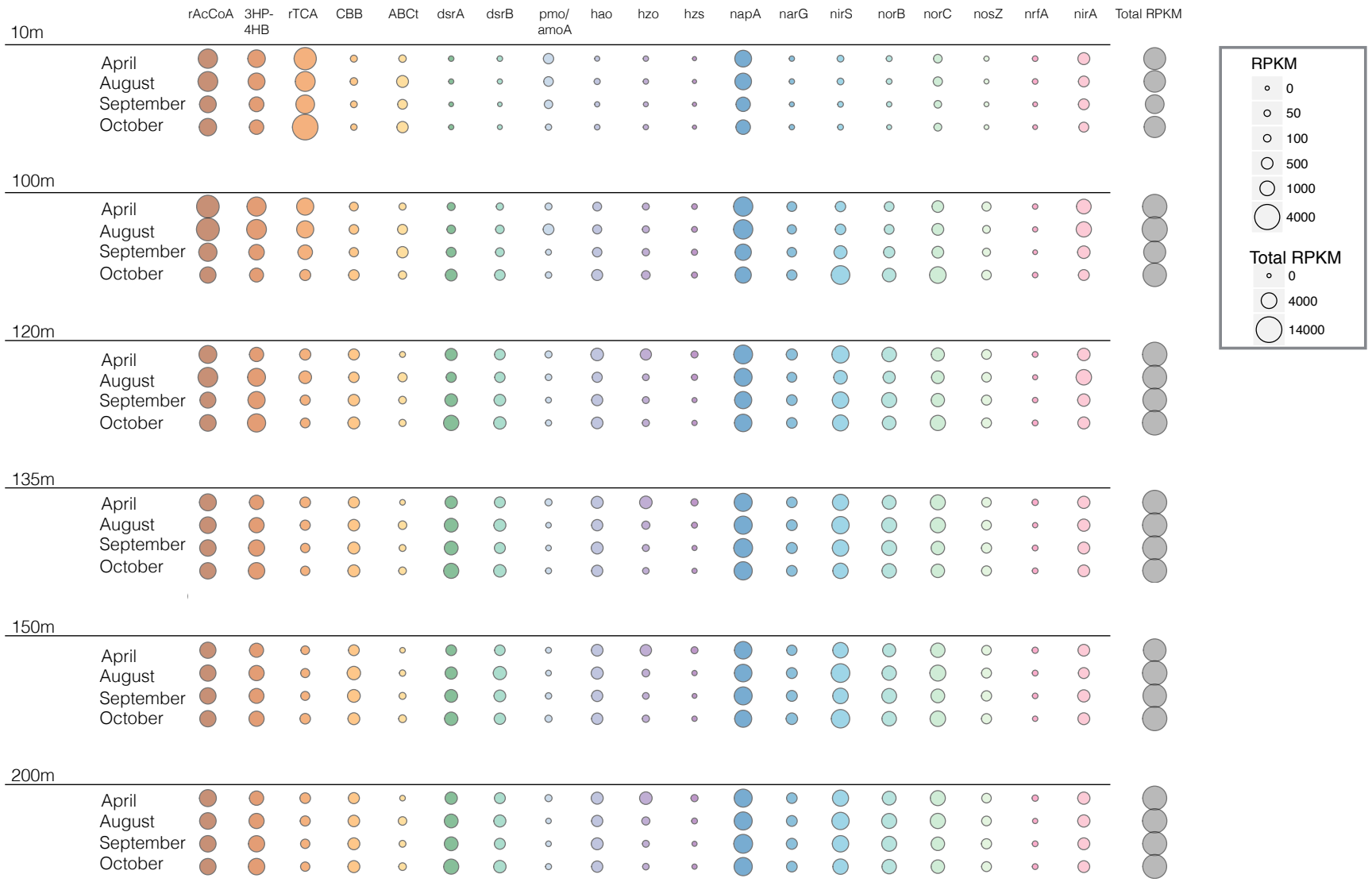

Figure D.4: *RPKM counts for functional genes.* RPKM for genes involved in C-fixation (rAcCoA=CO dehydrogenase, 3HP-4HB= acetyl CoA carboxylase in archaea, rTCA= 2-oxoglutarate synthase, CBB=Ribulose-1,5-bisphosphate carboxylase/oxygenase), C-degradation (ABCt=ABC transporter), sulphide oxidation (*dsrA* and *B*= reversible dissimilatory sulphate reductase), nitrification (*pmo/amoA*=ammonia monooxygenase, *hao*=hydroxylamine oxidoreductase), anammox (*hzo*=hydrazine dehydrogenase, *hzs*=hydrazine synthase), NO_3^- reduction (*napA*=periplasmic dissimilatory nitrate reductase, *narG*=membrane-bound dissimilatory reductase), denitrification (*nirS*=nitrite reductase, *norBC*=nitric oxide reductase, *nosZ*=nitrous oxide reductase), DNRA (*nrfA*=dissimilatory periplamic cytochrome c nitrite reductase, *nirA*=assimilatory nitrite reductase) and total RPKM for all the ORFs detected in the metagenomic samples.

Table D.2: *List of genes and their acronyms used in this paper for the metagenomic analysis.*

Gene name	Abbreviation	Process associated	Metacyc number
CO dehydrogenase	*rAcCoA*	C-fixation	1.2.7.4
Acetyl CoA carboxylase in archaea	*3HP-4HB*	C-fixation	6.4.1.2, 2.1.3.15
2-oxoglutarate synthase	*rTCA*	C-fixation	1.2.7.3
Ribulose-1,5-bisphosphate carboxylase/oxygenase	*CBB*	C-fixation	4.1.1.39
ABC transporter	*ABCt*	C-degradation	K12536, K05648 (KEGG)
Reversible dissimilatory sulphate reductase	*dsrA and B*	HS- oxidation	1.8.99.5
Ammonia monooxygenase	*pmo/amoA*	Nitrification	1.14.99.39
Hydroxylamine oxidoreductase	*hao*	Nitrification	1.7.2.6
Hydrazine dehydrogenase	*hzo*	Anammox	1.7.2.8
Hydrazine synthase	*hzs*	Anammox	1.7.2.7
Periplasmic dissimilatory nitrate reductase	*napA*	NO_3^- reduction	1.10.2.2, 1.9.6.1
Membrane-bound dissimilatory reductase	*narG*	NO_3^- reduction	1.7.5.1
Nitrite reductase	*nirS*	Denitrification	1.7.2.1
Nitric oxide reductase	*norBC*	Denitrification	1.7.2.5
Nitrous oxide reductase	*nosZ*	Denitrification	1.7.5.2, 1.7.2.4
Dissimilatory periplamic cytochrome c nitrite reductase	*nrfA*	DNRA	1.7.2.2
Assimilatory nitrite reductase	*nirA*	DNRA	1.7.7.1

D.4 Energy availability and power supply

Table D.3: *Examples of free energy yields calculated for 2 months anoxic water column in SI (in kJ moles N^{-1}).*

Year	Month	Depth	ΔG_DEN	ΔG_AN	ΔG_DNRA
2016	9	90	-422.13	-427.65	-404.17
2016	9	100	-420.29	-427.03	-402.80
2016	9	120	-428.78	-417.42	-412.20
2016	9	135	-430.34	-417.97	-413.99
2016	9	150	-427.63	-417.91	-411.01
2016	9	165	-425.28	-433.30	-407.80
2016	9	200	-424.51	-435.57	-404.57
2016	10	90	-421.49	-413.11	-400.99
2016	10	100	-423.08	-436.70	-403.01
2016	10	120	-428.24	-418.04	-411.24
2016	10	135	-429.13	-418.00	-412.58
2016	10	150	-430.51	-439.02	-413.21
2016	10	165	-427.44	-415.54	-409.01
2016	10	200	-420.95	-415.35	-398.23

D.5 Methods supplement

Table D.4: *Sampling dates and type of ^{15}N-labeled incubations.*

Month	Exact date of sampling	Type of ^{15}N labeled-incubation
January 2015	14 January 2015	$^{15}NO_3^-$ (10μM), $^{15}NH_4^+$ & $^{14}NO_3^-$ (10μM&10μM)
February 2015	11 February 2015	/
March 2015	11 March 2015	$^{15}NO_3^-$ (10μM), $^{15}NH_4^+$ & $^{14}NO_3^-$ (10μM&10μM)
April 2015	8 April 2015	$^{15}NO_3^-$ (10μM), $^{15}NH_4^+$ & $^{14}NO_3^-$ (10μM&10μM)
May 2015	13 May 2015	$^{15}NO_3^-$ (10μM), $^{15}NH_4^+$ & $^{14}NO_3^-$ (10μM&10μM)
June 2015	3 June 2015	$^{15}NO_3^-$ (10μM), $^{15}NH_4^+$ & $^{14}NO_3^-$ (10μM&10μM),
July 2015	8 July 2015	$^{15}NO_3^-$ (10μM), $^{15}NH_4^+$ & $^{14}NO_3^-$ (10μM&10μM)
August 2015	12 August 2015	$^{15}NO_3^-$ (10μM), $^{15}NH_4^+$ & $^{14}NO_3^-$ (10μM&10μM)
September 2015	9 September 2015	$^{15}NO_3^-$ (10μM), $^{15}NH_4^+$ & $^{14}NO_3^-$ (10μM&10μM)
October 2015	22 October 2015	$^{15}NO_3^-$ (10μM), $^{15}NH_4^+$ & $^{14}NO_3^-$ (10μM&10μM)
November 2015	18 November 2015	$^{15}NO_3^-$ (10μM), $^{15}NH_4^+$ & $^{14}NO_3^-$ (10μM&10μM)
December 2015	9 December 2015	$^{15}NO_3^-$ (10μM), $^{15}NH_4^+$ & $^{14}NO_3^-$ (10μM&10μM)
January 2016	13 January 2016	/
February 2016	4 February 2016	$^{15}NO_3^-$ (10μM), $^{15}NH_4^+$ & $^{14}NO_3^-$ (10μM&10μM)
March 2016	16 March 2016	$^{15}NO_3^-$ (10μM), $^{15}NH_4^+$ & $^{14}NO_3^-$ (10μM&10μM)
April 2016	13 April 2016	$^{15}NO_3^-$ (10μM), $^{15}NH_4^+$ & $^{14}NO_3^-$ (10μM&10μM)
May 2016	11 May 2016	$^{15}NO_3^-$ (10μM), $^{15}NH_4^+$ & $^{14}NO_3^-$ (10μM&10μM)
June 2016	1 June 2016	$^{15}NO_3^-$ (10μM), $^{15}NH_4^+$ & $^{14}NO_3^-$ (10μM&10μM)
July 2016	13 July 2016	$^{15}NO_3^-$ (10μM), $^{15}NH_4^+$ & $^{14}NO_3^-$ (10μM&10μM)
August 2016	10 August 2016	$^{15}NO_3^-$ (10μM), $^{15}NH_4^+$ & $^{14}NO_3^-$ (10μM&10μM)
September 2016	14 September 2016	$^{15}NO_3^-$ (10μM), $^{15}NH_4^+$ & $^{14}NO_3^-$ (10μM&10μM)
October 2016	12 October 2016	$^{15}NO_3^-$ (10μM), $^{15}NH_4^+$ & $^{14}NO_3^-$ (10μM&10μM)
November 2016	9 November 2016	$^{15}NO_3^-$ (10μM), $^{15}NH_4^+$ & $^{14}NO_3^-$ (10μM&10μM)
December 2016	14 December 2016	$^{15}NO_3^-$ (10μM), $^{15}NH_4^+$ & $^{14}NO_3^-$ (10μM&10μM)

Table D.5: *Accession numbers for NCBI raw reads of samples.*

Sample name	Accession number
SI_118_April2016_10_MG	PRJNA468231
SI_118_April2016_100_MG	PRJNA468232
SI_118_April2016_120_MG	PRJNA468233
SI_118_April2016_135_MG	PRJNA468234
SI_118_April2016_150_MG	PRJNA468235
SI_118_April2016_200_MG	PRJNA468236
SI_122_August2016_10_MG	PRJNA468237
SI_122_August2016_100_MG	PRJNA468238
SI_122_ August2016_120_MG	PRJNA468239
SI_122_ August2016_135_MG	PRJNA468240
SI_122_ August2016_150_MG	PRJNA468241
SI_122_ August2016_200_MG	PRJNA468242
SI_123_September2016_10_MG	PRJNA468243
SI_123_ September2016_100_MG	PRJNA468244
SI_123_ September2016_120_MG	PRJNA468245
SI_123_ September2016_135_MG	PRJNA468246
SI_123_ September2016_150_MG	PRJNA468247
SI_123_ September2016_200_MG	PRJNA468248
SI_124_October2016_10_MG	PRJNA468249
SI_124_ October2016_100_MG	PRJNA468250
SI_124_ October2016_120_MG	PRJNA468251
SI_124_ October2016_135_MG	PRJNA468253
SI_124_ October2016_150_MG	PRJNA468254
SI_124_ October2016_200_MG	PRJNA468255